THE SEPARATION OF ATOMIC AND MOLECULAR GASES FROM HELIUM BY CATAPHORESIS

Thesis by

Donald Sherwood Remer

In Partial Fulfillment of the Requirements

For the Degree of

Doctor of Philosophy

California Institute of Technology

Pasadena, California

1970

(Submitted May 12, 1970)

ACKNOWLEDGMENTS

I want to express my appreciation to Professor F. H. Shair for introducing me to the subject of cataphoresis and for his contributions which were far too numerous to be mentioned here.

I would also like to express my gratitude to the Chemical Engineering shop personnel and the Chemistry Glassworking shop personnel for their work in the design and construction of the apparatus.

During my graduate studies I have received support from an Atlantic-Richfield Fellowship, a National Science Foundation Graduate Traineeship, a National Science Teaching Assistant Summer Fellowship, several Graduate Research Assistantships, and a Teaching Assistantship.

The experimental work was supported in part with funds provided by the United States Atomic Energy Commission.

Thanks to my wife, Louise, and my family and friends for the many ways they have encouraged and helped me.

ABSTRACT

The cataphoretic purification of helium was investigated for binary mixtures of He with Ar, Ne, N_2, O_2, CO, and CO_2 in a DC glow discharge. An experimental technique was developed to continuously measure the composition in the anode end-bulb without sample withdrawal. Discharge currents ranged from 10 ma to 100 ma. Total gas pressure ranged from 2 torr to 9 torr. Initial compositions of the minority component in He ranged from 1.2 mole percent to 7.5 mole percent.

The cataphoretic separation of Ar and Ne from He was found to be in agreement with previous investigators. The cataphoretic separation of N_2, O_2, and CO from He was found to be similar to noble gas systems in that the steady-state separation improved with (1) increasing discharge current, (2) increasing gas pressure, and (3) decreasing initial composition of the minority component. In the He-CO_2 mixture, the CO_2 dissociated to CO plus O_2 . The fraction of CO_2 dissociated was directly proportional to the current and pressure and independent of initial composition.

The experimental results for the separation of Ar, Ne, N_2, O_2, and CO from He were interpreted in the framework of a recently proposed theoretical model involving an electrostatic Peclet number. In the model the electric field was assumed to be constant. This assumption was checked experimentally and the maximum variation in the electric field was 35% in time and 30% in position. Consequently, the

assumption of constant electric field introduced no more than 55% variation in the electrostatic Peclet number during a separation.

To aid in the design of new cataphoretic systems, the following design criteria were developed and tested in detail: (1) electric field independent of discharge current, (2) electric field directly proportional to total pressure, (3) ion fraction of impurity directly proportional to discharge current, and (4) ion fraction of impurity independent of total pressure. Although these assumptions are approximate, they enabled the steady-state concentration profile to be predicted to within 25% for 75% of the data. The theoretical model was also tested with respect to the characteristic time associated with transient cataphoresis. Over 80% of the data was within a factor of two of the calculated characteristic times.

The electrostatic Peclet number ranged in value from 0.13 to 4.33. Back-calculated ion fractions of the impurity component ranged in value from 4.8×10^{-6} to 178×10^{-6}.

TABLE OF CONTENTS

LIST OF FIGURES

LIST OF TABLES

LIST OF TABLES

Appendix E

NOMENCLATURE

D	diffusion coefficient, cm^2/sec
D^+	diffusion coefficient of ions, cm^2/sec
E	axial electric field defined in Eq. (21), volts/cm
$\overline{E}_a$	average value of the electric field near the anode end of the positive column, volts/cm
E_a	electric field near the anode end of the positive column, volts/cm
E_a^h	high-value of the electric field near the anode end of the positive column, volts/cm
E_a^ℓ	low-value of the electric field near the anode end of the positive column, volts/cm
$\overline{E}_c$	average value of the electric field near the cathode end of the positive column, volts/cm
E_c	electric field near the cathode end of the positive column, volts/cm
E_c^h	high-value of the electric field near the cathode end of the positive column, volts/cm
E_c^ℓ	low-value of the electric field near the cathode end of the positive column, volts/cm
F	fraction of CO_2 dissociated
J_o	Bessel function of the first kind (of order zero)
K	coefficient defined in Eq. (23)
L	length of discharge tube, cm
N_a	concentration of metal vapor, atoms/cc
N_o	concentration of metal vapor atoms near the cathode, atoms/cc
N_w	concentration of metal vapor near the walls, atoms/cc
P	total gas pressure, mm Hg
P_c	collision probability of electrons, cm^2/cm^3

R	radius of discharge tube, cm
S	mean distance traveled between ionic formation and neutralization, cm
T	gas temperature, ^{o}K
T_e	electron temperature, ^{o}K
V	voltage, volts
V_o	mean electron energy, volts
V_1, V_2	voltage at electric-field probes 1 and 2, volts
X	impurity component
b	constant defined in Table E-13, volts/cm
d	distance between probes, cm
i^+	current of positive ions defined in Eq. (13)
i	discharge current, ma
k	constant introduced in Eq. (15), min^{-1}
m	slope of electric-field line, volts/cm/mm Hg
n^-	density of electrons, electrons/cc
n_a	density of impurity, atoms/cc
n_a^*	original density of impurity, atoms/cc
n_a^+	concentration of metal ions, ions/cc
n_+	density of impurity ions, ions/cc
n_o	density of impurity neutrals, atoms/cc
n_+/n_o	fraction of impurity ionization
n_o^o	initial mole percentage of impurity
r	radius, cm

t	time, min
t_c	characteristic time for cataphoresis, min
t_c^E	characteristic time for cataphoresis from the experiment, min
t_c^M	characteristic time for cataphoresis from the model, min
$u_1, u_2 \cdots$	eigenvalues defined in Eq. (32)
v	defined in Eq. (18)
x	axial position, cm
θ_F	degree of ionization of the impurity defined in Eq. (18)
$\theta(\eta,\tau)$	dimensionless concentration of impurity at a position η at a time τ
$\theta(1,\infty)$	dimensionless concentration of impurity at the anode at steady state
α	electrostatic Peclet number
α_{BGW}	a function of the ionization mechanism
β^*	an average ionization probability
β	a dimensionless grouping which represents the ratio of the forced diffusion effect to the ordinary diffusion effect
δ	dimensionless volume of cathode
ϵ	dimensionless volume of anode
η	dimensionless distance coordinate
λ	mean free path of electrons, cm
μ	ionic mobility, cm^2/volt/sec
μ^+	ionic mobility of metal ions, cm^2/volt/sec
μ_A^+	ionic mobility of A^+ ions, cm^2/volt/sec

ν	mole fraction
π	3.14
τ	dimensionless time
τ_c	dimensionless characteristic time
τ_c^E	dimensionless characteristic time from the experiment
τ_c^M	dimensionless characteristic time from the model
τ_o	dimensionless separation factor at t = 0
τ_t	dimensionless separation factor at a time t
τ_∞	dimensionless separation factor at infinite time
τ_{BGW}	dimensionless separation factor

I. INTRODUCTION

When a pure gas is the conducting medium in a direct-current glow discharge, positive ions of the gas are formed and drift toward the cathode because of the electric field. If the pure gas is replaced by a binary mixture of gases, then the component with the lowest ionization potential will be selectively ionized and drift toward the cathode, producing an increase in concentration of this component near the cathode. The preferential ionization of gases in a glow discharge and the subsequent increase in concentration of a component near the cathode is referred to as cataphoresis.

Literature Survey

Cataphoresis was first observed by Baly [1] in 1893. He reported that several binary mixtures of gases (CO_2-H_2, N_2-H_2, CO-H_2, SO_2-H_2, I_2-H_2, Hg-H_2, CO_2-CO, N_2-CO_2, and CO_2-SO_2) exhibited an increase in concentration of one of the components near the cathode. Baly's qualitative results were based on spectroscopic measurements. In 1898, Thomson [2] qualitatively observed cataphoresis in a H_2-Cl_2 mixture with Cl_2 being enriched near the anode. No further investigations of cataphoresis in molecular gases were made until 1939 when Groth and Harteck [3] reported on the cataphoretic purification of H_2-D_2. In 1953 more data on the separation of hydrogen and deuterium were reported by Beckey, Groth, and Welge [4]. They explained the increase in deuterium concentration near the cathode by assuming that dissociation rates and mechanisms were identical for the isotopes and that the recombination proceeds by ternary collisions. Since H atoms

have a speed approximately $\sqrt{2}$ times as great as that of the deuterium atoms, the three-body recombination rate was higher for hydrogen than for deuterium. Consequently, there was a higher concentration of D and D^+ than of H and H^+. The net effect was deuterium enrichment at the cathode. They were unable to detect the separation of Xe isotopes. This result is consistent with their explanation of the hydrogen-deuterium separation because Xe isotopes have molecular weights which only differ by a small amount; therefore, the speeds of the isotopes are nearly equal.

Except for the aforementioned investigations [1-4] the study of cataphoresis has been limited to mixtures of monatomic gases.

The first qualitative studies of the cataphoretic separation of noble gas mixtures were performed by Skaupy [5] in 1916. He worked with binary mixtures of He, Ar, and Ne, and found that the gas with the lower ionization potential always appeared to be increased in concentration at the cathode. In 1925, Skaupy and Bobek [6] obtained the first quantitative measurement of cataphoresis by using a gas interferometer to measure the indices of refraction. Results were reported for binary mixtures of He-Ar and He-Ne in the pressure range 3 mm Hg to 10 mm Hg at a current of about 500 ma. They concluded that the separation of inert gases increased with increasing current and decreased with increasing pressure.

In 1933 Penning [7] observed cataphoresis in mixtures of Ne-Ar-Hg. He made the first quantitative measurements on cataphoresis using optical spectroscopy. In his experiments Hg was enriched at the cathode. To this date all the work on cataphoresis had been

experimental; then Druyvesteyn [8], in 1935, presented the first theoretical attempt to explain Penning's results for metal ions in noble gases. Druyvesteyn showed that the ambipolar diffusion of positive ions from the positive column to the wall gave rise to a radial concentration profile. In addition, he was apparently the first experimentalist to utilize the principle of cataphoresis in a practical application. He kept metal vapor from attacking a glass window in a metal-noble gas discharge by placing the window near the anode.

In 1954 Riesz and Dieke [9] reported quantitative spectroscopic measurements of cataphoresis in binary mixtures of He-Ne, Ar-Ne, Kr-Ar, and Kr-Xe. Investigations were performed in the pressure range of 3.2 mm Hg to 5.5 mm Hg and the current range 10 ma to 30 ma. They found that the steady-state separation increased both with increasing pressure and increasing current. This pressure effect is the antithesis of the results previously reported by Skaupy and Bobek [6]. Later experimenters [15,16] have confirmed Riesz and Dieke's conclusion that cataphoretic separation increases with increasing pressure. Riesz and Dieke also observed that the separation decreased as the mass of the preferentially ionized component increased. For the cases they investigated, it was observed that the minority component always increased in composition near the cathode whether it had a higher or a lower ionization potential than the majority component.

In 1958 Kenty [10] observed the cataphoretic separation of Hg vapor (ionization potential of 10.4 eV) in binary mixtures with the inert gases He, Ne, Ar, Kr, and Xe (ionization potentials from 24.5 eV to 12.1 eV). He noted that Hg moved in a retrograde direction, that

is, toward the anode in the binary mixture with Xe. In all the other cases Hg moved toward the cathode as would be expected because of the lower ionization potential of Hg. Kenty attributed the retrograde behavior of Hg in Xe to the increased drift of neutral Hg atoms toward the anode because of the large cross section of Hg for electron impact and the small cross section of Xe for electron impact with electrons of about 1 eV energy (Ramsauer effect [11]).

Loeb [12], in 1958, presented a qualitative discussion on the mechanism of cataphoretic separation in inert gas glow discharges. He attributed the preferential ionization of the minority gas to two mechanisms, namely charge exchange and hybridization. If, in a binary mixture, the minority gas has a lower ionization potential, then it can be separated near the cathode because the minority gas is almost completely ionized by the process of charge exchange. However, Loeb points out that under certain conditions, some of the ions present may be hybrid ions such as $NeHe^+$ and $NeAr^+$. These hybrid ions have been observed by Oskam [13] and Pahl [14]. Consequently, in some cases, the minority gas which may have a higher ionization potential could still be separated near the cathode as was observed by Riesz and Dicke [9]. Loeb implies that a real understanding of cataphoresis can only be obtained by a microscopic analysis.

In 1959 Matveeva [15] performed the first direct quantitative measurements of cataphoresis. Samples were removed from the discharge tube and subjected to a mass spectrometer analysis. Matveeva investigated binary mixtures of He, Ar, and Ne and found that the separation was a function of minority gas concentration, discharge current,

discharge pressure, and the distance between electrodes. In the pressure range of 1.5 mm Hg to 4 mm Hg and a current range of 25 to 400 ma, the separation increased with increasing pressure and increasing current. Matveeva measured the concentration near the anode by removing several samples as a function of time in a binary mixture of He-Ar, and she observed that there was a continuous decrease of minority gas (argon) concentration near the anode for about fifteen minutes. She found that the time required to reach an apparent steady state was relatively independent of the discharge current and the initial composition of the mixture; however, increasing the length of the discharge tube increased the time to reach steady state.

In 1962 Schmeltekopf [16] reported on the cataphoretic separation of He-Ne mixtures in experiments where a mass spectrometer was used for quantitative analysis. Schmeltekopf found that the Ne concentration always increased near the cathode irrespective of whether Ne was the minority or majority component. This result is a contradiction of Riesz and Dieke's [9] conclusion that the concentration of minority component (whether it had the lower or higher ionization potential) was always increased near the cathode. In order to resolve this discrepancy Schmeltekopf also used an optical technique similar to the one used by Riesz and Dieke. Comparison of the optical data with the more reliable mass spectrometer data showed that the optical measurements were inaccurate near the cathode. A possible reason for erroneous optical measurements is the increase in degree of ionization of the minority component because of a shift in the electron

energy distribution function near the cathode.

All the work up to this time had been restricted to batch systems. Then, in 1962, Schmeltekopf [16] reported qualitative results on the separation of Ne from a binary mixture of He-Ne in a flowing system. In 1966 Flinn and Price [18] performed the first quantitative measurements on cataphoresis in a flowing system. They used a microthermal conductivity gauge similar to one described by Grew and Ibbs [19]. The removal of samples from the discharge system tended to disturb the system for about 7 minutes. Their investigation of binary mixtures of helium and argon indicated that the composition of argon near the cathode increased with increasing current and decreased with increasing flow rate. The separation was found to be relatively independent of the pressure for a given inlet composition. The theory presented was inadequate to explain their experimental results. Their analytical treatment predicted the wrong pressure and concentration dependence when compared to their experimental data. They concluded that the lack of agreement between the experimental data and the analytical solution was probably due to an inadequate theory and lack of knowledge as to the types and concentration of the ions existing in the gas mixture discharge.

Until the last few years, a satisfactory theoretical model for cataphoresis had not been formulated. In 1967 Freudenthal [20,21] developed a linearized model for steady state and transient cataphoresis when no end-bulbs are present. In 1968 Shair and Remer [22] developed a linearized model for steady state and transient

cataphoresis for the general case including end-bulbs. When the degree of ionization is low, their results reduce to those presented by Freudenthal for the special case of no end-bulbs. The basic assumptions in the model were that after electrical breakdown, the level of ionization of the impurity, and the axial electric field remained constant. It was demonstrated that for these conditions a system involving rapid ionization-recombination reactions with electrodiffusion was equivalent to a system in which no reaction occurred, but in which the effective ion mobility was a product of the true ion mobility and the fraction of impurity ionization. Agreement was found between this model and the experimental data reported by Matveeva [15] for mixtures of rare gases and by Beckey, Groth, and Welge [4] for mixtures of hydrogen and deuterium. Both of these sets of data were taken in systems with end-bulbs. In 1969 Sosnowski [77] measured cataphoresis in a He-Cd laser discharge tube. He found good agreement between his data and the theoretical model proposed by Shair and Remer [22].

The development of these recent theories [20-22] for cataphoresis indicated the need for a method by which the gas composition within end-bulbs could be measured continuously and without sample withdrawal. The quantitative data reported by Schmeltekopf [17] was for the steady-state separation. The transient data reported by Riesz and Dieke [9] were qualitative with respect to composition. The data reported by Matveeva [15] were the closest to being continuous and quantitative. She withdrew several discrete samples from the

end-bulbs as a function of time. Until this time no one had taken continuous and quantitative measurements of cataphoresis as a function of time. In 1969 Remer and Shair [23] reported results for such a technique in which continuous and quantitative cataphoretic measurements were performed in a He-Ar mixture. The measurements were recorded without removing samples from the system by using a 60-watt light bulb filament as a thermal conductivity detector and placing the filament directly behind a porous molybdenum screen serving as the anode.

Applications of Cataphoresis

Cataphoresis has been used successfully for purification of noble gases in preparation for experiments where low impurity levels are very important [24-28]. Miller [24] purified neon by using cataphoresis in order to determine the effect of argon impurity on the breakdown potential of neon. Loeb, Westberg, and Huang [25] used cataphoresis to separate Kr and N_2 impurities from Ar in order to study the spark breakdown potential of Ar . Purification of Ar produced breakdown properties entirely different from those previously observed. Oskam and Mittelstadt [26] employed cataphoresis to remove impurities in helium to study the ion mobilities of He^+ and He_2^+ in their parent gases from the afterglow in a helium plasma. Druyvesteyn and Penning [27] used cataphoresis to remove argon from neon before determining the first Townsend coefficient in neon. Using cataphoresis, Benton [28] was able to carry out work on metastable He and to measure the cross section for the deactivation of metastable He by

other gases. It was felt by Benton that these investigations would have been very difficult if not impossible to conduct without the use of cataphoresis.

In addition to using cataphoresis as a gas purification technique, Hogervorst and Freudenthal [29] employed cataphoresis to measure binary diffusion coefficients for neon-argon mixtures between 300 and 650°K.

Over twenty-five different binary mixtures have been separated by cataphoresis. These mixtures are identified for ready reference in Fig. 1. Cataphoresis is not limited to binary mixtures. Skaupy [5] observed qualitatively that in a ternary mixture of He, Ne and Ar, the mixture was enriched in He near the anode, Ne near the center of the tube, and Ar at the cathode. Possibly a multicomponent mixture could be separated by using several cataphoretic systems in series and removing one component in each chamber. If one pass through the system did not yield the required separation, then recycle could be used.

There are many potential commercial applications for an effective cataphoretic system. In helium-cooled nuclear reactors there is a build-up of Xe, Kr and other impurities. By bleeding off a steady stream of coolant from the reactor, these impurities could possibly be removed by cataphoresis.

Separation of the isotopes H_2 and D_2 (which have been separated by Groth [3,4]) would be very important in both research and commercial applications.

FIG. 1

Some Binary Mixtures which Have Been Separated by Cataphoresis

Numbers in boxes refer to references

CATHODE / COMPONENT NEAR	He	Ne	Ar	Kr	Xe	Na	Mg	Hg	Cl_2	I_2	CO	SO_2	CO_2	N_2	O_2	H_2	D_2
He																	
Ne	9 *																
Ar	23 *	15 31															
Kr			9														
Xe				9				10									
Na	30	30	30	30													
Mg		8															
Hg	10	8 10	10	10													
Cl_2																	
I_2																	
CO	*												1				
SO_2													1				
CO_2	*													1			
N_2	*																
O_2	*																
H_2								1	2	1	1	1	1	1			
D_2																3 4	

*Present investigation by D. S. Remer and F. H. Shair

Recently, Sosnowski [77] investigated the influence of cataphoresis on the operation of a He-Cd laser discharge. In earlier designs of He-Cd laser discharge tubes, it was thought necessary to locate Cd sources at a number of discrete points along the tube to obtain a unifom Cd distribution. However, his results indicate that at high currents it is only necessary to use a single source of Cd near the anode. The Cd will be transported toward the cathode by cataphoresis. A theoretical model for cataphoresis would aid in the design and performance of future systems of this type.

Purpose of This Investigation

At the time the author began his research project, no adequate theory existed for predicting cataphoretic separation of gas mixtures and no quantitative experimental results were reported in the literature for molecular gases except H_2 and D_2 . Also, continuous and quantitative measurements of the cataphoretic purification as a function of time had not been reported. The potential applications for cataphoretic separations serve as an impetus to study cataphoresis both experimentally and theoretically.

The main goal of the present experimental investigation was to check on the theory put forth by Shair and Remer [22]. The project was divided into three parts. In the first part, an experimental method was developed to measure the composition during cataphoresis. An inexpensive thermal conductivity technique was designed to take continuous and quantitative measurements without removing a sample. This technique has been previously described by Remer and Shair [23]. The

second part of the project was to collect steady-state and transient separation data especially for molecular gases. Cataphoresis was investigated in six gas mixtures: He-Ar, He-Ne, He-N_2, He-O_2, He-CO, and He-CO_2. The separation of O_2, N_2, and CO from He had not been previously investigated. The third part of this project consisted of comparing the experimental results to the model proposed for cataphoresis. Also, to facilitate the design of future cataphoretic separation systems, design criteria were developed and tested in detail.

Outline of Thesis

This thesis is divided into five major chapters: I. Introduction, II. Theory, III. Experimental Apparatus and Procedure, IV. Experimental Results, and V. Comparison of Theory and Experiment.

In Chapter I there was a literature survey, followed by a discussion of the present and future applications of cataphoresis. The purpose of the investigation was explained, and the thesis format was outlined.

In Chapter II the development of the theory for cataphoresis is described starting with the early work by Druyvesteyn [8] in 1935 and concluding with the most recent contributions by Shair and Remer [22].

In Chapter III the equipment including the vacuum, electrical, and water systems are described and the experimental procedure is outlined.

In Chapter IV the treatment of the data and the calculation procedure are explained. This is followed by a discussion of the experimental results and the quantities calculated from the data.

In Chapter V the experimental results are compared to the predictions of the recently developed theoretical model for cataphoresis, and design criteria are introduced to aid in the design of future cataphoretic separators.

II. THEORY

The theory of cataphoresis has been investigated for the purpose of predicting the spatial and time dependence of the axial concentration gradient occurring in a DC glow discharge containing gas mixtures at pressures of several torr. The discussion is limited to binary mixtures where one of the components is present in a small amount, usually less than 10 mole %. This component is referred to as the impurity and the other gas is called the majority component. In most cases the impurity gas has a lower ionization potential than the majority gas, but this is not mandatory [16].

In this chapter the development of the theory of cataphoresis is described, starting with the early work by Druyvesteyn [8] in 1935, followed by the work of Schmeltekopf [16], and Beckey, Groth and Welge [4], and concluding with the most recent contributions by Freudenthal [20,21] and Shair and Remer [22].

Druyvesteyn [8] presented the first theory to describe cataphoresis. The impetus for his work was Penning's [7] observation that a metal vapor impurity moved toward the cathode in a noble gas discharge. Druyvesteyn's analysis was for a binary mixture composed of a metal vapor impurity in a noble gas. Because of mathematical complexity, Druyvesteyn divided the problem into two parts. First, he investigated the axial dependence of the concentration of the metal vapor, $N_a(x)$, and second, he analyzed the radial dependence, $N_a(r)$, of the metal vapor concentration.

In the first part of the problem Druyvesteyn assumed that the concentration of metal atoms, $N_a(x)$, was constant over the cross section of the tube. He equated the ionic flux of metal vapor ions in one direction to the diffusional flux of neutral atoms of metal vapor in the opposite direction to obtain

$$-D \frac{dN_a(x)}{dx} \pi R^2 = \mu^+ E n_a^+ \int_0^R J_o\left(\frac{2.4r}{R}\right) 2\pi r \, dr$$

$$= 1.36 \, n_a^+ \mu^+ E R^2 \qquad (1)$$

where R is the radius of the tube, D is the diffusion coefficient of the metal atoms in the noble gas, E is the longitudinal electric field, and μ^+ and n_a^+ are the ionic mobility and concentration of the metal ions, respectively. Although he does not state it, he assumed that the diffusional flux of metal ions was negligible:

$$D^+ \frac{dn_a^+(x)}{dx} \pi R^2 << D \frac{dN_a(x)}{dx} \pi R^2 \qquad (2)$$

This is a good assumption when the degree of ionization of the metal vapor is low [21].

It is important to note that Druyvesteyn's entire discussion was limited to the steady state analysis. He did not treat the time dependence of cataphoresis. In order to solve Eq. (1), the dependence of n_a^+ on the distance from the cathode x must be known. Druyvesteyn therefore divided the system into two regions

(A) $n_a^+ = n^-$ for small x

(B) $n_a^+ \ll n^-$ for large x

where n^- is the concentration of electrons.

For region (A) he integrated Eq. (1) using

$$n_a^+ = \frac{1.9 \times 10^{11} \sqrt{V_o}\, i}{\lambda R^2 E} \tag{3}$$

to yield a linear decrease in the concentration of metal vapor as a function of the distance x from the cathode

$$N_a(x) = N_o - \frac{8.3 \times 10^{10} \mu^+ \sqrt{V_o}\, i}{\lambda D R^2} x \tag{4}$$

where V_o is the mean electron energy, i the discharge current, λ the mean free path of electrons, and N_o the concentration of metal vapor atoms near the cathode. This equation gives only the relative distribution of metal vapor unless the absolute value of the metal vapor concentration is known at some position x.

The axial gradient of the metal vapor concentration was obtained by taking the derivative of Eq. (4)

$$\frac{dN_a}{dx} = - \frac{8.3 \times 10^{10} \mu^+ \sqrt{V_o}}{\lambda D R^2} i \tag{5}$$

Penning [7] experimentally determined a value for $dN_a/dx = -1.7 \times 10^{13}$ atoms/cm^4 at a distance of 3 to 4 cm from the cathode in a 90% Ne - 10% Ar mixture with Hg vapor impurity. From Eq. (5),

Druyvesteyn calculated a value for $dN_a/dx = -1.2 \times 10^{13}$ atoms/cm^4. Several assumptions were made in Druyvesteyn's calculation because experimental values of the transport properties were not available. However, since Druyvesteyn's work in 1935, more recent transport data have appeared in the literature [37,51].

Druyvesteyn calculated a value of $D_{Hg-Ne} = 8.7$ cm^2/sec at $T = 300^oK$ and $P = 12$ mm Hg with formula (846) in Jeans [50]. However, if the diffusivity is recalculated using Eq. (8.2-44) in Hirschfelder, Curtiss, and Bird [37] with more recent values of the force constants for Hg and Ne [37], then a value of $D_{Hg-Ne} = 15.5$ cm^2/sec is obtained; see Appendix A for calculations.

Druyvesteyn extrapolated the mobility data of Tyndall and Powell [52] for Hg^+ in He to obtain a value for the mobility of Hg^+ in Ne (250 cm^2/volt/sec at 12 mm Hg and 300^oK.) However, in 1957 Chanin and Biondi [51] reported the mobilities of Hg^+ in Ne and Hg^+ in Ar. If Blanc's law [36] is assumed valid for Hg^+ in the Ar-Ne mixture, then the mobility of Hg^+ in a 10% Ar - 90% Ne mixture can be calculated directly to yield 309 cm^2/volt/sec at 300^oK and 12 mm Hg.

When Druyvesteyn's calculation is repeated using the more recent data for mobility and diffusivity, a value of $dN_a/dx = -0.8 \times 10^{13}$ atoms/cm^4 is obtained. (The details of these calculations are presented in Appendix A). This calculated value of dN_a/dx is a factor of two lower than the experimental value obtained by Penning. Druyvesteyn's calculated value of dN_a/dx was -1.2×10^{13} atoms/cm^4 which was fortuitously closer to the

experimental results than the value calculated with more recent transport data.

In region (B) Druyvesteyn introduced two new quantities, S and β^* . The term S was defined as the mean distance traveled by the ions in the direction of the cathode between their formation and subsequent neutralization on the wall. The number of ionizations of metal atoms per cm^3 was $n^- N_a \beta^*$ where β^* is a function of the electron temperature. Equation (1) takes the form

$$-D \frac{dN_a}{dx} \pi R^2 = (1.36) n^- \beta^* S R^2 \left(N_a + \frac{1}{2} \frac{dN_a}{dx} S\right) \tag{6}$$

The solution is

$$N_a = N_o e^{-Ax} \tag{7}$$

where

$$A = \frac{-0.43\ n^- \beta^* S}{D + 0.22\ n^- \beta^* S^2} = \frac{-2.1 \times 10^{10}\ i\beta^*/(\lambda\sqrt{V_o})}{D + \dfrac{0.28 \times 10^{10} i \beta^* R^2 E}{\lambda\ V_o^{3/2}}}$$

In the second part of the problem Druyvesteyn investigated the radial dependence of the ion concentration of the metal vapor. He assumed the concentration $N_a(r)$ to be independent of the distance to the cathode. Again, as for the axial case, Druyvesteyn divided the system into two regions

(A) $n_a^+ = n^-$ for large R

(B) $n_a^+ << n^-$ for small R .

For case (A) the solution is

$$N_a = N_w - n^- \frac{2\mu^+ V_o}{3D} J_o\left(\frac{2.4r}{R}\right) \tag{8}$$

where N_w is the concentration of metal vapor near the walls. For case (B) the result is

$$N_a = N_o J_o \left(\sqrt{\frac{-\beta^* n^-}{D}}\, r \right) \tag{9}$$

In summary, Druyvesteyn's solution is given by Eqs. (4), (7), (8) and (9).

Druyvesteyn did not discuss the relative importance of the axial concentration gradients (Eqs. (4) and (7)) and the radial concentration gradients (Eqs. (8) and (9)) to the cataphoretic purification of the metal vapor from the noble gas. However, when the ionization degree of the impurity component is low, which is usually the case for cataphoretic separations, then the influence of the radial concentration gradient on the axial gradient can be neglected [20,21].

Since Druyvesteyn's development was not restricted to metal atoms, Schmeltekopf [16,17] applied Druyvesteyn's theory to a binary mixture of noble gases. Schmeltekopf transformed Eqs. (4) and (7) into terms of the gas temperature, T , and pressure, P , by introducing several modifications. First, he used an expression for the electron mobility taken from Loeb [53]; second, Schmeltekopf assumed a Maxwellian distribution of electron velocities; and third, he used the Einstein expression to relate the mobility and *diffusion*

coefficient to the gas temperature. His results were

$$N_a = N_o - \frac{2.63 \times 10^{15} P_c \sqrt{T_e}\, P\, i}{T^2 R^2} x \tag{10}$$

for small x and

$$N_a = N_o e^{-\frac{1.36 \mu^+ E}{\pi D} x} = N_o e^{-1.5 \times 10^6 \frac{E}{T} x} \tag{11}$$

for large x, where P_c is the collision probability for electrons and T_e is the electron temperature.

In the derivation of Eq. (11), Schmeltekopf assumed that the impurity atoms are completely ionized, $n_a^+ = N_a$. This assumption is invalid because the level of ionization of the impurity atoms is $\sim 10^{-5}$ to 10^{-6}. This point will be discussed later.

Schmeltekopf [16] reported experimental data for the cataphoretic purification of Ne from He. In Fig. 4 of Schmeltekopf's paper he summarized results for the relative concentration of Ne to He as a function of distance x from the cathode for a range of currents. According to Druyvesteyn's theory as modified by Schmeltekopf, dN_a/dx should be proportional to i

$$\frac{dN_a}{dx} = -2.63 \times 10^{15} \frac{P_c T_e^{1/2} P}{T^2 R^2} i \tag{12}$$

and, therefore, the slopes of the curves should be proportional to the current. However, the slopes of these curves appeared to be relatively independent of the current in the range of 20 ma to 100 ma. Schmeltekopf concluded that the data were in clear disagreement with the current dependence as predicted by the theory of Druyvesteyn.

Beckey, Groth, and Welge [4] (referred to as BGW) investigated cataphoresis in H_2-D_2 mixtures. In their steady-state analysis, which was similar to Druyvesteyn's, they equated fluxes but did not separate the discharge into two regions. They introduced a quantity α_{BGW} which is a function of the ionization mechanism of H_2 and D_2. The solution to their steady-state analysis is

$$\ell n\, \tau_{BGW} = \frac{i^+ L(\alpha_{BGW} - 1)}{N_a \pi R^2 D} \tag{13}$$

with $i^+ = 1.36R^2\, n^+ \mu^+ e E$, where τ_{BGW} is the separation factor defined by

$$\tau_{BGW} = \left(\frac{\nu_c^{D_2}}{\nu_c^{H_2}}\right)\left(\frac{\nu_a^{H_2}}{\nu_a^{D_2}}\right) \tag{14}$$

and $n^+ e$ is the charge density. The quantity ν is the mole fraction of D_2 or H_2 in the vicinity of the cathode c, or anode a. An absolute value for the separation factor could not be calculated unless a value for α_{BGW} was assumed; however, relative changes in the value of τ_{BGW} could be compared to the experimental data. Linear plots were obtained for $\ell n\, \tau_{BGW}$ versus i and $\ell n\, \tau_{BGW}$ versus L, where L is the length of the discharge tube.

In addition to their steady-state analysis, BGW presented an ad hoc approach for the time-dependence of the separation factor. The separation factor as a function of time τ_t, was assumed to be

$$\tau_t = \tau_\infty - (\tau_\infty - \tau_o)\, e^{-kt} \tag{15}$$

where τ_∞ and τ_o are the separation factors as $t \to \infty$ and $t \to 0$, respectively. A plot of $\log(\tau_\infty - \tau)$ versus time was linear as predicted from Eq. (15).

In 1966 Freudenthal [20,21,31] treated the steady state analysis for the axial concentration gradient by introducing the quantity θ_F which is the degree of ionization of the impurity

$$\theta_F = \frac{n_a^+}{N_a} \tag{16}$$

where n_a^+ and N_a are the average ion-number density and the neutral atom-number density of the impurity. The degree of ionization was assumed independent of the axial position x.

Freudenthal equated the ionic flux to the diffusional flux similarly to Druyvesteyn and Schmeltekopf

$$\pi R^2 D \frac{dN_a}{dx} = n_a^+ \mu_a^+ E \pi R^2 \tag{17}$$

However, at this point he was able to substitute $n_a^+ = \theta_F N_a$ from Eq. (16) into Eq. (17). This is the critical point where the other investigators went astray. Druyvesteyn got involved in microscopic quantities β^* and S which are difficult, if not impossible, to measure. Schmeltekopf, essentially assumed that $\theta_F = 1$, which is incorrect because $\theta_F \sim 10^{-6}$.

Freudenthal's solution after integrating Eq. (17) was

$$n_a(x) = n_a^* A e^{-vx/D} \tag{18}$$

with

$$A = \frac{vLD}{1 - e^{-vL/D}}$$

where n_a^* is the original density of the impurity and $v = \mu_a^+ \theta_F E$. The length of the discharge tube is L.

Freudenthal's results in Eq. (13) were almost the same as Schmeltekopf's results in Eq. (7), except for the factor θ_F in the exponential term.

Freudenthal then examined the impurity density as a function of position x and time t. The basic equation is

$$\frac{\partial n_a(x,t)}{\partial t} = D \frac{\partial^2 n_a(x,t)}{\partial x^2} + v \left[\frac{\partial n_a(x,t)}{\partial x} \right] \qquad (19)$$

This is the ordinary diffusion equation with an added term to account for the transport of the ions in the electric field. There is a misprint in Freudenthal's paper [20] relative to this equation. The minus sign in front of $v[\frac{\partial n_a(x,t)}{\partial x}]$ should be a positive sign to be consistent with his solutions to the steady state case. However, this has been taken into account in his solution and does not affect the results.

Freudenthal solved Eq. (19) for a system without end-bulbs. He states that it is a rather complicated problem to determine the time-dependent cataphoresis theoretically for a system with end-bulbs.

Shair and Remer [22] presented a theoretical model for transient and steady-state cataphoresis starting with the macroscopic equations of continuity for a system including end-bulbs. Their general results reduce to Freudenthal's for the special case when the end-bulbs have zero volume,

$$\delta = \varepsilon = 0$$

and the level of ionization is low

$$\frac{n_+}{n_o + n_+} \simeq \frac{n_+}{n_o}$$

The basic assumptions in their model are that the level of ionization of the impurity, and the axial electric field remain constant. It was demonstrated that under these conditions a system involving rapid ionization-recombination reactions was equivalent to a system in which no reaction occurred, but in which the effective ion mobility was a product of the true ion mobility and the fraction of impurity ionization. The influence of end-bulbs which are commonly employed in experiments was analyzed and found to influence greatly the characteristic time required to reach steady state. Agreement was found between the model and available experimental data. Particular emphasis was placed upon mass spectrometer date reported by Matveeva [15] and Beckey, Groth, and Welge [4]. These data were for mixtures of rare gases and for mixtures of H_2-D_2. Both experiments involved end-bulbs. The ordinary diffusion case, associated with the collapse of the steady-state cataphoretic profile, was also analyzed for a system containing end-bulbs. The theoretical model proposed by Shair and Remer [22] is presented in Appendix B.

In their model, it is important to note that only electron-impact ionization processes were considered. Whereas the ionization process was taken to be homogeneous in character, the main loss of charged particles was considered to be through ambipolar diffusion to

the walls where recombination occurred; this has been the starting point in the development of other theories concerning the positive column [32,41] . In other words, the tube wall was assumed to be a sink for ions, that is, all ions diffusing to the wall were assumed to be lost. Moreover, the recombination was assumed to be rapid as compared to the characteristic times associated with the diffusion processes; therefore, the system was diffusion limited. These assumptions break down at high pressures [41].

Recently, Sosnowski [77] utilized the theoretical model proposed by Shair and Remer [22] to interpret cataphoresis in a He-Cd laser discharge tube. He obtained good agreement between the data and the model for the composition of Cd as a function of position in the discharge tube for a range of current of 6 ma to 60 ma.

III. EXPERIMENTAL EQUIPMENT AND PROCEDURE

Introduction

The basic experiment consists of producing a plasma by supplying DC power through electrodes into a glass discharge tube containing a binary gas mixture at a pressure of several torr. The purification of the gas mixture is investigated as a function of the initial mixture composition, the discharge current, and the gas pressure. The composition is measured by a thermal conductivity probe inserted in the anode end-bulb. The electric field is measured with a high-impedance voltmeter placed across two floating probes at a known distance of separation in the positive column of the glow discharge.

This chapter is divided into two sections. First a description of the experimental apparatus, and second a discussion of the experimental procedure.

A photograph of the experimental equipment is shown in Fig. 60.

Equipment

The description of the experimental apparatus will be divided into three parts: (1) the vacuum system, (2) the water system, and (3) the electrical system.

Vacuum system. The vacuum system is composed of the gas supply section, Fig. 2, and the discharge chamber plus detector, Fig. 3. The pressure is reduced to about one micron with a Welch Duo-Seal Vacuum Pump, Model 1400B, with a free air displacement of 21 ℓ/min. The pressure is reduced to less than 0.01 microns with a Consolidated

Vacuum Corporation (CVC) Diffusion Pump, Model PMCS-2C. A baffle is located between the mixing chamber and the diffusion pump to reduce contamination of the system from the diffusion pump fluid vapors. This baffle is similar to the Chevron ring-baffle described in CVC Bulletin 10-1. A CVC Vacuum-Gate Valve, Model VSTM2, is used to isolate the baffle and pumps from the mixing chamber.

The gases used in this experiment are stored in high-pressure cylinders up to 2,000 psig. Single-stage Matheson Regulators, Models 1L580 and 3300, are used for regulating the delivery pressure at about 15 psig.

The He, Ar, N_2, O_2 and Ne are supplied by Linde. The He and Ar are standard grade, the N_2 is high-purity dry grade, the O_2 is commercial grade, and the Ne is research grade. The CO and CO_2 are supplied by Matheson. The CO is C.P. grade and the CO_2 is commercial grade.

High-vacuum stopcocks of borosilicate glass, supplied by Eck and Krebs, are used throughout the vacuum system. Universal type stopcock adapters are used to reduce the possibility of stopcock leakage.

Pressures are measured by using a Universal McLeod Gage manufactured by Todd Scientific Company. Pressures between 0.1 micron and 25 mm Hg can be measured. There are three scales with ranges of 5-25 mm Hg, 0.5 - 5 mm Hg, and 0.0001 - 0.5 mm Hg. An Eck and Krebs McLeod Gage, Model 2184, is used for measuring pressures down to 0.01 microns. Mixtures are prepared by using an absolute pressure manometer and a Welch Cathetometer, Model 0068A. After preparing the mixtures they are stored in bulbs connected to the mixing chamber.

The water-cooled discharge chamber and detector are shown in Fig. 3. The water-jacketed discharge tube is 1 cm in outside diameter and 70 cm long. The cathode end-bulb which also has a water jacket is connected to the end of the discharge tube. The volume of this bulb is 312 cc. Inserted into the cathode end-bulb is an electrode which is connected by soft-solder to a one-inch kovar glass-to-metal seal. The 1/2-inch diameter cathode is composed of a solid molybdenum tip threaded into a hollow copper tube which is cooled with water. Stainless-steel tubes, 1/8-inch diameter, are used to supply cooling water to the cathode. Initially, a solid cathode without water-cooling was used; however, expansion and contraction caused by repeated heating and cooling of the electrode produced cracking of the pyrex glass at the end of the discharge tube and fracturing of the kovar seal. Molybdenum was selected for the electrode tip because it sputters less than other common electrode materials and, therefore, reduces the tendency of glass fracture near the cathode.

On the other end of the discharge tube is the anode which is 3 cm long. The anode is a porous molybdenum screen rolled and packed tightly inside a 3/8-inch kovar glass-to-metal seal that is grounded. Behind the anode is the detector which is a commercial General Electric 60-watt, 120-volt light bulb immersed in a constant-temperature water bath. The volume of the bulb is 133 cc.

Water system. Water is utilized for two purposes in this experiment. First, water is used as a coolant in four locations: (1) the diffusion pump, (2) the Tamson circulation thermostat, (3) the discharge chamber, and (4) the cathode. Second, water is used to

maintain a constant-temperature bath for the thermal conductivity detector. A flow diagram for the water system is illustrated in Fig. 4.

The use of water as a cooling medium will be discussed first. When the diffusion pump is operating, a nominal cooling-water rate of 1/5-gallon per minute is required to prevent damage to the diffusion pump oil. This water is supplied through line #9 (line numbers are shown in Fig. 4) at about 20°C and exits through line #10 at about 45-55°C. Line #11 supplies water to the boiler quench coil which is provided in case rapid shut-down of the pump is required.

The Tamson circulation thermostat requires cooling water which enters via line #5 and exits via line #6 at the rate of approximately 0.1 gallon per minute. This cooling water is necessary when the thermostat controls the water temperature at several degrees above ambient because the heat generated by friction at the Tamson circulation pump must be removed due to the efficient insulation of the thermostat bath. Otherwise, the temperature would rise above the designated set point of 30°C.

The discharge tube and cathode chamber are cooled by water entering the discharge tube via line #7 and flowing through the jacket surrounding the tube and chamber; refer to Figs. 3 and 4. This cooling water exits by line #8 at about the rate of one gallon per minute.

The hollow cathode is water cooled by distilled water which is gravity fed from the water reservoir via line #2; refer to Figs. 3 and 4. This water is returned to the reservoir by line #1 using a Cole-Parmar Oscillating Type Pump, Model 7103-1. Thermal expansion of the

cathode which resulted in fracturing of the kovar seal was eliminated by water-cooling the cathode.

In addition to the use of water as a coolant, it is also used for maintaining a constant-temperature bath. The Tamson Circulation-Thermostat, Model TZ3, is utilized to control the water temperature to within $\pm$ 0.02°C in the constant-temperature bath surrounding the thermal conductivity detector. The temperature of the bath is monitored with a Braun thermometer (A.S.T.M. 56C) which has a range of 19-35°C with subdivisions of 0.01°C. Water exits from the Tamson thermostat and enters the constant-temperature bath via line #4. Line #3 serves as the water return line to the Tamson thermostat. Water is circulated through lines #3 and #4 by a combination force and suction pump. Use of a magnetic stirrer, Precision Scientific Company, Model 65904, improved the water temperature control in the bath.

Electrical systems. There are three distinct electrical systems used in this experiment. They are (1) the power-supply circuit for the electrical discharge, (2) the detector circuit for monitoring the thermal conductivity, and (3) the electrical circuit for measuring the electric field.

The power to initiate and sustain the glow discharge is supplied by a CVC High-Voltage Power Supply, Model No. LC-031. It is a variable voltage (0 to 5,000 volts) full-wave rectified, high reactance, DC power supply with an output current rating of 300 ma for continuous service. The power-supply output is filtered with a π-section filter. The ripple factor [44] for the filter is 3×10^{-4}

which corresponds to a ripple voltage of about 1.5 volts for a 5,000 volt input to the filter. A ballast resistance of 7,500 ohms is placed in series with the discharge tube to stabilize the discharge [11,16]. The voltage across the discharge tube is measured with a Triolab Vacuum-Tube Voltmeter, Model No. 106-1, connected across a voltage divider with a divider ratio of 200:1. This voltage-divider ratio was determined with a Keithley Model 601 Electrometer to within $\pm$ 2%. The current through the discharge tube is measured with a Simpson DC Milliammeter, Model No. 1150-1 (0-100 ma and 0-500 ma), with an accuracy of $\pm$ 1% of full scale. A Hewlett Packard, Model 122A Dual-Beam Oscilloscope is connected across a one-ohm resistor in series with the discharge tube to monitor any AC interference. The electrical circuit for the apparatus used to furnish power for the glow discharge is shown in Fig. 5.

The composition in the anode end-bulb is determined by monitoring the thermal conductivity of the mixture. The detector probe is a filament in a commercial G.E. 60-watt, 120-volt light bulb. This coiled-coil filament is made from 0.0046 cm diameter tungsten wire which is initially 53 cm long. After the first coiling, the filament length is reduced to 8.6 cm and the diameter is increased to 0.018 cm. This coil which consists of approximately 1200 turns is coiled again, making the filament 1.6 cm long. The filament is represented by R-5 in the detector circuit shown in Fig. 6. The power for this circuit is supplied by a Dressen-Barnes, Model 20-5, five-volt regulated power supply.

The resistance changes in the filament are monitored by measuring the voltage drop across R-4; refer to Fig. 6. This voltage drop is amplified by a Leeds and Northrup Stabilized DC Microvolt Amplifier, Model 9835-B. The output from the amplifier is monitored continuously on a Leeds and Northrup Speedomax W/L Millivolt Recorder. When calibration runs are initiated, the potential drop across R-4 is set to approximately zero by adjusting two Spectral Potentiometers, Model 860, which are designated by R-6 and R-7 in Fig. 6.

There are five major components needed to measure the electric field. These components are (1) the electric field probes, (2) the voltage divider probe, (3) the electrometer, (4) the isolation amplifier, and (5) the recorder.

Two sets of electric field probes are sealed with pyrex glass into the discharge tube; see Fig. 3. These probes are located so that they are in the positive column of the glow discharge. Each set of probes consists of two probes spaced 21 mm apart. The tungsten probes are 1/2 mm in diameter and about 45 mm long. The probes are coated with Pyrex glass over a length of about 34 mm. The outside diameter of these coated probes is about 1.5 mm. Both ends of the probes are left uncoated. The tip of the probe in the discharge tube is left uncoated over a length of 2 mm. A silver-solder ball is attached to the other end of the probe to facilitate the connection of an electrical lead. To insure a good vacuum seal at the Pyrex-tungsten interface, the outside of the seal is coated with glyptal paint. For each set of electric field probes, one of the two probes is floating at a higher potential. This probe is referred to as the

high-voltage probe and the other probe in the set is called the low-voltage probe.

The low-voltage probe is connected to the input of a Keithley, Model 5103A, 1000:1 voltage-divider probe with input resistance of 10^{12} ohms and an accuracy of ± 5%; refer to Fig. 7. The purpose of this probe is to drop the potential to within a range that can be monitored with the electrometer. The output of the voltage-divider probe is connected to a Keithley Model 6012 triaxial-to-coaxial adapter.

This adapter is connected to the input of a Keithley Model 601 electrometer with voltmeter accuracy of ±1% of full scale. The high-voltage probe is connected to the low-input terminal on the electrometer. The current output from the electrometer is accurate to ±5% with recorders that have an input impedance of 1.4 KΩ .

A voltage divider converts the full-scale output from the electrometer to full-scale input for the isolation amplifier. The output from the electrometer is connected to the input of a Fluke, Model A88, isolation amplifier with gain accuracy of ±2% . This amplifier is used to provide, first, high isolation of the input from ground, and second, high isolation of the input from the output. The isolation amplifier relieves the necessity of using a recorder having a high leakage resistance and high input resistance. The voltage divider located between the electrometer and amplifier converts the full-scale output from the electrometer to full-scale input for the isolation amplifier. The output from the isolation amplifier is monitored on a Leeds and Northrup Speedomax W/L millivolt recorder with an

accuracy of $\pm$0.25% of full scale. The voltage divider between the amplifier and the recorder converts the full-scale output from the isolation amplifier to a full-scale input to the recorder. A switch is used so that the electric field can be monitored at either set of probes during a cataphoretic test.

Procedure

The experimental procedure for the preparation of gas mixtures and for the calibration of the detector is described in this section.

The gases are mixed in a glass cylinder that is approximately 2 inches in diameter and 19 inches long; refer to Fig. 2. The system is evacuated to less than 0.01 micron and then flushed out with helium several times. The CVC vacuum-gate valve is closed and helium is added to a pressure P_1 . The pressure is measured by using a mercury absolute-pressure manometer and a cathetometer with subdivisions of 0.005 mm Hg. The second gas is added and the total pressure P_2 is recorded. Assuming ideal gas behavior, the percentage of the components in the binary mixture is then calculated. The time required for mixing is determined from the results in Cook [45]. The mixture is then stored in a 3-liter flask connected to the mixing cylinder.

The detector that is used to monitor the composition of the gas mixture at the anode during cataphoresis is calibrated by the following technique. For one composition of the gas mixture, the voltage drop across the resistor R-4 (refer to Fig. 6) is measured as a function of the gas pressure at constant temperature. The temperature is maintained to within $\pm 0.02^{\circ}C$ by immersing the detector in a water bath.

This procedure is replicated for different compositions of a specified binary gas mixture. As an example, results for the voltage drop as a function of pressure with composition as a parameter is shown in Fig. 8 for He-CO. From these results, cross-plots are made of the composition as a function of the voltage drop with pressure as a parameter. This calibration curve is shown in Fig. 9 for He-CO. A known mixture of helium and argon obtained from Matheson was used to check the mixture preparation and calibration procedure. The calibration curves were checked after six months, and the results were reproducible; refer to Fig. 8.

During a cataphoretic purification test, the voltage drop across resistor R-4 is measured as a function of time. The voltage drop is usually in the range of 0 to 200 microvolts. This signal is amplified and recorded continuously. Since the pressure is known, the composition as a function of time is obtained from the composition-calibration curves. This technique has been described previously by Remer and Shair [23]; refer to Appendix C.

IV. EXPERIMENTAL RESULTS

Introduction

The experimental program was designed to measure cataphoresis in binary mixtures of helium with atomic and molecular gases. The gas mixtures investigated were He-Ar, He-Ne, He-N_2, He-O_2, He-CO, and He-CO_2. Helium is the majority component and the other gas is the impurity. The independent variables in the experiment were the discharge current, the initial composition of the gas mixture, and the total pressure of the gas mixture. The three measured dependent variables were the composition in the anode end-bulb, the axial electric field in the positive column of the glow discharge, and the time for cataphoresis. The composition and the electric field were measured continuously, commencing after the discharge was initiated and terminating when the discharge was extinguished. Three important quantities could be calculated from the model of cataphoresis with the data from the experimental measurements. These calculated quantities were (1) the electrostatic Peclet number, (2) the fraction of impurity ionization, and (3) the characteristic time for the separation.

For all the experimental tests, the initial composition of the impurity gas was less than 7.5 mole %. The discharge currents were between 5 milliamperes and 100 milliamperes. At currents less than 5 ma, the discharge could not be sustained, and for currents greater than 100 ma, the glass seals would fracture. The range of the gas pressure was between 2 mm Hg and 9 mm Hg. At higher pressures the breakdown potential of the gas mixture could not always be attained

with the power supply. The time for the separation was usually several minutes.

All compositions are stated in mole %. Whenever a pressure is reported, it is always the total gas pressure. The current density in ma/cm^2 can be calculated from the measured current by dividing by the cross-sectional area of the discharge tube which is 0.502 cm^2.

This chapter is divided into two parts. First, there is a discussion of the treatment of the composition and electric field data, followed by the calculation procedure for both the electrostatic Peclet number and the ionization fraction of the impurity. Second, there is a presentation and discussion of the results for the impurity composition at the anode, the axial electric field, the electrostatic Peclet number, and the ionization fraction of the impurity as a function of the pressure, current, and initial composition of the mixture. There is also a discussion of the ionization mechanisms. The characteristic time for cataphoresis is discussed in Chapter V.

Treatment of the Data and the Calculation Procedure

In this section the treatment of the composition and electric field data, and the calculation procedure for both the electrostatic Peclet number and the fraction of impurity ionization are discussed.

Composition data. The quantity $\theta(\eta,\tau)$ is the ratio of the impurity composition for an axial position η at a time τ, divided by the initial impurity composition. This relationship is valid when the fraction of impurity ionization is small; refer to Appendix B. The value of η varies from zero at the cathode to one at the anode.

The composition of the impurity gas is continuously measured in the anode end-bulb ($\eta = 1$) during cataphoresis. When this measured result is divided by the initial composition of the impurity gas, the value of $\theta(1,\tau)$ is obtained. Initially at $\tau = 0$ the impurity is uniformly dispersed throughout the system before electrical breakdown, and $\theta(\eta,0) = 1$. After breakdown, the impurity is driven toward the cathode as cataphoresis proceeds and $\theta(1,\tau)$ decreases from 1.0 to the steady state value $\theta(1,\infty)$. Therefore, one measurement of the effectiveness of the separation is the value of $\theta(1,\infty)$. The smaller the value of $\theta(1,\infty)$, the better the separation. A complete separation of the impurity from helium would result in a value of $\theta(1,\infty) = 0$. The actual measurement of $\theta(1,\tau)$ and the calibration procedure have been discussed in Chapter III.

Electric field. The axial electric field was measured by the floating probe technique [70 to 72]. The electric field E is the voltage difference between two points divided by the distance d between the two points.

$$E = \frac{V_2 - V_1}{d} \tag{20}$$

The value of d was 21 mm for all the experimental measurements reported herein. The field was measured near both ends of the positive column. The position of the probes was 7 cm and 9.1 cm from each end of the tube. The electric field near the anode end of the positive column was designated by E_a; similarly, the electric field near the cathode end was designated by E_c. During the cataphoretic separation, the values of E_a and E_c varied because of the changing composition.

The highest and lowest values of the field at the anode end of the positive column were represented by E_a^h and E_a^ℓ, and similarly near the cathode end of the positive column, E_c^h and E_c^ℓ. The average values of E_a and E_c during cataphoresis were taken as

$$\overline{E}_a = \frac{E_a^\ell + E_a^h}{2} \qquad \text{and} \qquad \overline{E}_c = \frac{E_c^\ell + E_c^h}{2}$$

The value of E reported in the experimental results section of this chapter was the average of these two values, namely,

$$E = \frac{\overline{E}_a + \overline{E}_c}{2} \tag{21}$$

For example, with the 4.8% N_2 mixture at 25 ma and 6.0 mm Hg, the values of E_a^ℓ, E_a^h, E_c^ℓ, E_c^h, $\overline{E}_a$, $\overline{E}_c$, and E are summarized below in volts/cm.

$E_a^\ell = 29.3$, $E_a^h = 32.8$ $\rightarrow$ $\overline{E}_a = 31.1$

$E_c^\ell = 32.6$, $E_c^h = 36.9$ $\rightarrow$ $\overline{E}_c = 34.75$

$\overline{E}_a = 31.1$, $\overline{E}_c = 34.75$ $\rightarrow$ $E = 32.9$

The maximum variation of E in the experiments reported herein was 35% in time and 30% in position.

The calculational procedure for the electrostatic Peclet number and the fraction of impurity ionization will now be discussed.

Electrostatic Peclet number. The electrostatic Peclet number α was calculated from the following implicit equation for α, using experimental results for $\theta(1,\infty)$.

$$\theta(1,\infty) = K e^{-\alpha} \tag{22}$$

where

$$K = \frac{1 + \delta + \varepsilon}{\delta + \varepsilon e^{-\alpha} - \frac{e^{-\alpha}}{2} + \frac{1}{\alpha}} \tag{23}$$

These equations were derived by Shair and Remer [22]; refer to Eqs. (13) and (18) in Appendix B. The quantity δ is the ratio of the volume of the bulb surrounding the cathode to the volume of the discharge tube. Similarly, ε is the ratio of the volume of the bulb surrounding the anode to the volume of the discharge tube. In the experimental system the value of ε was 4.2 and δ was 8.9. The results for α as a function of $\theta(1,\infty)$ are summarized in Fig. 10 and Table E-1.

Ion Fraction. The fraction of impurity atoms ionized is $n_+/(n_o + n_+)$ where n_+ and n_o are the density of impurity ions and neutrals, respectively. When the degree of ionization is low, then $n_+ << n_o$, and $n_+/(n_o + n_+) \sim n_+/n_o$. The electrostatic Peclet number α is given by

$$\alpha = \left(\frac{n_+}{n_o + n_+}\right)\beta \sim \left(\frac{n_+}{n_o}\right)\beta \tag{24}$$

where $\beta = \mu EL/D$. The product of the ionic mobility μ and the electric field E is the drift velocity of the ion through a distance L . From a qualitative viewpoint, the numerator μEL represents the magnitude of the forced diffusion of the ions in one direction because of the electric field, and the diffusion coefficient D in the denominator represents the diffusion of the neutrals in the opposite direction because of the concentration gradient. Hence a low value of β means that forced diffusion is small in comparison to ordinary diffusion. The purification by cataphoresis becomes more effective as the value of β increases.

The fraction of impurity ionization was calculated by rearranging Eq. (24).

$$\frac{n_+}{n_o} = \frac{D\alpha}{\mu EL} \tag{25}$$

The quantity D is the binary diffusion coefficient of the gas mixture He-X, where X is one of the following gases: Ar, Ne, N_2, O_2, CO, or CO_2. The values of D for He-N_2 and He-O_2 were experimental results reported by Seager, Geerstrom, and Giddings [48]. The diffusion coefficients for He-Ar and He-Ne were experimental results reported by Srivastava [39,40] that were corrected for temperature by the method suggested in Cobine [11]. The experimental results for He-Ar, He-Ne, He-N_2, He-O_2, and He-CO_2 agreed to within 7% of those calculated from theory using the technique described by Hirschfelder, Curtiss, and Bird [37]. The diffusion coefficient for He-CO was calculated from theory [37]. The diffusivities were assumed to be inversely proportional to pressure and independent of composition [46]. The values used for D in

cm^2/sec are summarized below for 760 mm Hg and 298^oK.

Gas Mixture	D (cm^2/sec)	Reference
He-Ar	0.729	[38]
He-Ne	1.05	[40]
He-N_2	0.687	[48]
He-O_2	0.729	[48]
He-CO	0.721	[37]
He-CO_2	0.612	[48]

The quantity μ is the ionic mobility of the impurity ion diffusing through He. For example, in a He-Ar mixture, the value of μ is for Ar^+ diffusing through He. The values used for the mobilities of Ar^+ in He, Ne^+ in He, and O_2^+ in He were taken from experimental results reported in the literature [26,33,49]. The mobility for N_2^+ in He was assumed equal to the value for O_2^+ in He. The mobility of CO^+ in He was calculated with Blanc's law [53] using the data for CO^+ in CO from Varney [61] and CO^+ in He extrapolated from McDaniel [62]. The mobilities were assumed to be inversely proportional to pressure and independent of composition [12]. The value of the mobility is positive for positive ions and negative for negative ions. The values used for μ in $cm^2/volt/sec$ are summarized below for 760 mm Hg and 298^oK.

Gas Mixture	$(cm^2/volt/sec)$	Reference
He-Ar	22.4	[33]
He-Ne	16.2	[26]
$He-N_2$	11.8	[49]
$He-O_2$	11.8	[49]
He-CO	22.0	[53,61,62]

The length of the discharge tube was 70 cm. This is the value of L in Eq. (25).

Discussion of the Results

He-Ar. Cataphoresis in a He-Ar mixture was investigated as a function of the discharge current and the total gas pressure. The initial composition of the gas mixture was 4.7% Ar. The current range was 25 ma to 75 ma and the pressure range was 3.2 mm Hg to 8.9 mm Hg.

The effect of current and pressure on the steady-state composition at the anode $\theta(1,\infty)$ is shown in Figs. 12 and 17. The purification of Ar from He was found to be enhanced with increasing current and increasing pressure. However, the current had a much stronger influence on the purification than the pressure; refer to Figs. 12 and 17. For example, increasing the current from 25 ma to 100 ma at 3.2 mm Hg changed the separation factor $\theta(1,\infty)$ from 0.915 to 0.245, whereas increasing the pressure from 3.2 mm Hg to 8.9 mm Hg at 25 ma only changed the separation factor $\theta(1,\infty)$ from 0.915 to 0.790. The pressure and current dependence of cataphoresis in the He-Ar mixtures was in agreement with previously reported results [9,15].

The influence of current and pressure on the calculated electrostatic Peclet number α is shown in Figs. 34 and 39. Unless otherwise stated, the lines through the points represent the best fit of the data. The value of α was found to increase with increasing current. This result is in agreement with the theory [22]. The value of α was found to increase linearly with increasing pressure. The pressure dependence of α is a function of the ionization mechanism which will be discussed later. The magnitude of the electrostatic Peclet number varied from α equal to 0.13 (at 25 ma and 3.2 mm Hg) to α equal to 3.92 (at 100 ma and 8.9 mm Hg).

The effect of current and pressure on the electric field E is illustrated in Figs. 25 and 31. The electric field was found to increase with increasing pressure and to decrease with increasing current. The electric field was a linear function of pressure. The values of E were between 8.5 volts/cm and 20.0 volts/cm. The lowest value of E , 8.5 volts/cm, occurred at the lowest pressure, 3.2 mm Hg, and the highest current, 100 ma. The highest value of E , 20.0 volts/cm, occurred at the highest pressure, 8.9 mm Hg, and the lowest current, 25 ma.

The influence of current and pressure on the ion fraction n_+/n_o is shown in Figs. 43, 48 and 49. The ion fraction increased with pressure and with current. However, the value of n_+/n_o was a much stronger function of current than pressure; refer to Figs. 43 and 48. The value of n_+/n_o increased by about 30% for a range of pressure of 3.2 mm Hg to 8.9 mm Hg. However, the value of n_+/n_o increased by a factor of 20 for a range of current of 25 ma to 100 ma. The values

for n_+/n_o were in the range of 5×10^{-6} to 133×10^{-6}. The value of n_+/n_o equal to 5×10^{-6} corresponded to the lowest current, 25 ma, and the lowest pressure, 3.2 mm Hg (also 5.5 mm Hg). The highest value of n_+/n_o equal to 133×10^{-6} corresponded to the highest current of 100 ma and the highest pressure of 8.9 mm Hg. A summary of the results for cataphoresis in He-Ar mixtures is presented in Table E-2.

The ionization mechanism in a He-Ar mixture during cataphoresis may proceed by three paths. The first path is electron impact of Ar neutrals to form Ar^+.

$$e^- + Ar \rightarrow Ar^+ + 2e^- \qquad (26)$$

The second path is the formation of Ar_2^+ by the Hornbeck-Molnar process [57]. This process involves formation of an excited atom Ar^* via the following reaction:

$$e^- + Ar \rightarrow Ar^* + e^-$$

This step is possible because the energy of the excited atom Ar^* is between 11.5 eV and 11.7 eV which is lower than the ionization potential of Ar, 15.76 eV from Reed [56]. The second step is ionization of Ar by the following reaction:

$$Ar^* + Ar \rightarrow Ar_2^+ + e^-$$

The third path is the formation of Ar_2^+ by a three-body impact process [53].

$$Ar^+ + 2Ar \rightarrow Ar_2^+ + Ar$$

This reaction can occur because the Ar^+ has an appearance potential of 15.76 eV which is larger than the appearance potential for Ar_2^+ of 15.06 eV [18,26]. This process is pressure dependent and is favored by high pressure and high percentage of Ar. This may explain why the results for n_+/n_o increased with increasing pressure.

The ratio of rate constants for the formation of atomic ions Ar^+ to molecular ions Ar_2^+ is about 18, based on the results reported by Dahler, Franklin, Munson and Field [58]. Therefore, most ions are formed by electron impact, Eq. (26). This is in agreement with the experimental results that n_+/n_o increased only slightly with increasing pressure.

He-Ne. Cataphoresis in He-Ne mixtures was examined as a function of current, pressure and initial percentage of Ne. Two sets of experiments were performed. The first set of experimental data was taken at a constant pressure to investigate the effect of current and initial composition on cataphoresis. The second set of data was taken at a constant initial composition and a constant current to examine the effect of pressure on cataphoresis.

In the first set of data, the total pressure was held constant at 6.0 mm Hg. The initial compositions were 2.4% Ne and 4.8% Ne. The current range was 25 ma to 75 ma for the 2.4% Ne mixture and 25 ma to 100 ma for the 4.8% Ne mixture.

The second set of data was taken for an initial composition of 2.4% Ne at a current of 50 ma. The pressure range was between 3.5 mm Hg and 9.1 mm Hg.

The influence of current, initial percentage of Ne, and pressure on the steady-state composition near the anode $\theta(1,\infty)$ is shown in Figs. 13 and 18. The purification of Ne from He by cataphoresis was found to be enhanced with increasing current or with increasing pressure, or with decreasing initial percentage of Ne. The separation factor at the anode $\theta(1,\infty)$ varied from 0.900 at 25 ma and 6.0 mm Hg for a mixture with initial composition of 4.8% Ne to 0.251 at 75 ma and 6.0 mm Hg for a mixture with initial composition of 2.4% Ne. The pressure, current, and initial composition dependence of cataphoresis in He-Ne mixtures was in agreement with previously reported results [9,15,16].

The effect of current, pressure, and initial percentage of Ne on the electrostatic Peclet number α is shown in Figs. 35 and 40. For a given initial percentage of Ne, the value of α was found to increase with increasing current. Currents greater than 100 ma were not investigated because fracture of the glass-to-kovar seals resulted near the cathode. For a given current, the electrostatic Peclet number decreased as the initial percentage of Ne increased. The value for α increased with increasing pressure. For example, at a current of 50 ma with an initial composition of 2.4% Ne, the electrostatic Peclet number increased from 0.62 at 3.5 mm Hg. to 1.10 at 9.1 mm Hg. The values of α for the He-Ne tests were in the range of 0.22 to 1.72. The low value of α equal to 0.22 occurred at a discharge current of 25 ma and a pressure of 6.0 mm Hg for the mixture with an initial composition of 2.4% Ne. The upper value of α equal to 1.72

occurred at 75 ma and 6.0 mm Hg for the 2.4% Ne mixture.

The influence of current, pressure, and initial composition on the electric field E is shown in Figs. 26 and 32. The value of E varied only slightly over the entire range of currents investigated. The electric field was relatively independent of pressure. The values of E were between 11.1 volts/cm and 12.6 volts/cm. In comparison with the other mixtures studied, the variation of electric field in He-Ne mixtures was very small. Very recently, Gaur and Chanin [68] reported electric field measurements in He-Ne at pressures generally higher than those investigated herein. However, they reported a value of 11.0 volts/cm at 7 mm Hg and 10 ma. This is in agreement with the value reported herein of 11.9 volts/cm at 6.0 mm Hg and 25 ma.

The influence of current, pressure, and initial composition on the ion fraction n_+/n_o is shown in Figs. 44 and 49. The ion fraction increased with increasing current and decreased with increasing initial percentage of Ne. The value of n_+/n_o also increased with increasing pressure. For example, at a current of 50 ma and an initial composition of 2.4% Ne, the ion fraction increased from 48.3×10^{-6} at 3.5 mm Hg to 82.3×10^{-6} at 9.1 mm Hg. At high pressures, the value of n_+/n_o appeared to be reaching a limiting value. Higher pressures were not investigated because the breakdown voltage could not be reached with the power supply. The values of n_+/n_o for the He-Ne data are in the range of 11.0×10^{-6} to 139×10^{-6}. The lowest value of n_+/n_o equal to 11.0×10^{-6} occurred at 25 ma and 6.0 mm Hg for the mixture with an initial composition of 4.8% Ne. The highest value of n_+/n_o equal to 139×10^{-6} occurred at 75 ma and

6.0 mm Hg for the 2.4% Ne mixture. The results for cataphoresis in He-Ne mixtures are summarized in Table E-3.

The experimental results for He-Ne mixtures were consistent with the model for cataphoresis [22]. The value of $\theta(1,\infty)$ decreased with increasing current because of the increase in α caused by the increase in the ion-production rate. The pressure dependence of cataphoresis is again believed to be a function of ionization mechanism as in He-Ar mixtures.

The ionization mechanism in a He-Ne mixture during cataphoresis is primarily direct electron impact of neutral Ne atoms when the percentage of Ne > 0.1% [31].

$$e^- + Ne \rightarrow Ne^+ + 2e^-$$

The production of Ne^+ ions by electron impact increases as the percentage of Ne increases [31].

The formation of Ne^+ ions by the Penning reaction [53,54] via the helium metastable atoms, He^*, is energetically impossible because the energy of He^* is between 19.81 eV and 20.96 eV [55] and the ionization potential for Ne taken from Reed [56] is 21.56 eV.

$$He^* + Ne \rightarrow Ne^+ + He + e^-$$

At low percentages of Ne (< 0.1% Ne), the following charge exchange reaction may occur [55]

$$He_2^+ + Ne \rightarrow Ne^+ + 2\ He$$

because the energy of the He_2^+ molecular ion, 23.2 eV [36], is larger

than the ionization energy of Ne, 21.56 eV [56]. At high pressures of approximately 5 mm Hg, the molecular ion is probably formed by a three-body impact process [31,36].

$$He^+ + 2He \rightarrow He_2^+ + He$$

At low pressures, the molecular ion He_2^+ is most likely formed by the following steps [31,36]:

$$e^- + He \rightarrow He^* + e^-$$

$$He^* + He \rightarrow He_2^+ + e^-$$

Gaur and Chanin [68] in a recent publication performed an ionic analysis of cataphoresis in He-Ne mixtures. They observed He_2^+, Ne^+, Ne_2^+, and $HeNe^+$ ions. Their work was limited to mixtures with 0.05% Ne or less. The complex ion $HeNe^+$ was postulated to occur via a three-body collision.

In conclusion, for the cataphoretic experiments reported herein, the ionization of Ne by direct electron impact will predominate because of the high initial percentage of Ne which was 2.4% Ne to 4.8% Ne.

A three-minute, 16 mm film was taken to illustrate the change in color produced by the formation of the axial concentration gradient during cataphoresis in a He-Ne mixture. The best pictures were obtained using Kodak Ektachrome EF Film, type 7242 at 16 frames per second with a f/5.6 setting. Overexposed films were obtained using f/2 - f/2.8 and f/4 settings.

He-N_2. Cataphoresis in He-N_2 mixtures was investigated as a function of discharge current, initial composition, and total pressure. The first set of experimental data was taken at a constant pressure to examine the effect of current and initial composition on cataphoresis. The second set of data was taken at a constant initial composition and a constant current to examine the effect of pressure on cataphoresis.

In the first set of data the total pressure was held constant at 6.3 mm Hg. The initial compositions were 1.2% N_2, 2.2% N_2, and 4.8% N_2 . The current levels were 5 ma to 20 ma for the 1.2% N_2 mixture, 7.5 ma to 50 ma for the 2.2% N_2 mixture, and 15 ma to 75 ma for the 4.8% N_2 mixture.

The second set of data was taken for an initial composition of 4.8% N_2 at a current level of 50 ma. The pressure range investigated was 2.2 mm Hg to 8.8 mm Hg.

The effect of current, initial composition, and pressure on the steady-state composition near the anode $\theta(1,\infty)$ is shown in Figs. 14, 19 and 22. The purification of N_2 from He by cataphoresis was found to increase with increasing current or with increasing pressure, or with decreasing the initial percentage of N_2 .

The influence of discharge current on the separation was very significant; refer to Fig. 14. For example, the value of $\theta(1,\infty)$ decreased from 0.864 at 15 ma to 0.021 at 75 ma in the mixture with initial composition of 4.8% N_2 and a pressure of 6.3 mm Hg. The value of $\theta(1,\infty)$ equal to 0.021 represents 0.1% N_2 in He which is almost a

fifty-fold reduction in the percentage of N_2 near the anode as compared with the initial composition of 4.8% N_2 in He.

The effect of pressure on the separation is shown in Fig. 19. The separation was improved by increasing the pressure up to about 4 mm Hg. At higher pressures the separation became almost independent of pressure.

The influence of initial composition on the separation is presented in Fig. 22 which is a cross-plot of the data in Fig. 14. The separation decreased significantly as the initial percentage of N_2 increased. For example, at 15 ma and 6.3 mm Hg, the value of $\theta(1,\infty)$ increased from 0.100 at 1.2% N_2 to 0.864 at 4.8% N_2.

The effect of current, pressure, and initial percentage of N_2 on the electrostatic Peclet number α is illustrated in Figs. 36 and 40. The value of α increased with increasing current. For low currents the value of α increased linearly with current. At high currents the increase in α became nonlinear. This effect was probably caused by the large increase in the ion fraction at high currents. For a given current, α decreased as the initial percentage of N_2 increased; refer to Fig. 36. The value of α increased with increasing pressure by a factor of 2 in the pressure range of about 2 to 9 mm Hg at a current of 50 ma; refer to Fig. 40. The influence of pressure on α was significant at low pressures and became less important at pressures greater than about 4 mm Hg. The values of α varied from 0.21 to 4.33. The low value of 0.21 occurred at a current of 15 ma and a pressure of 6.3 mm Hg for an initial composition of 4.8% N_2. The upper value of 4.33 occurred with a pressure of 6.3 mm Hg at 75 ma for

the 4.8% N_2 mixture, 50 ma for the 2.2% N_2 mixture, and 20 ma for the 1.2% N_2 mixture.

The effect of current on the electric field is shown in Fig. 27 for several initial compositions. For example, the electric field decreased about 20% in the range of currents investigated for the 2.2% N_2 and 4.8% N_2 mixtures. The electric field was an increasing linear function of pressure; refer to Fig. 32. For example, the electric field increased from 15.8 volts/cm at 2.2 mm Hg to 36.4 volts/cm at 8.8 mm Hg for the mixture with initial composition of 4.8% N_2 at 50 ma.

The calculated ion fraction n_+/n_o as a function of current, pressure, and initial composition is shown in Figs. 45 and 49. The value of n_+/n_o increased with current. At low currents n_+/n_o was approximately proportional to current; at high currents n_+/n_o increased in a nonlinear manner with current. The pressure dependence of n_+/n_o is shown in Fig. 49. The ion fraction increased with pressure in the range of about 2 mm Hg to 4 mm Hg. The value of n_+/n_o appeared to go through a maximum near 4 mm Hg, and the value of n_+/n_o decreased with further increases in pressure. The influence of pressure on the ion fraction was smaller than the effect of current. For example, the value of n_+/n_o was between 50.0×10^{-6} and 77.2×10^{-6} for the range of pressures of 2.2 mm Hg to 8.8 mm Hg with the 4.8% N_2 mixture at 50 ma. In comparison, the value of n_+/n_o increased from 5.2×10^{-6} at 15 ma to 131×10^{-6} at 75 ma for the 4.8% N_2 mixture. The values of the calculated ion fraction were between 5.2×10^{-6} and 167.5×10^{-6}. The low value of 5.2×10^{-6} occurred at a current of 15 ma and a pressure of 6.3 mm Hg with an initial composition of

4.8% N_2 . The upper value for n_+/n_o of 167.5 occurred at 50 ma and 6.3 mm Hg with the 2.2% N_2 mixture. A summary of the results for cataphoresis in He-N_2 mixtures is presented in Table E-4.

The ionization mechanisms in a He-N_2 mixture during cataphoresis will now be considered. Electron impact of N_2 which has an ionization potential of 15.57 volts may produce N_2^+ [11].

$$e^- + N_2 \rightarrow N_2^+ + 2e^- \qquad (27)$$

The dissociation of N_2 to $N^+ + N$ has a very high ionization potential of 24.5 volts [11]. The cross section for dissociative ionization is very small and, therefore, this reaction was improbable [36,59]. Dissociation of N_2 by electron impact requires only 9.6 volts [53].

$$e^- + N_2 \rightarrow N + N + e^-$$

The ionization of atomic nitrogen which requires only 14.5 volts may then occur.

$$N + e^- \rightarrow N^+ + 2e^-$$

Helium has a very high ionization potential of 24.6 volts [56]. Ionization via excited atoms has been reported [53]. The appearance potential of He_2^+ is 23.2 volts and is formed from

$$He + e^- \rightarrow He^* + e^-$$

followed by

$$He^* + He \rightarrow He_2^+$$

Charge exchange of the He_2^+ with N_2 may have taken place because the

ionization potential of N_2 is 15.57 volts [11].

$$He_2^+ + N_2 \rightarrow N_2^+ + 2He$$

Loeb's [53] spectroscopic observations indicated that in a 0.5% N_2 + He mixture the color was determined by the N_2 . Most probably the N_2 in the He-N_2 mixtures investigated herein was ionized via electron impact and charge exchange.

He-O_2. Cataphoresis in He-O_2 mixtures was investigated as a function of discharge current, total gas pressure, and initial composition. Two sets of experiments were conducted. The first set of data was taken at a constant pressure to determine the influence of current and initial composition on the cataphoretic purification. The second set of experiments was taken at a constant current and initial composition to study the effect of pressure on cataphoresis.

In the first set of data the pressure was held constant at 6.0 mm Hg. The initial compositions were 2.2% O_2, 4.1% O_2, and 5.0% O_2 . The current range studied was 15 ma to 85 ma.

The second set of data was taken for an initial composition of 5.0% O_2 at a current of 50 ma. The pressure range examined was 2.1 mm Hg to 7.5 mm Hg.

The effect of current, pressure, and initial composition on the steady-state composition at the anode $\theta(1,\infty)$ is shown in Figs. 15, 20, and 23. The purification of O_2 from He improved by increasing the current or increasing the pressure or decreasing the initial percentage of O_2 . The separation of O_2 from He increased significantly by

increasing the current; refer to Fig. 15. For example, the value of $\theta(1,\infty)$ decreased from 0.764 at 20 ma to 0.020 at 85 ma with a 5.0% O_2 mixture at a pressure of 6.0 mm Hg. The lowest value of $\theta(1,\infty)$ that could be measured with the present instrumentation was 0.020, however, lower values of $\theta(1,\infty)$ probably occurred. The separation of O_2 from He was improved by increasing the pressure up to 4.0 mm Hg; however, further increases in pressure produced no subsequent improvement in the purification; refer to Fig. 20. A cross-plot of the results in Fig. 15 indicates that $\theta(1,\infty)$ increased with increasing initial percentage of O_2; see Fig. 23. For example, the value of $\theta(1,\infty)$ increased by a factor of about 8 at 15 ma when the initial composition increased from 1.2% O_2 to 4.8% O_2 .

The influence of current, pressure and initial percentage of O_2 on the calculated electrostatic Peclet number α is shown in Figs. 37 and 40. The value of α was found to increase with increasing current; refer to Fig. 37. The current dependence of α was in agreement with the model [22] because increasing the current should have increased α by increasing the ion-production rate. The value of α increased with pressure up to 4.0 mm Hg and then became relatively pressure independent; see Fig. 40. The electrostatic Peclet number decreased with increasing initial percentage of O_2. For example, at 35 ma the value of α was reduced from 2.69 to 0.84 by increasing the initial composition of O_2 from 2.2% O_2 to 5.0% O_2 at a pressure of 6.0 mm Hg. The values for α were between 0.38 and 4.32. The low value of 0.38 corresponded to the 5.0% O_2 mixture at a current of 20 ma and a pressure of 6.0 mm Hg. The high value of 4.32 corresponded to a pressure of

6.0 mm Hg with the 5.0% O_2, 4.1% O_2, and 2.2% O_2 mixtures at 85 ma, 72.5 ma, and 42.5 ma, respectively.

The effect of current, pressure, and initial composition on the electric field E is illustrated in Figs. 28 and 32. The electric field increased in a linear manner with increasing pressure and decreasing current. The values of E ranged from a low value of 13.6 volts/cm for a current of 50 ma and a pressure of 2.1 mm Hg with a 5.0% O_2 mixture, to a high value of 30.4 volts/cm for a current of 20 ma and a pressure of 6.0 mm Hg with a 4.1% O_2 mixture. The values of E generally increased with increasing percentage of O_2. This is in agreement with Headrick and Duffendack [83]. Several of the E versus i curves cross at low currents for the He-O_2, He-N_2, and He-Ne mixtures; refer to Figs. 26 to 28. This is not unexpected because, for example, He-Ne mixtures undergo a maximum in the electric field versus composition curve at about 5% Ne [32]. In addition, these values of the electric field where the curves cross are within the error limits described in Appendix D.

The influence of current, pressure and initial composition on the calculated ion fraction n_+/n_o is shown in Figs. 46 and 49. The ion fraction increased in almost a linear manner with increasing current at low current levels. For higher currents, the value of n_+/n_o increased more rapidly; refer to Fig. 46. The ion fraction decreased with increasing pressure. The effect of pressure on n_+/n_o was much less than the current dependence. The value of n_+/n_o increased when the initial percentage of O_2 was decreased. For example, at a pressure of 6.0 mm Hg and a current of 25 ma the ion fraction increased from

27×10^{-6} to 106×10^{-6} when the initial percentage of O_2 was dropped from 5.0% O_2 to 2.2% O_2 . The range for n_+/n_o was 11.4×10^{-6} to 178×10^{-6}. The low value for n_+/n_o of 11.4×10^{-6} occurred at a current of 20 ma and a pressure of 6.0 mm Hg with an initial composition of 5.0% O_2. The highest value of n_+/n_o equal to 178×10^{-6} occurred at 42.5 ma and 6.0 mm Hg with the 2.2% O_2 mixture. A summary of these results for cataphoresis in He-O_2 mixtures is shown in Table E-5.

The ionization mechanism for cataphoresis in He-O_2 mixtures may be direct electron impact of O_2 [11].

$$e^- + O_2 \rightarrow O_2^+ + 2e^- \quad (12.5 \text{ eV})$$

At higher energies than is probably present during cataphoresis, dissociative ionization to $O^+ + O$ at 20 eV has been observed [67]. The dissociation energy of O_2 is 5 volts, and the ionization potential of O is 13.5 volts [36]. The attachment of electrons to O_2 has been summarized by McDaniel [62]. The chemistry of electrical discharges in O_2 has been investigated by Rundle [70].

He-CO. Cataphoresis in He-CO mixtures was investigated as a function of discharge current, total gas pressure, and initial composition. Two sets of experiments were performed. The first set of experimental data was taken at a constant pressure to examine the effect of current on cataphoresis. The second set of data was taken at a constant current to examine the effect of pressure on cataphoresis. Both sets of data were taken for several initial compositions.

In the first set of data the pressure was held constant at 6.3 mm Hg. The initial compositions were 1.2% CO, 2.3% CO, and 4.9% CO. The current range examined was 15 ma to 75 ma.

The second set of data was taken for an initial composition of 1.2% CO, 2.3% CO, and 4.9% CO at a current level of 50 ma. The pressure range investigated was about 2 mm Hg to 9 mm Hg.

The effect of current, pressure, and initial composition on the steady-state composition at the anode $\theta(1,\infty)$ is shown in Figs. 16, 21, and 24. The purification of CO from He was found to be enhanced with increasing current or with increasing pressure, or with decreasing the initial percentage of CO. The steady-state separation factor $\theta(1,\infty)$ appeared to decrease linearly with increasing pressure. At low initial percentage of CO the pressure effect became unimportant; refer to Fig. 21.

The effect of current, pressure, and the initial percentage of CO on the calculated electrostatic Peclet number α is shown in Figs. 38, 41 and 42. The value of α was found to increase linearly with increasing current and increasing pressure. The current dependence of α agreed with the theory [22]. The pressure dependence of α was believed to be a function of the ionization mechanism. The electrostatic Peclet number decreased when the initial percentage of CO was increased. The values for α ranged from 0.40 to 2.21. The lowest value for α of 0.40 corresponded to the 4.9% CO mixture at 15 ma and 6.3 mm Hg, whereas the highest value for α of 2.21 corresponded to the 1.2% CO mixture at 75 ma and 6.3 mm Hg.

The effect of pressure, current and composition on the electric field E is illustrated in Figs. 29 and 33. The electric field was found to be a linear function of pressure and a linear function of current. The electric field increased with increasing pressure and decreased with increasing current. The values of E were between 11.1 volts/cm and 35.8 volts/cm. The lowest value for E of 11.1 volts/cm occurred with the 1.2% CO mixture at a current of 50 ma and a pressure of 2.5 mm Hg. The highest value for E of 35.8 volts/cm occurred with the 4.9% CO mixture at 50 ma and 8.8 mm Hg.

The influence of current, pressure and initial composition on the ion fraction n_+/n_o is shown in Figs. 47, 49 to 51. The ion fraction was a linearly increasing function of current; refer to Fig. 47. This is probably the main reason why the purification was improved by increasing the current. The ion fraction decreased with increasing pressure for the 1.2% CO mixture. However, with the 2.3% CO mixture and especially with the 4.9% CO mixture, the value of n_+/n_o was relatively independent of the pressure; refer to Fig. 50. This explains why increasing the pressure was less effective for enhancing the purification of the 1.2% CO mixture than the 4.9% CO mixture. The ion fraction increased with decreasing percentage of CO. This is the reason for the increasing effectiveness of separation with decreasing initial percentage of CO; refer to Fig. 21. The values for n_+/n_o were in the range of 5.9×10^{-6} to 70.2×10^{-6}. The lowest value for n_+/n_o of 5.9×10^{-6} occurred with a 4.9% CO mixture at a pressure of 6.3 mm Hg and a current of 15 ma. The highest value for n_+/n_o of 70.2×10^{-6} occurred with the 1.2% CO mixture

at 2.5 mm Hg and 50 ma. A summary of the results for cataphoresis in He-CO mixtures is shown in Table E-6.

An excellent discussion of the ionization of CO by electron impact is given by Reed [56] and by Gaydon [63]. The ionization mechanism may be the ionization of CO by electron impact to form a positive molecular ion CO^+ [11,56].

$$e^- + CO \rightarrow CO^+ + 2e^- \quad (14.1 \text{ eV})$$

Hagstrom [64,65] has reported that dissociative ionization occurs at high energies around 20.9 eV to 23.2 eV, but these are not important in cataphoresis. Dissociative electron capture has been observed by Cottrell [66].

He-CO_2. The He-CO_2 mixture behaved differently than the other mixtures investigated. In the five mixtures He-Ar, He-Ne, He-N_2, He-O_2, and He-CO only cataphoresis occurred. In the He-CO_2 mixture, a fraction of the CO_2 dissociated into CO and O_2 . The dissociation proceeded by the following reaction

$$2CO_2 \rightarrow 2CO + O_2 \quad (28)$$

After the initial stages where dissociation predominated, cataphoresis was then observed in the resulting quaternary mixture of He, CO_2, CO, and O_2 . When the discharge was extinguished, the gases diffused back to a uniform concentration profile in the axial direction. The difference between the thermal conductivity of the initial mixture of He-CO_2 and the final mixture of He, CO_2, CO, and O_2 was used to calculate the fraction of CO_2 dissociated.

The fraction of CO_2 dissociated was determined in two steps. First, the change in thermal conductivity of the mixture was obtained by measuring the detector output; refer to Figs. 55 and 56. Second, this thermal conductivity was related to the fraction of CO_2 dissociated; refer to Fig. 57.

The experimental measurements were taken for a mixture with an initial composition of 4.7% CO_2 and 7.5% CO_2. The current range examined was 10 ma to 65 ma and the pressure range was 2.2 mm Hg to 7.9 mm Hg for the 4.7% CO_2 mixture. The current range was 30 ma to 60 ma and the pressure 6.0 mm Hg for the 7.5% CO_2 mixture.

The fraction of CO_2 dissociated was directly proportional to the current and independent of the initial percentage of CO_2; refer to Fig. 58. The fraction of CO_2 dissociated increased from 0.11 to 0.67 when the current was increased from 10 ma to 65 ma at 6.0 mm Hg. The dissociation of CO_2 was directly proportional to the pressure; refer to Fig. 59. The fraction of CO_2 dissociated increased from 0.17 to 0.64 when the pressure was increased from 2.2 mm Hg to 7.9 mm Hg. The results for the dissociation of CO_2 are summarized in Table E-7.

After initiation of the discharge in the He-CO_2 mixture, the thermal conductivity of the mixture in the anode end-bulb initially decreased. This decrease in the thermal conductivity of the mixture was a result of the diminution of the mole fraction of He because of the increase in moles formed by the dissociation reaction. Since helium has a larger thermal conductivity than the impurity gas, the thermal conductivity of the mixture in the anode end-bulb increased

for all the other mixtures studied because the impurity gas was driven toward the cathode by cataphoresis. A calculation of the thermal conductivity of the mixture resulting from the dissociation of CO_2 to CO and O_2 indicated that the thermal conductivity decreased as the fraction of CO_2 dissociated increased. The result of these calculations are shown in Fig. 57 for a mixture with initial composition of 5.0% CO_2.

The values of the thermal conductivities that were used in the calculations are summarized below for 298°K [37].

Gas	Thermal Conductivity (cal/sec gm °K)
He	3,850
O_2	615
CO	600
CO_2	386

Because helium was the major component and because the thermal conductivity of helium is much higher than any of the other gases, the calculated and experimental values of the thermal conductivity were a linear function of composition in the range investigated; refer to Figs. 55 and 56.

A comment is required to explain why the dissociation of CO_2 via the following reaction was not observed in this study.

$$CO_2 \rightarrow C + O_2 \qquad (29)$$

The reaction described in Eq. (28) was energetically favored because it occurred at 5.5 eV [73] compared to 26.6 eV [56] for the reaction

described in Eq. (29). Blackwood and McTaggert [74] and O'Driscoll [75] have also observed the dissociation of CO_2 via the reaction described in Eq. (28) in a similar discharge during their investigations of the reaction of C with atomic gases and the study of graphite oxidation. The results reported herein are in agreement with the very recent publication by Buser and Sullivan [78] in 1970. Buser and Sullivan [78] and McTaggart [73] suggest the following ionization mechanism:

$$e + CO_2 \rightarrow CO_2^* + e$$

$$CO_2^* \rightarrow CO + O$$

V. COMPARISON OF THEORY AND EXPERIMENT

The purpose of this chapter is to check the theoretical model for cataphoresis which admittedly has many assumptions because of the very complex physical processes occurring in the discharge and to develop rule-of-thumb criteria for the design of cataphoretic separators.

The chapter is divided into two parts. First, the magnitude of the steady-state separation calculated from the model is compared to the experiment, and second, the characteristic time for cataphoresis calculated from the model is compared to the experiment.

The first part of this chapter is subdivided into five sections which are (1) a discussion of the variables which comprise the electrostatic Peclet number α, (2) an introduction to the assumptions associated with the prediction of α, (3) a quantitative discussion of these assumptions, (4) the calculation of α and $\theta(1,\infty)$, and (5) a comparison of the model to the experimental data for $\theta(1,\infty)$.

Discussion of the Variables which Comprise the Electrostatic Peclet Number

The main limitation to the model for cataphoresis is the necessity of having to know a priori the value of the electrostatic Peclet number α which is

$$\alpha = \frac{\mu E L}{D} \frac{n_+}{n_o}$$

for the case where $n_+/(n_o + n_+) \simeq n_+/n_o$. It is necessary to know the value of five quantities to calculate α. These five quantities are

summarized in Table 1.

Table 1: Definition of Terms in the Electrostatic Peclet Number

No.	Symbol	Definition	Units
1	L	Discharge Tube Length	cm
2	D	Binary Diffusion Coefficient	cm^2/sec
3	μ	Ionic Mobility	$cm^2/volt/sec$
4	E	Electric Field	V/cm
5	n_+/n_o	Ion Fraction	---

Discharge Tube Length. The length of the discharge tube L can be easily measured.

Diffusion Coefficient. The diffusion coefficient of the gas mixture D can be calculated from the theory in Hirschfelder, Curtiss, and Bird [37]. The experimental results for D have been summarized by Reid and Sherwood [46]. For the gas mixtures investigated herein, the experimental values of D are reported in the literature [37,38,40,48] except for He-CO. The agreement between the calculated and experimental values were within 7% for He-Ne and within 3% for the other mixtures [46]. Therefore, the values of D are readily available either from theory [37] or from reported experimental data [46].

Ionic Mobility. The theoretical methods for calculating the mobilities of ions in gases have been summarized by von Engel [36],

McDaniel [49], Tyndall [52], and Loeb [53]. The agreement between the experimental results and the theory is about 20% [43,49,53]. Calculating the ionic mobility from theory is difficult [43]. The experimental data, when available, are preferred instead of the theoretical values. Experimental values of the mobilities were used in the work described herein.

Electric Field. The data for the electric field E of single components are abundant [32,36,49,53,59,62]; however, the data for E in mixtures are rarely available [32]. Therefore, the values of E during the cataphoretic separation of gases must be measured in order to calculate α. The value of E can be measured as discussed in Chapter III.

Ion Fraction. The fraction of impurity ionization n_+/n_o for gas mixtures is not available in the literature. Recently, however, Gaur and Chanin [68] measured the degree of ionization during cataphoresis in He-Ne mixtures. In their experiment the initial composition of Ne was $\leq$ 0.05% Ne which is a factor of 50 less than the initial percentage of Ne examined herein. The current investigation by Ravimohan and Shair [69] utilizing a microwave cavity to measure the electron density may prove helpful in estimating an upper bound for the ion fraction.

Summary. The two transport properties D and μ can be obtained from the collections of experimental data in the literature or from theoretical calculations. The theoretical calculations for D are easier than for μ and agree more closely with the experimental results.

The major difficulty in predicting α is manifested by the problems of obtaining adequate data for E and n_+/n_o. The value of n_+/n_o is more of a problem than E because it is harder to measure n_+/n_o. In addition, the value of n_+/n_o varies over a wider range than E. For example, the measured E reported in Chapter IV varied by a factor of 4.3 from a maximum value of 36.4 volts/cm to a minimum value of 8.5 volts/cm. In comparison, the calculated n_+/n_o varied by a factor of 37 from a maximum value of 178×10^{-6} to a minimum value of 4.8×10^{-6}. These results are summarized in Table 2.

Before one uses the theoretical model for cataphoresis to design systems for separating gas mixtures, it is necessary to have experimental data on E and n_+/n_o to calculate α. Since these measurements are very difficult and require an excessive expenditure of time and resources, the use of cataphoresis as a practical separation technique is severely limited unless α can be estimated by developing rule-of-

Table 2: Range of Measured E and Calculated n_+/n_o

Range of E	E	n_o^o	i	P
Maximum	36.4 V/cm	4.8% N_2	50 ma	8.8 mm Hg
Minimum	8.5 V/cm	4.7% Ar	100 ma	3.2 mm Hg
Ratio of Maximum E to Minimum E = $\frac{36.4 \text{ V/cm}}{8.5 \text{ V/cm}}$ = 4.3				
Range of n_+/n_o	n_+/n_o	n_o^o	i	P
Maximum	178×10^{-6}	2.2% O_2	42.5 ma	6.0 mm Hg
Minimum	4.8×10^{-6}	4.7% Ar	25 ma	3.2 mm Hg
Ratio of Maximum n_+/n_o to minimum n_+/n_o = $\frac{178 \times 10^{-6}}{4.8 \times 10^{-6}}$ = 37				

thumb methods for predicting the current and pressure dependence of E and n_+/n_o .

Introduction to the Assumptions Associated with the Prediction of α

Is it possible to make some rule-of-thumb assumptions about estimating α that will yield reasonable results for designing systems to separate gases by cataphoresis? This important question will be considered here.

The quantities L, D, and μ present practically no problem as previously explained. In addition, the ratio of μ/D is pressure independent [53]. Therefore, $\mu L/D$ is a constant for a gas mixture at a fixed temperature. It is assumed that both D and μ are independent of the composition [37,53].

The two key parameters are the electric field E and the ion fraction n_+/n_o . In the experimental data described in Chapter IV, it was observed that E was directly proportional to the pressure P and relatively independent of the current i . The ion fraction was approximately directly proportional to the current except at high currents, and the effect of pressure on n_+/n_o was usually considerably less than the effect of current on n_+/n_o .

Based on these observations, several rule-of-thumb assumptions are made. First, to calculate α versus i , the electric field is assumed constant and independent of i , and n_+/n_o is assumed directly proportional to i . Second, to calculate α versus P , the ion fraction is assumed constant and independent of P , and E is assumed directly proportional to P . These assumptions are summarized

in Table 3.

Table 3: Rule-of-Thumb Assumptions

1. Assumptions to Calculate α vs i
   (constant P and n_o^o)
   A. E independent of i
   B. n_+/n_o directly proportional to i
2. Assumptions to Calculate α vs P
   (constant i and n_o^o)
   A. E directly proportional to P
   B. n_+/n_o independent of P

Discussion of the Assumptions

Each assumption will be compared to the experimental results reported in Chapter IV. The experimental results are summarized in Appendix E, Tables E-2 to E-6.

Assumption 1.A: The experimental values of E decreased slightly with increasing current rather than being constant as assumed in 1.A; refer to Figs. 25 to 29. The best, typical, and worst cases from these figures are summarized in Table 4.

Table 4: Check of Assumption 1.A

Agreement	Maximum Value of E (V/cm)	Minimum Value of E (V/cm)	Ratio of Maximum to Minimum	n_o^o (mole %)	P (mm Hg)	i (ma)
worst	12.6	8.5	1.48	4.7% Ar	3.2	25-100
typical	27.3	21.6	1.26	2.2% N_2	6.3	7.5-50
best	11.9	11.4	1.04	2.4% Ne	6.0	25-75

The basis of comparison was the ratio of the maximum value of E (at the lowest current) to the minimum value of E (at the highest current) for a gas mixture at constant n_o^o and P.

The worst case was the 4.7% Ar mixture at 3.2 mm Hg where the value of E decreased from 12.6 volts/cm at 25 ma to 8.5 volts/cm at 100 ma. This 32.5% decrease in E was for a 400% increase in current. In conclusion, the maximum decrease in E was 32.5% for the range of currents investigated at a constant n_o^o and P.

Assumption 1.B: The assumption that n_+/n_o is directly proportional to current was a good assumption at low currents, but at high currents there was usually a nonlinear increase in current. When a straight line was drawn through the values of n_+/n_o corresponding to the two lowest measured currents, then the deviation from linear behavior for the highest current was about a factor of 1.5 for He-Ar and He-N_2 and about a factor of 2 for He-O_2. The values of n_+/n_o were linear with current for He-CO in the entire range of 15 ma to 75 ma.

The values of n_+/n_o as a function of i were obtained by drawing a straight line through the two values of n_+/n_o which corresponded to the two lowest measured currents. The subsequent values of n_+/n_o calculated from this line are referred to as the predicted values of n_+/n_o from assumption 1.B. The values of n_+/n_o calculated from the experimental data as previously described in Chapter IV are referred to as the calculated values. These calculated values of n_+/n_o are shown in Figs. 43 to 47. A comparison of the predicted

and calculated values of n_+/n_o are summarized in Table 5 for the best, typical, and worst cases.

Table 5: Check of Assumption 1.B

Agreement	Calculated $\frac{n_+}{n_o} \times 10^6$	Predicted $\frac{n_+}{n_o} \times 10^6$	Ratio of Calculated to Predicted	n_o^o (mole %)	P (mm Hg)	i (ma)
worst	170	69.9	2.43	4.1% O_2	6.0	72.5
typical	168	126	1.33	2.2% N_2	6.3	50
best	17.4	17.2	1.01	4.9% CO	6.3	75

In conclusion, the assumption that n_+/n_o is directly proportional to i varied from excellent for the He-CO mixtures to poor for the He-O_2 mixtures; refer to Table 5. The effect of this assumption on the prediction of α and $\theta(1,\infty)$ will be discussed later.

Assumption 2.A: For a given gas mixture, the measured electric field was a linear function of pressure for a constant initial composition and a constant current; refer to Figs. 30 to 33. The lines in these figures are described by the following equation.

$$E = mP + b \qquad P_1 < P < P_2$$

The values of m and b were calculated using the method of least-squares for constant n_o^o and i [42,76]. The results for m and b are summarized in Table E-13. For a discharge tube of 8 mm diameter, these are good design equations for calculating E . The E versus P data for He-O_2 had the most scatter and the data for He-N_2 had

the least scatter; refer to Fig. 32. The results shown in Fig. 32 are summarized in Table 6. The predicted values of E were obtained

Table 6: Check of Assumption 2.A

$i = 50$ ma , $n_o^o = 5.0\%$ O_2		
Measured E (V/cm)	Predicted E (V/cm)	P (mm Hg)
13.6	15.9	2.1
19.8	17.4	2.7
20.3	20.6	4.0
26.8	25.5	6.0
28.0	29.1	7.5
$i = 50$ ma , $n_o^o = 4.8\%$ N_2		
Measured E (V/cm)	Predicted E (V/cm)	P (mm Hg)
15.8	15.8	2.2
17.7	17.4	2.7
21.7	22.4	4.3
29.2	28.7	6.3
36.4	36.5	8.8

by using the above design equation with the appropriate m and b .

In conclusion, the assumption that E is directly proportional to P is within 17% for the range investigated.

Assumption 2.B: The ion fraction increased with increasing pressure for He-Ar and He-Ne mixtures. The ion fraction generally decreased with P for the He-N_2, He-O_2, and He-CO mixtures; refer to Figs. 48 to 50. The salient features of these figures are summarized in Table 7. The basis of comparison was the ratio of the maximum

Table 7: Check of Assumption 2.B

Agreement	Maximum Value of $\frac{n_+}{n_o} \times 10^6$	Minimum Value of $\frac{n_+}{n_o} \times 10^6$	Ratio of Maximum and Minimum Values	n_o^o (mole %)	P (mm Hg)	i (ma)
worst	70.2	35.9	1.96	1.2% CO	2.5-8.7	50
typical	77.2	50.0	1.54	4.8% N_2	2.2-8.8	50
best	12.9	11.8	1.09	4.9% CO	2.8-8.8	50

value of n_+/n_o to the minimum value of n_+/n_o for a given gas mixture at a constant n_o^o and i . The worst case was the 1.2% CO mixture at 50 ma where the value of n_+/n_o decreased by a factor of 1.96 as P increased by a factor of about 3.5. The best case was the 4.9% CO mixture at 50 ma where the value of n_+/n_o decreased by only a factor of 1.09 as P increased by a factor of about 3.1.

In conclusion, the assumption that n_+/n_o is independent of P is excellent in some cases, for example, the 4.9% CO mixture at 50 ma, and fair in other cases, for example, the 1.2% CO mixture at 50 ma. The effect of this assumption on the prediction of α and $\theta(1,\infty)$ will be discussed later.

A qualitative summary of the assumptions for each gas mixture is presented in Table 8.

Table 8: Qualitative Summary of Assumptions for Each Mixture

Gas Mixture	Assumption 1.A E Independent of i	Assumption 1.B n_+/n_o Directly Proportional to i	Assumption 2.A E Directly Proportional to P	Assumption 2.B n_+/n_o Independent of P
He-Ar	Fair	Fair	Excellent	Fair (improves with i)
He-Ne	Excellent	Good	Excellent	Poor
He-N_2	Good	Fair	Excellent	Fair
He-O_2	Good	Poor	Very Good	Fair
He-CO	Good	Excellent	Excellent	Excellent (low n_o^o) Poor (high n_o^o)

Calculation of α and $\theta(1,\infty)$

The electrostatic Peclet number was estimated by using the rule-of-thumb assumptions. The results of these calculations are in Appendix E, Tables E-8 to E-12. The details of these calculations for the electric field and the ion fraction are now described.

α versus i. For each gas mixture at a constant n_o^o and P, the values of n_+/n_o versus i were estimated by using the values of n_+/n_o for the two lowest measured currents and assuming that n_+/n_o was directly proportional to i . The measured value of

E at the second lowest current was used for the electric field, and this value of E was assumed constant and independent of i .

α versus P . For each gas mixture at a constant n_o^o and i, the values of E as a function of P were predicted by the equation describing the best straight line through the experimental data. The line was obtained by the method of least squares. The value for n_+/n_o was assumed constant and independent of P . The value for n_+/n_o was taken as the calculated value closest to a pressure of 6.0 mm Hg. For He-Ar, He-Ne, He-O_2, He-N_2, and He-CO, these values of P were 5.5, 6.0, 6.0, 6.3, and 6.3 mm Hg, respectively.

θ(1,∞) versus i and P . The values of θ(1,∞) versus i and θ(1,∞) versus P were calculated from Eqs. (22) and (23)

$$\theta(1,\infty) = Ke^{-\alpha} \tag{22}$$

$$K = \frac{1 + \delta + \varepsilon}{\delta + \varepsilon e^{-\alpha} - \frac{e^{-\alpha}}{2} + \frac{1}{\alpha}} \tag{23}$$

by using the estimated values of α versus i and α versus P . The results of these calculations are summarized in Tables E-8 to E-12. These calculated values will now be compared to the experimental measurements for θ(1,∞) .

Comparison of the Model to the Experimental Data for θ(1,∞)

The value of θ(1,∞) calculated from the model by using the estimated values of α are compared to the experimental measurements of θ(1,∞) as a function of i and P .

$\theta(1,\infty)$ versus i . The agreement between the calculated values and the measured results for $\theta(1,\infty)$ as a function of i are shown in Figs. 12 to 16. The agreement in general is good considering that $\theta(1,\infty)$ is proportional to $e^{-\alpha}$. The values of α were estimated using assumptions 1.A and 1.B. The salient features of these figures are now discussed.

He-Ar. The agreement between the model and the data for $\theta(1,\infty)$ versus i was good except at high currents approaching 100 ma. The values of $\theta(1,\infty)$ calculated from the model were between a factor of 1.38 to 2.07 times higher than the measured values at 100 ma; refer to Table 9 and Fig. 12.

Table 9: Comparison of Calculated and Measured Values of $\theta(1,\infty)$ for He-Ar. Calculated Values Obtained with Assumptions 1.A and 1.B

i = 100 ma , n_o^o = 4.7% Ar			
Calculated $\theta(1,\infty)$	Measured $\theta(1,\infty)$	Ratio of Calculated to Measured	P (mm Hg)
0.338	0.245	1.38	3.2
0.207	0.138	1.50	5.5
0.062	0.030	2.07	8.9

The main reason for this result was that the values of n_+/n_o were estimated a factor of about 1.5 times too low at high currents because of the nonlinear increase in n_+/n_o .

He-Ne. The agreement between the model and the experiment for $\theta(1,\infty)$ as a function of i was very good except at high currents approaching 100 ma for the 4.8% Ne mixture. When the current was increased, the agreement became worse as shown in Table 10 and Fig. 13.

Table 10: Comparison of Calculated and Measured Values of $\theta(1,\infty)$ for He-Ne. Calculated Values Obtained with Assumptions 1.A and 1.B

P = 6.0 mm Hg , n_o^o = 4.8% Ne			
Calculated $\theta(1,\infty)$	Measured $\theta(1,\infty)$	Ratio of Calculated to Measured	i (ma)
0.915	0.900	1.02	25
0.631	0.631	1.00	50
0.420	0.458	0.92	75
0.270	0.403	0.67	100

The value of $\theta(1,\infty)$ calculated from the model at 100 ma was 33% lower than the measured value. The calculated value of $\theta(1,\infty)$ was too low at 100 ma because the value of n_+/n_o was estimated a factor of 1.36 too high. The experimental value of $\theta(1,\infty)$ appeared to be leveling off at high currents for the 4.8% Ne mixture.

He-N_2. The agreement between the model and the experiment for $\theta(1,\infty)$ as a function of i was good. The calculated value of $\theta(1,\infty)$ was generally higher than the measured value. For the 4.8% N_2 mixture the ratio between the calculated and measured values of $\theta(1,\infty)$

increased from 1.00 to 3.86 as the current increased from 15 ma to 75 ma; refer to Table 11 and Fig. 14. The reason for this departure of the

Table 11: Comparison of Calculated and Measured Values of $\theta(1,\infty)$ for He-N_2 with n_o^o of 4.8% N_2 . Calculated Values Obtained with Assumptions 1.A and 1.B

P = 6.3 mm Hg , n_o^o = 4.8% N_2			
Calculated $\theta(1,\infty)$	Measured $\theta(1,\infty)$	Ratio of Calculated to Measured	i (ma)
0.865	0.864	1.00	15
0.600	0.600	1.00	25
0.236	0.173	1.36	50
0.081	0.021	3.86	75

calculated and measured values at high current was that the values of n_+/n_o were estimated too low at currents greater than 25 ma. For example, at 100 ma the estimated value of n_+/n_o was approximately 50% low.

The calculated values of $\theta(1,\infty)$ were always higher than (or equal to) the measured values except for the 2.2% N_2 mixture at 6.3 mm Hg and 25 ma; refer to Table 12. The ratio of the calculated to the measured value was 0.88. This effect occurred because the ratio of the calculated to predicted value of n_+/n_o was 1.05 as compared to the ratio of the measured to estimated value of E which was 0.89. The product of these two ratios was less than 1.0, and the net result was an increase in α which produced a resulting decrease in the calculated value of $\theta(1,\infty)$. This is an example of one of the only cases where Assumption 1.B introduced a larger error than Assumption 1.A.

He-O_2. The agreement between the model and the experiment was

Table 12: Comparison of Calculated and Measured Values of $\theta(1,\infty)$ for He-N_2 with n_o^o of 2.2% N_2. Calculated Values Obtained with Assumptions 1.A and 1.B

P = 6.3 mm Hg , n_o^o = 2.2% N_2			
Calculated $\theta(1,\infty)$	Measured $\theta(1,\infty)$	Ratio of Calculated to Measured	i (ma)
0.737	0.728	1.01	7.5
0.445	0.445	1.00	15
0.213	0.241	0.88	25
0.029	0.022	1.32	50

good at low currents, but the agreement departed significantly as the current increased; see Table 13 and Fig. 13. Analogous to the discussion

Table 13: Comparison of Calculated and Measured Values of $\theta(1,\infty)$ for He-0_2. Calculated Values Obtained with Assumptions 1.A and 1.B

P = 6.0 mm Hg , n_o^o = 5.0% 0_2			
Calculated $\theta(1,\infty)$	Measured $\theta(1,\infty)$	Ratio of Calculated to Measured	i (ma)
0.782	0.764	1.02	20
0.536	0.536	1.00	35
0.356	0.344	1.03	50
0.171	0.080	2.14	75
0.126	0.020	6.30	85

for He-Ar and He-N_2, the departure of the measured and the calculated value of $\theta(1,\infty)$ was caused by the nonlinear increase of n_+/n_o at high currents. At 85 ma, the estimated value of n_+/n_o was too low by about a factor of 2 for the 5.0% 0_2 mixture at 6.0 mm Hg.

He-CO. The value of $\theta(1,\infty)$ calculated from the model was generally lower than the experimental data for He-CO. A summary of the results for a 4.9% CO mixture is shown in Table 14 and Fig. 16.

Table 14: Comparison of Calculated and Measured Values of $\theta(1,\infty)$ for He-CO. Calculated Values Obtained with Assumptions 1.A and 1.B

P = 6.3 mm Hg , n_o^o = 4.9% CO			
Calculated $\theta(1,\infty)$	Measured $\theta(1,\infty)$	Ratio of Calculated to Measured	i (ma)
0.765	0.755	1.01	15
0.699	0.698	1.00	25
0.548	0.575	0.95	50
0.420	0.482	0.87	75

The worst agreement for the He-CO mixtures occurred for the 1.2% CO mixture at 75 ma and 6.3 mm Hg. The ratio of the calculated to measured value of $\theta(1,\infty)$ was 0.682. The agreement between the calculated and measured results for $\theta(1,\infty)$ were generally good because assumption 1.B was excellent, that is, the ion fraction was directly proportional to i. The calculated values of $\theta(1,\infty)$ were generally lower than the experimental measurements because E decreased by about a factor of 1.2 with increasing current rather than being constant as assumed in Assumption 1.A.

$\theta(1,\infty)$ versus P . The agreement between the calculated values and the measured results for $\theta(1,\infty)$ as a function of P are shown in Figs. 17 to 21. The agreement in general is good considering that $\theta(1,\infty)$ is proportional to $e^{-\alpha}$. The values of α were estimated utilizing Assumptions 2.A and 2.B. The salient characteristics of these results are now discussed.

He-Ar. The values of $\theta(1,\infty)$ versus P calculated from the model were lower than the experimental results for pressures less than about 6 mm Hg and higher than the experimental results for pressures greater than 6 mm Hg. The agreement between the calculated and measured values of $\theta(1,\infty)$ are shown in Table 15 and Fig. 17. The ratio

Table 15: Comparison of Calculated and Measured Values of $\theta(1,\infty)$ for He-Ar at 100 ma. Calculated Values Obtained with Assumptions 2.A and 2.B

i = 100 ma , n_o^o = 4.7% Ar			
Calculated $\theta(1,\infty)$	Measured $\theta(1,\infty)$	Ratio of Calculated to Measured	i (ma)
0.213	0.245	0.87	3.2
0.138	0.138	1.00	5.5
0.070	0.030	2.33	8.9

of the calculated to measured values of $\theta(1,\infty)$ varied from 0.87 at 3.2 mm Hg to 2.33 at 8.9 mm Hg. This result occurred because n_+/n_o increased with P by a factor of 1.4 between 3.2 mm Hg and 8.9 mm Hg

rather than being constant as assumed in Assumption 2.B.

The data for He-Ar were taken at a constant pressure as a function of current, and at a constant current as a function of pressure. This enabled a comparison between the first set of assumptions (1.A and 1.B) and the second set of assumptions (2.A and 2.B). The results in Tables 9 and 15 are for the same experimental points using the two different sets of assumptions. This comparison is summarized in Table 16. The agreement is better (except at 8.9 mm Hg)

Table 16: Comparison of Calculated and Measured Values of $\theta(1,\infty)$ Using Both Sets of Assumptions for He-Ar at 100 ma

i = 100 ma , n_o^o = 4.7% Ar		
Ratio of Calculated to Measured $\theta(1,\infty)$ Using Assumptions 1.A and 1.B (from Table 9)	Ratio of Calculated to Measured $\theta(1,\infty)$ Using Assumptions 2.A and 2.B (from Table 15)	P (mm Hg)
1.38	0.87	3.2
1.50	1.00	5.5
2.07	2.33	8.9

using Assumptions 2.A and 2.B. Therefore, the use of the second set of assumptions (2.A and 2.B) are recommended for He-Ar at high currents around 100 ma.

The same comparison is made in Table 17 for He-Ar at a low current of 25 ma. Again as before, the second set of assumptions

Table 17: Comparison of Calculated and Measured Values of $\theta(1,\infty)$ for He-Ar at 25 ma. Calculated Values Obtained with Assumptions 1.A and 1.B, and Assumptions 2.A and 2.B

$i = 25$ ma , $n_o^o = 4.7\%$ Ar			
Calculated $\theta(1,\infty)$ Using Assumptions 1.A and 1.B			
Calculated $\theta(1,\infty)$	Measured $\theta(1,\infty)$	Ratio of Calculated to Measured	P (mm Hg)
0.931	0.915	1.017	3.2
0.915	0.894	1.023	5.5
0.829	0.790	1.049	8.9
Calculated $\theta(1,\infty)$ Using Assumptions 2.A and 2.B			
0.915	0.915	1.000	3.2
0.896	0.894	1.002	5.5
0.867	0.790	1.097	8.9

(2.A and 2.B) are recommended for He-Ar at 25 ma except at high pressures around 8.9 mm Hg.

In conclusion, the second set of assumptions gave better agreement between the calculated and measured values of $\theta(1,\infty)$ except at high pressures around 8.9 mm Hg where the first set of assumptions gave closer agreement.

He-Ne. The values of $\theta(1,\infty)$ versus P that were calculated from the model are lower than the experimental results for $\theta(1,\infty)$

at pressures less than about 6.0 mm Hg and higher at pressures greater than 6 mm Hg. The agreement between the calculated and measured values of $\theta(1,\infty)$ are shown in Table 18 and Fig. 18. The ratio of the

Table 18: Comparison of Calculated and Measured Values of $\theta(1,\infty)$ for He-Ne. Calculated Values Obtained with Assumptions 2.A and 2.B

$i = 50$ ma , $n_o^o = 2.4\%$ Ne			
Calculated $\theta(1,\infty)$	Measured $\theta(1,\infty)$	Ratio of Calculated to Measured	P (mm Hg)
0.476	0.635	0.75	3.5
0.468	0.483	0.97	6.0
0.460	0.430	1.07	9.1

calculated to measured values of $\theta(1,\infty)$ varied from 0.75 at 3.5 mm Hg to 1.07 at 9.1 mm Hg. This result occurred because n_+/n_o increased with pressure by a factor of 1.7 from 3.5 mm Hg to 9.1 mm Hg.

He-N_2. The values of $\theta(1,\infty)$ versus P calculated from the model were higher than the experimental values at pressures less than about 6 mm Hg and lower at pressures greater than 6 mm Hg. The agreement between the model and the measurements are shown in Table 19 and Fig. 19. The ratio of the calculated to measured values of $\theta(1,\infty)$ varied from a high of 1.42 to a low of 0.64 in the pressure range

Table 19: Comparison of Calculated and Measured Values of $\theta(1,\infty)$ for He-N_2 . Calculated Values Obtained with Assumptions 2.A and 2.B

i = 50 ma , n_o^o = 4.8% N_2			
Calculated $\theta(1,\infty)$	Measured $\theta(1,\infty)$	Ratio of Calculated to Measured	P (mm Hg)
0.412	0.379	1.09	2.2
0.372	0.275	1.35	2.7
0.270	0.190	1.42	4.3
0.177	0.173	1.02	6.3
0.103	0.160	0.64	8.8

2.2 mm Hg to 8.8 mm Hg. The worst agreement occurred at a pressure of 4.3 mm Hg because the value of n_+/n_o was estimated about 20% too low. The ratio of calculated to measured values of $\theta(1,\infty)$ went through a maximum near 4.3 mm Hg because the ion fraction went through a maximum there; see Table 19 and Fig. 49.

He-O_2. The results for He-O_2 were similar to those for He-N_2. The agreement between the model and the data are shown in Fig. 20. The salient feature of this figure is that the calculated values of $\theta(1,\infty)$ are higher than the observed values for pressures less than about 6.0 mm Hg. The experimental data for $\theta(1,\infty)$ were higher than the calculated values at P greater than 6.0 mm Hg. This result occurred because the value of n_+/n_o decreased with increasing pressure rather than being constant as assumed in Assumption 2.B. The

ratio of the calculated to the measured value of $\theta(1,\infty)$ varied from 1.06 to 1.29 for the pressure range of 2.1 mm Hg to 7.5 mm Hg.

He-CO. The agreement between $\theta(1,\infty)$ calculated from the model and measured in the experiment are shown in Fig. 21. The important features are summarized in Table 20. The agreement improved markedly

Table 20: Comparison of Calculated and Measured Values of $\theta(1,\infty)$ for He-CO. Calculated Values Obtained with Assumptions 2.A and 2.B

Calculated $\theta(1,\infty)$	Measured $\theta(1,\infty)$	Ratio of Calculated to Measured	P (mm Hg)
i = 50 ma , n_o^o = 4.9% CO			
0.715	0.711	1.006	2.8
0.652	0.654	0.997	4.4
0.579	0.575	1.007	6.3
0.492	0.472	1.042	8.8
i = 50 ma , n_o^o = 1.2% CO			
0.457	0.261	1.751	2.5
0.332	0.248	1.339	4.4
0.236	0.233	1.013	6.3
0.153	0.218	0.702	8.7

as the percentage of CO increased from 1.2% CO to 4.9% CO because n_+/n_o became more independent of P . For example, the value of n_+/n_o varied by a factor of only 1.09 for the 4.9% CO mixture in

the pressure range of 2.8 mm Hg to 8.8 mm Hg, whereas the value of n_+/n_o varied by a factor of 1.96 for the 1.2% CO mixture in the pressure range of 2.5 mm Hg to 8.7 mm Hg. The agreement between the calculated and measured values of $\theta(1,\infty)$ for the 4.9% CO mixture was excellent because the ion fraction was linear with i, and n_+/n_o was independent of P, satisfying Assumptions 2.A and 2.B.

Conclusion to First Part of Chapter

Near the beginning of this chapter, the question was posed whether some rule-of-thumb assumptions could be used to estimate α for designing systems to separate gases by cataphoresis using the model and only a few experimental values of n_+/n_o and E. These approximate methods gave very satisfactory results for predicting $\theta(1,\infty)$ versus i and $\theta(1,\infty)$ versus P. This technique is recommended for designing systems to separate gases by cataphoresis taking into account the following limitations. The assumptions for estimating E were very good; the pressure dependence of E was particularly accurate because of the linear relationship between E and P. The assumptions for estimating n_+/n_o were generally not as good as those for estimating E. At high currents a nonlinear effect may occur for n_+/n_o versus i. Also, at low initial percentages of impurity, for example the 1.2% CO mixture, the value of n_+/n_o may be a strong function of P. A qualitative summary of the assumptions is shown in Table 8 for each mixture.

In the second part of the chapter, the characteristic time for cataphoresis calculated from the model is compared to the experimental results. This part of the chapter is subdivided into five sections

which are (1) the definition of the characteristic time for cataphoresis t_c, and the dimensionless characteristic time τ_c, (2) the calculation of τ_c and t_c from the model, (3) the calculation of t_c and τ_c from the experiment, (4) a comparison of the characteristic times from the model and experiment, and (5) a discussion of the dependence of t_c on P, n_o^o, and i.

Definition of t_c and τ_c for Cataphoresis

For the following discussion, the time for 63.2% of the total change in composition to occur at the anode is referred to as the characteristic time for the cataphoretic separation t_c. As defined by Shair and Remer [22], the dimensionless characteristic time τ_c is

$$\tau_c = \frac{Dt_c}{L^2} \tag{30}$$

where D is the binary diffusion coefficient for the mixture and L is the length of the discharge tube. The values for D and L are reported in Chapter IV.

Calculations of τ_c and t_c from the Model

The value of τ_c was calculated from the transient part of the solution to the model for cataphoresis; refer to Eq. (13) in Appendix B. This value for the characteristic time is

$$\tau_c^M = \frac{1}{\frac{\alpha^2}{4} + u_1^2} \tag{31}$$

for small α. The superscript M refers to the value calculated

from the model. The values of u_1 and α were required to calculate τ_c^M from Eq. (31). The term u_1 is a solution to the following equation which is derived in Appendix B, Eq. (19).

$$\tan u_1 = \frac{-(\delta + \varepsilon)u_1}{1 + \frac{\alpha}{2}(\delta - \varepsilon) - \delta\varepsilon\left(\frac{\alpha^2}{4} + u_1^2\right)} \tag{32}$$

The value of α was calculated from the experimental value of $\theta(1,\infty)$ and the steady-state solutions, Eqs. (22) and (23), as previously discussed in Chapter IV. An outline of these calculations is shown in Fig. 11. For a specified α, the value of u_1 was calculated from Eq. (32) by an iterative procedure. The results for u_1 as a function of α are summarized in Table E-14 for $\delta = 8.9$ and $\varepsilon = 4.2$. The value of τ_c^M calculated from Eq. (31) was a linear function of α

$$\tau_c^M = -0.61\alpha + 3.00 \tag{33}$$

for $\alpha < 1.36$. The results for τ_c^M as a function of α are summarized in Table E-14. Equation (33) was also used as an approximation of τ_c^M for values of α up to about 3. For the calculation of τ_c^M when $\alpha > 3$, more eigenvalues are required; refer to Shair and Cohen [79]. These calculations were not performed in the present investigation. The value of t_c^M was then calculated from Eq. (30) using the results for τ_c^M from Eq. (31).

Calculation of τ_c and t_c from the Experiment

The value of t_c was obtained from the composition versus time curve measured at the anode; refer to Fig. 61 or Fig. 1 in Appendix C. This value of t_c is denoted by t_c^E where the superscript E refers to the experiment. The composition versus time curves were checked to see if they were first order. The values of t_c were calculated for several cases using the three different methods suggested by Shilling [80]. The three methods gave the same values for t_c within 1%. This implies that the transient response was definitely first order. The remaining values of t_c^E were obtained from the response curve by using the value of t when cataphoresis was 63.2% completed.

The results for τ_c^E were then calculated from Eq. (30). An outline of these calculations is shown in Fig. 11. The results for τ_c^E, τ_c^M, t_c^E and t_c^M are summarized in Tables E-15 through E-19.

Comparison of t_c^E and t_c^M

The agreement between the model and the experiment for t_c was within 25% for 50% of the data and within a factor of 2 for 82% of the data. The calculated values from the model were about 20% lower than the experimental values for He-Ne and He-N_2 mixtures and higher by a factor of about 2.2 for the He-CO mixtures.

He-Ar. The ratio of t_c^M/t_c^E for He-Ar varied from a high of 1.50 to a low of 0.875; however, for five out of eight of the comparisons, the ratio of t_c^M/t_c^E was between 0.875 and 0.98.

He-Ne. The ratio of t_c^M/t_c^E for He-Ne varied from 0.24 to 1.53; however, for six out of nine of the comparisons, the ratio of t_c^M/t_c^E was between 0.63 and 0.95.

He-N_2. The ratio of t_c^M/t_c^E for He-N_2 varied from 0.51 to 1.36; however, for ten out of twelve of the comparisons, the ratio of t_c^M/t_c^E was between 0.51 and 0.97.

He-O_2. The ratio of t_c^M/t_c^E varied from 0.49 to 2.42; however, for ten out of thirteen of the comparisons, the ratio of t_c^M/t_c^E was between 0.49 and 1.15.

He-CO. The ratio of t_c^M/t_c^E varied from 0.94 to 5.14; however, for sixteen out of twenty-one of the comparisons, the ratio of t_c^M/t_c^E was 0.94 to 1.81.

Summary. The range of t_c^M/t_c^E for each gas mixture is summarized in Table 21. The average of the values of t_c^M/t_c^E was between 0.80 and 1.04 for all the mixtures except He-CO, which was 2.23.

Discussion of the Dependence of t_c on P, n_o^o, and i

Since the diffusion coefficient is inversely proportional to the pressure P, the characteristic time t_c is predicted to be directly proportional to P. The data generally agree with this prediction; refer to Figs. 52 to 54 and Tables E-2 to E-6. In these figures the values of t_c vary between 1/2 minute and 4 minutes, and the values of P vary between about 2 mm Hg and 9 mm Hg. The conclusion that t_c is directly proportional to P is in agreement with other experimental observations [4,15].

Table 21 : Range of t_c^M/t_c^E for Each Gas Mixture

Gas Mixture	Maximum Value of t_c^M/t_c^E	Minimum Value of t_c^M/t_c^E	Average of the Values of t_c^M/t_c^E
He-Ar	1.50	0.875	1.04
He-Ne	1.53	0.24	0.83
He-N_2	1.36	0.51	0.80
He-O_2	2.42	0.65	0.995
He-CO	5.14	0.96	2.23

The model suggests that t_c should be relatively independent of the initial composition of the impurity n_o^o. The results in Fig. 54 for He-CO are in agreement with this prediction for a range of P between 2 mm Hg and 9 mm Hg and a range of n_o^o between 1.2% CO and 4.9% CO. The conclusion that t_c is relatively independent of n_o^o is in agreement with another experiment [15].

If heating effects upon the transport properties are negligible, then t_c should not be significantly influenced by the current. This is in agreement for the range of currents investigated which was about 5 ma to 100 ma. This is also in agreement with Matveeva [15].

In conclusion the qualitative agreement was very good between the measured value of t_c^E and the calculated value of t_c^M as a function of current, pressure, and initial composition. The quantitative agreement was within a factor of 2 for 80% of the data.

VI. CONCLUSIONS

1. A tungsten filament lamp was used as a Pirani gauge for continuous gas analysis. This proved to be a very inexpensive and effective technique for obtaining quantitative data on the cataphoretic separation without requiring the removal of a sample from the system.

2. The cataphoretic separation of Ar and Ne from He was found to be in agreement with previous investigations.

3. Cataphoresis was an effective technique for separating diatomic gases from He. The cataphoretic separation of N_2, O_2, and CO from He was found to be similar to noble gas systems in that the steady-state separation improved with (1) increasing discharge current, (2) increasing total gas pressure, and (3) decreasing initial composition of the minority component.

4. In the He-CO_2 mixture, the CO_2 dissociated to O_2 and CO. The extent of dissociation was proportional to the current and pressure and independent of the initial composition. Dissociation may occur in other cases when cataphoresis is utilized to separate polyatomic gases.

5. In a recently proposed theoretical model involving an electrostatic Peclet number, one of the basic assumptions was that the electric field is a constant which is independent of time and position. This assumption was checked experimentally and the maximum variation in the electric field was 35% in time and 30% in position. Therefore, the assumption of constant electric field introduced no more than 55% variation in the electrostatic Peclet number during a separation.

6. To aid in the construction of new cataphoretic separator systems, design criteria were developed and checked. First, to calculate the electrostatic Peclet number as a function of current, the following two assumptions were used.

   1.A. The electric field was assumed constant and independent of the discharge current.

   1.B. The ion fraction was assumed directly proportional to the discharge current.

   Second, to calculate the electrostatic Peclet number as a function of the total pressure, the following two assumptions were used.

   2.A. The electric field was assumed directly proportional to pressure.

   2.B. The ion fraction was assumed constant and independent of pressure.

   These assumptions, although approximate, enabled the steady-state separation to be predicted to within 25% for 75% of the data.

7. The theoretical model was also checked with respect to the characteristic time associated with transient cataphoresis. The characteristic times for cataphoresis obtained from the experiment were compared to the values calculated from the model. The agreement was within a factor of 2 for about 80% of the data. The values of α used in these comparisons were calculated from the steady-state solution of the model and the experimental data for the steady-state separation at the anode.

8. The values of the calculated electrostatic Peclet number ranged from 0.13 to 4.33. These results were calculated from the steady-

state solution of the model and the experimental value for the steady-state separation at the anode. The calculated values of the ion fraction of the impurity component ranged from 4.8×10^{-6} to 178×10^{-6} .

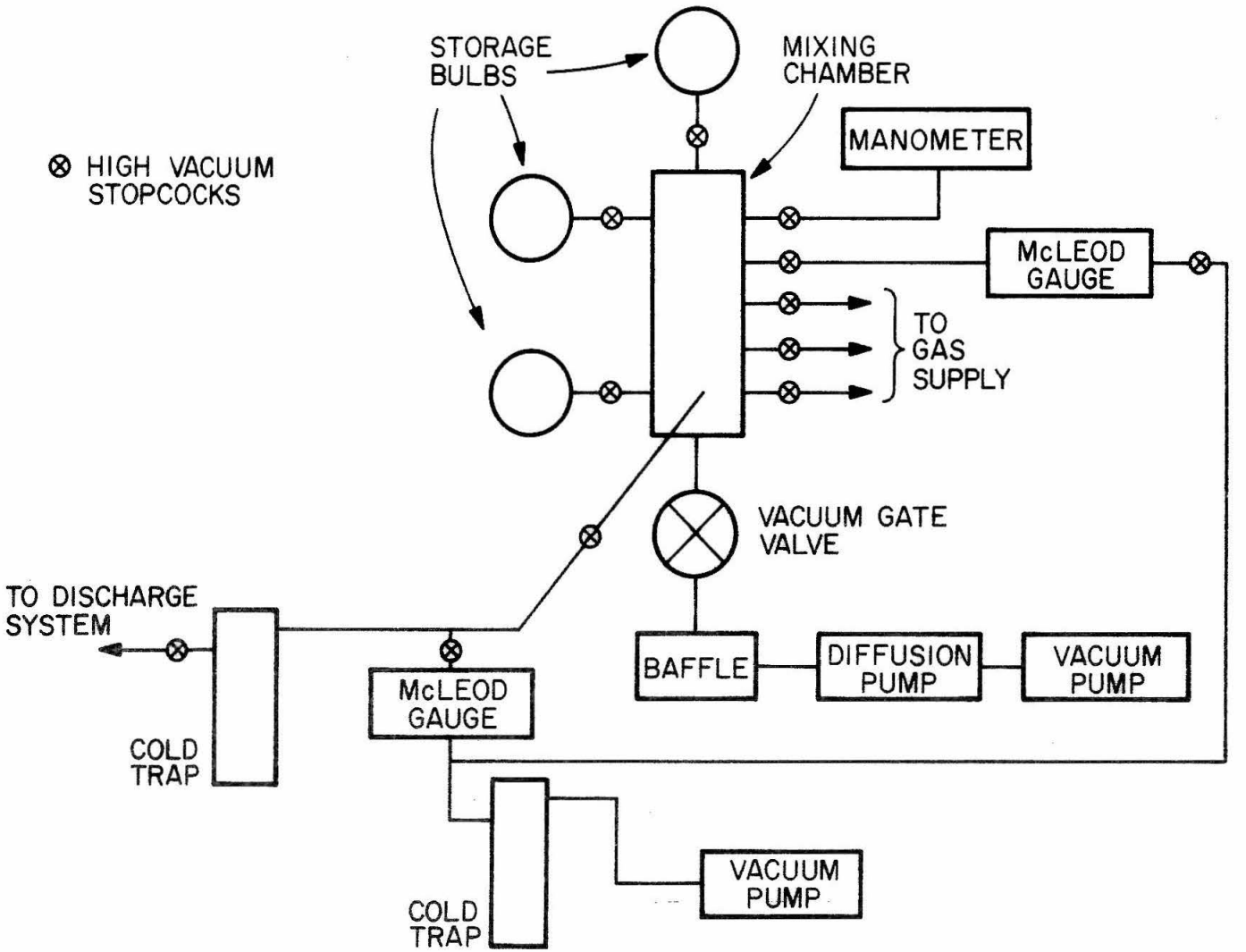

Figure 2. Block Diagram of Gas Supply System

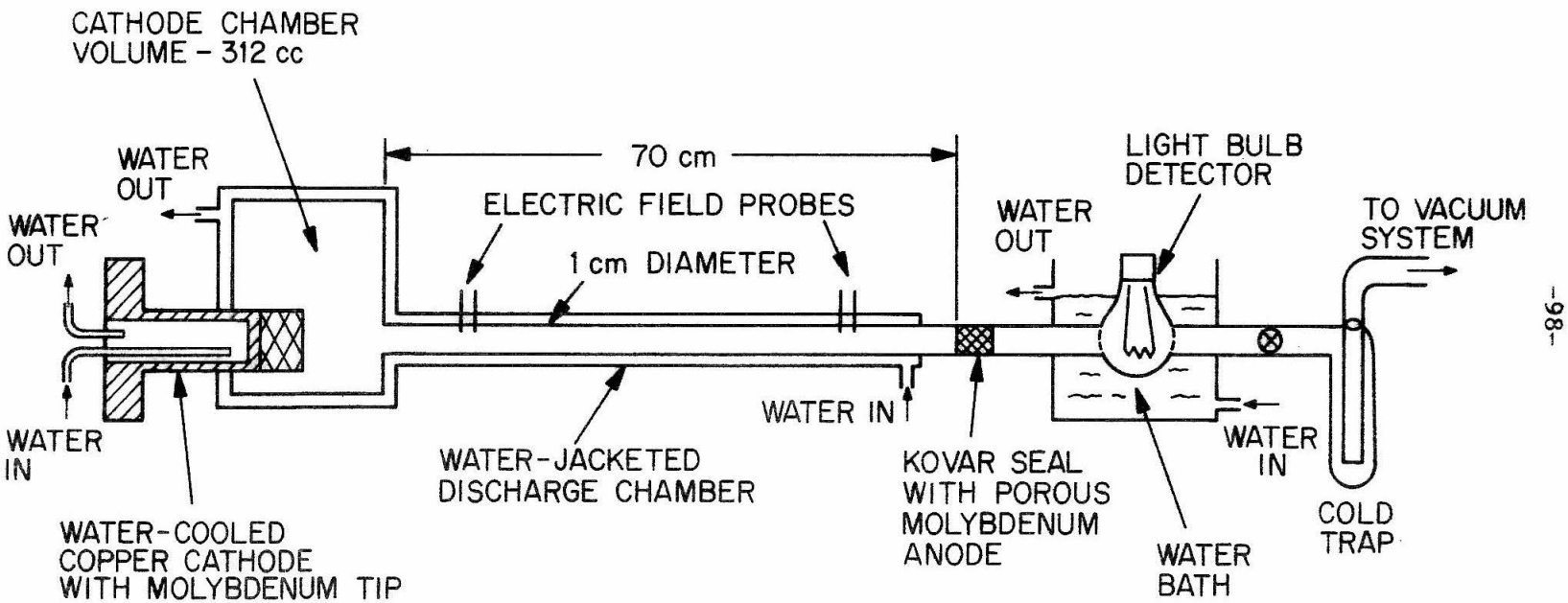

Figure 3. Diagram of Discharge Chamber and Detector

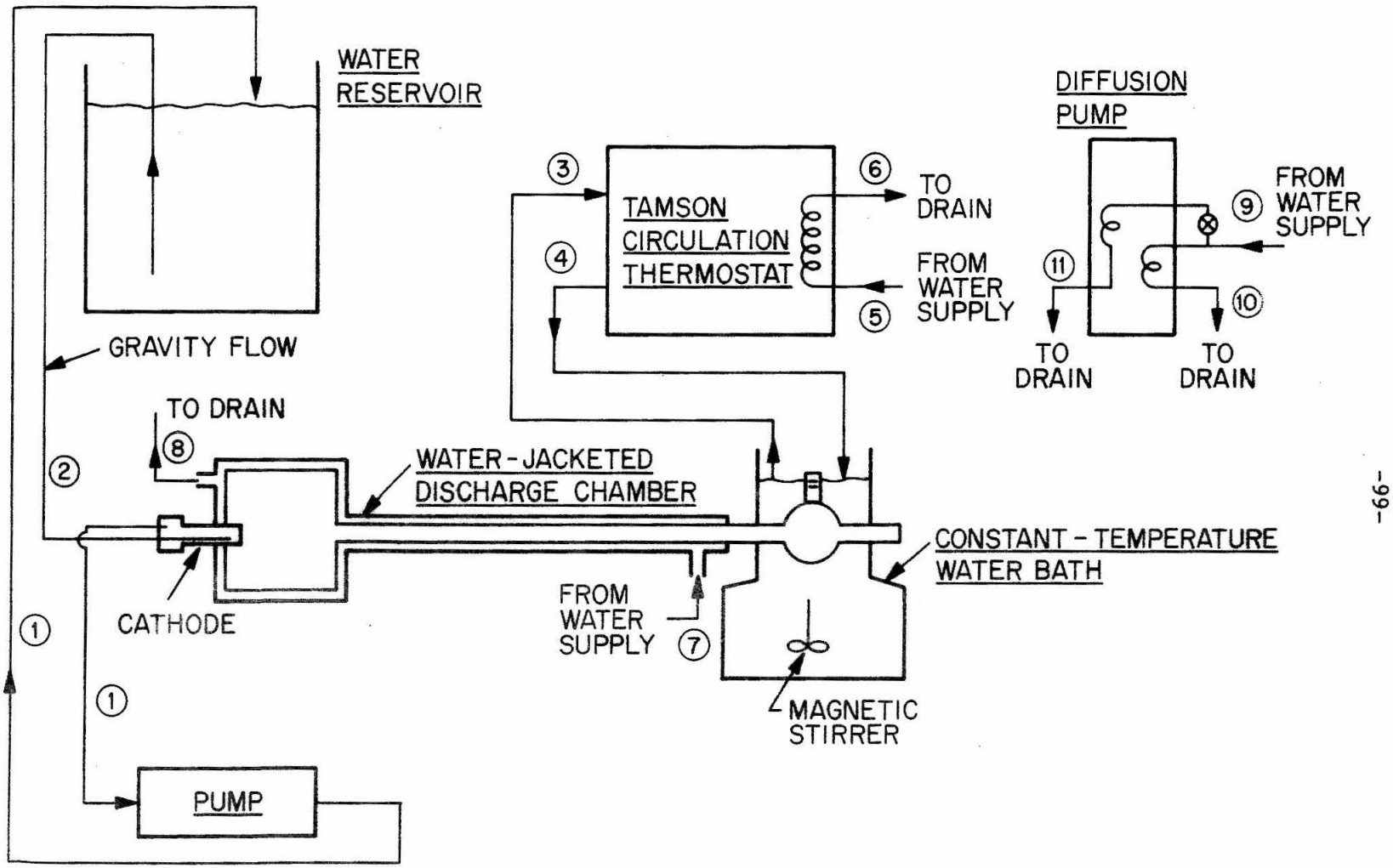

Figure 4. Flow Diagram of the Water System

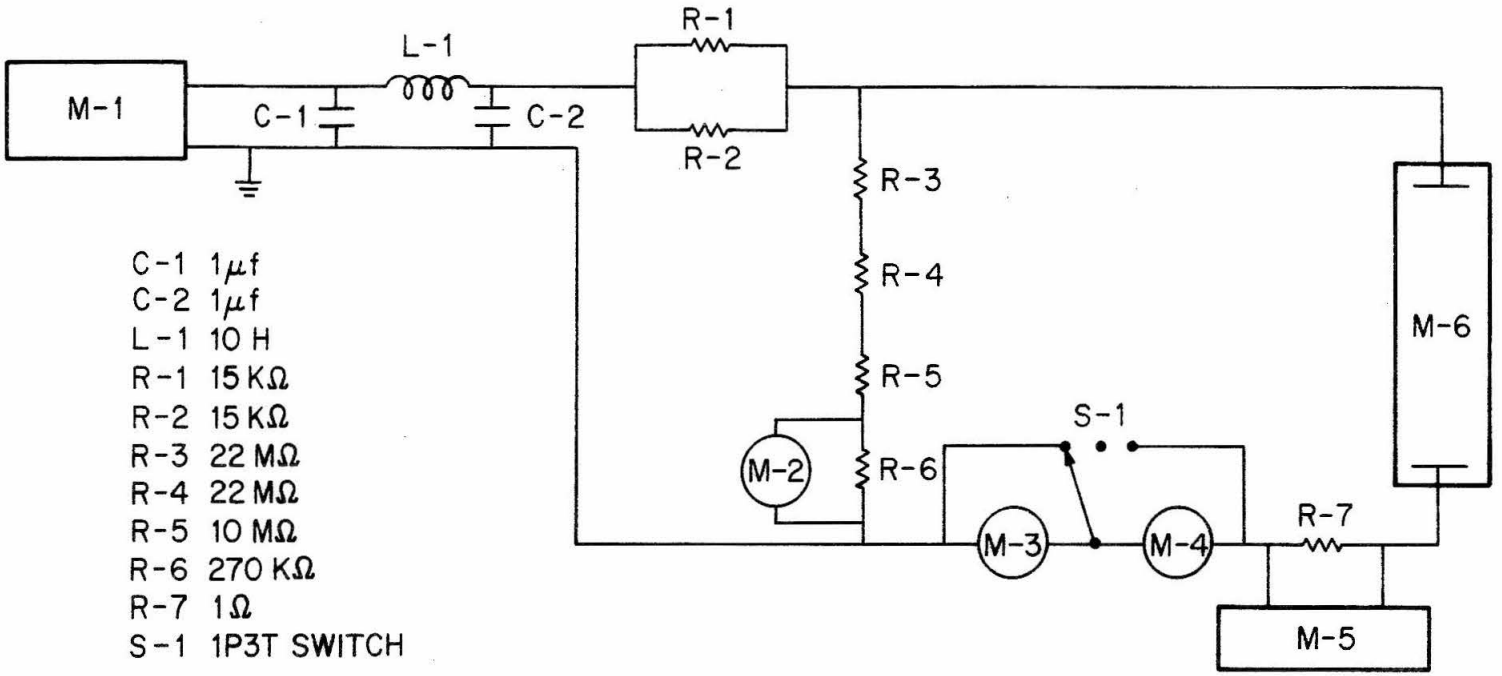

M-1 CVC HIGH-VOLTAGE POWER SUPPLY, MODEL NO. LC-031. 5000 VOLTS, 300 mA.

M-2 TRIOLAB VTVM MODEL NO. 106-1, 30 VOLTS.

M-3 SIMPSON DC MILLIAMMETER, MODEL NO. 1150-1, 100 mA.

M-4 SIMPSON DC MILLIAMMETER, MODEL NO. 1150-1, 500 mA.

M-5 HEWLETT PACKARD, DUAL BEAM OSCILLOSCOPE, MODEL NO. 122AR.

M-6 CATAPHORETIC DISCHARGE TUBE.

Figure 5. Power-Supply Circuit

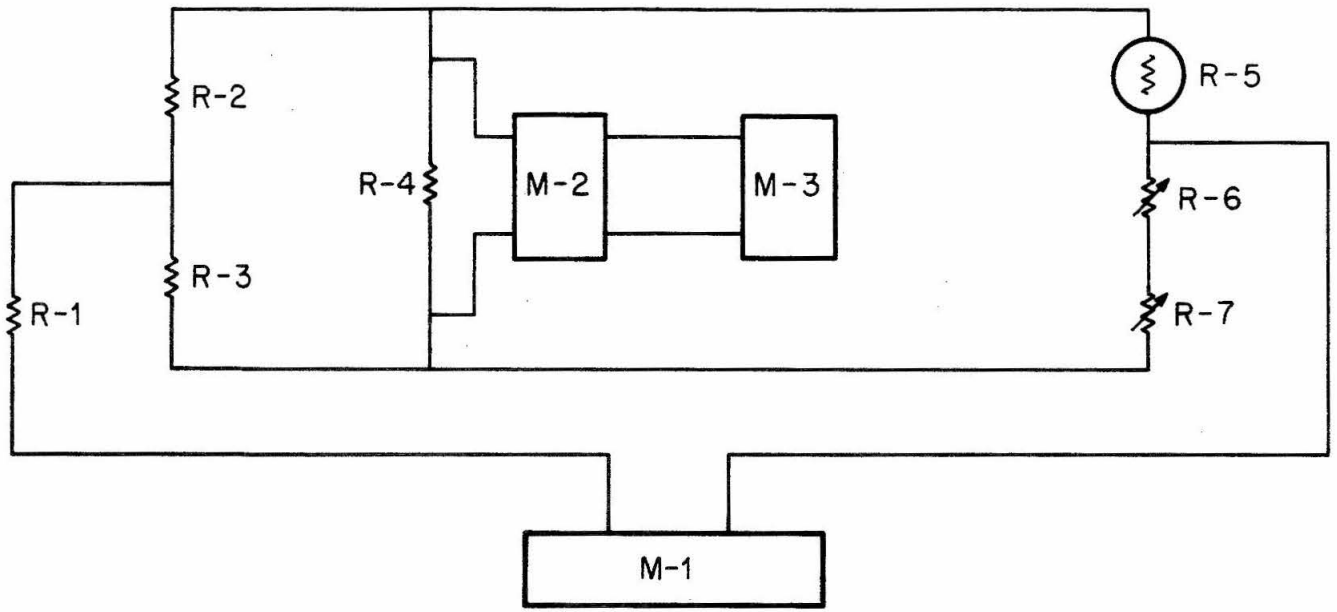

R-1 120Ω
R-2 0.75Ω
R-3 18Ω
R-4 47Ω
R-5 60-WATT LIGHT BULB
R-6 25Ω POTENTIOMETER
R-7 500Ω POTENTIOMETER

M-1 DRESSEN-BARNES, MODEL 20-5, REGULATED POWER SUPPLY, 5 VOLTS D.C., 750 MILLIAMPS.

M-2 L & N STABILIZED D.C. MICROVOLT AMPLIFIER 9835-B.

M-3 L & N SPEEDOMAX W/L RECORDER.

Figure 6. Detector Circuit

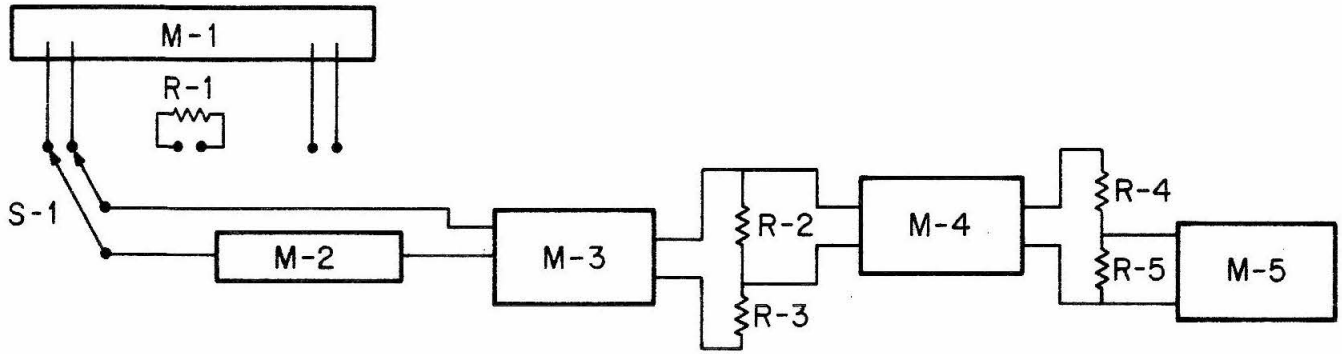

R-1 100KΩ
R-2 2Ω
R-3 1400Ω
R-4 45Ω
R-5 1000Ω
S-1 2P3T SWITCH

M-1 DISCHARGE TUBE.

M-2 KEITHLEY MODEL 6103A,
1000:1 VOLTAGE DIVIDER PROBE.

M-3 KEITHLEY MODEL 602 ELECTROMETER.

M-4 FLUKE MODEL A88 ISOLATION AMPLIFIER.

M-5 LEEDS & NORTHRUP SPEEDOMAX
W/L RECORDER.

Figure 7. Electric-Field Circuit

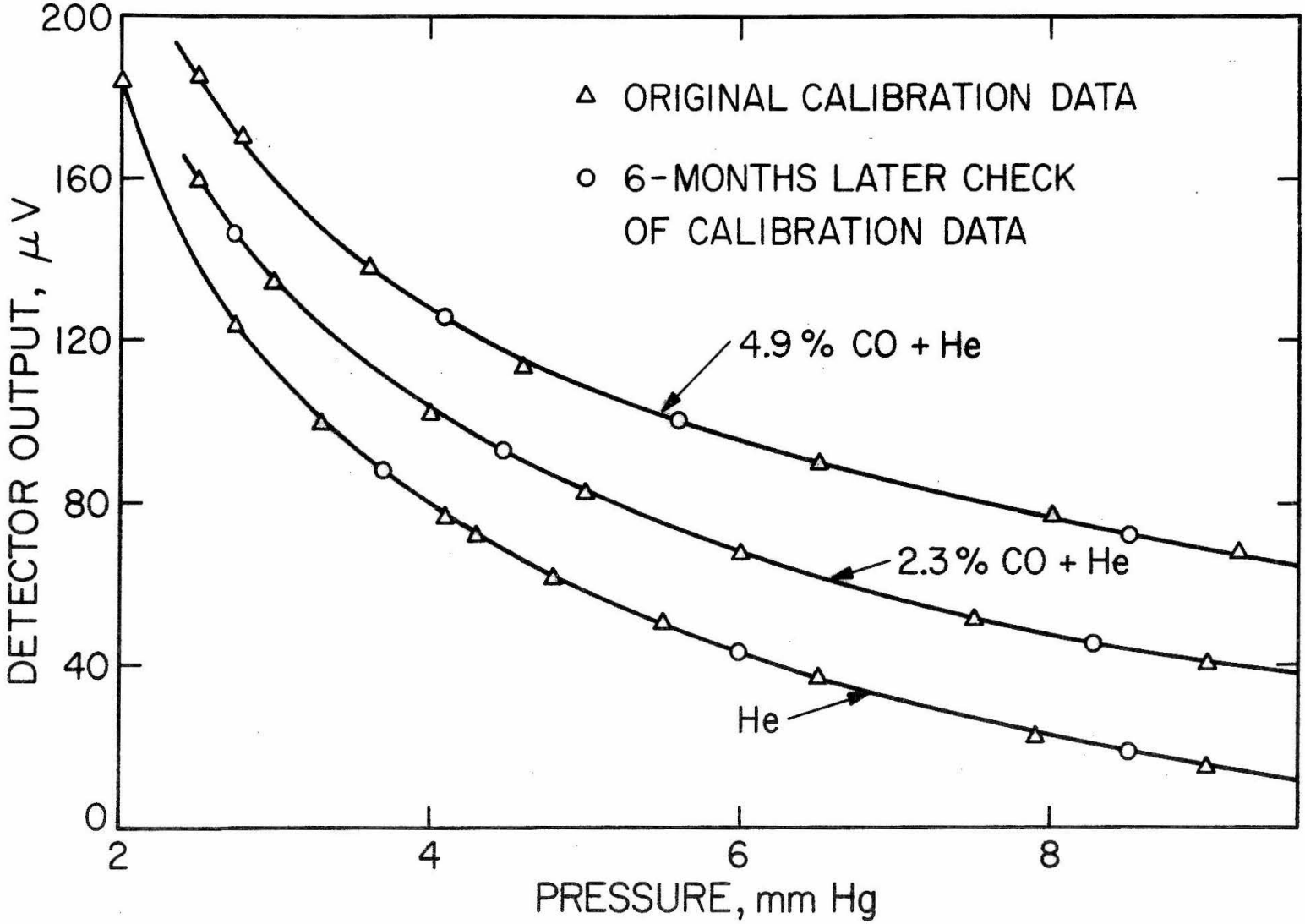

Figure 8. Pressure Calibration for He-CO

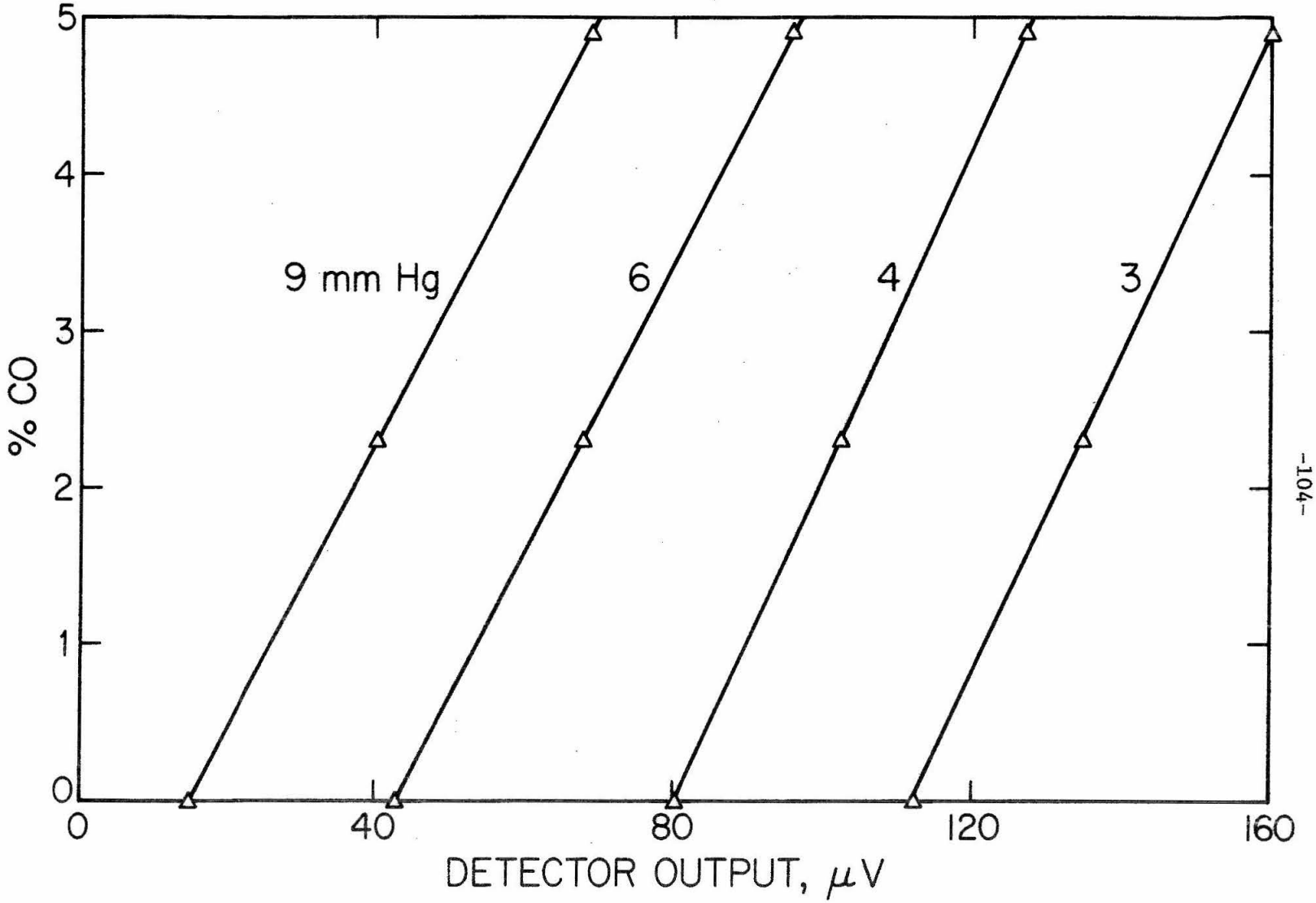

Figure 9. Composition Calibration for He-CO

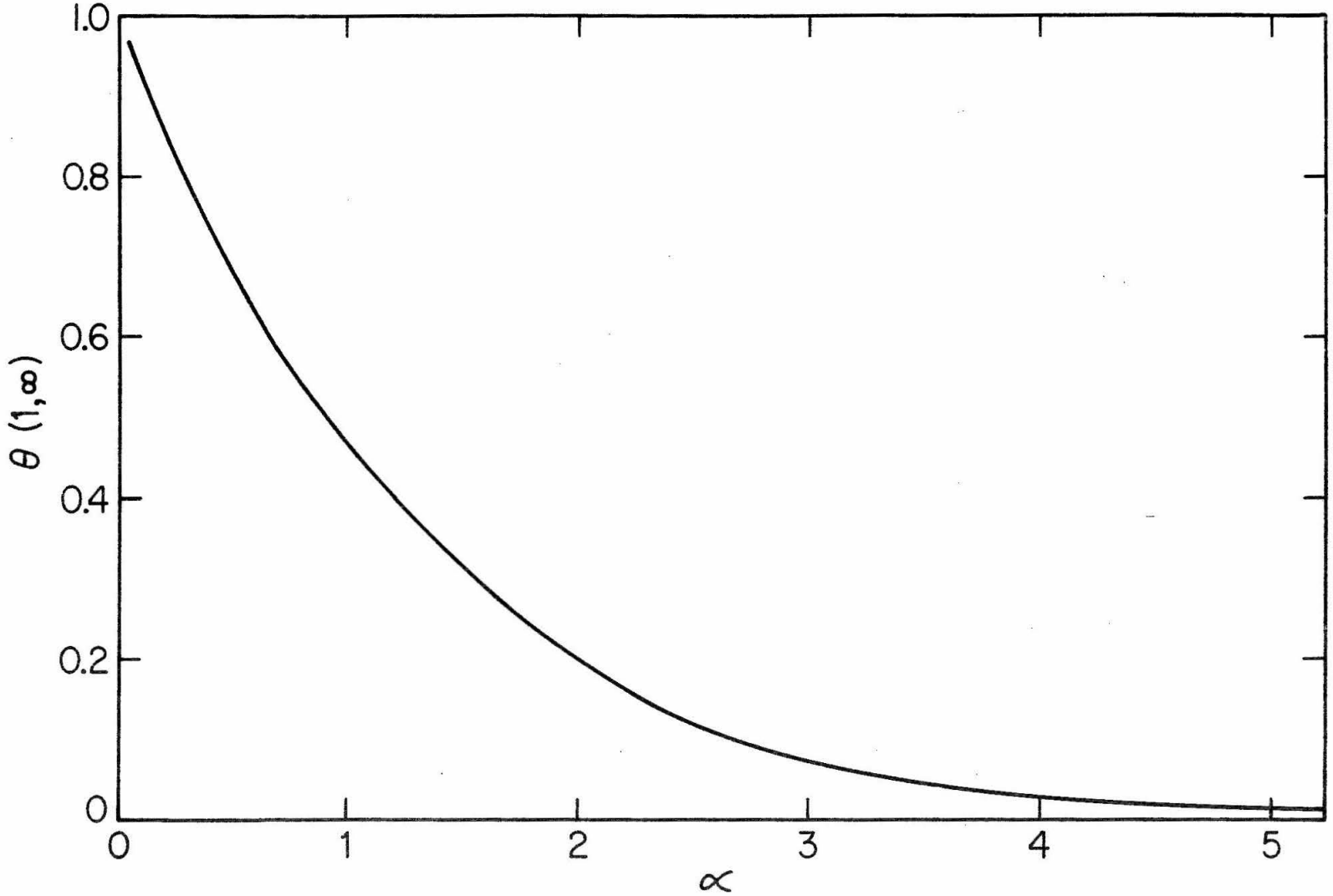

Figure 10. The Variation of Steady-State Separation with Electrostatic Peclet Number as Calculated from Model for $\delta = 8.9$ and $\varepsilon = 4.2$

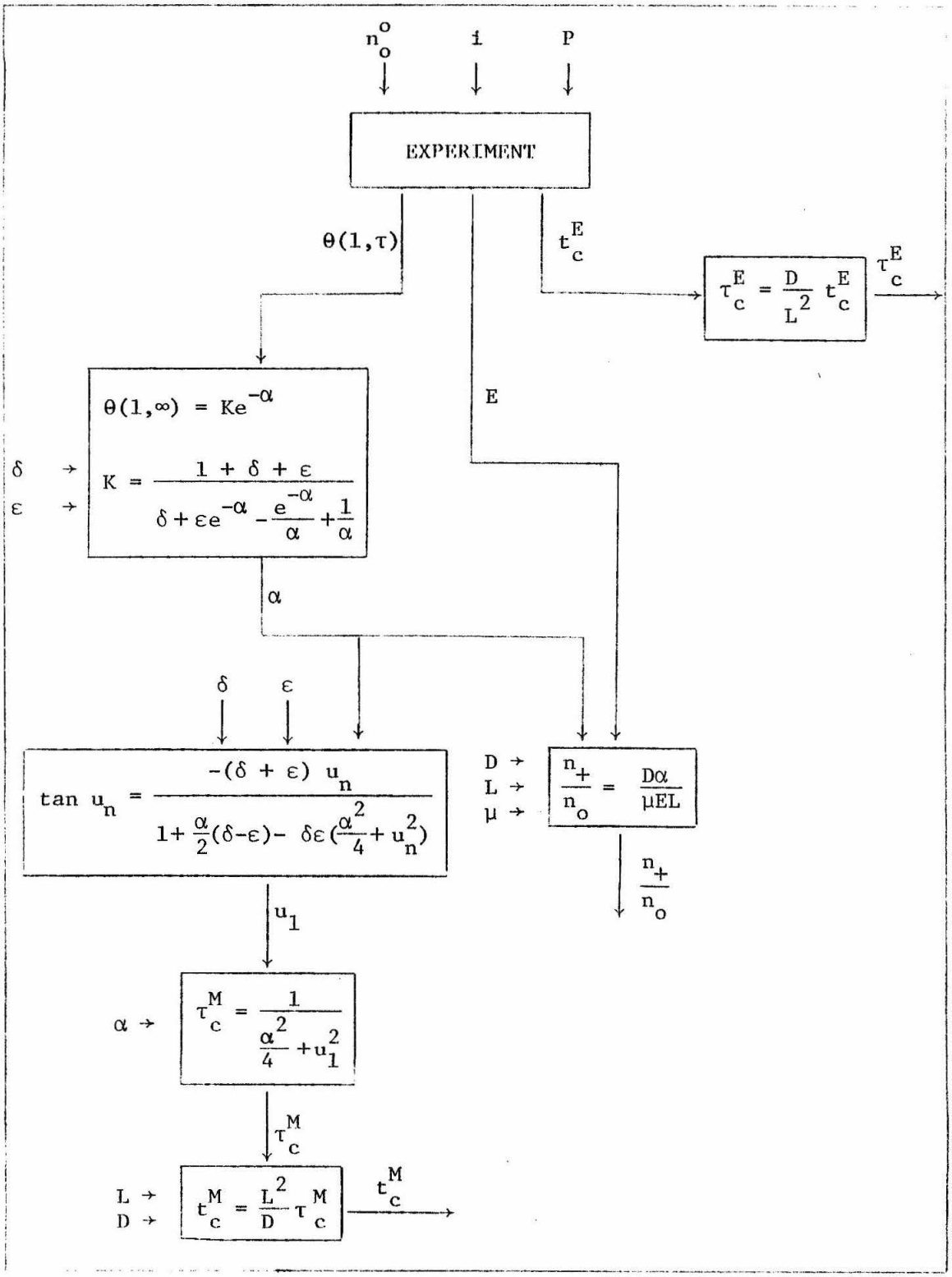

Figure 11. Block Diagram of Calculations

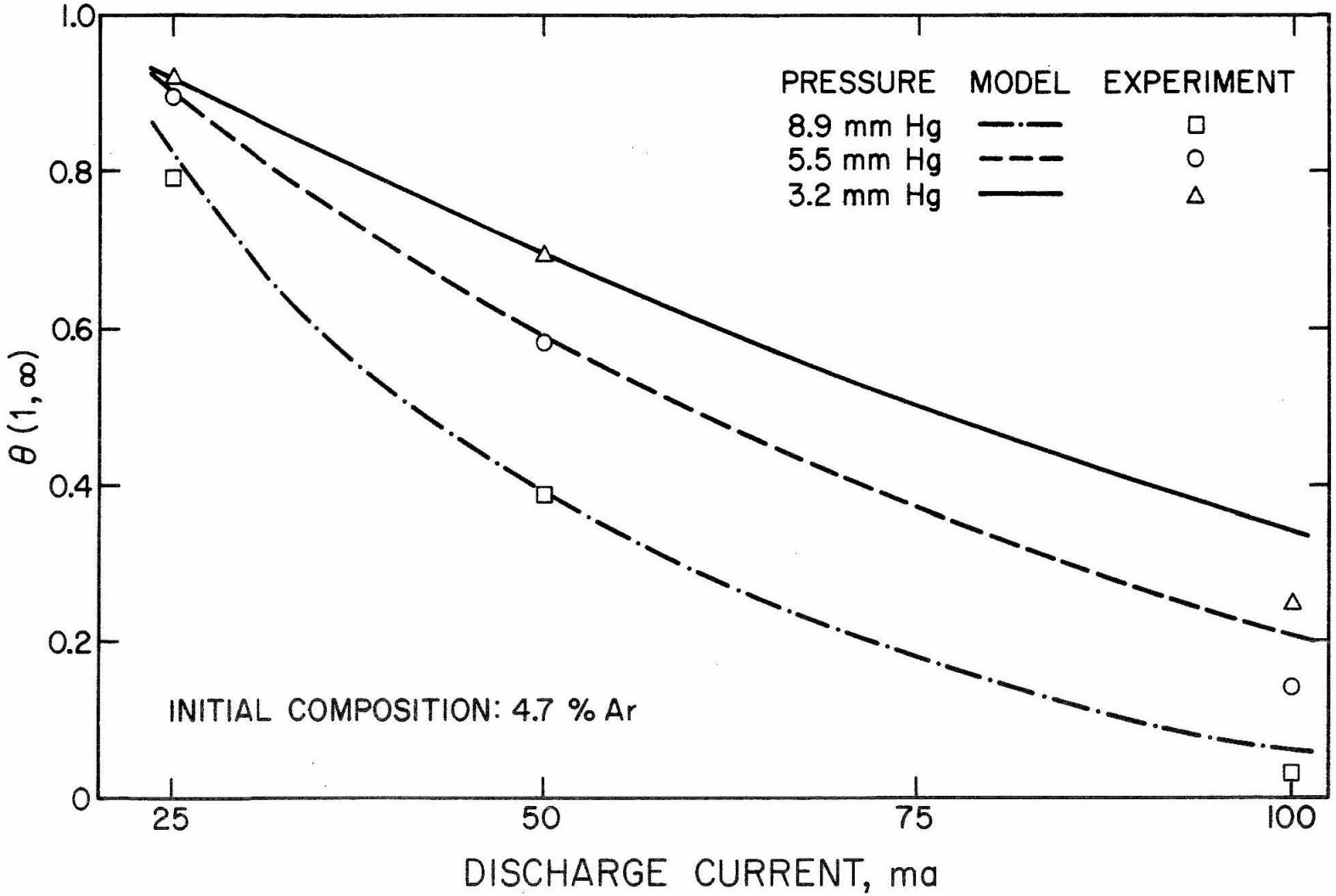

Figure 12. Comparison of Model and Experiment for Steady-State Separation as a Function of Discharge Current in He-Ar for Different Pressures

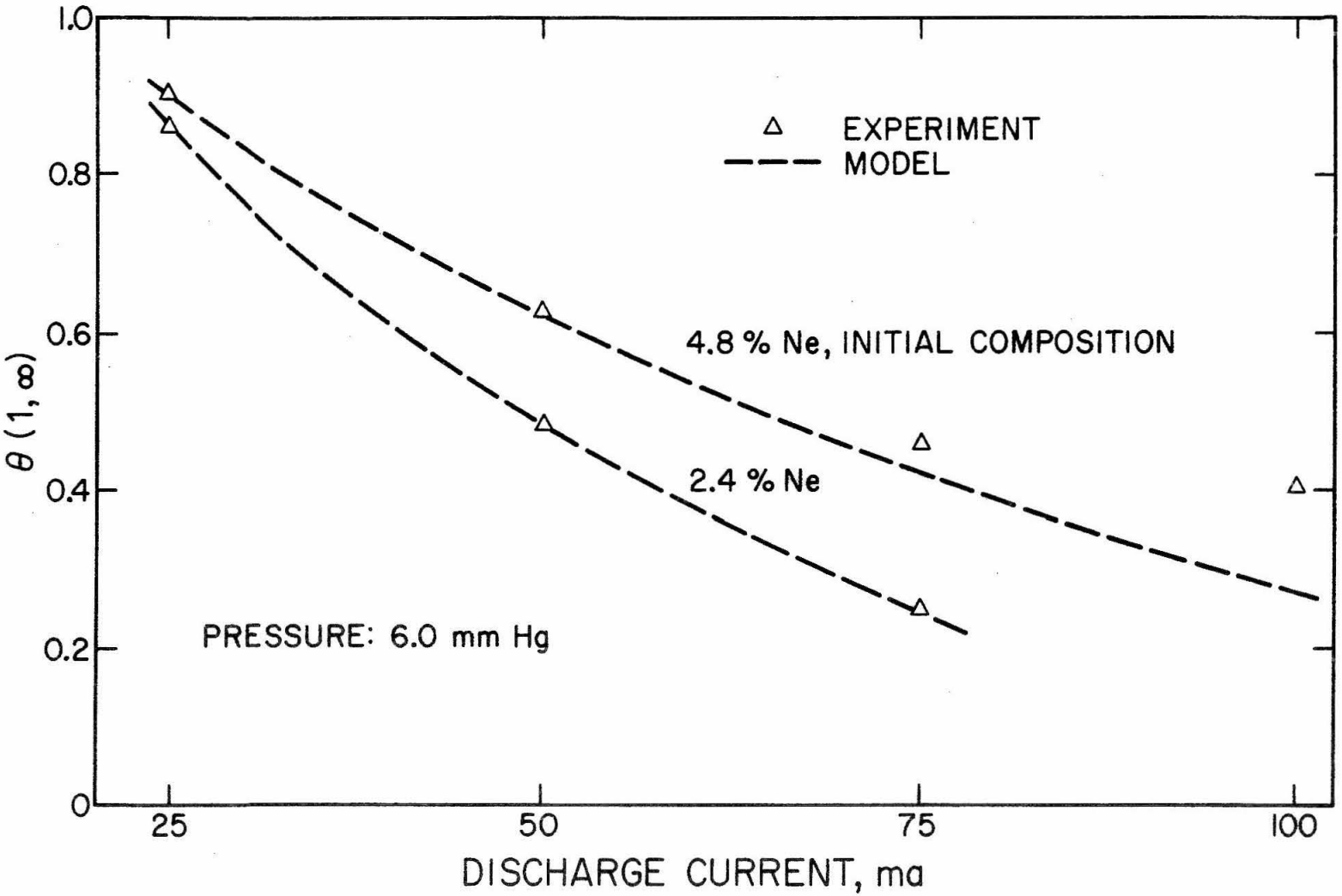

Figure 13. Comparison of Model and Experiment for Steady-State Separation as a Function of Discharge Current in He-Ne for Different Initial Compositions

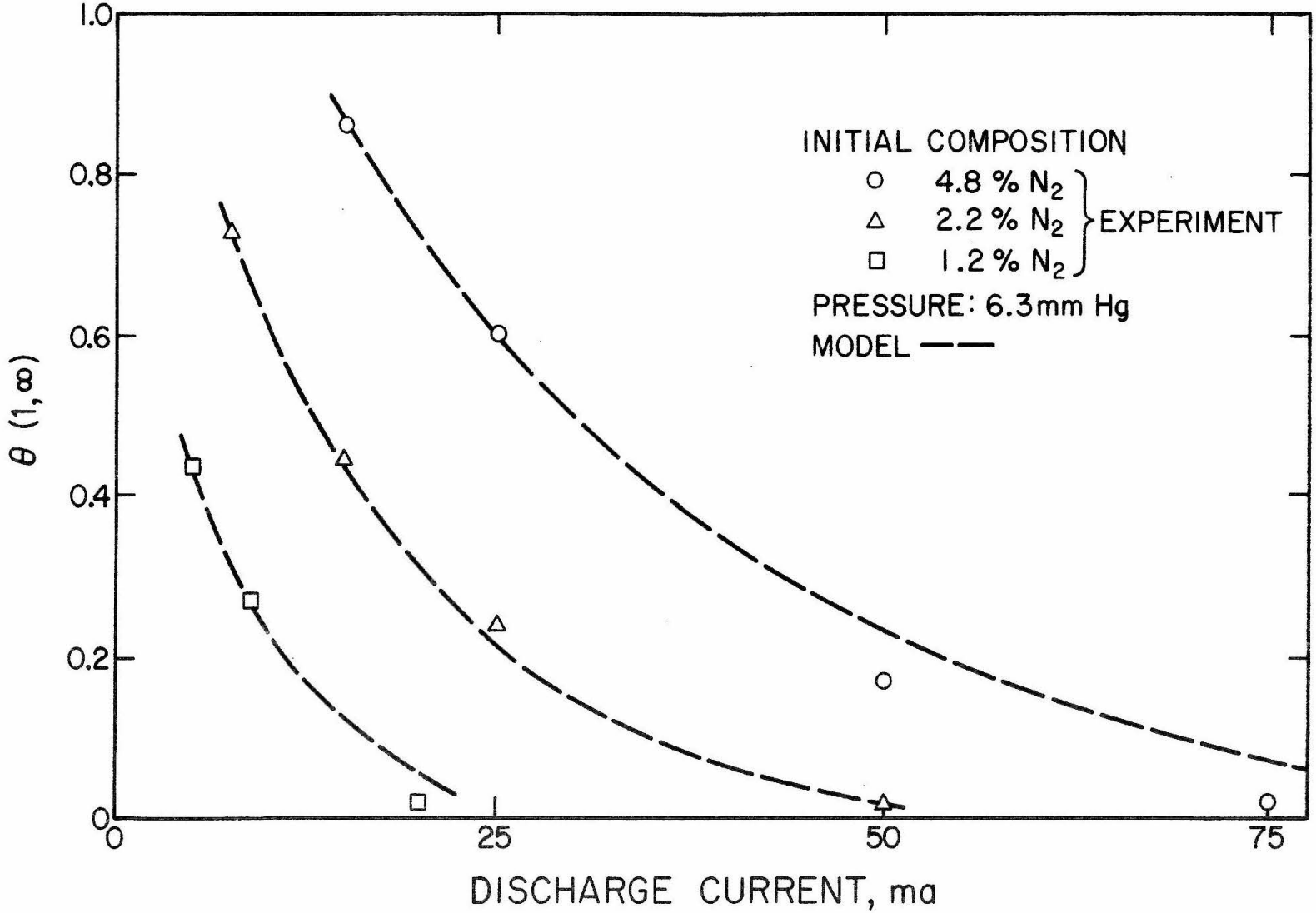

Figure 14. Comparison of Model and Experiment for Steady-State Separation as a Function of Discharge Current in He-N_2 for Different Initial Compositions

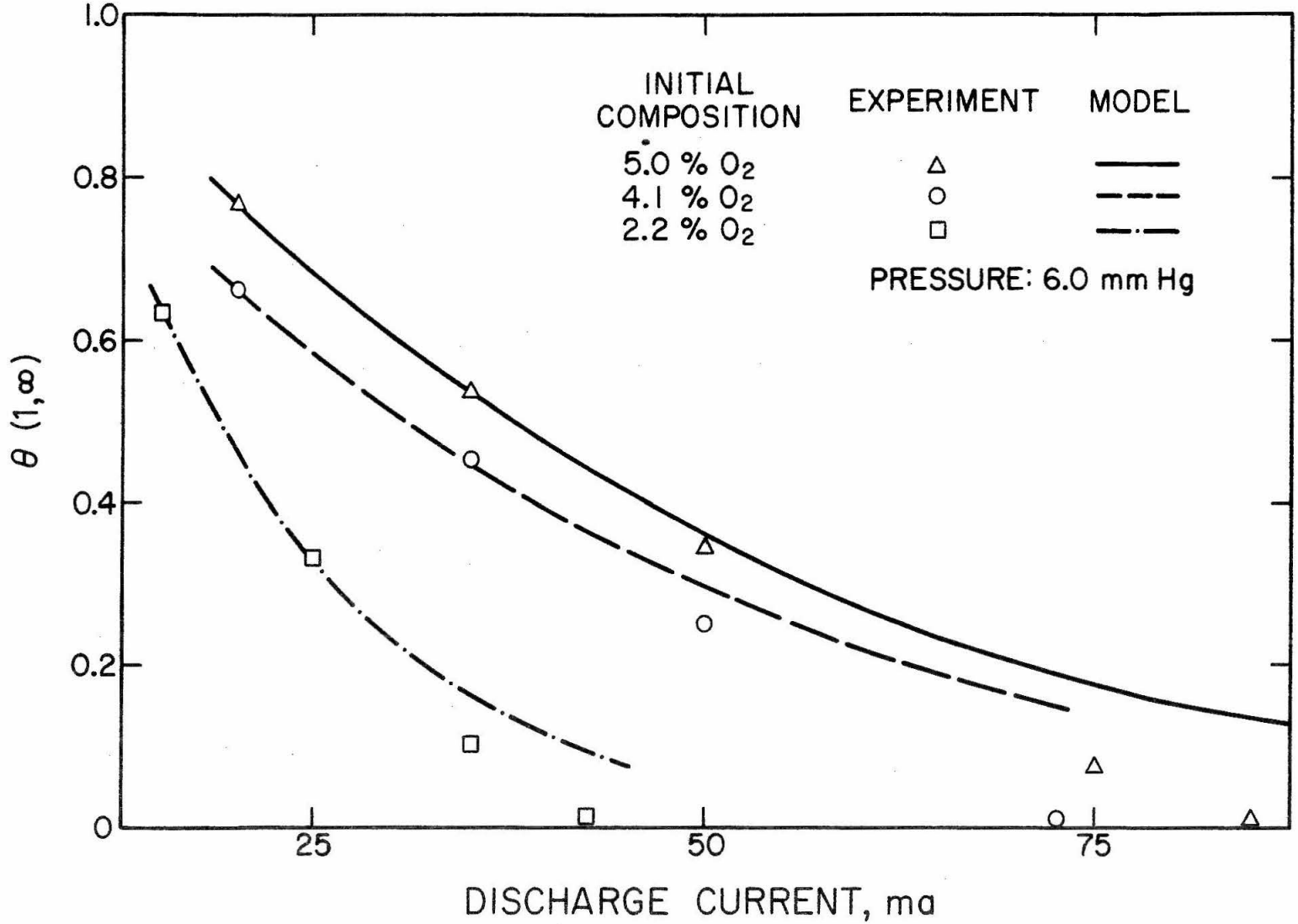

Figure 15. Comparison of Model and Experiment for Steady-State Separation as a Function of Discharge Current in He-O_2 for Different Initial Compositions

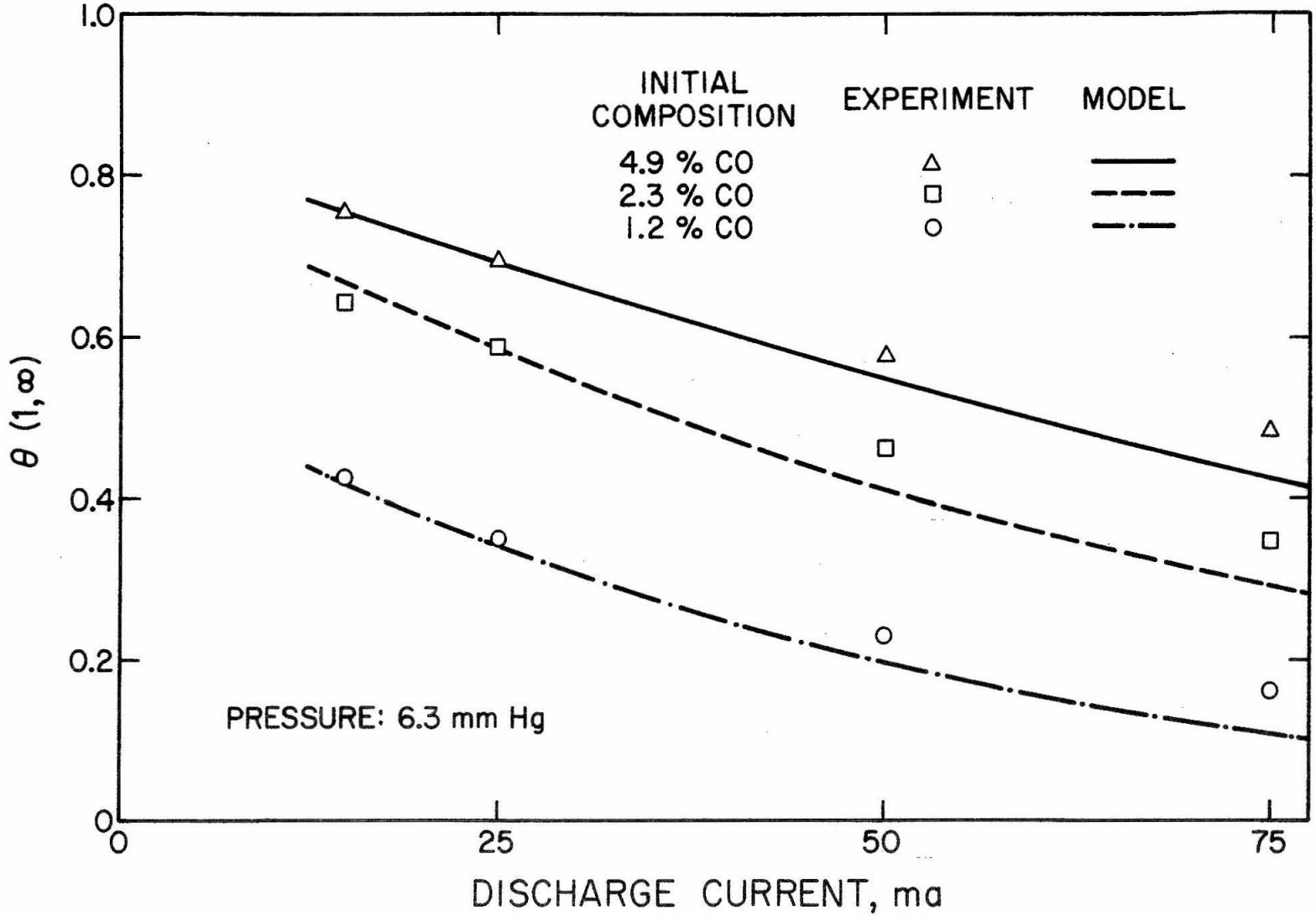

Figure 16. Comparison of Model and Experiment for Steady-State Separation as a Function of Discharge Current in He-CO for Different Initial Compositions

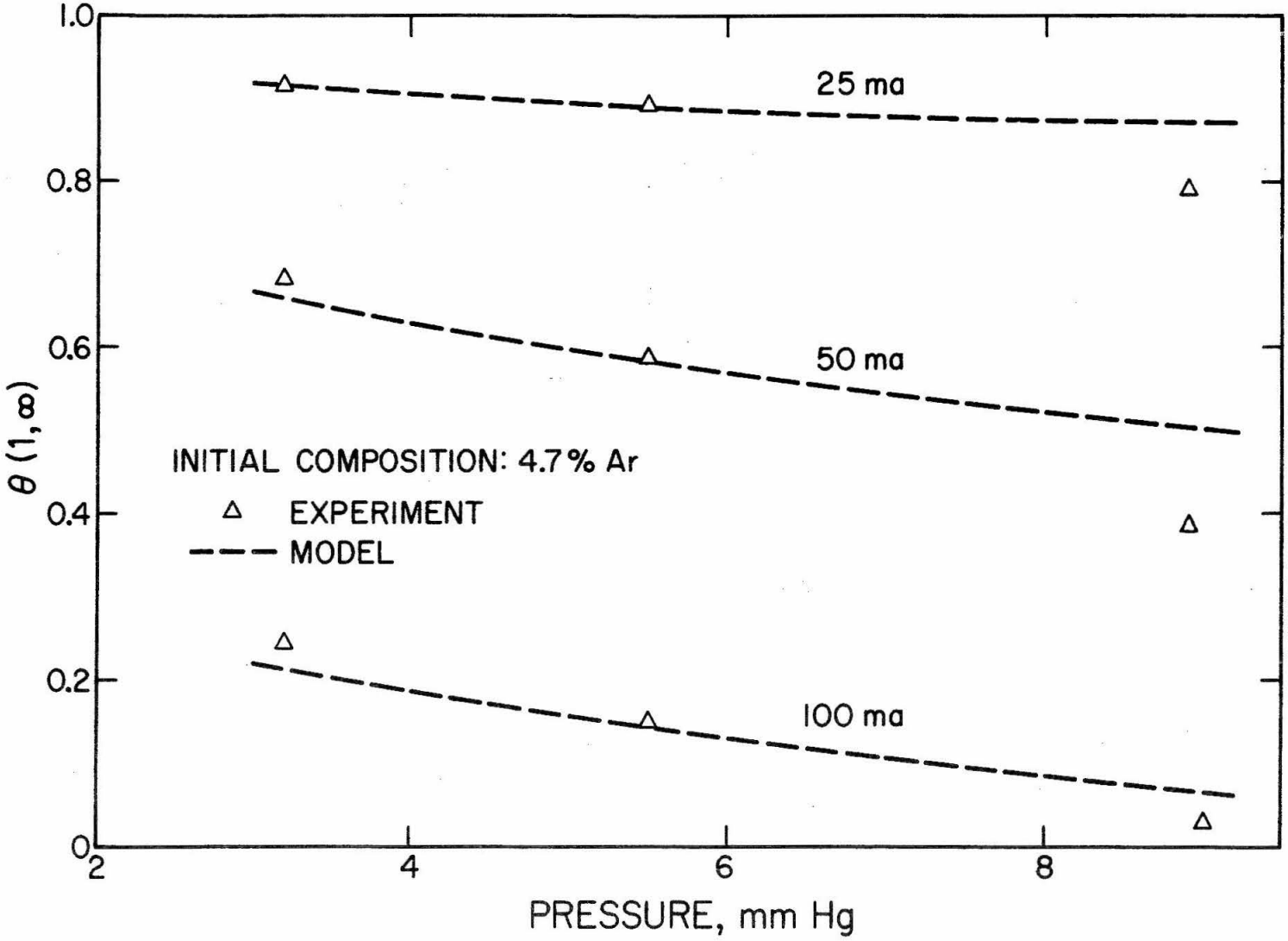

Figure 17. Comparison of Model and Experiment for Steady-State Separation as a Function of Pressure in He-Ar for Different Discharge Currents

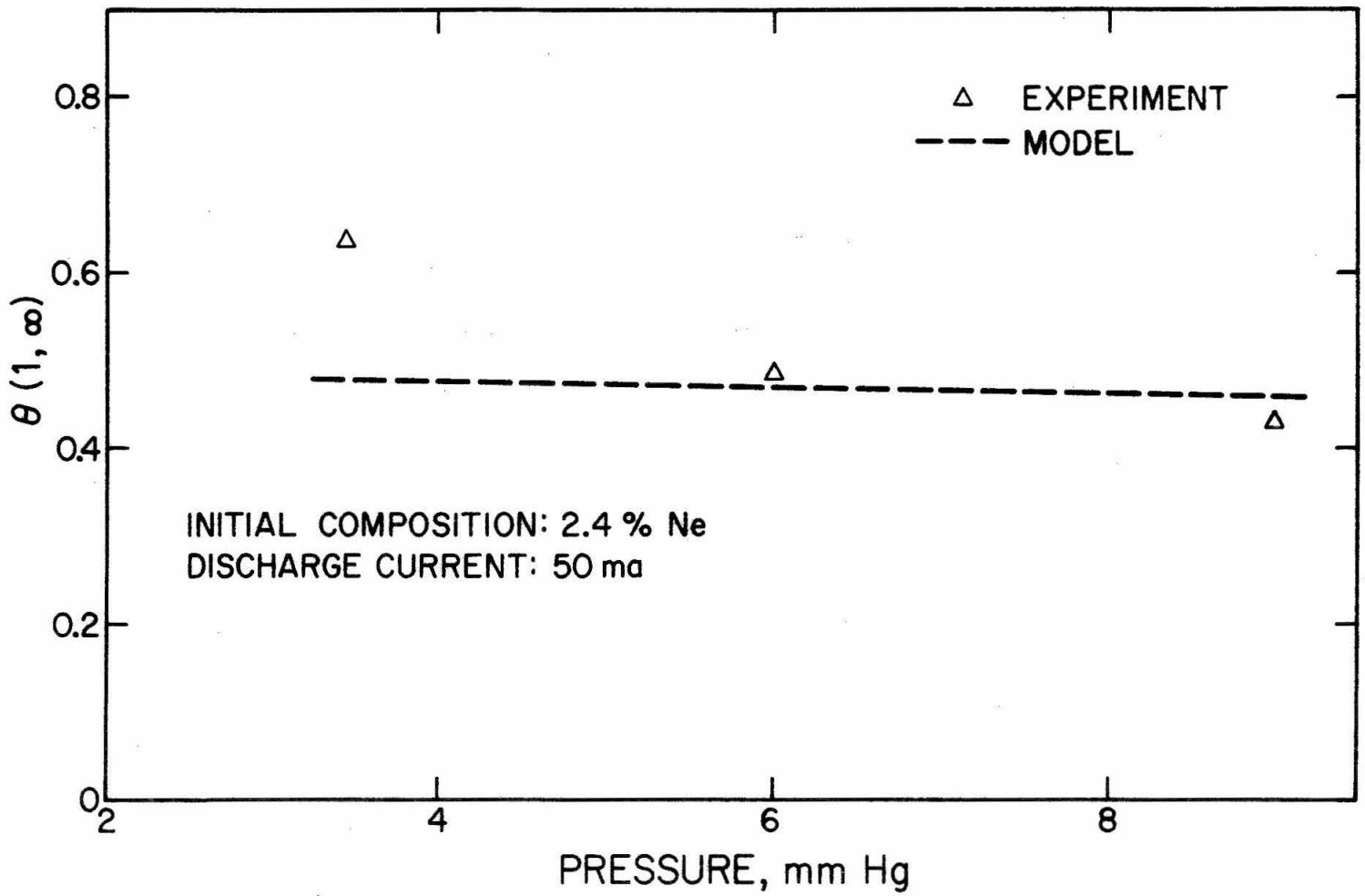

Figure 18. Comparison of Model and Experiment for Steady-State Separation as a Function of Pressure in He-Ne

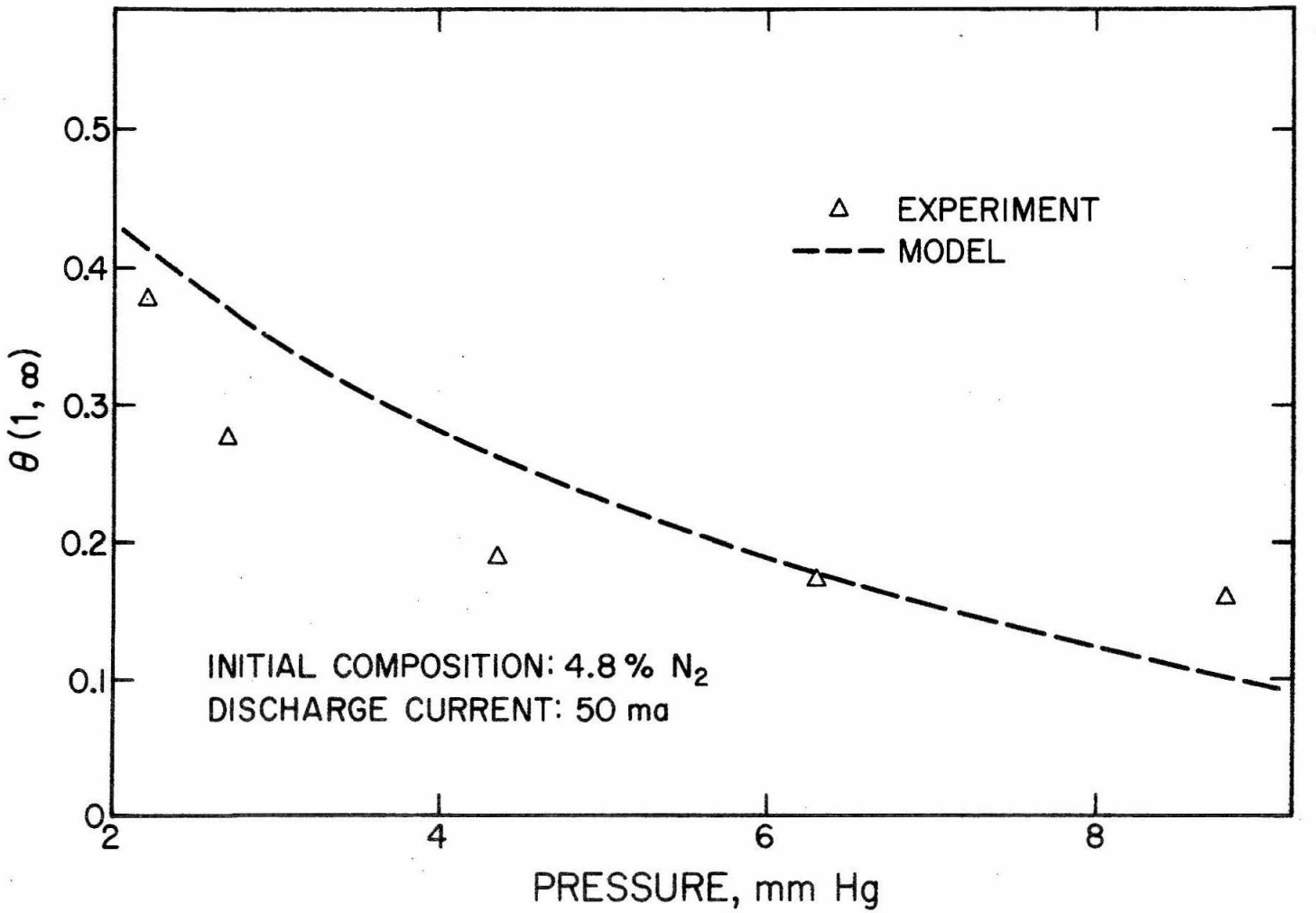

Figure 19. Comparison of Model and Experiment for Steady-State Separation as a Function of Pressure in $He-N_2$

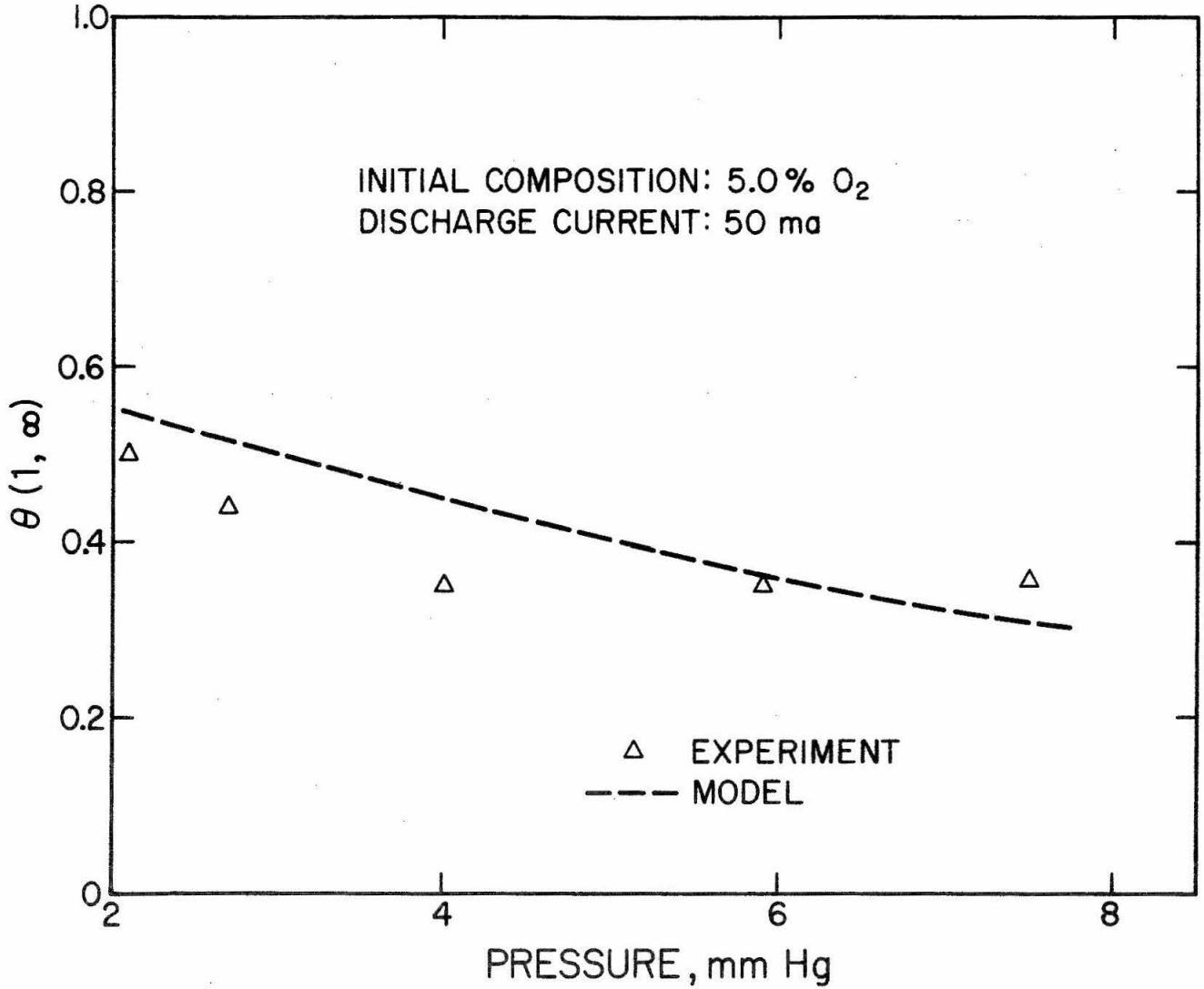

Figure 20. Comparison of Model and Experiment for Steady-State Separation as a Function of Pressure in He-O_2

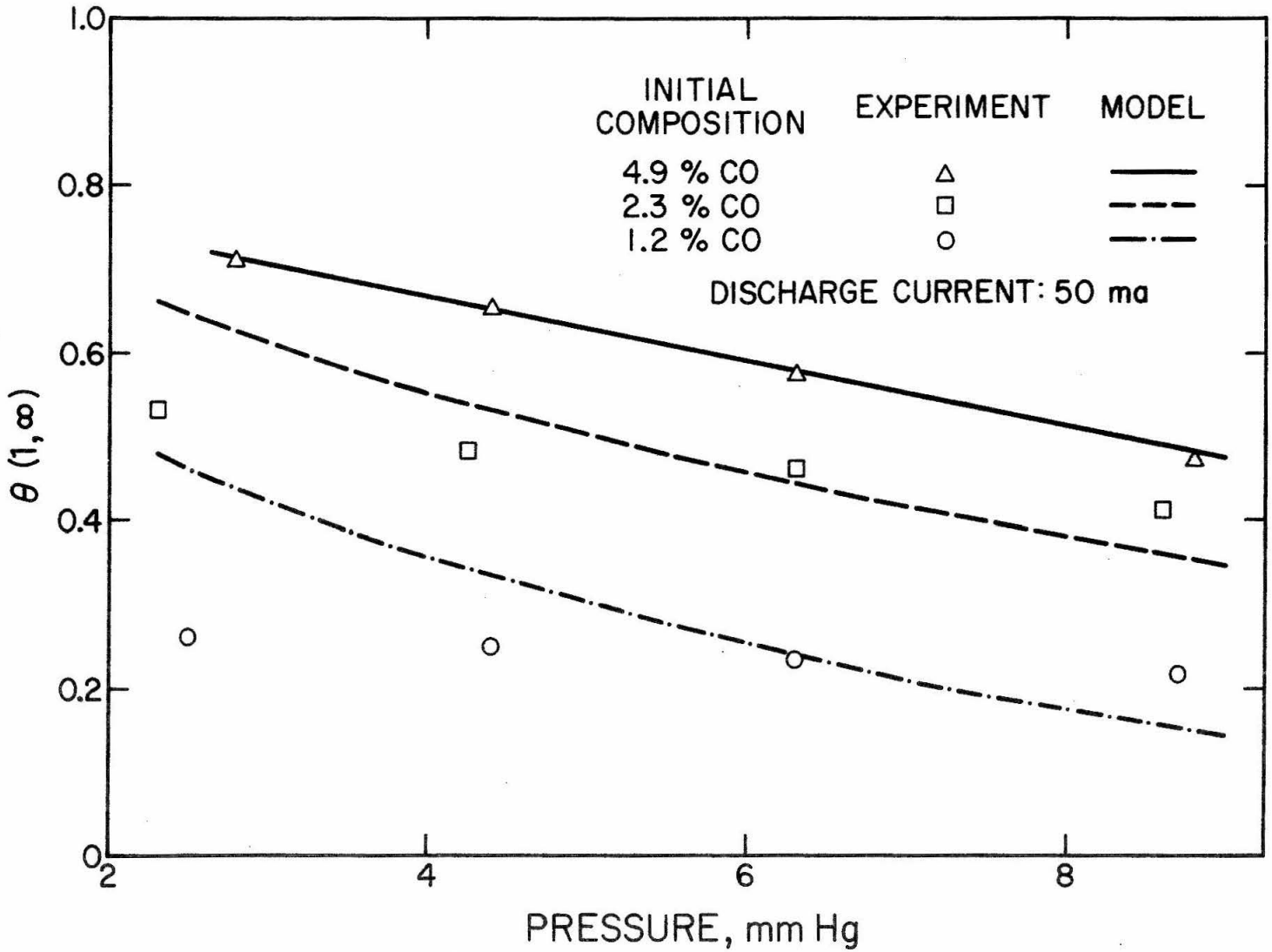

Figure 21. Comparison of Model and Experiment for Steady-State Separation as a Function of Pressure in He-CO for Different Initial Compositions

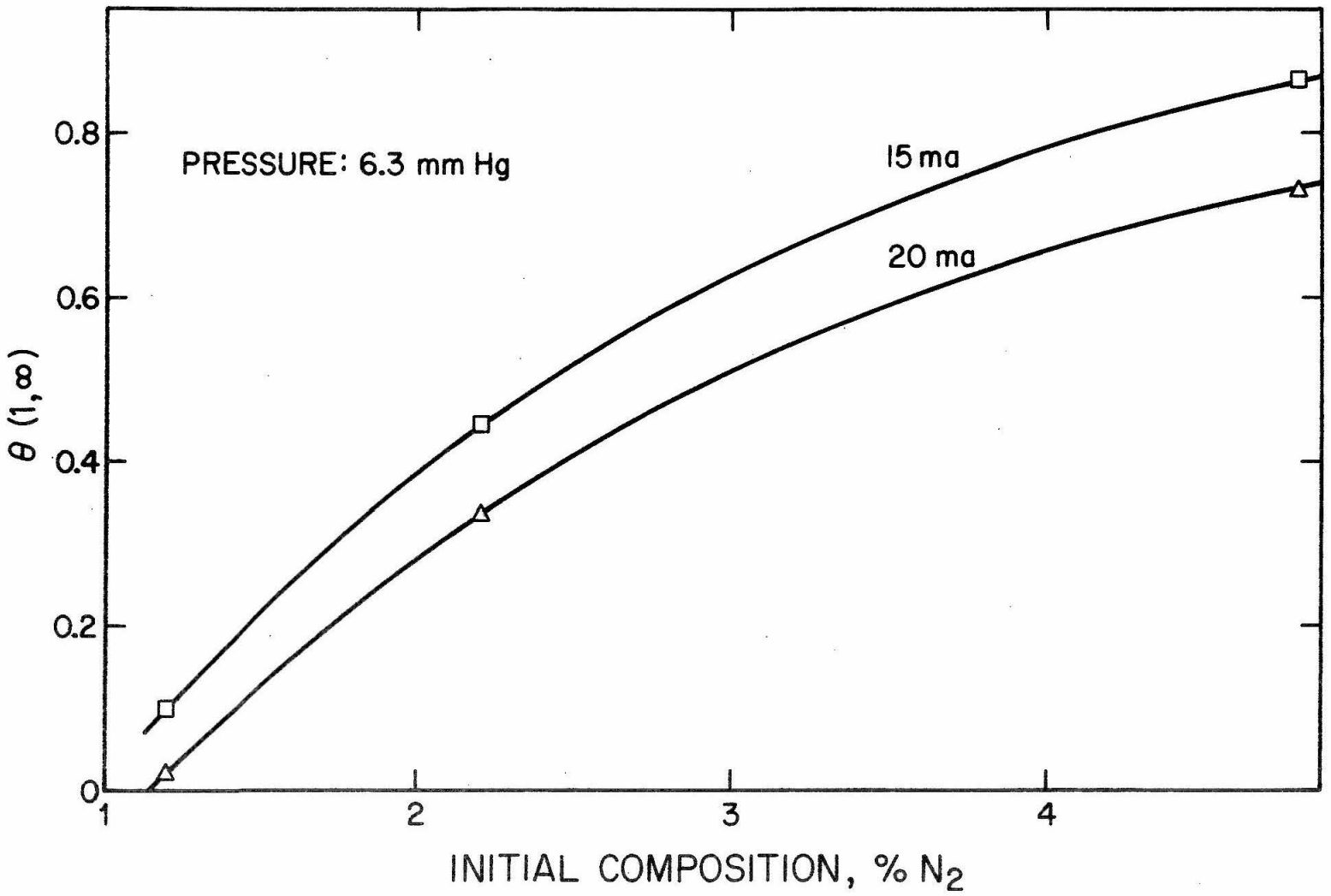

Figure 22. Steady-State Separation as a Function of Initial Composition in He-N_2 for Different Discharge Currents

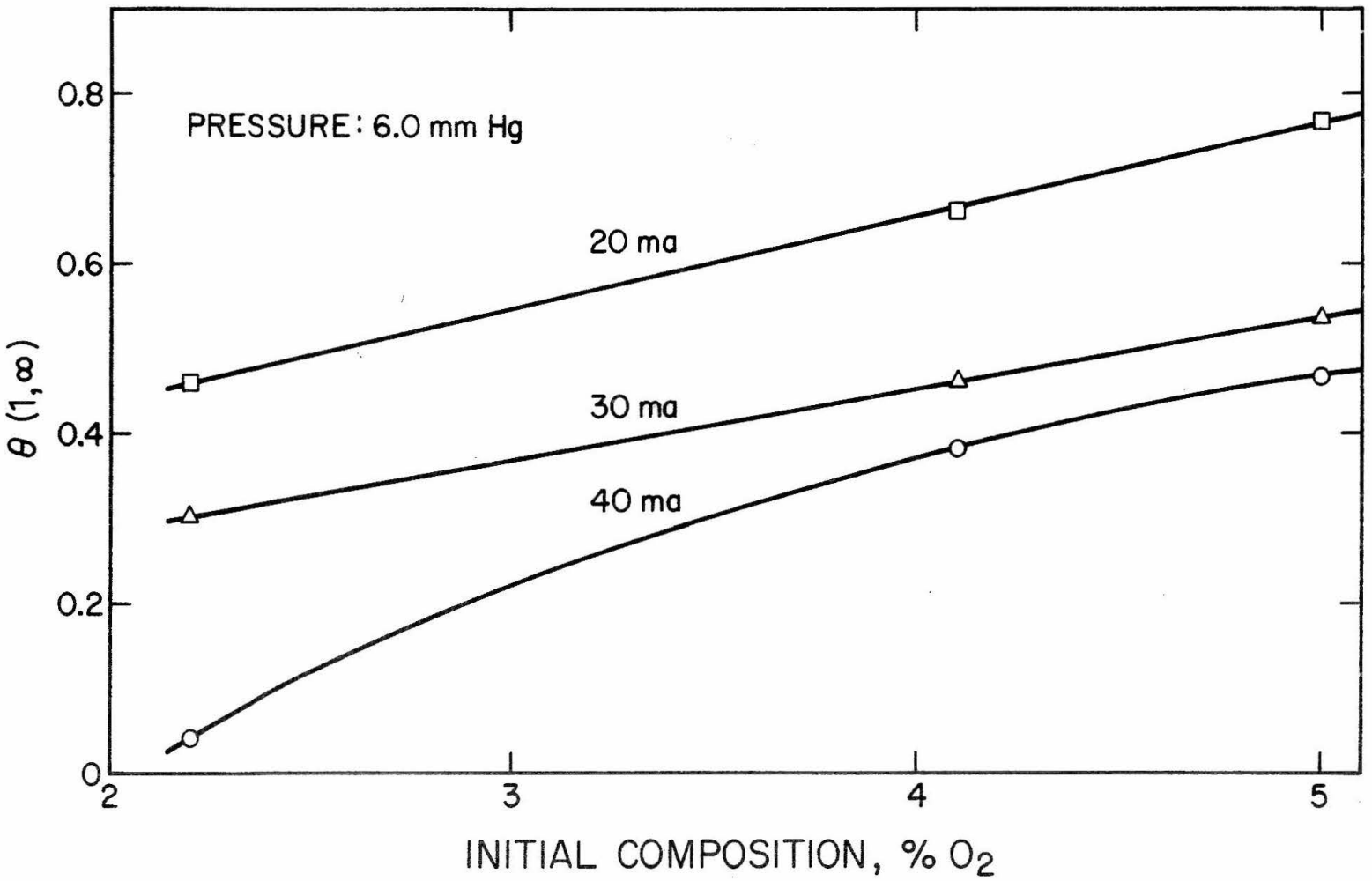

Figure 23. Steady-State Separation as a Function of Initial Composition in He-O_2 for Different Discharge Currents

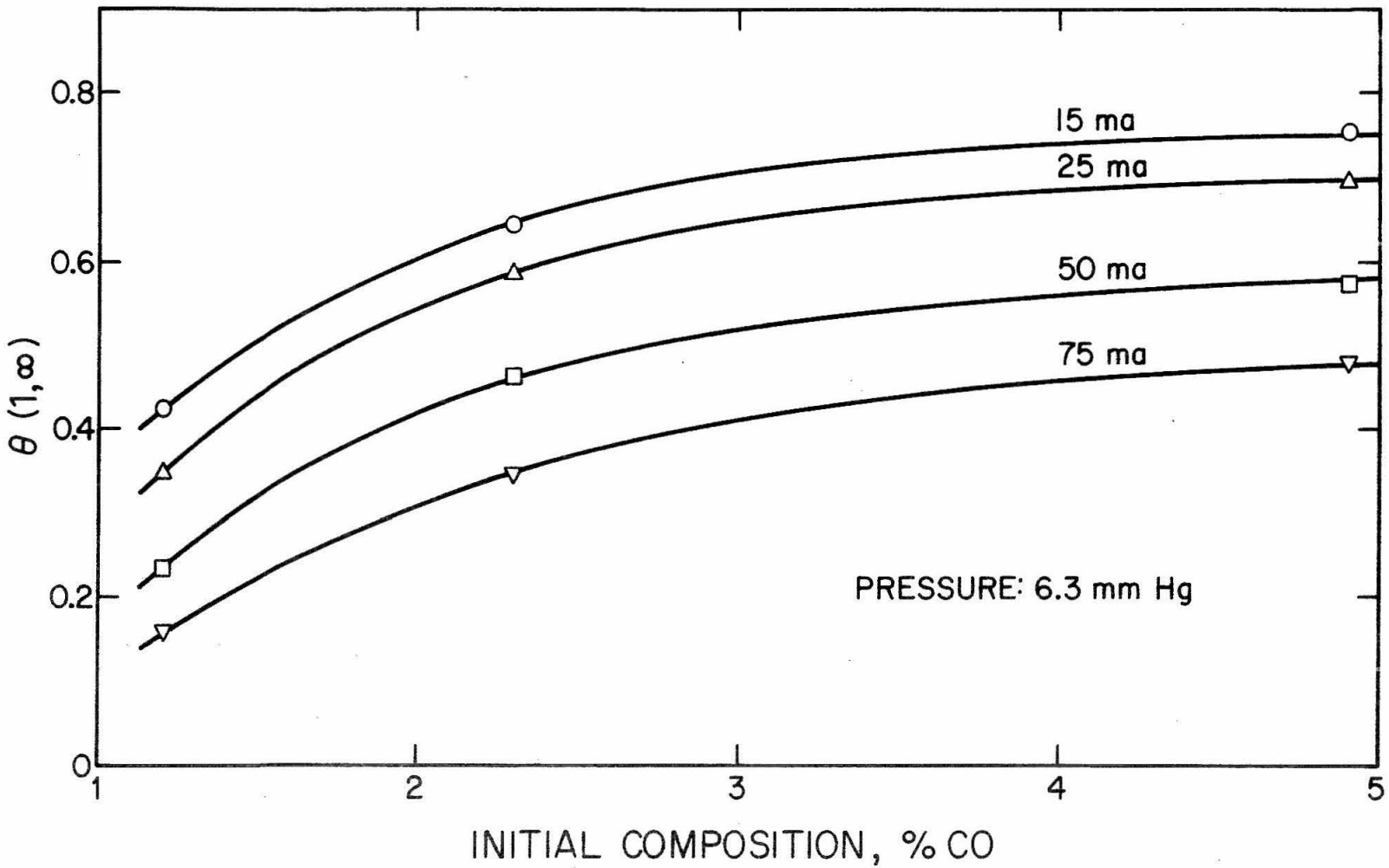

Figure 24. Steady-State Separation as a Function of Initial Composition in He-CO for Different Discharge Currents

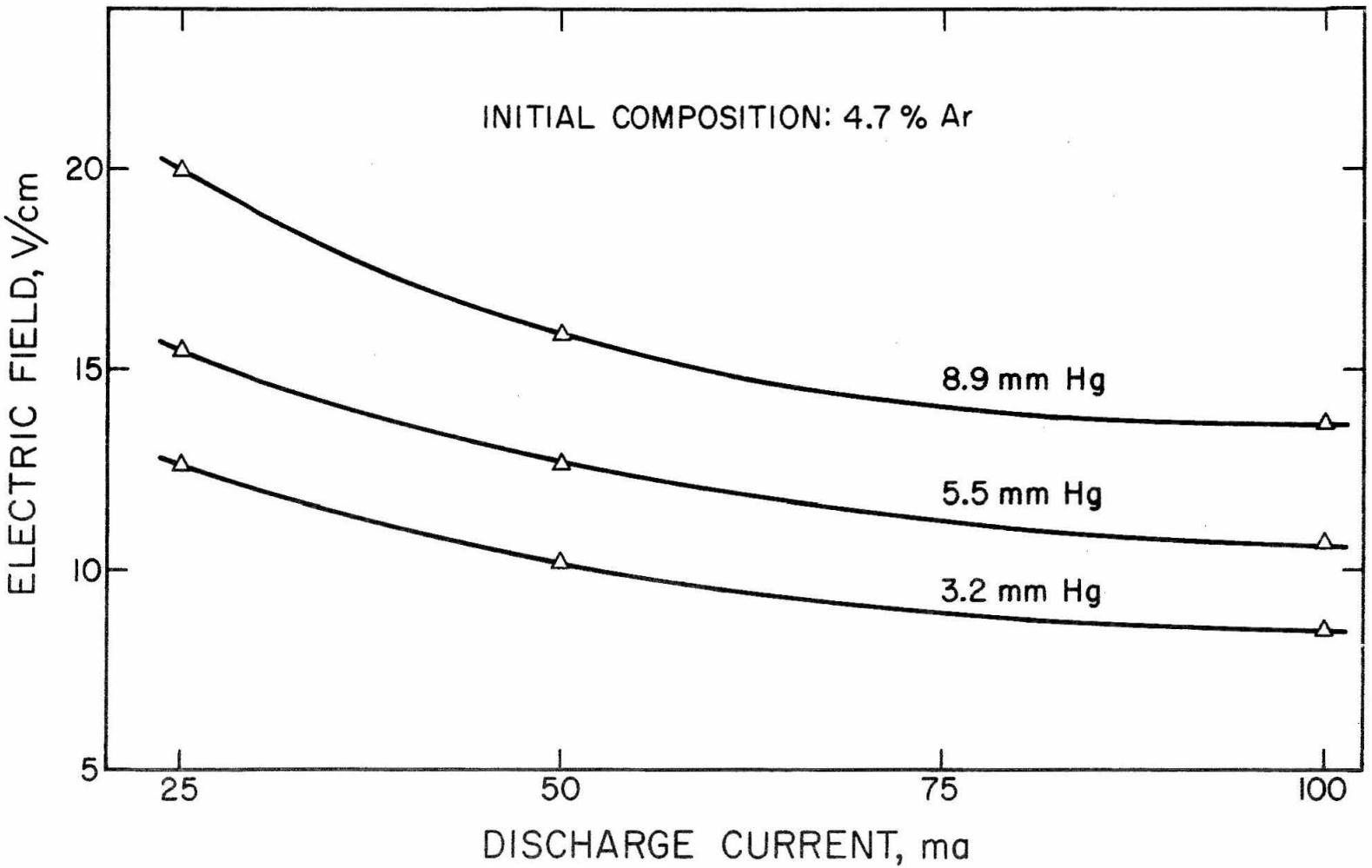

Figure 25. Measured Electric Field as a Function of Discharge Current in He-Ar for Different Pressures

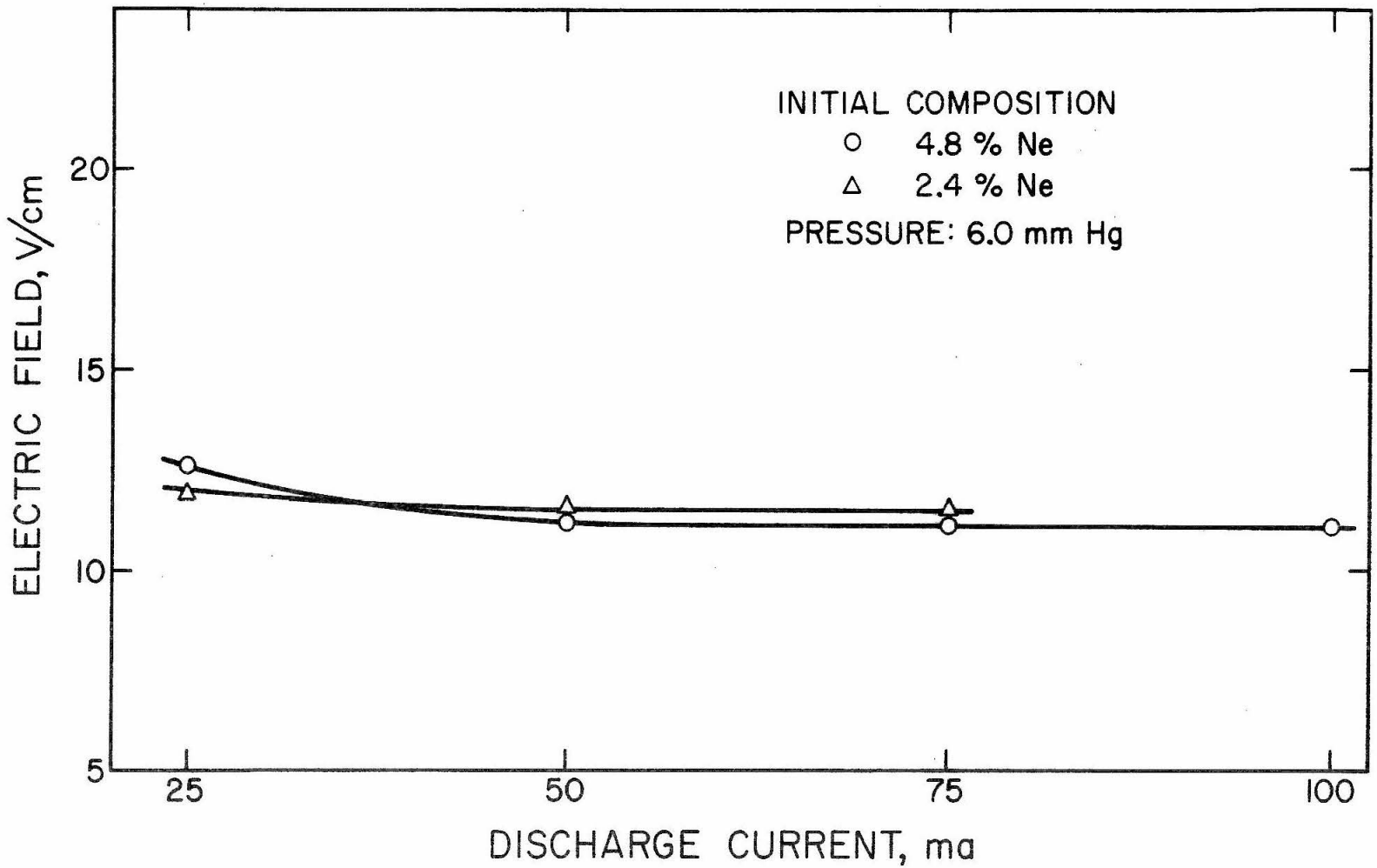

Figure 26. Measured Electric Field as a Function of Discharge Current in He-Ne for Different Initial Compositions

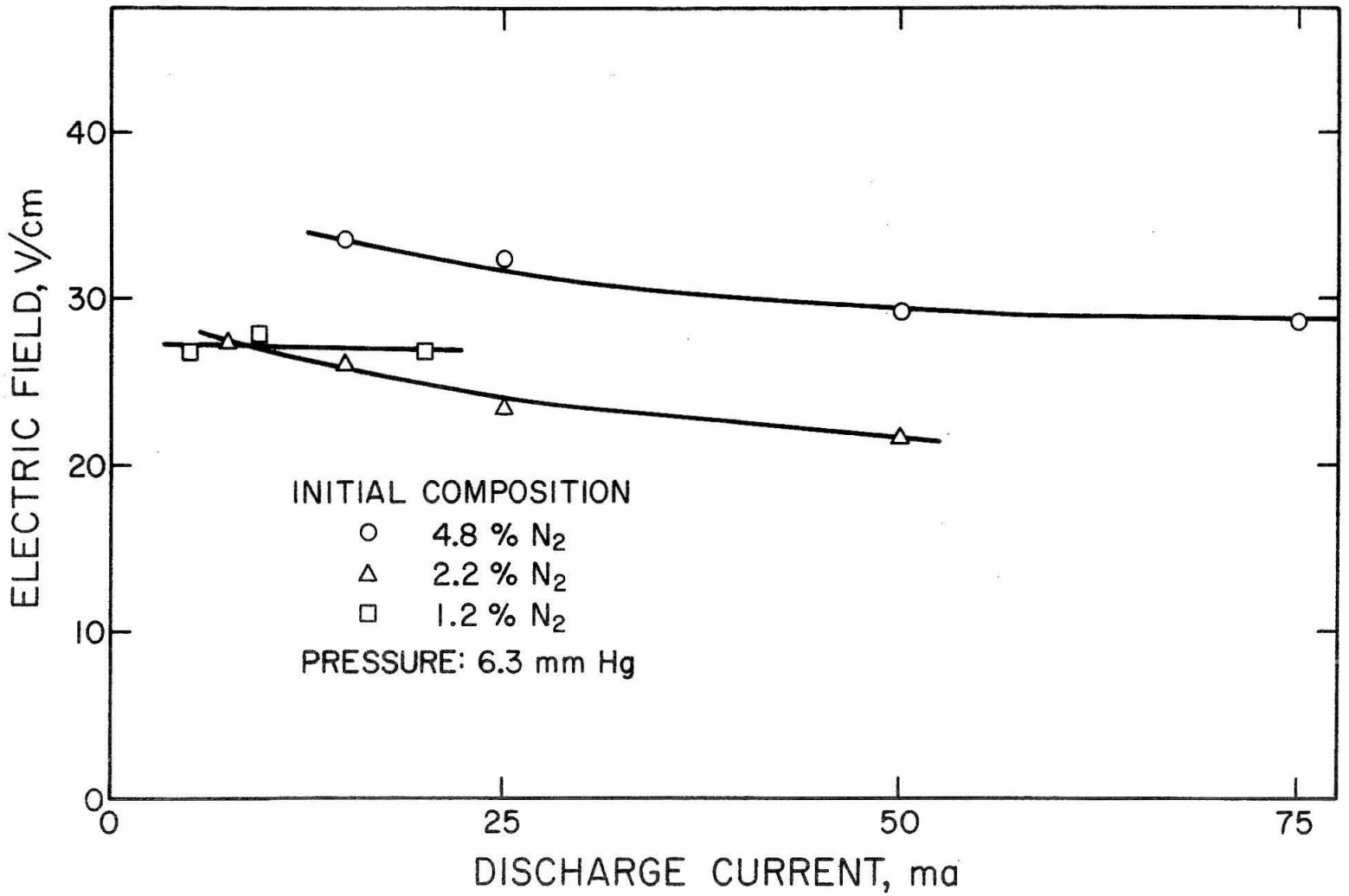

Figure 27. Measured Electric Field as a Function of Discharge Current in He-N_2 for Different Initial Compositions

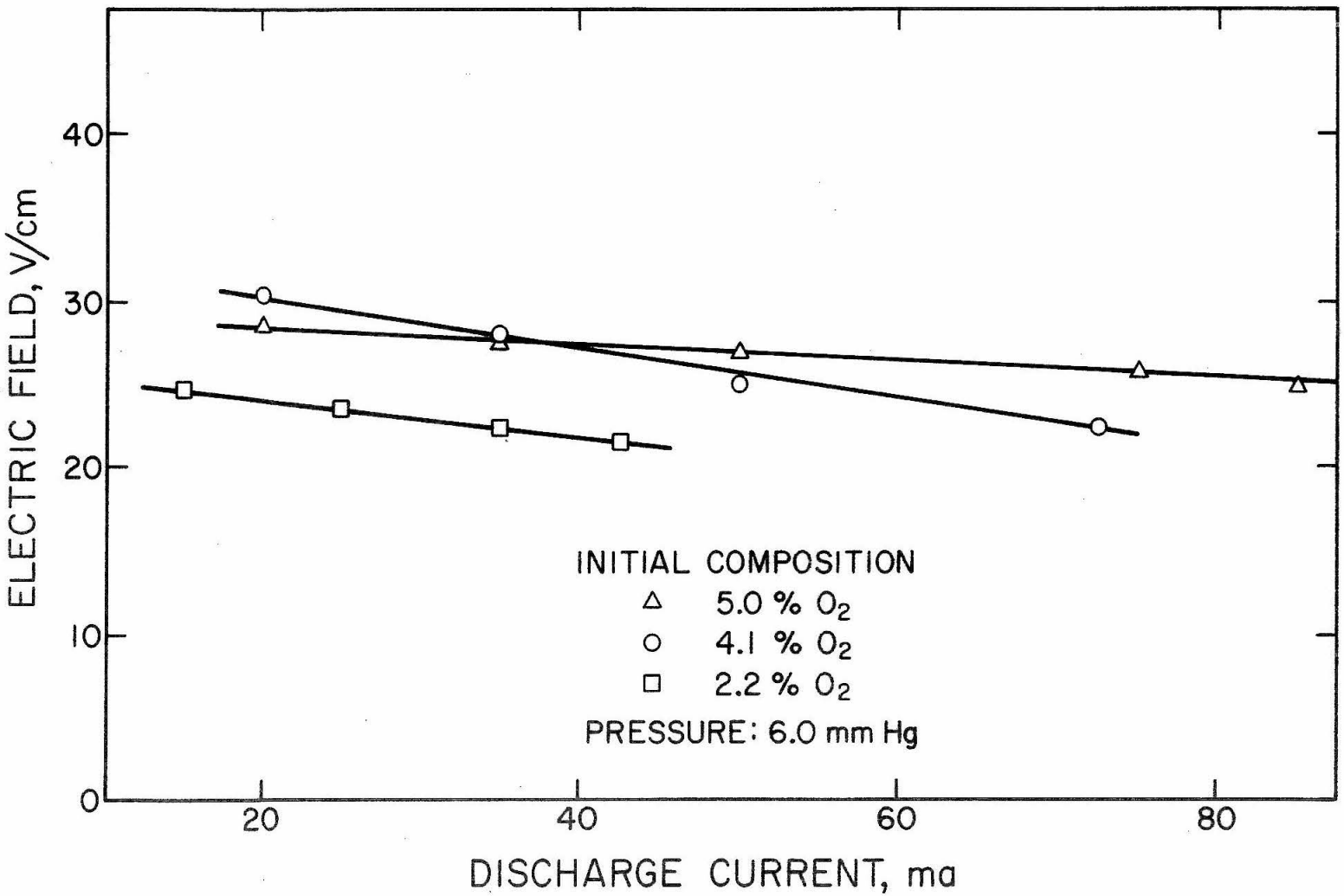

Figure 28. Measured Electric Field as a Function of Discharge Current in He-O_2 for Different Initial Compositions

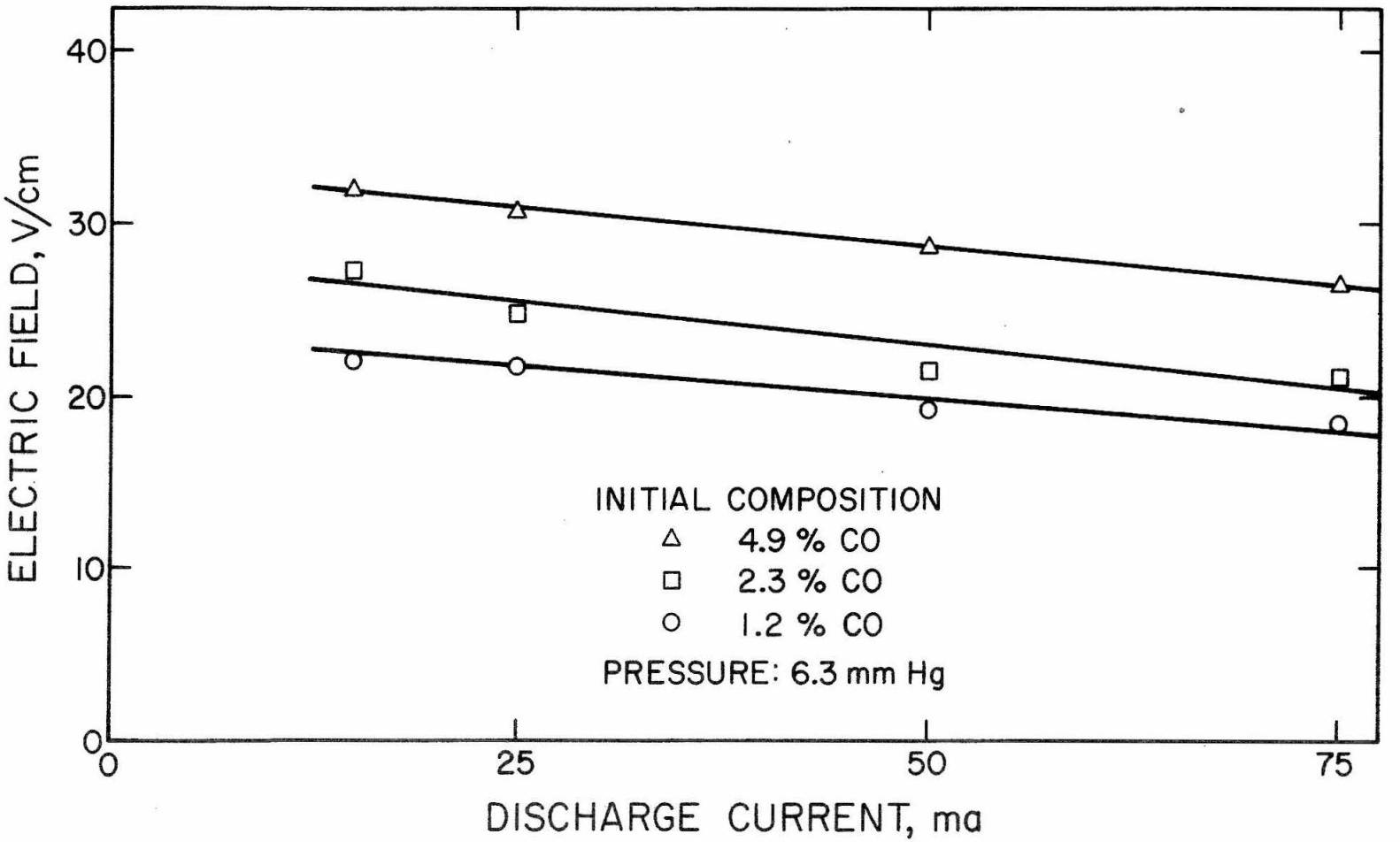

Figure 29. Measured Electric Field as a Function of Discharge Current in He-CO for Different Initial Compositions

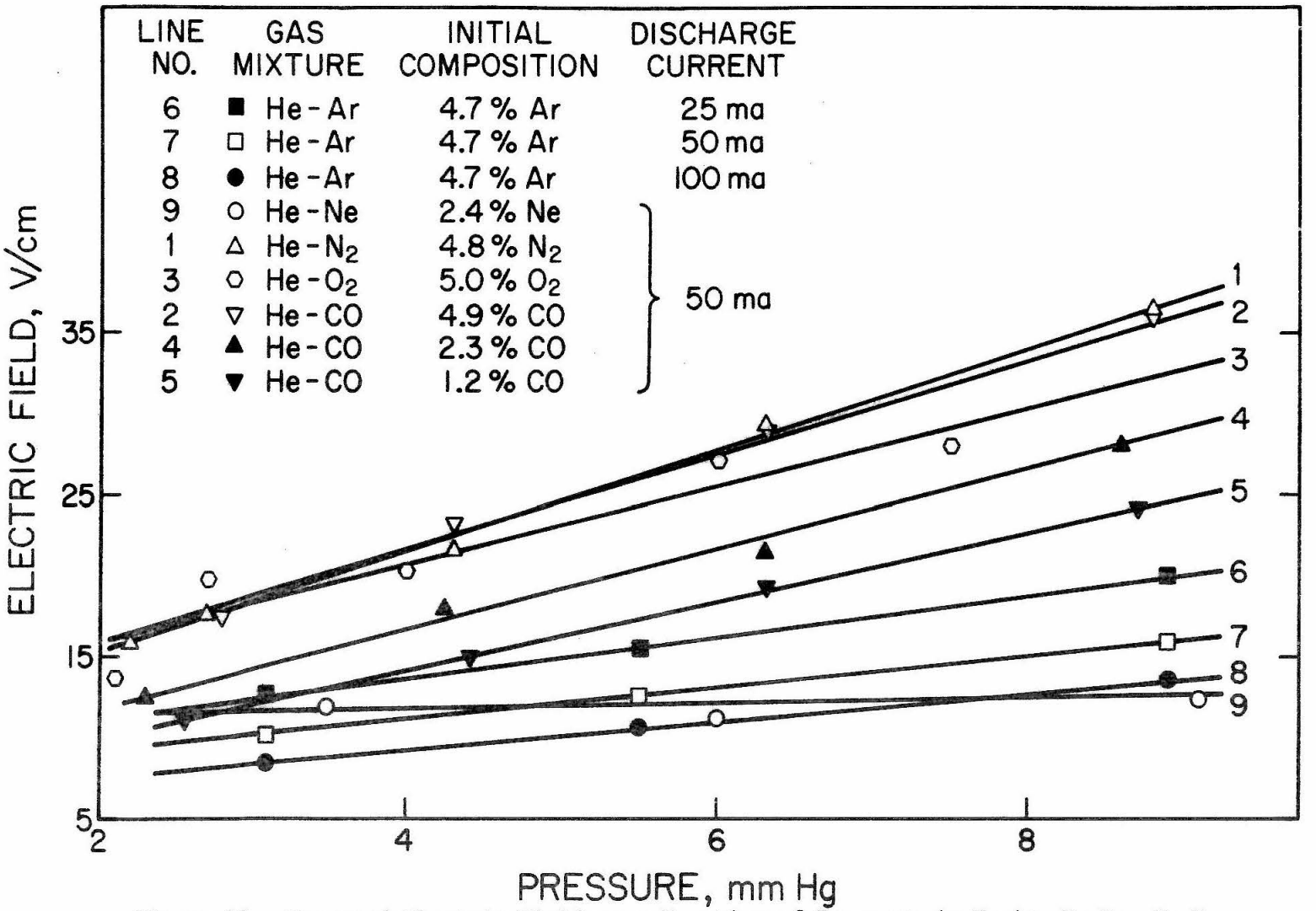

Figure 30. Measured Electric Field as a Function of Pressure in He-Ar, He-Ne, He-N_2, He-O_2, and He-CO

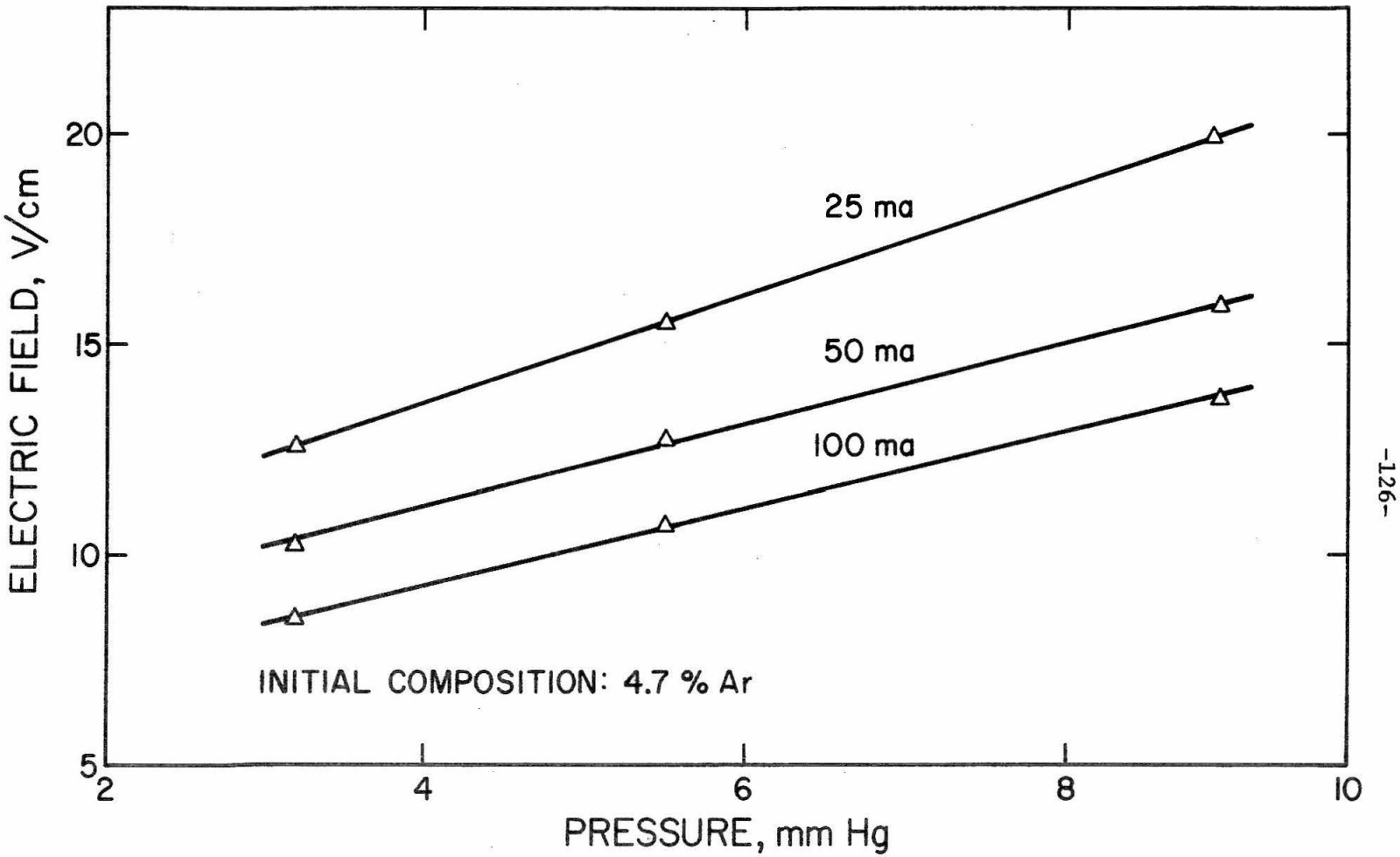

Figure 31. Measured Electric Field as a Function of Pressure in He-Ar for Different Discharge Currents

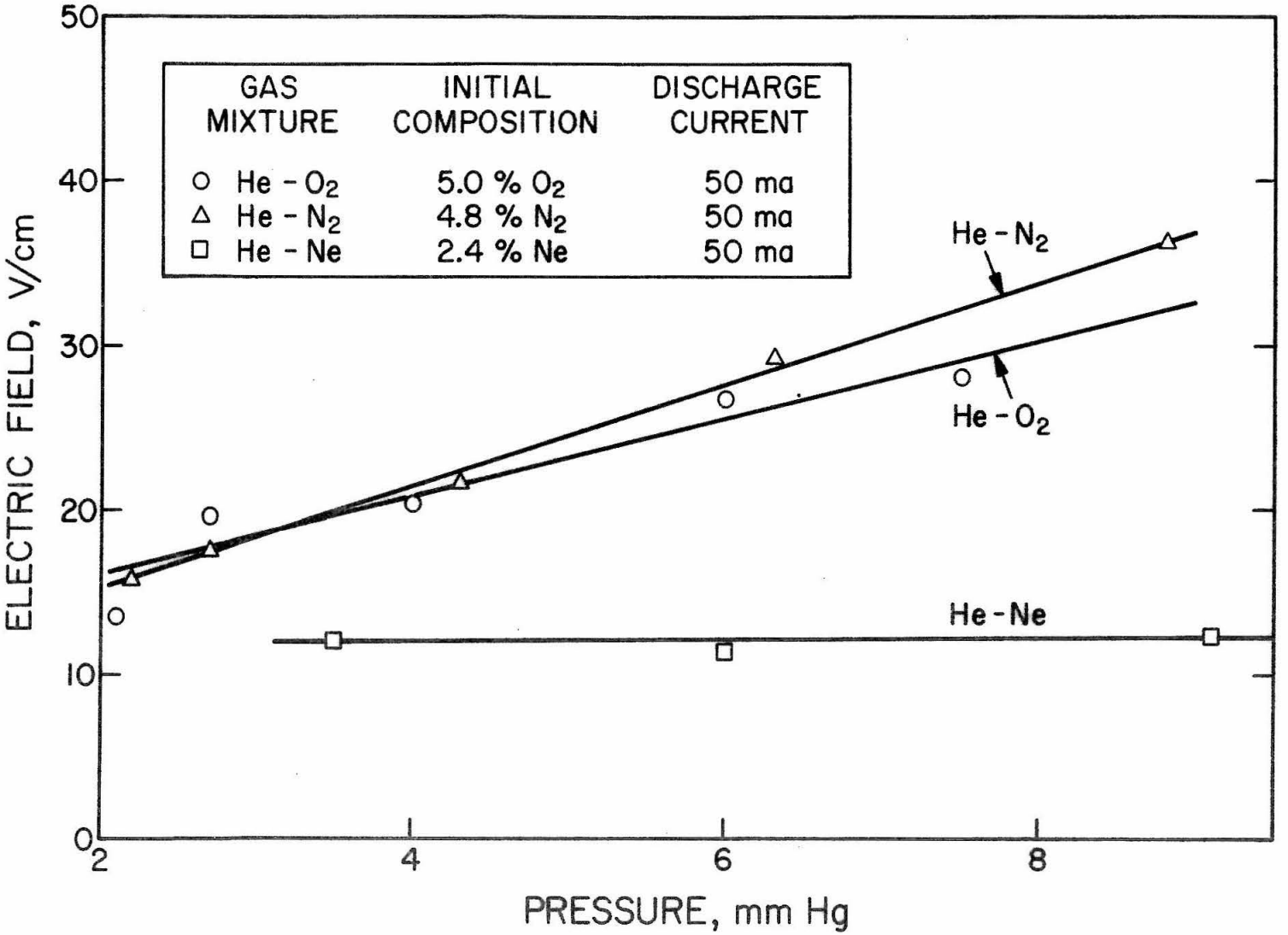

Figure 32. Measured Electric Field as a Function of Pressure in He-Ne, He-N_2 and He-O_2

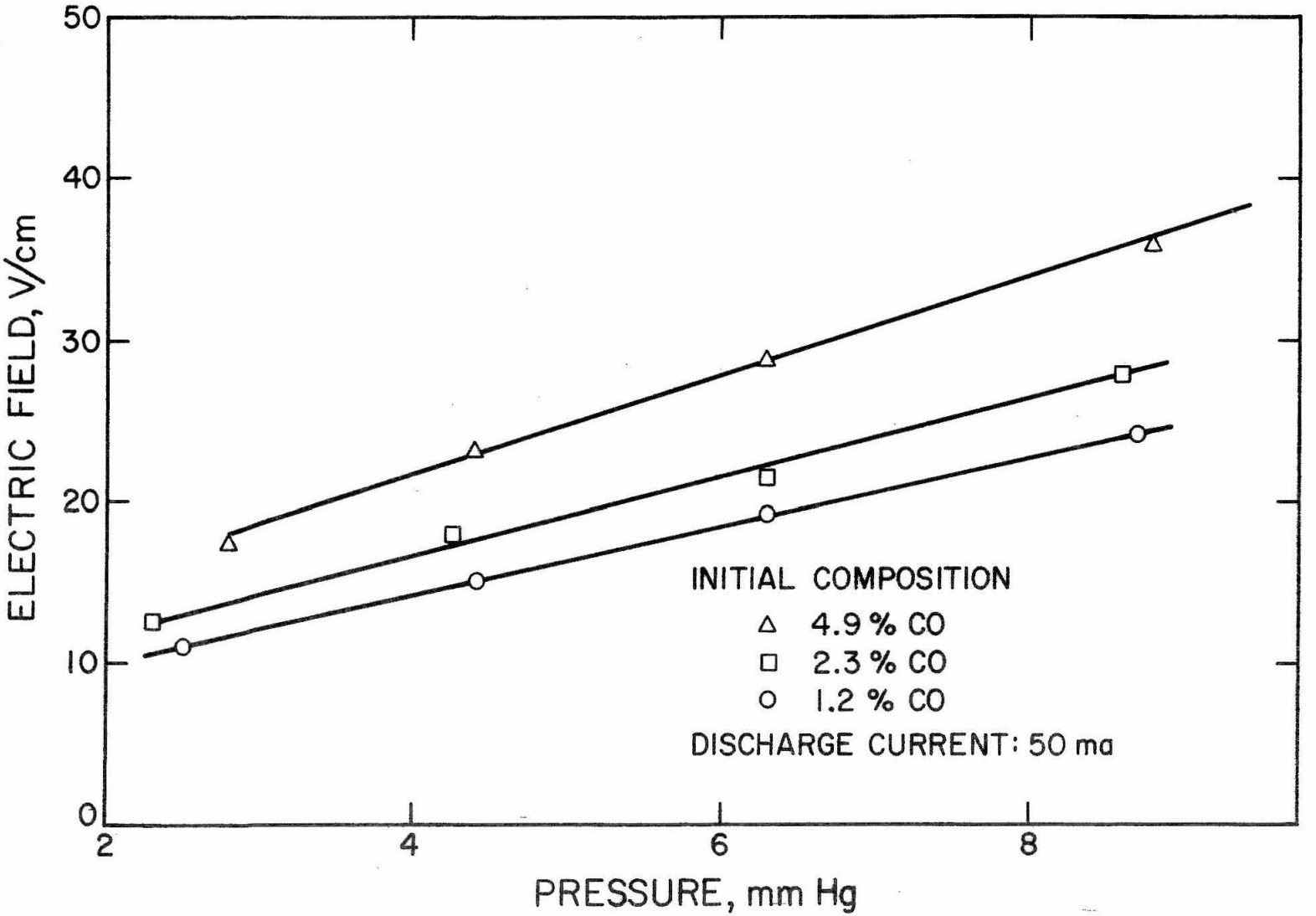

Figure 33. Measured Electric Field as a Function of Pressure in He-CO for Different Initial Compositions

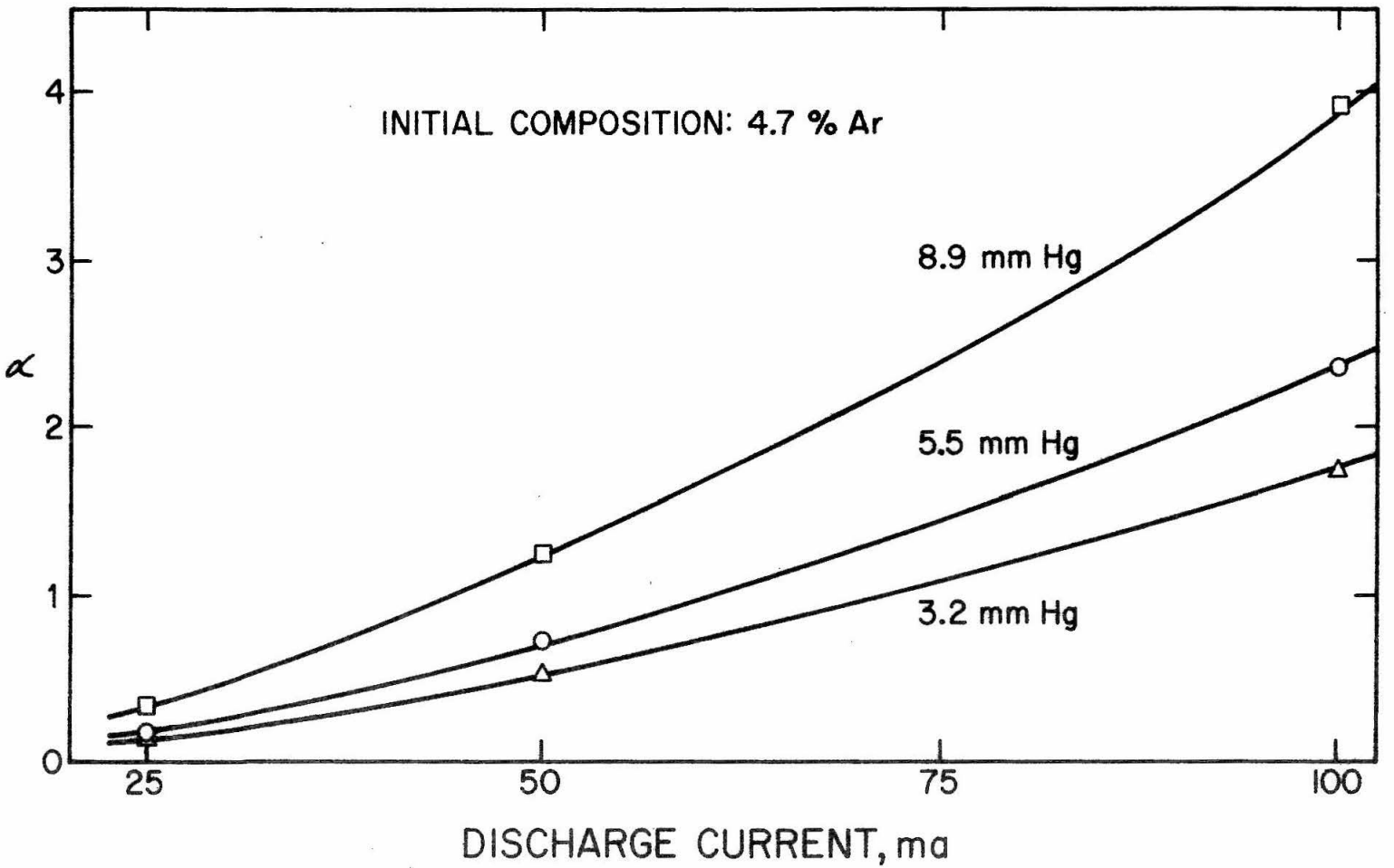

Figure 34. Calculated Electrostatic Peclet Number as a Function of Discharge Current in He-Ar for Different Pressures

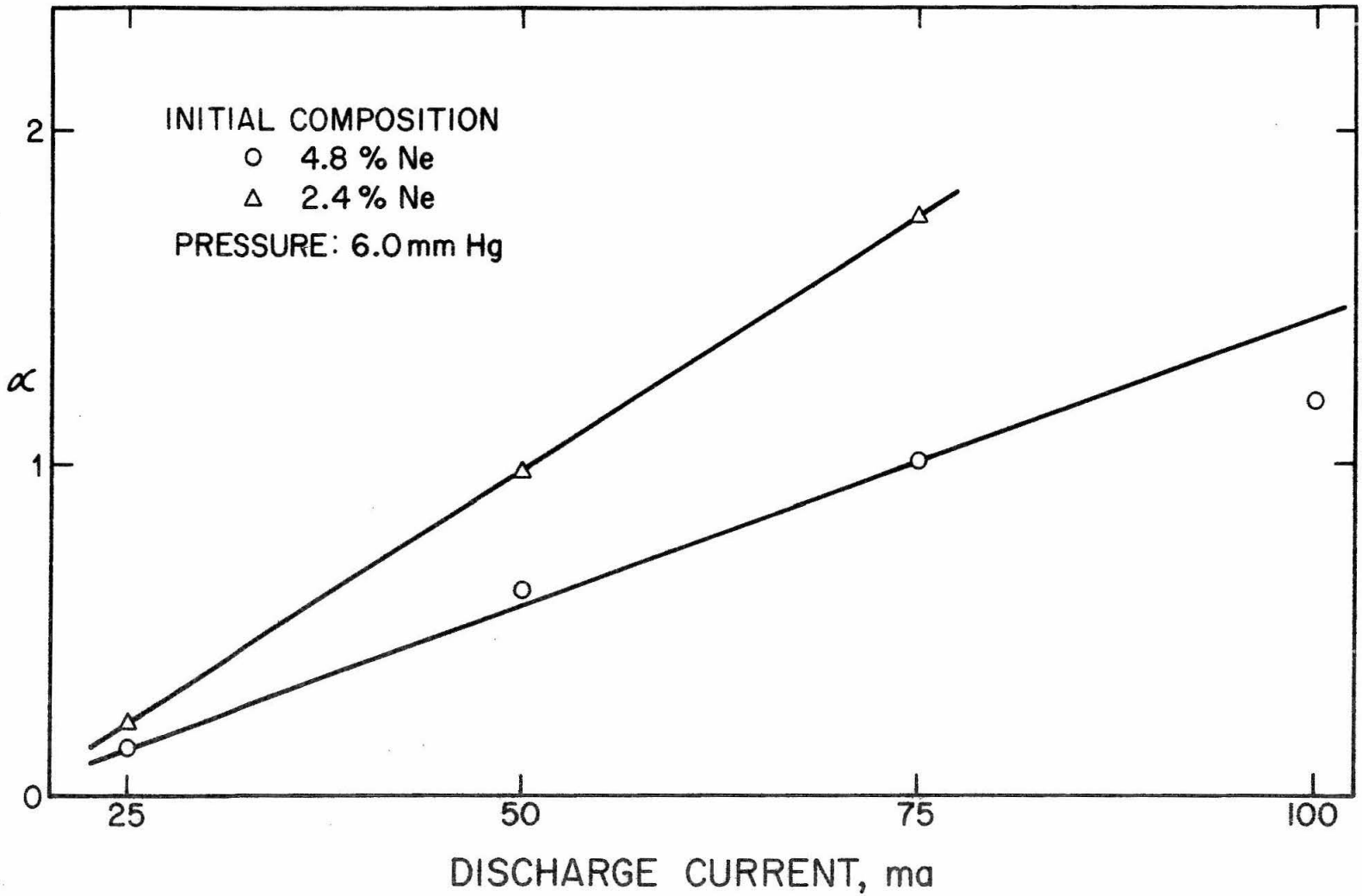

Figure 35. Calculated Electrostatic Peclet Number as a Function of Discharge Current in He-Ne for Different Initial Compositions

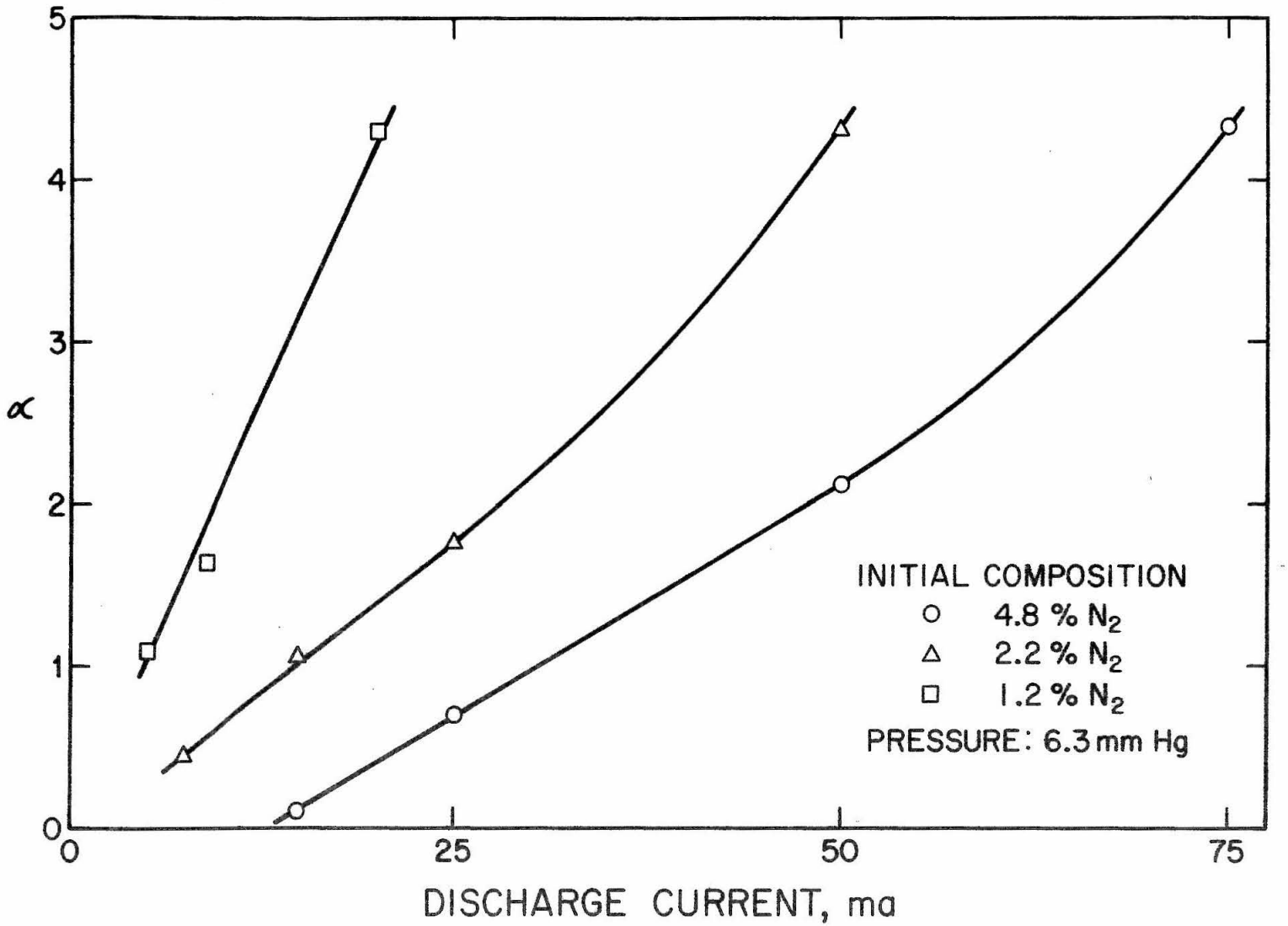

Figure 36. Calculated Electrostatic Peclet Number as a Function of Discharge Current in He-N_2 for Different Initial Compositions

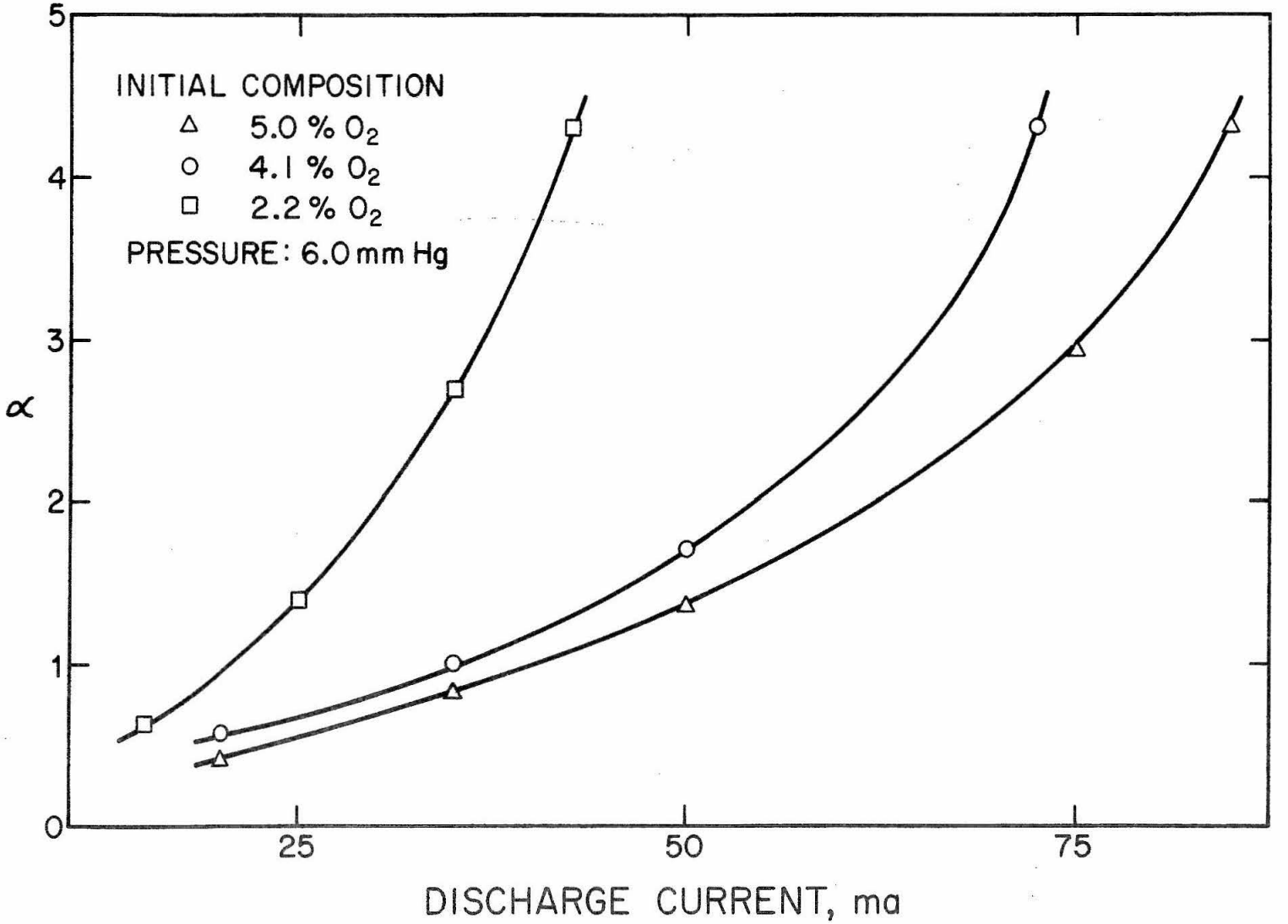

Figure 37. Calculated Electrostatic Peclet Number as a Function of Discharge Current in He-O_2 for Different Initial Compositions

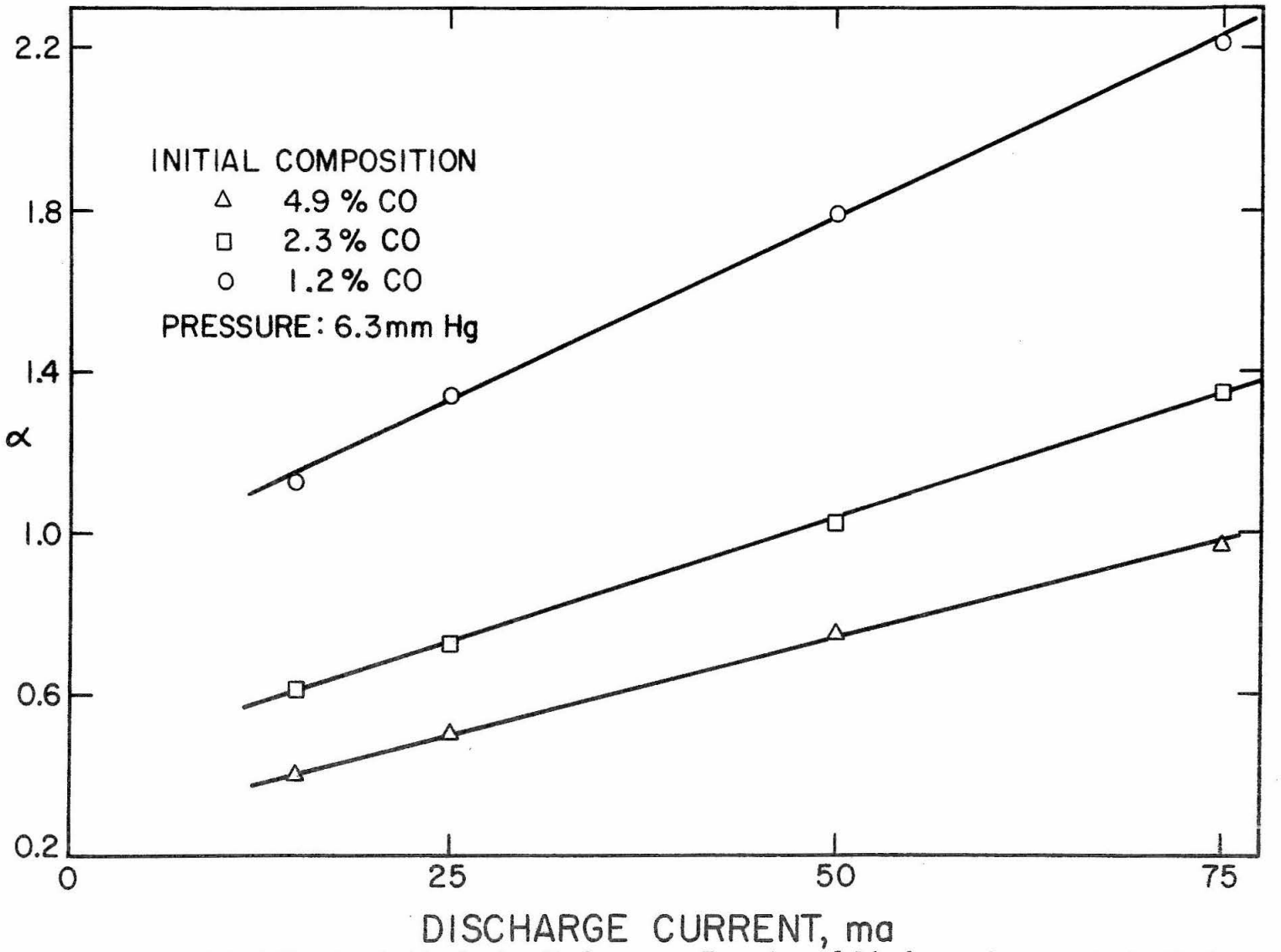

Figure 38. Calculated Electrostatic Peclet Number as a Function of Discharge Current in He-CO for Different Initial Compositions

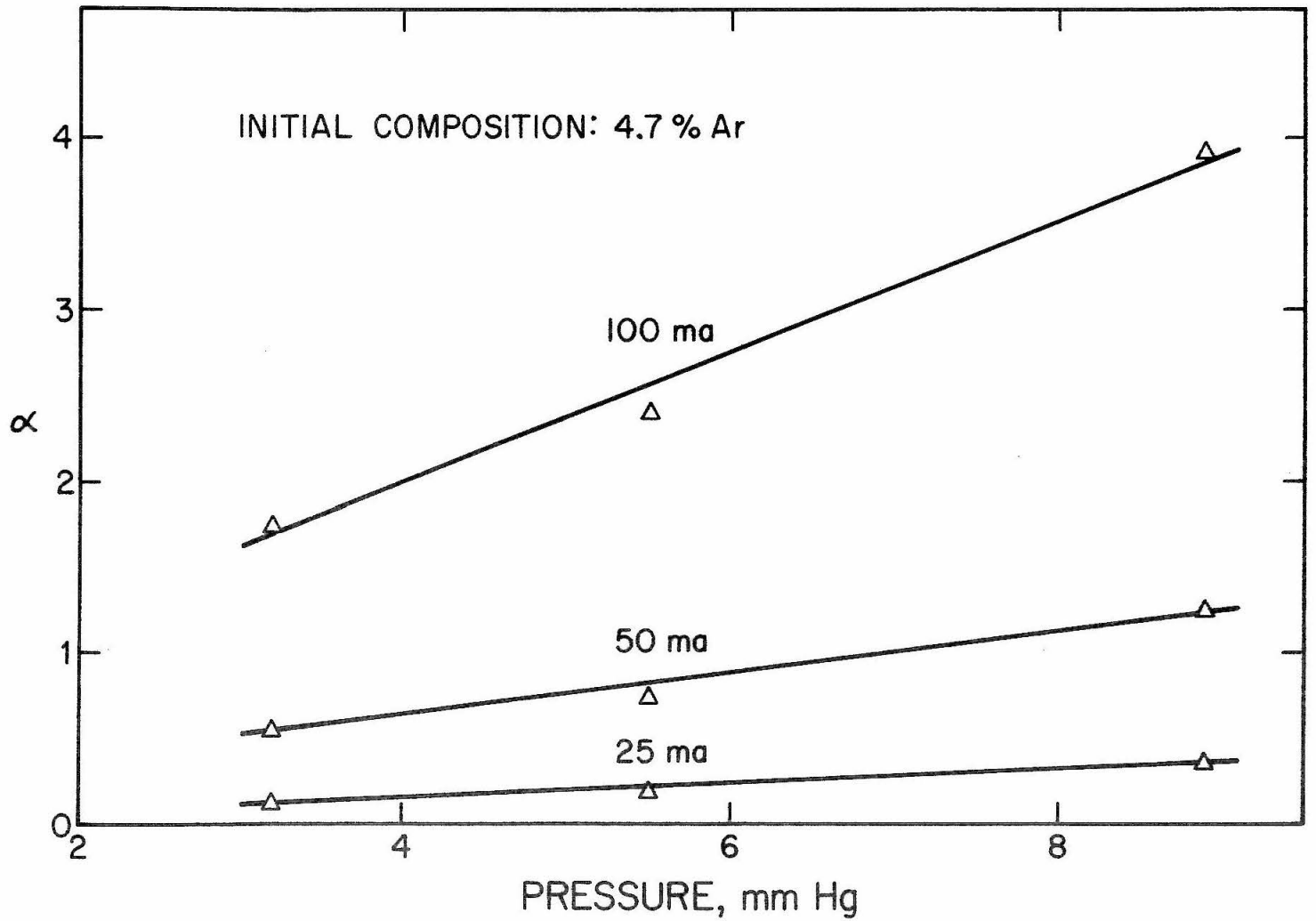

Figure 39. Calculated Electrostatic Peclet Number as a Function of Pressure in He-Ar for Different Discharge Currents

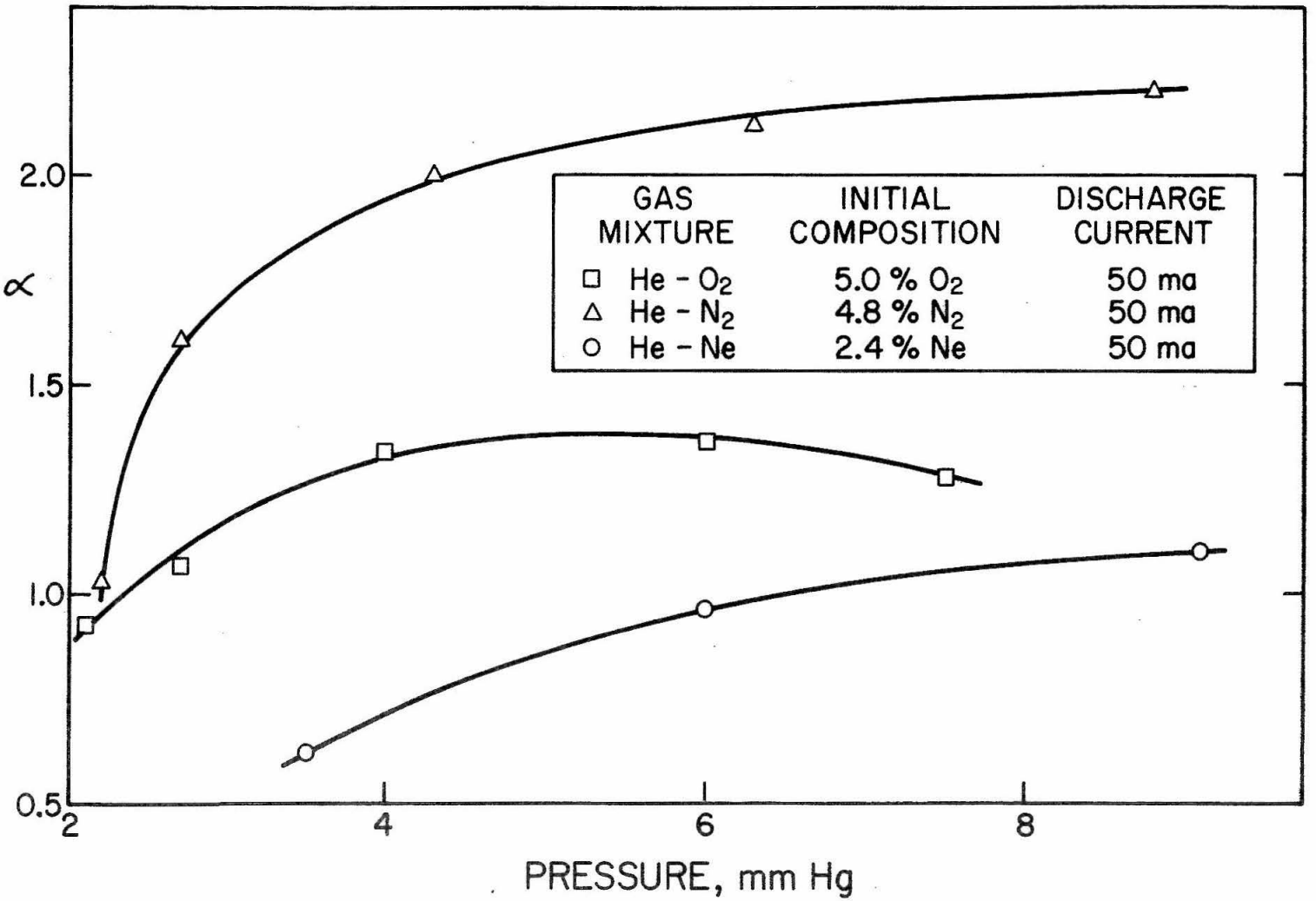

Figure 40. Calculated Electrostatic Peclet Number as a Function of Pressure in He-Ne, $He-N_2$, and $He-O_2$

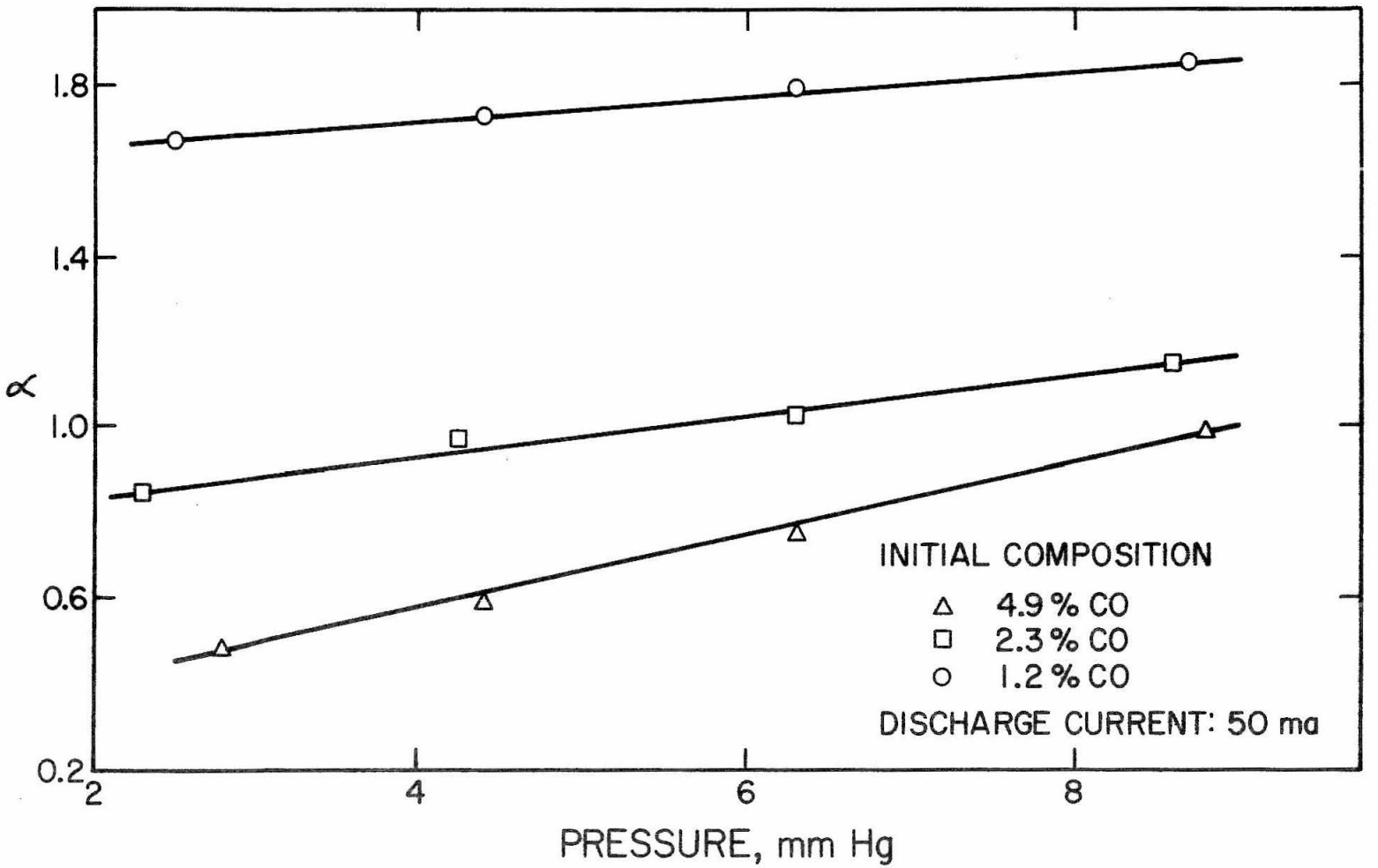

Figure 41. Calculated Electrostatic Peclet Number as a Function of Pressure in He-CO for Different Initial Compositions

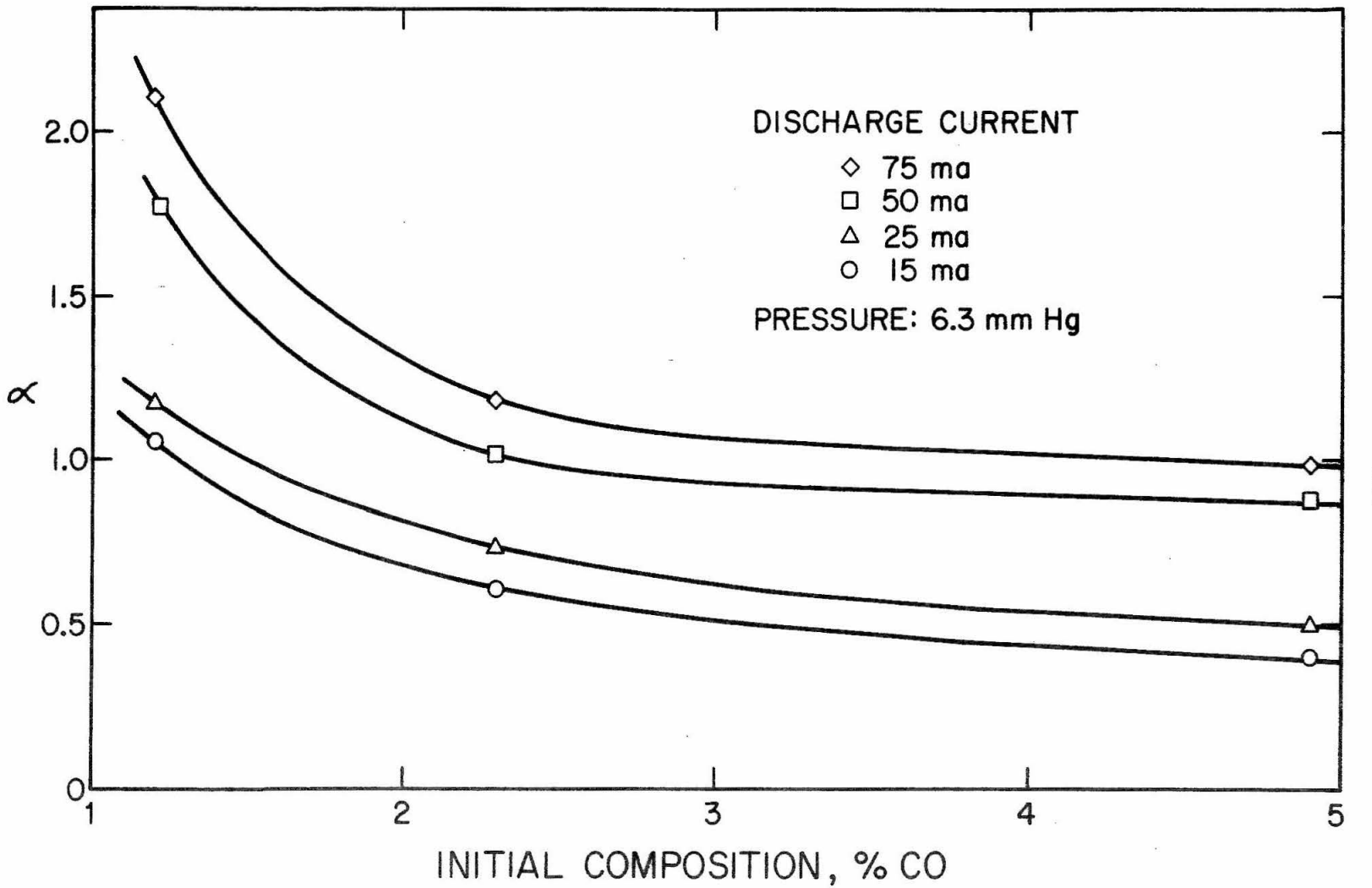

Figure 42. Calculated Electrostatic Peclet Number as a Function of Initial Composition for He-CO with Different Discharge Currents

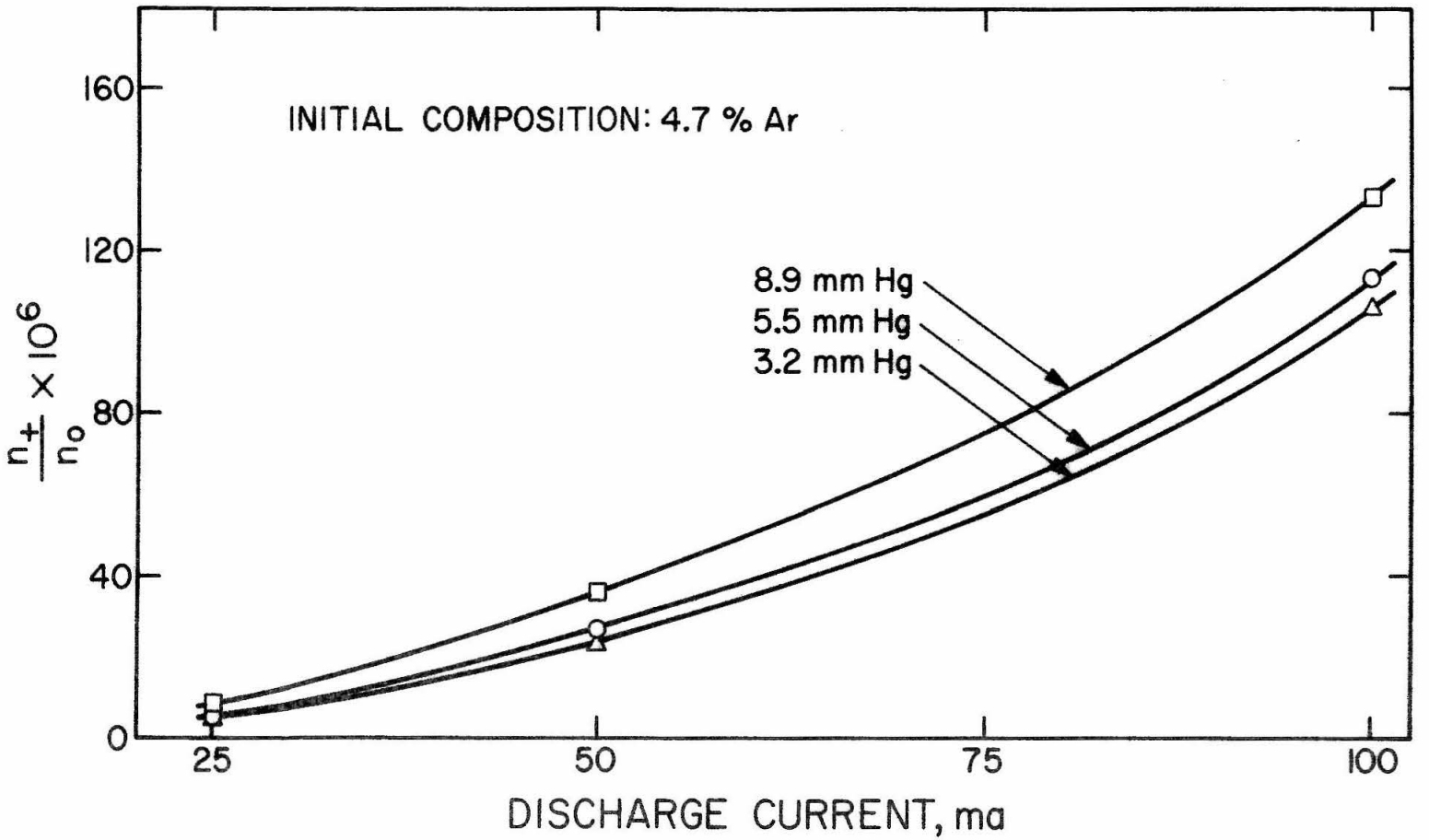

Figure 43. Calculated Ion Fraction as a Function of Discharge Current in He-Ar for Different Pressures

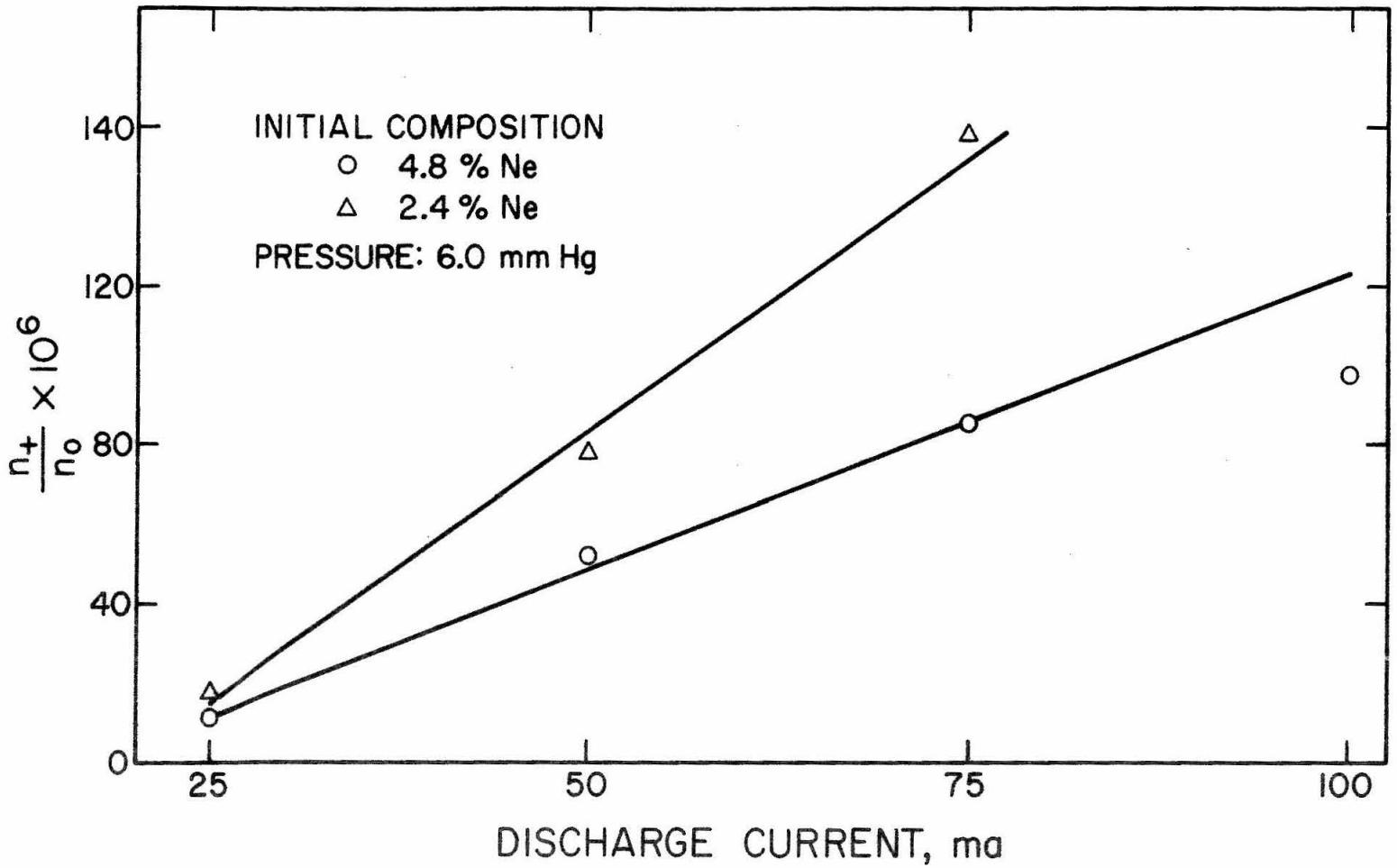

Figure 44. Calculated Ion Fraction as a Function of Discharge Current in He-Ne for Different Initial Compositions

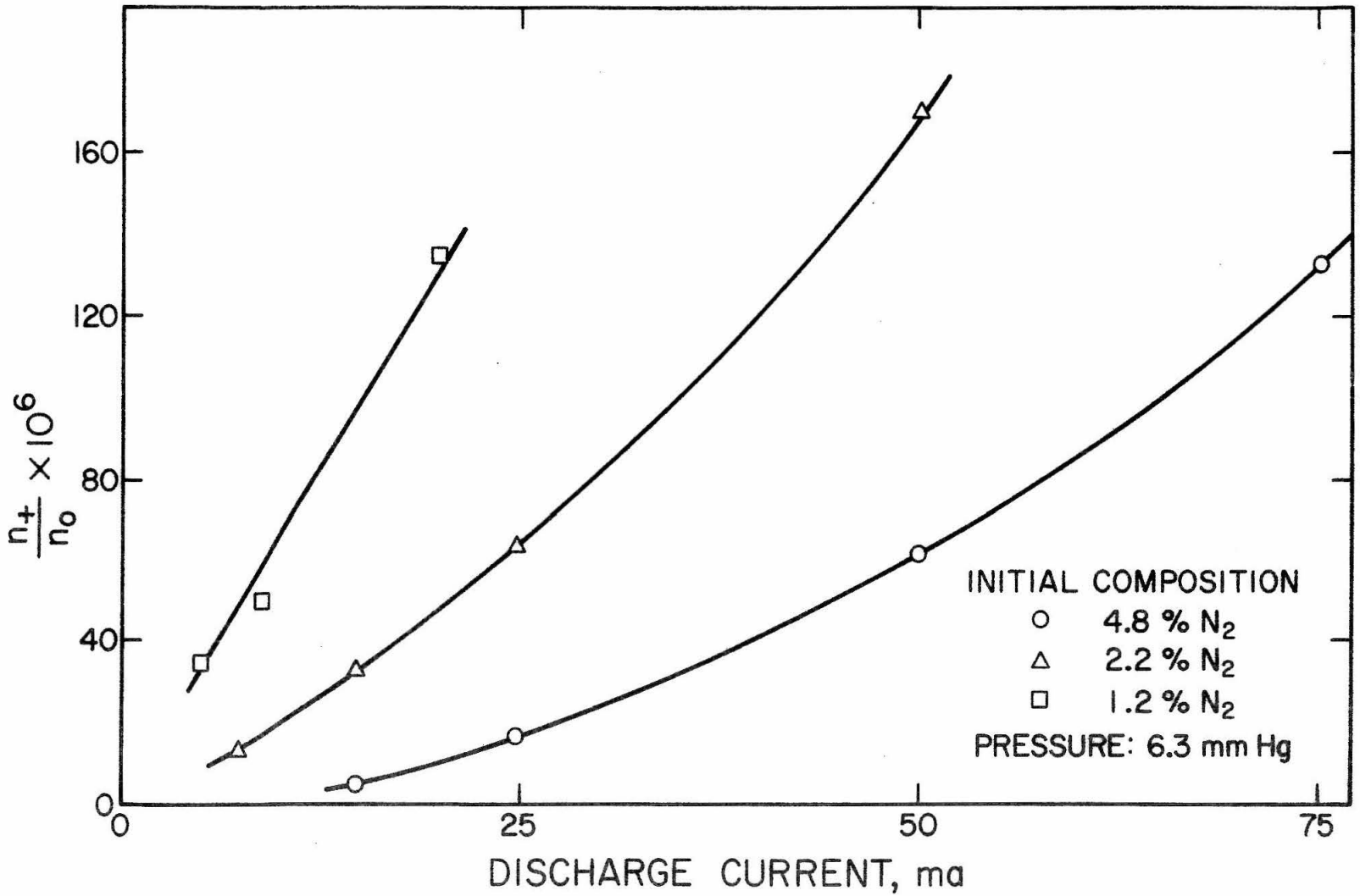

Figure 45. Calculated Ion Fraction as a Function of Discharge Current in He-N_2 for Different Initial Compositions

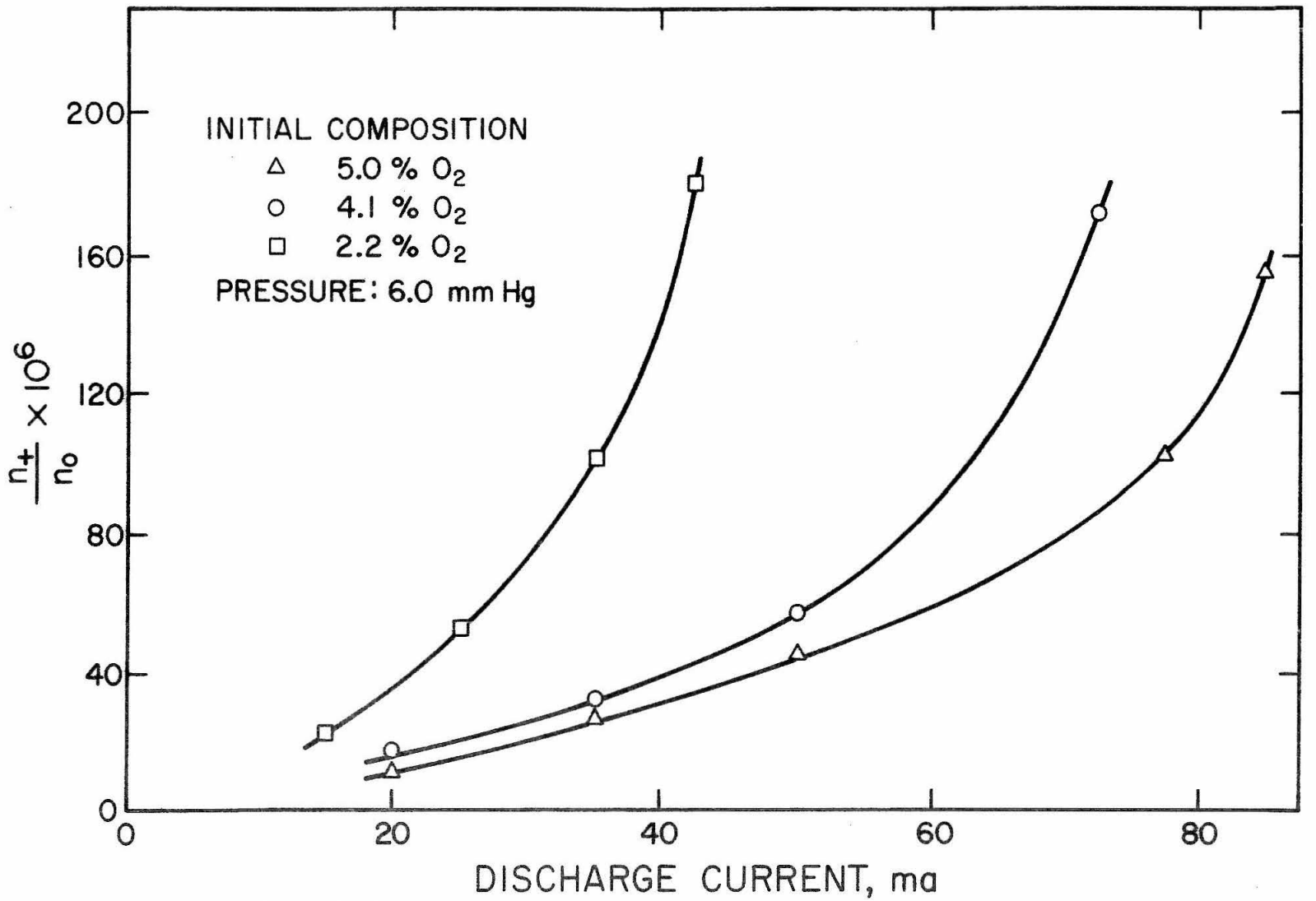

Figure 46. Calculated Ion Fraction as a Function of Discharge Current in He-O_2 for Different Initial Compositions

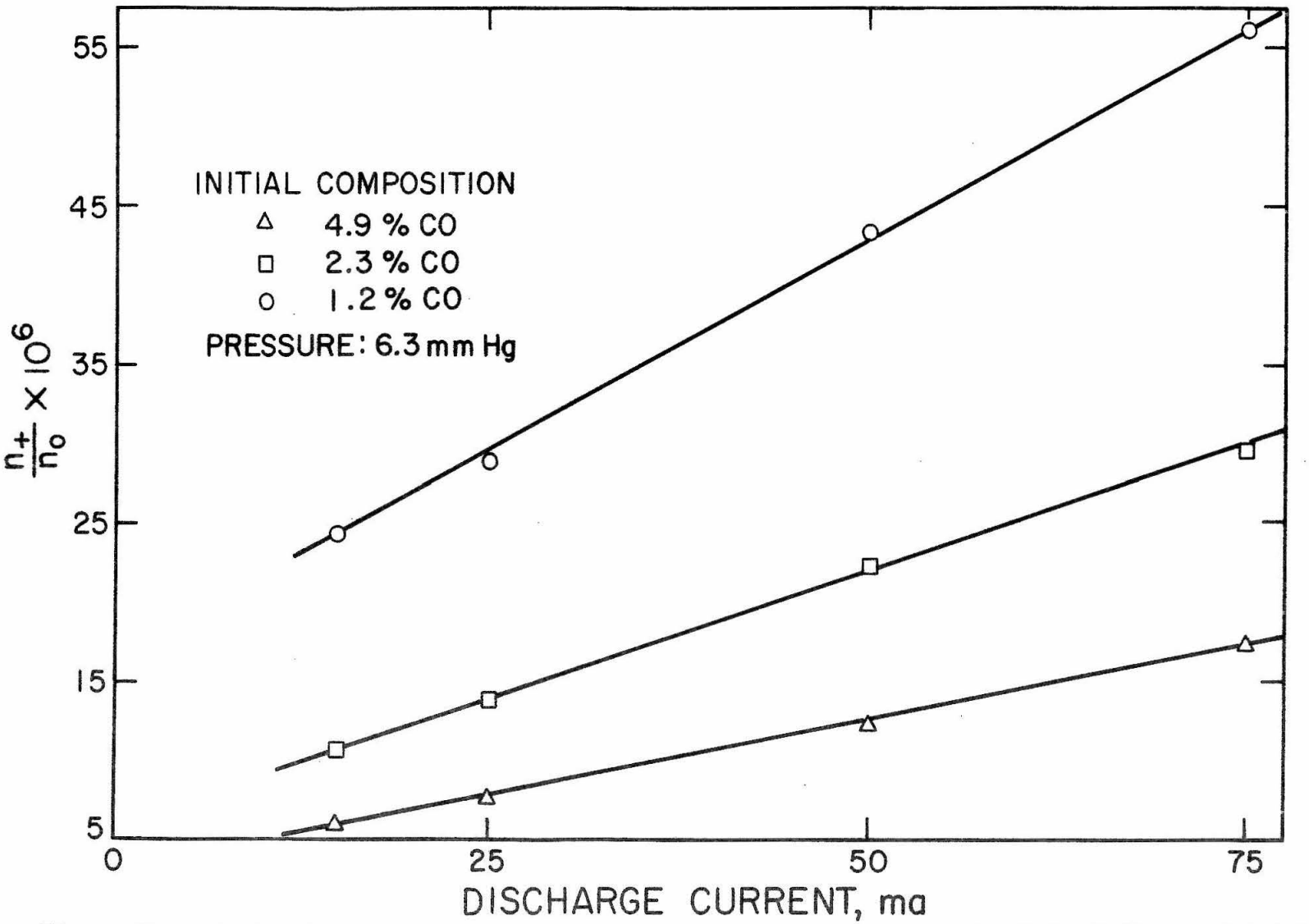

Figure 47. Calculated Ion Fraction as a Function of Discharge Current in He-CO for Different Initial Compositions

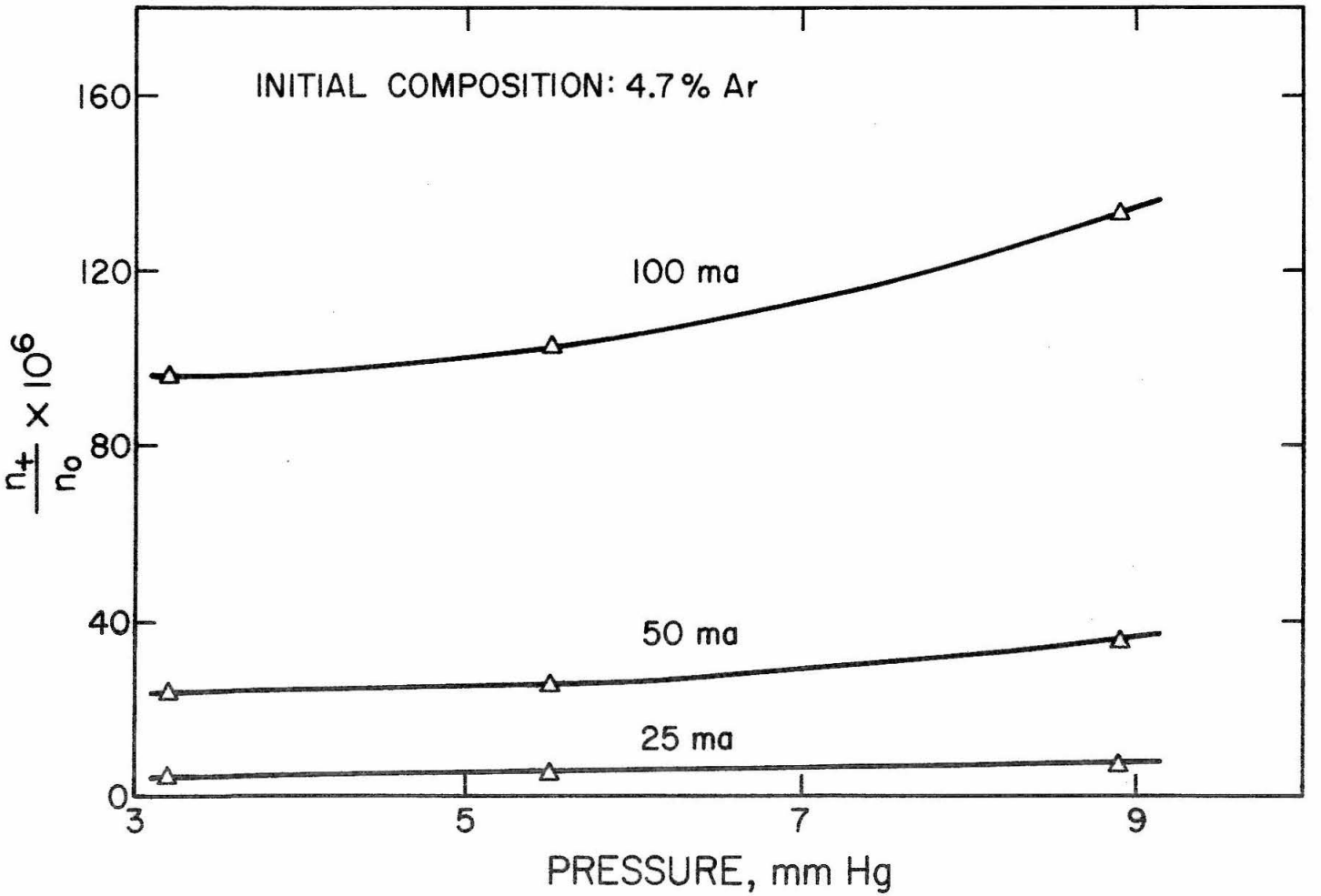

Figure 48. Calculated Ion Fraction as a Function of Pressure in He-Ar for Different Discharge Currents

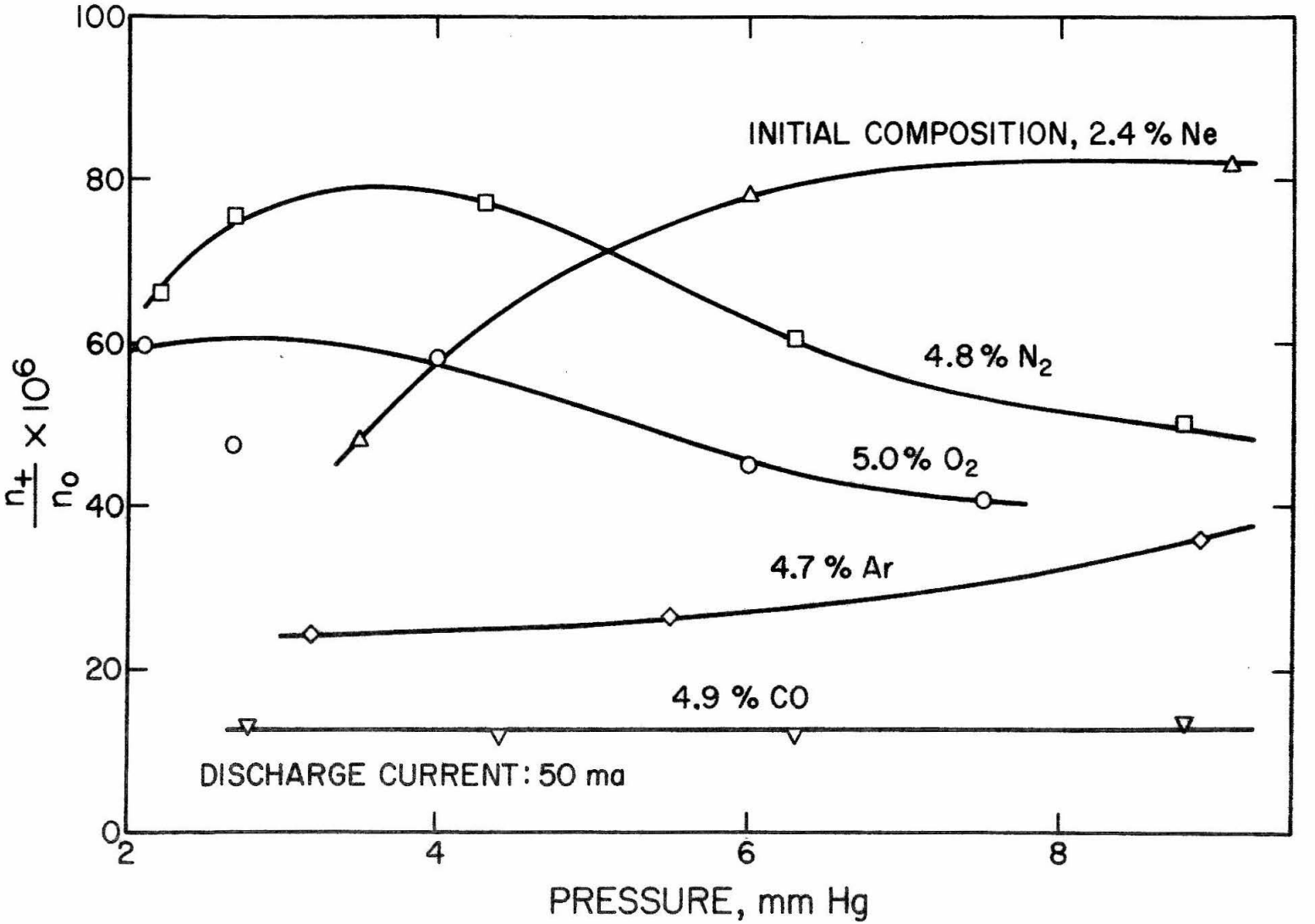

Figure 49. Calculated Ion Fraction as a Function of Pressure in He-Ar, He-Ne, He-N_2, He-O_2, and He-CO

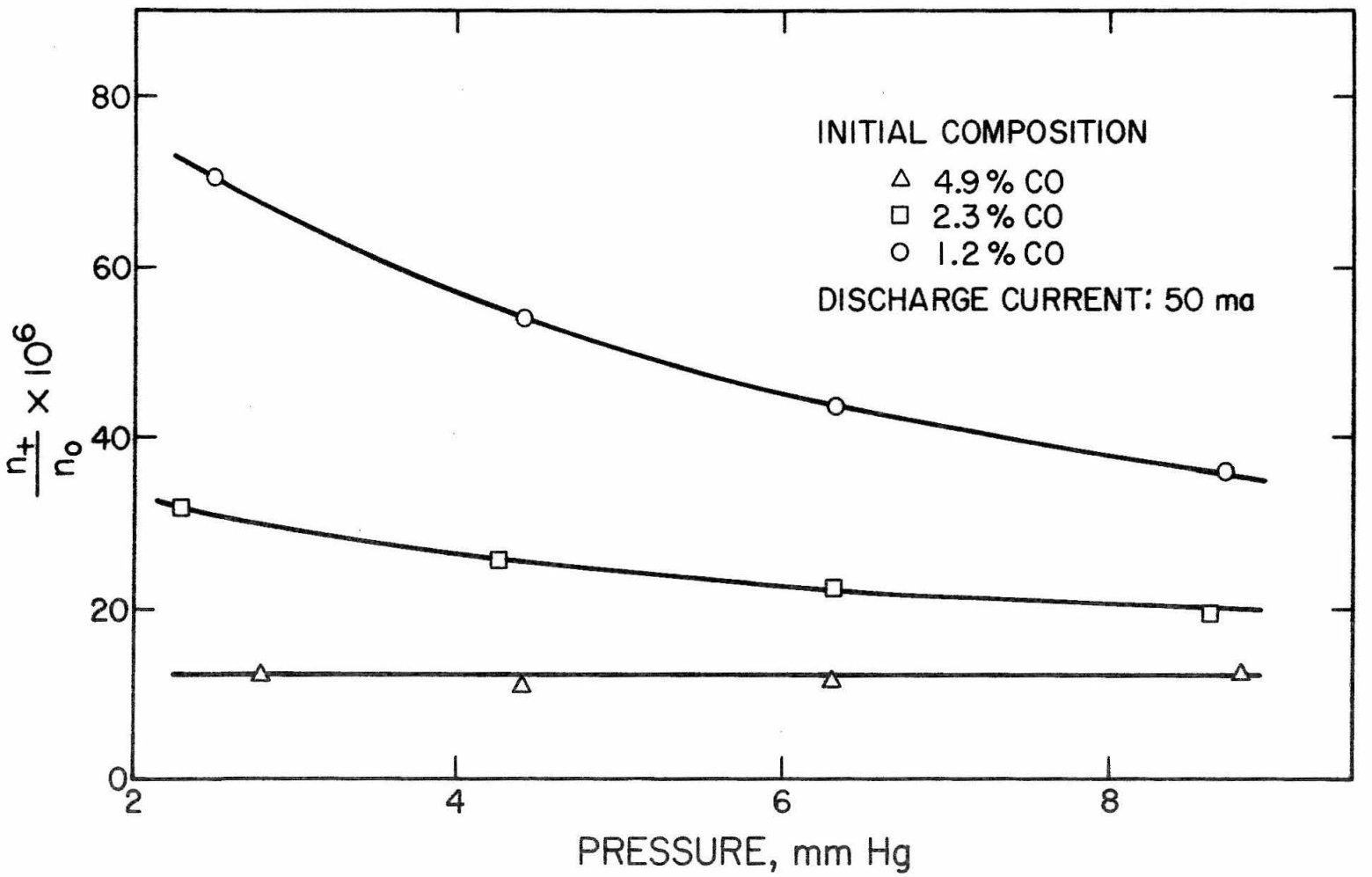

Figure 50. Calculated Ion Fraction as a Function of Pressure in He-CO for Different Initial Compositions

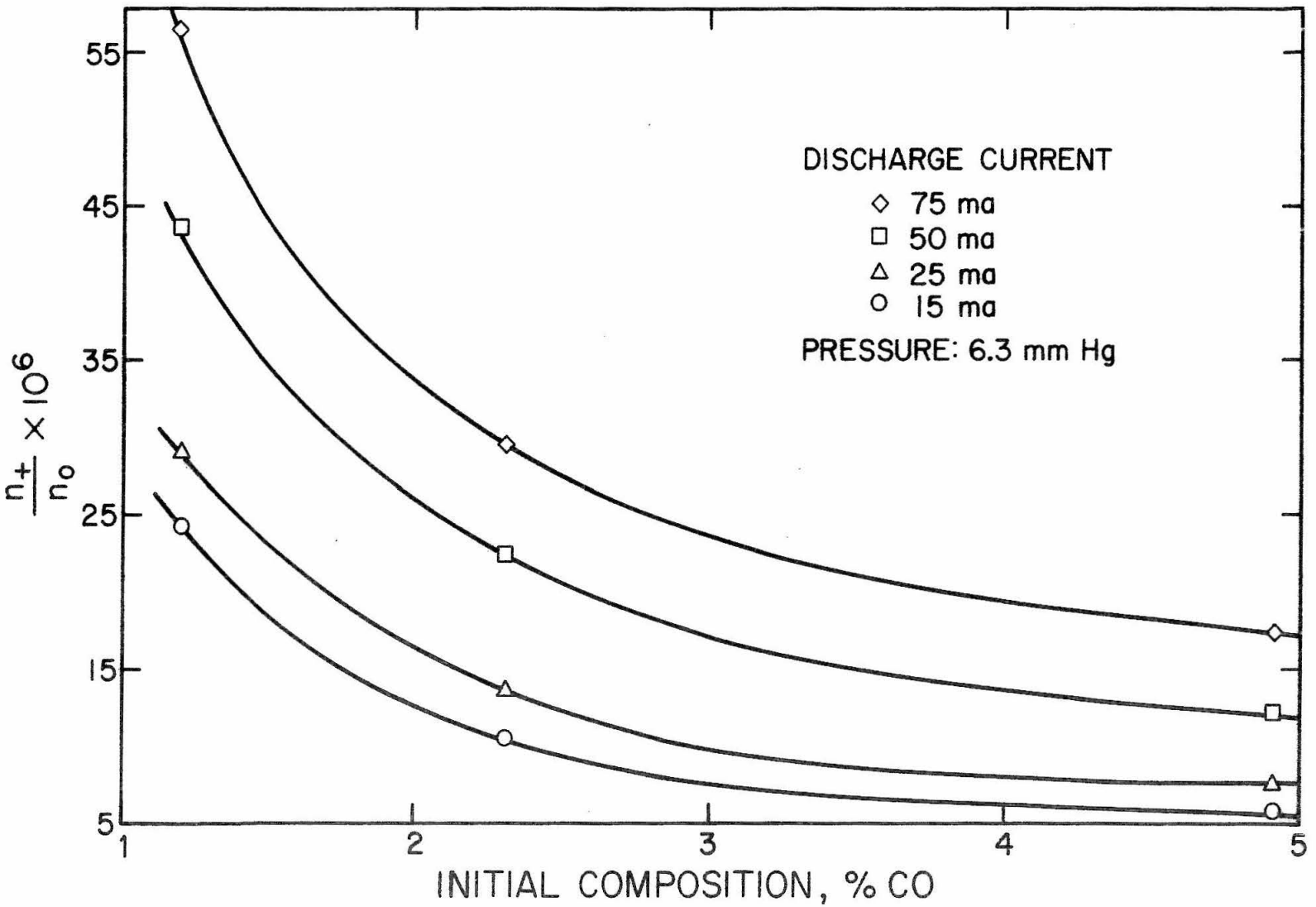

Figure 51. Calculated Ion Fraction as a Function of Initial Composition in He-CO for Different Discharge Currents

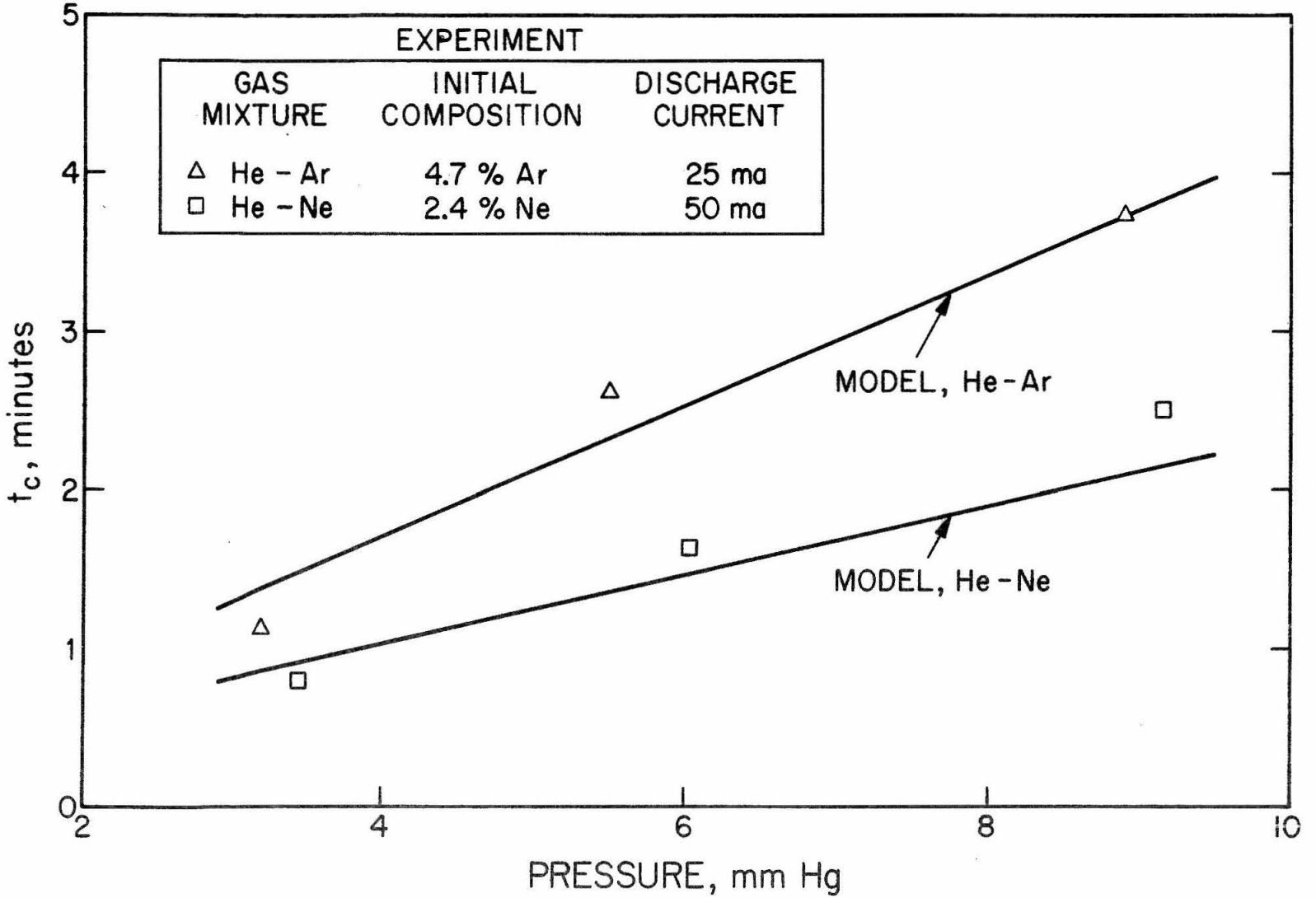

Figure 52. Comparison of Model and Experiment for Characteristic Time for Cataphoresis as a Function of Pressure in He-Ar and He-Ne

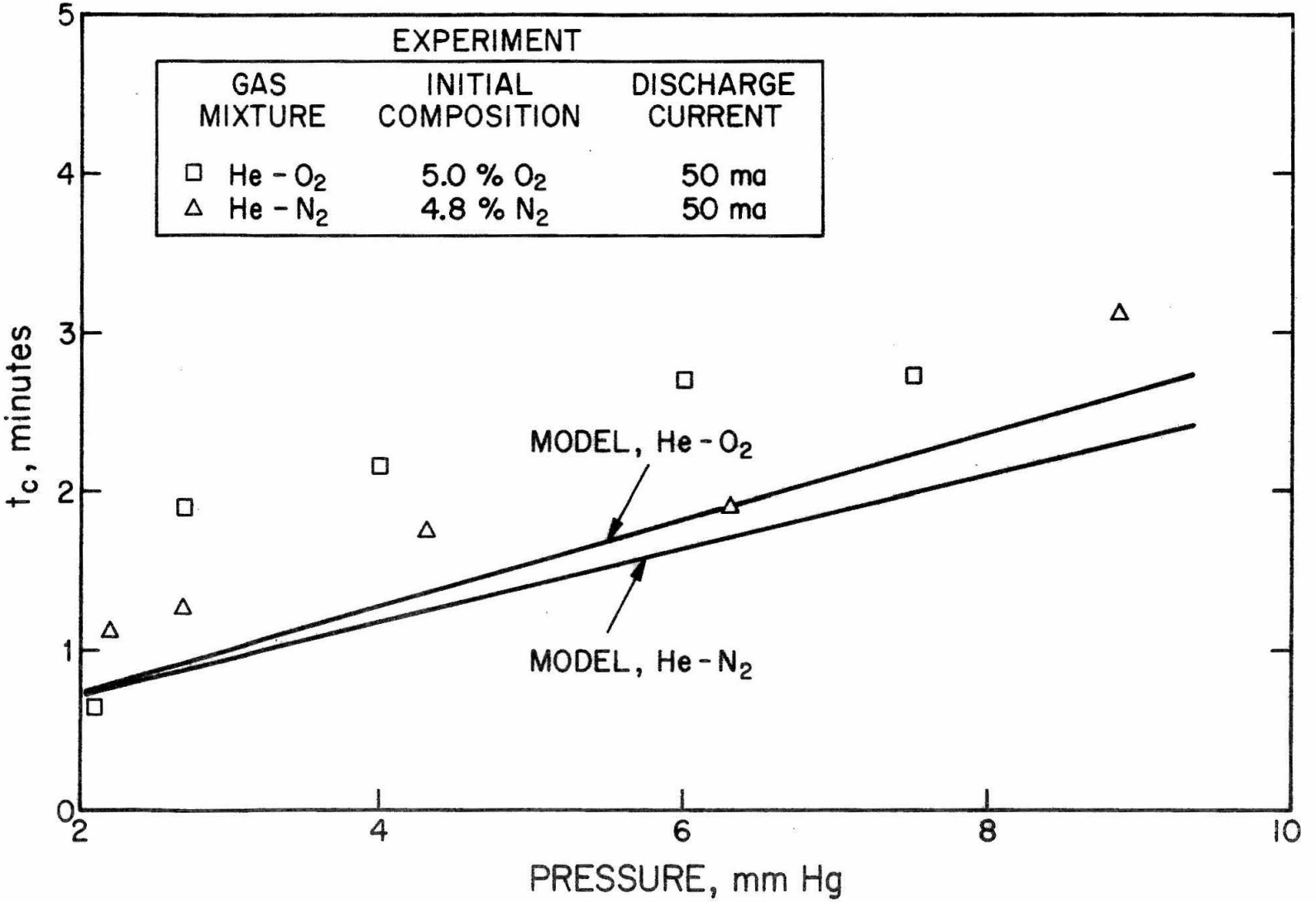

Figure 53. Comparison of Model and Experiment for Characteristic Time for Cataphoresis as a Function of Pressure in He-N_2 and He-O_2

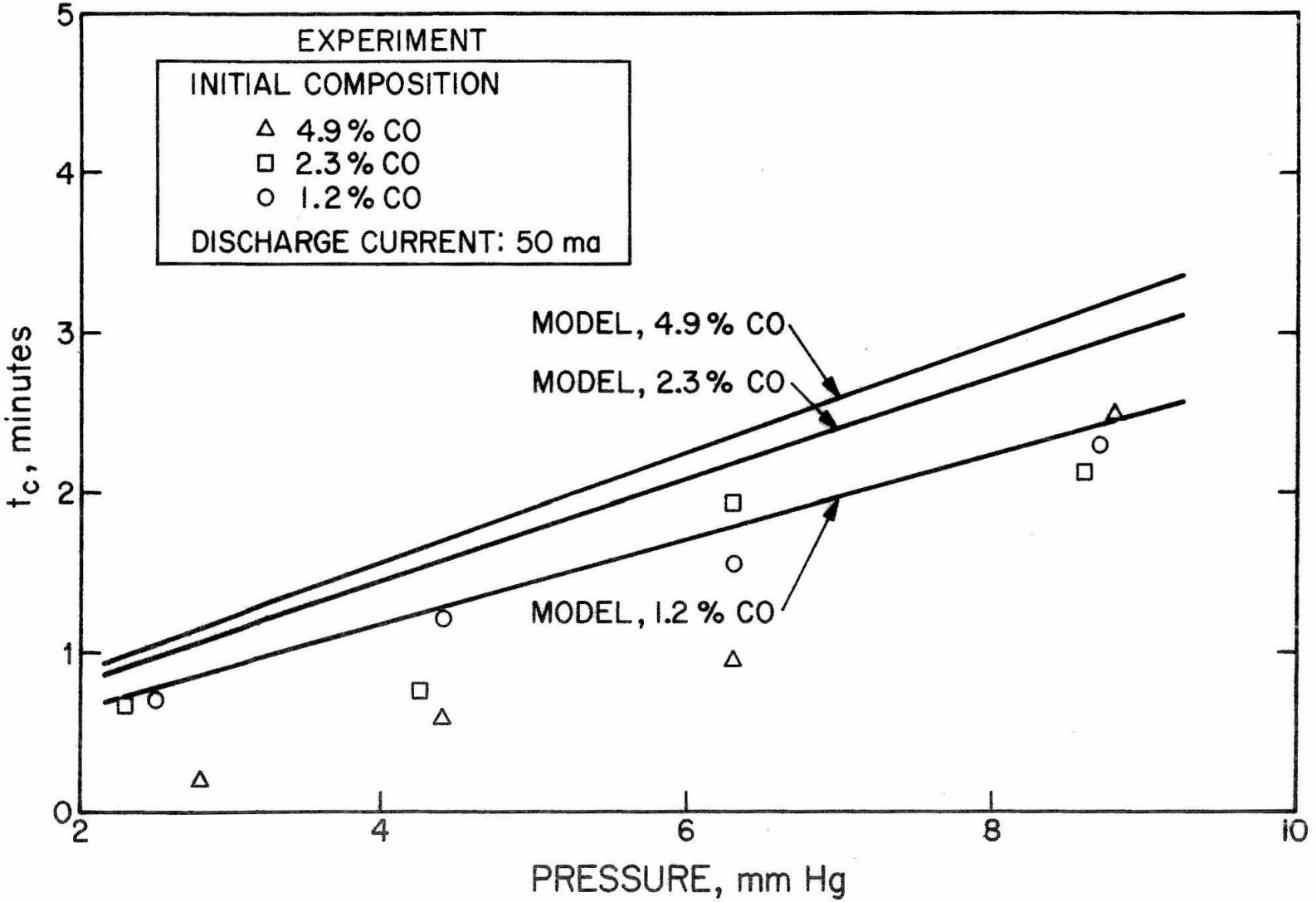

Figure 54. Comparison of Model and Experiment for Characteristic Time for Cataphoresis as a Function of Pressure in He-CO for Different Initial Compositions

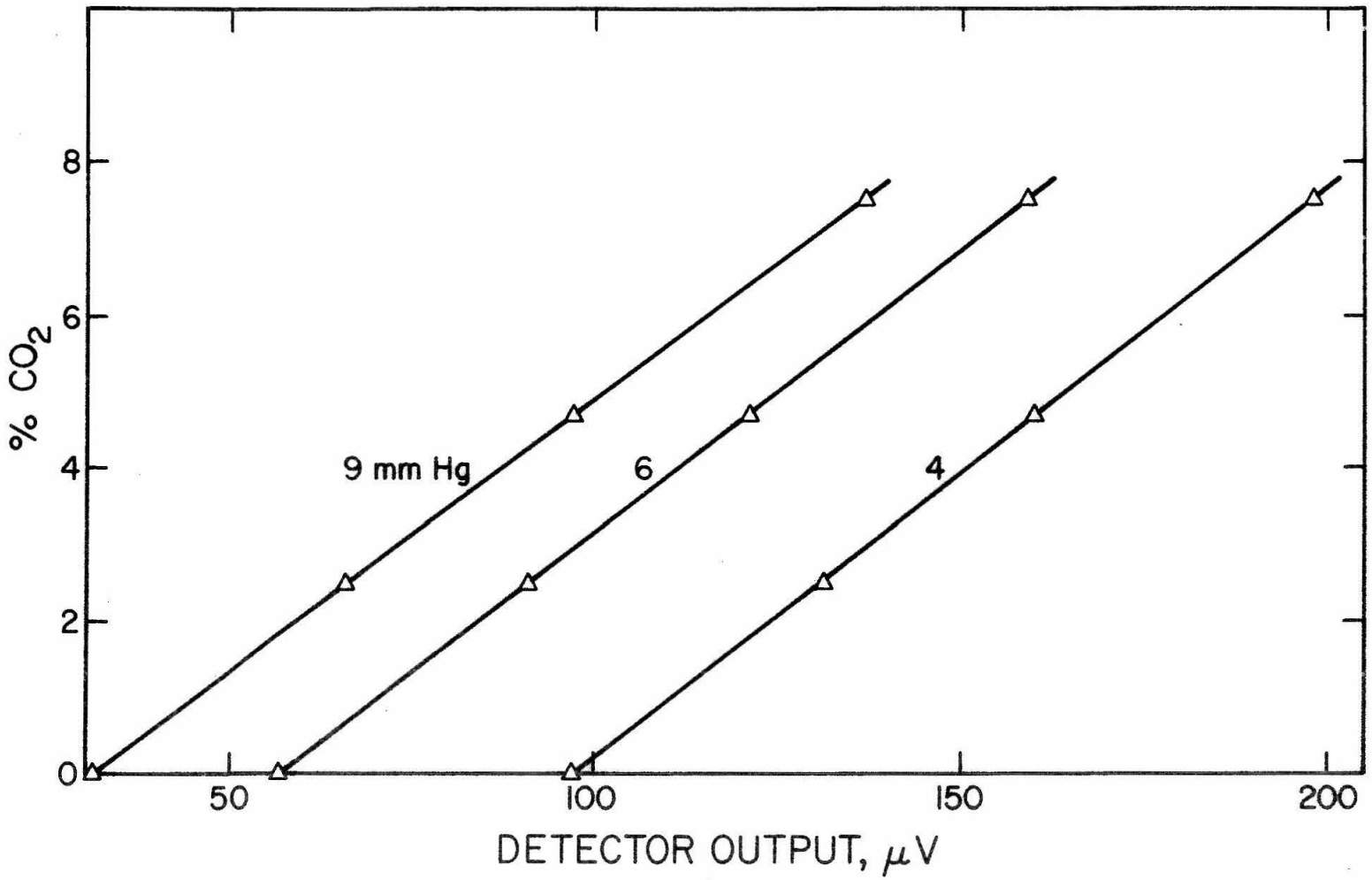

Figure 55. Composition Calibration for He-CO_2

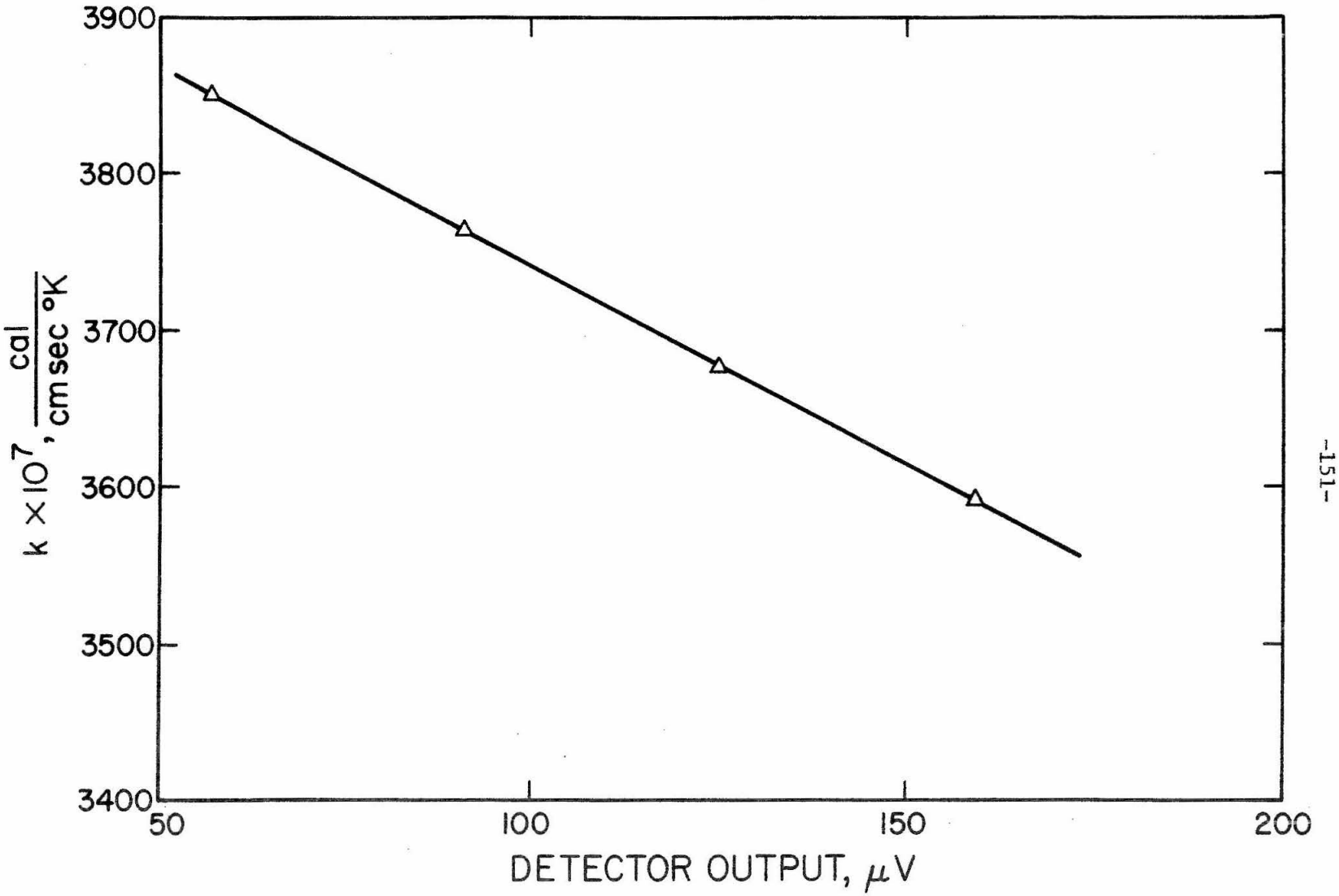

Figure 56. Calculated Values of Thermal Conductivity as a Function of Detector Output for He-CO_2 at 6.0 mm Hg

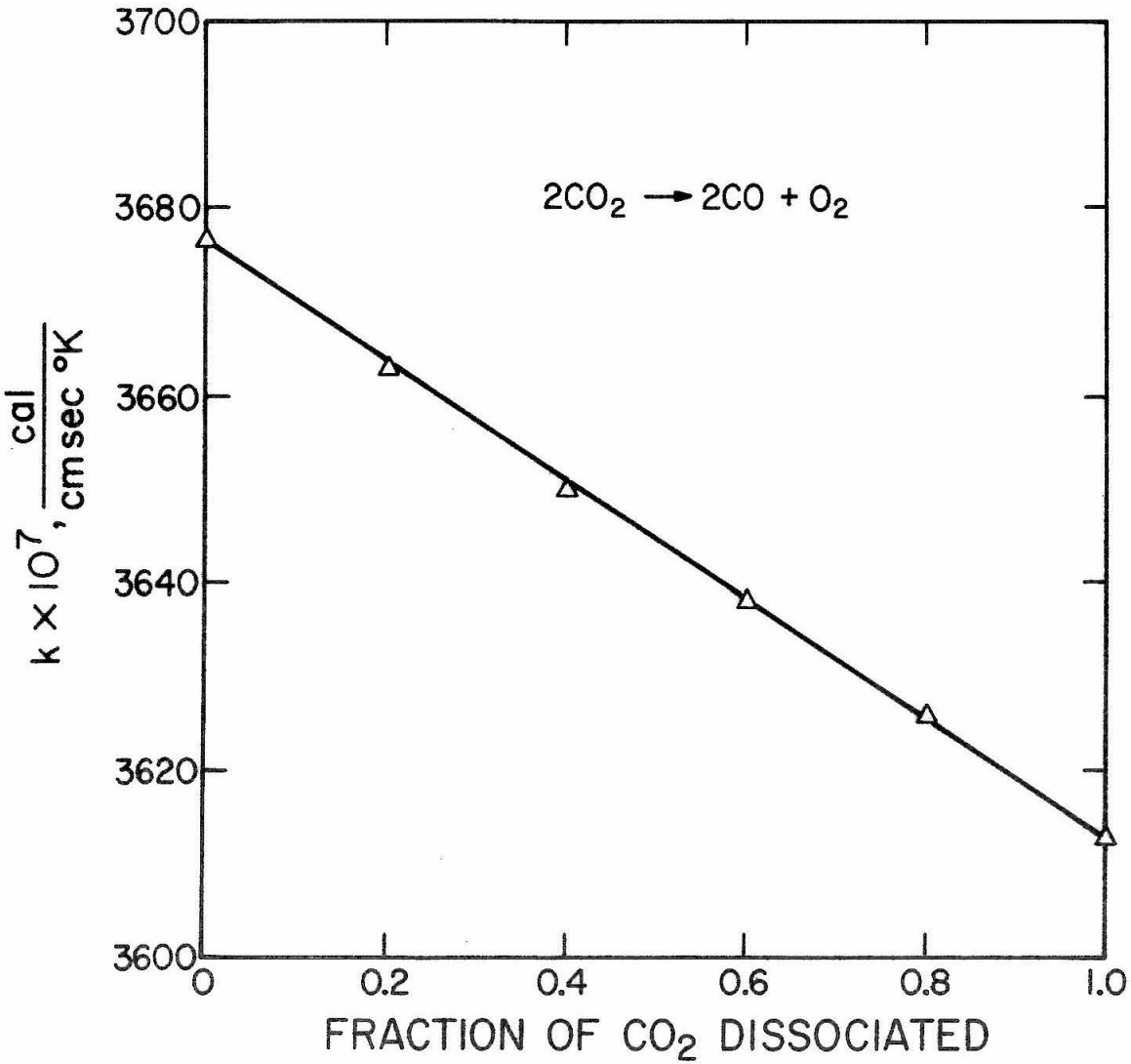

Figure 57. Thermal Conductivity as a Function of the Fraction of CO_2 Dissociated for Initial Composition of 5.0% CO_2

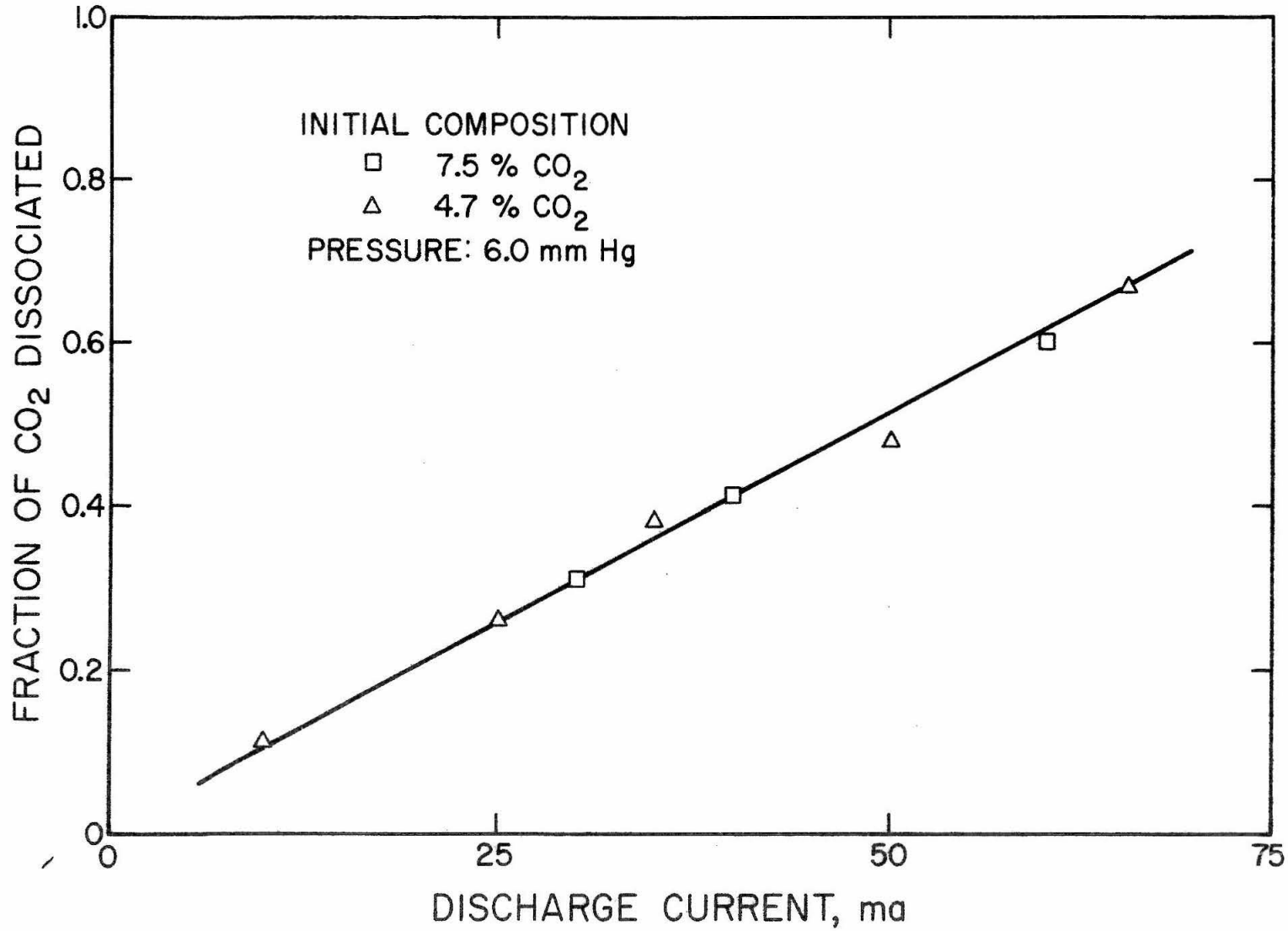

Figure 58. Fraction of CO_2 Dissociated as a Function of Discharge Current for He-CO_2

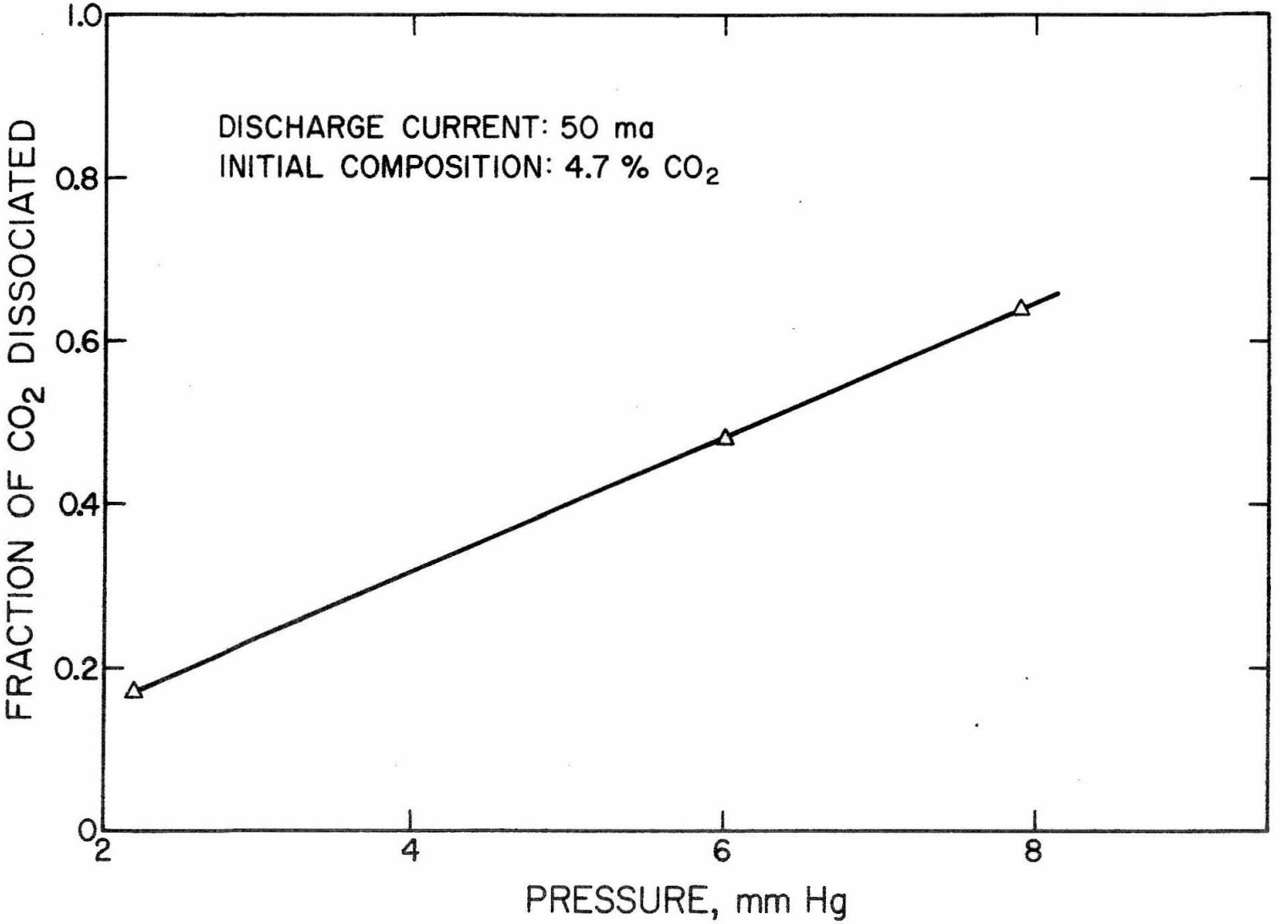

Figure 59. Fraction of CO_2 Dissociated as a Function of Pressure for He-CO_2

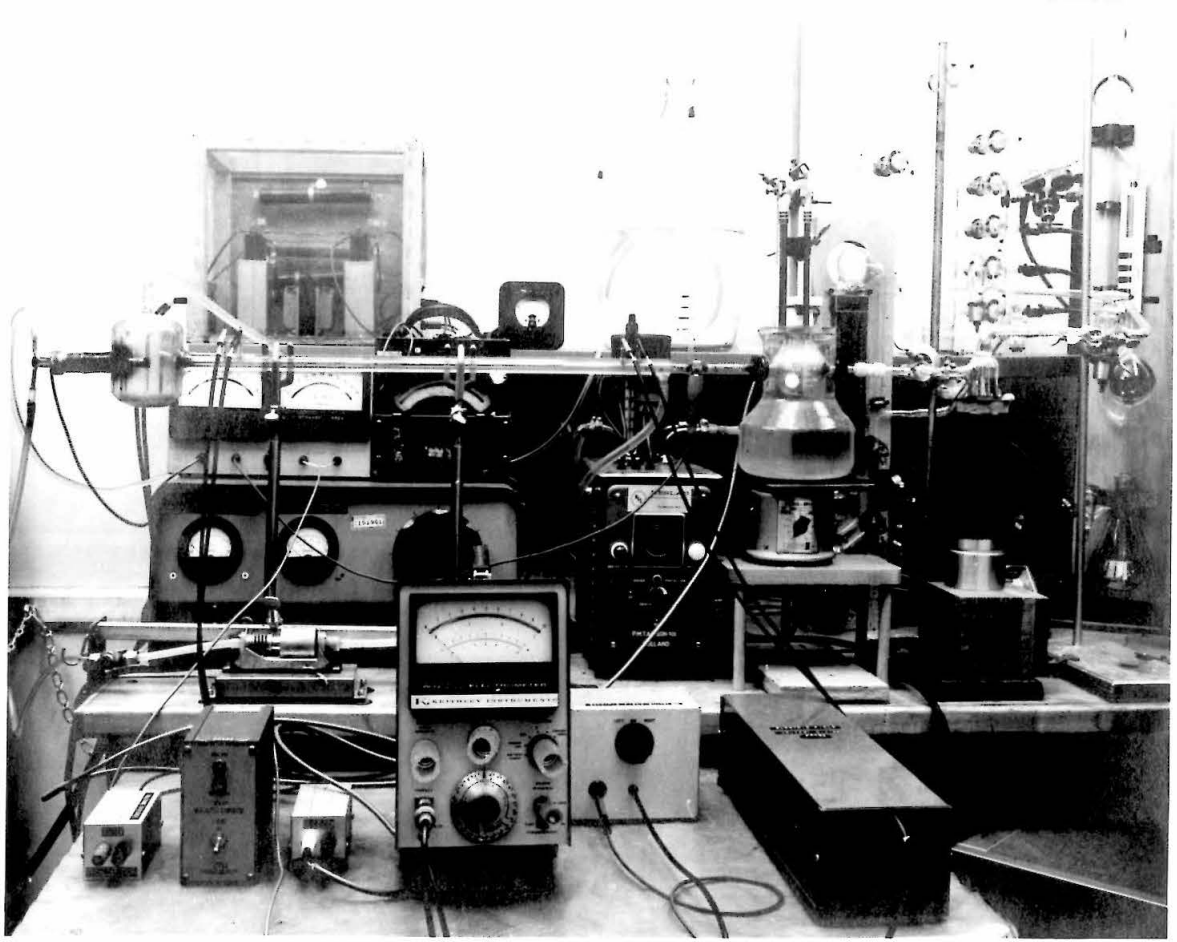

Fig. 60. Experimental System Excluding Some Vacuum Equipment and Electronics

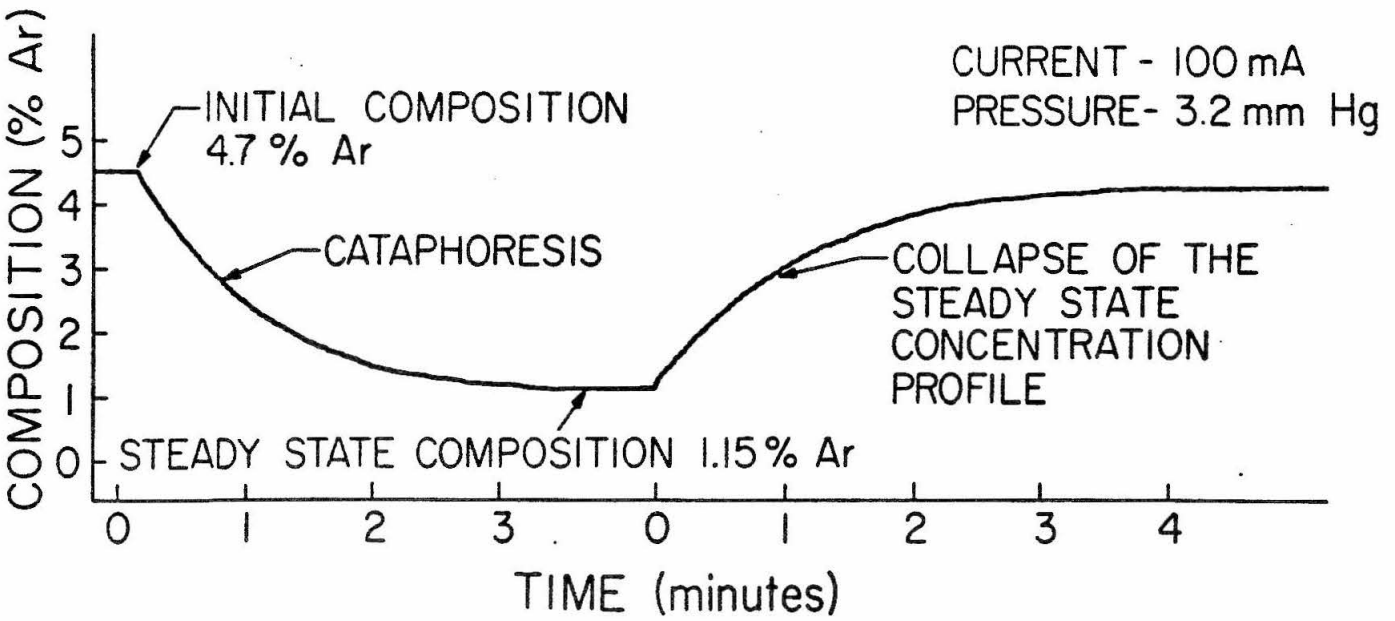

Fig. 61. Measured Composition of Argon in a He-Ar Mixture as a Function of Time in the Anode End-Bulb

IX. APPENDICES

APPENDIX A

The Application of New Data to Druyvesteyn's Calculation of the Axial Concentration Gradient

THE APPLICATION OF NEW DATA TO DRUYVESTEYN'S CALCULATION OF THE AXIAL CONCENTRATION GRADIENT

Druyvesteyn [8] calculated a value of $\frac{dNa}{dx} = -1.2 \times 10^{13}$ atoms/cm^4. The purpose of this appendix is to show that a value of $\frac{dNa}{dx} = -0.8 \times 10^{13}$ atoms/cm^4 is obtained when more recent values for transport properties are used in the calculation.

The following discussion will be divided into three parts. First, Druyvesteyn's calculation for $\frac{dNa}{dx}$ will be described. Second, recent transport properties will be presented. Finally, $\frac{dNa}{dx}$ will be calculated using the more recent values for the transport properties.

Druyvesteyn's Calculation for dNa/dx

Equation (11) in Druyvesteyn's paper [8] is

$$Na = N_o - 8.3 \times 10^{10} \frac{\mu_+ \sqrt{V_o}\, i}{\lambda DR^2} x \qquad (A.1)$$

The derivative of Eq. (A.1) is

$$\frac{dNa}{dx} = - \frac{8.3 \times 10^{10} \mu_+ \sqrt{V_o}\, i}{\lambda DR^2} \qquad (A.2)$$

Druyvesteyn neglected the argon in the calculation of dNa/dx for a 10% Ar - 90% Ne mixture. Values for the current and the tube radius were taken from Pennings [7] experiment where R = 0.6 cm and i = 0.03 amperes. He assumed V_o was 1 volt. The value for μ_+ was extrapolated from Tyndall and Powell's data [52]. Druyvesteyn's footnote #1 which is quoted below explains how μ_+ was obtained.

"Tyndall and Powell [52] have found for Hg^+ ions in He $\mu_+P = 9 \times 10^3$. As the mobility of alkali-ions in He is about three times greater than in Ne, we adopt for Hg^+ ions in Ne $\mu_+P = 3 \times 10^3$."

Druyvesteyn calculated the diffusion coefficient by means of formula (846) in Jeans [50]. He found $DP = 104$ where P is in mm Hg. The value of λ was taken to be $\lambda P = 0.2$. The values used by Druyvesteyn are summarized below. He did not specify a temperature.

Term	Magnitude	Reference
V_o	1 Volt	[8]
μ_+P	3×10^3 (P in mm Hg)	[52]
λP	0.2 (P in mm Hg)	[8]
DP	104 (P in mm Hg)	[50]
R	0.6 cm	[7]
i	0.03 amps	[7]

Substituting these values into the expression for dNa/dx, Druyvesteyn obtained for $P = 12$ mm Hg

$$\frac{dNa}{dx} = -1.2 \times 10^{13} \text{ atoms/cm}^4$$

His calculation was checked and this value was confirmed.

Determination of More Recent Transport Data

Chanin and Biondi [51] reported the mobilities of mercury ions in Ne and Ar at 300^oK to be

$$\mu_{Hg^+ \text{ in Ne}} = 5.95 \text{ cm}^2/\text{volt/sec}$$

and

$$\mu_{Hg^+ \text{ in Ar}} = 1.84 \text{ cm}^2/\text{volt/sec}$$

Assuming that Blanc's law [62] is valid for Hg^+ in the Ar-Ne mixture, then

$$\mu_{Hg^+ \text{ in Ar-Ne}} = \frac{\mu_{Hg^+/Ne} \; \mu_{Hg^+/Ar}}{\chi_{Ar} \mu_{Hg^+/Ne} + \chi_{Ne} \mu_{Hg^+/Ar}}$$

For a 10% Ar - 90% Ne mixture, then $\mu_{Hg^+ \text{ in 10\% Ar - 90\% Ne}} = 4.87$ cm^2/volt/sec at 300°K and 1 atm, or 309 cm^2/volt/sec at 300°K and 12 mm Hg. The mobility was assumed to be inversely proportional to P . It is important to note that Druyvesteyn had to use a "ball-park" number for the mobility of Hg^+ because data were not available at that time.

Druyvesteyn calculated D_{Hg-Ne} by neglecting the Ar percentage; this same assumption was also made here. The diffusion coefficient was calculated from Eq. (8.2-44) in Hirschfelder, Curtiss, and Bird [37] with the values in the following table which were obtained from pages 1110 and 1112 [37].

The value of σ^2_{Hg-Ne} was 8.10 $(^oA)^2$. Druyvesteyn used a value of $\sigma^2_{Hg-Ne} = 12$ $(^oA)^2$. The resulting calculated value of D_{Hg-Ne} was 15.5 cm^2/sec at 300°K and 12 mm Hg. Druyvesteyn calculated a value of DP = 104 or $D_{Hg-Ne} = 8.7$ cm^2/sec at 300°K and P = 12 mm Hg.

Term	Magnitude
T	300 ^{o}K (assumed)
P	12/760 atm
M_{Hg}	200.6 gms/gmole
M_{Ne}	20.2 gms/gmole
$(\epsilon/k)_{Hg}$	851 ^{o}K
$(\epsilon/k)_{Ne}$	35.7 ^{o}K
σ_{Hg}	2.898 ^{o}A
σ_{Hg}	2.789 ^{o}A

Recalculation of dNa/dx Using Recent Values for the Transport Properties

With the more recent values for the transport properties, mobility and diffusivity, the value of dNa/dx was recalculated from Eq. (A.2). The result was $dNa/dx = -0.8 \times 10^{3}$ atoms/cm^{4}. This value is 33% lower than the value calculated by Druyvesteyn, and a factor of two lower than the value measured by Penning [7]. The new results are compared to Druyvesteyn's results in the following table.

In Fig. A.1, there is a comparison of dNa/dx versus $\sqrt{V_o}$ using both Druyvesteyn's results and the new results. Druyvesteyn's results are about a factor of 1.5 times higher than the new results for the range of $\sqrt{V_o}$ from 1 to 6 volts.

	Druyvesteyn's Results	New Results
Transport Properties $T = 300^{o}K$ $P = 12$ mm Hg	$\mu_{Hg^+ \text{ in Ne}} = \frac{250 \text{ cm}^2}{\text{volt sec}}$ $D_{Hg\text{-}Ne} = \frac{8.7 \text{ cm}^2}{\text{sec}}$	$\mu_{Hg^+ \text{ in Ne-Ar}} = \frac{309 \text{ cm}^2}{\text{volt sec}}$ $D_{Hg\text{-}Ne} = \frac{15.5 \text{ cm}^2}{\text{sec}}$
Axial Gradient of Hg	$\frac{dNa}{dx} = \frac{-1.2 \times 10^{13} \text{ atoms}}{\text{cm}^4}$	$\frac{dNa}{dx} = \frac{-0.8 \times 10^{13} \text{ atoms}}{\text{cm}^4}$

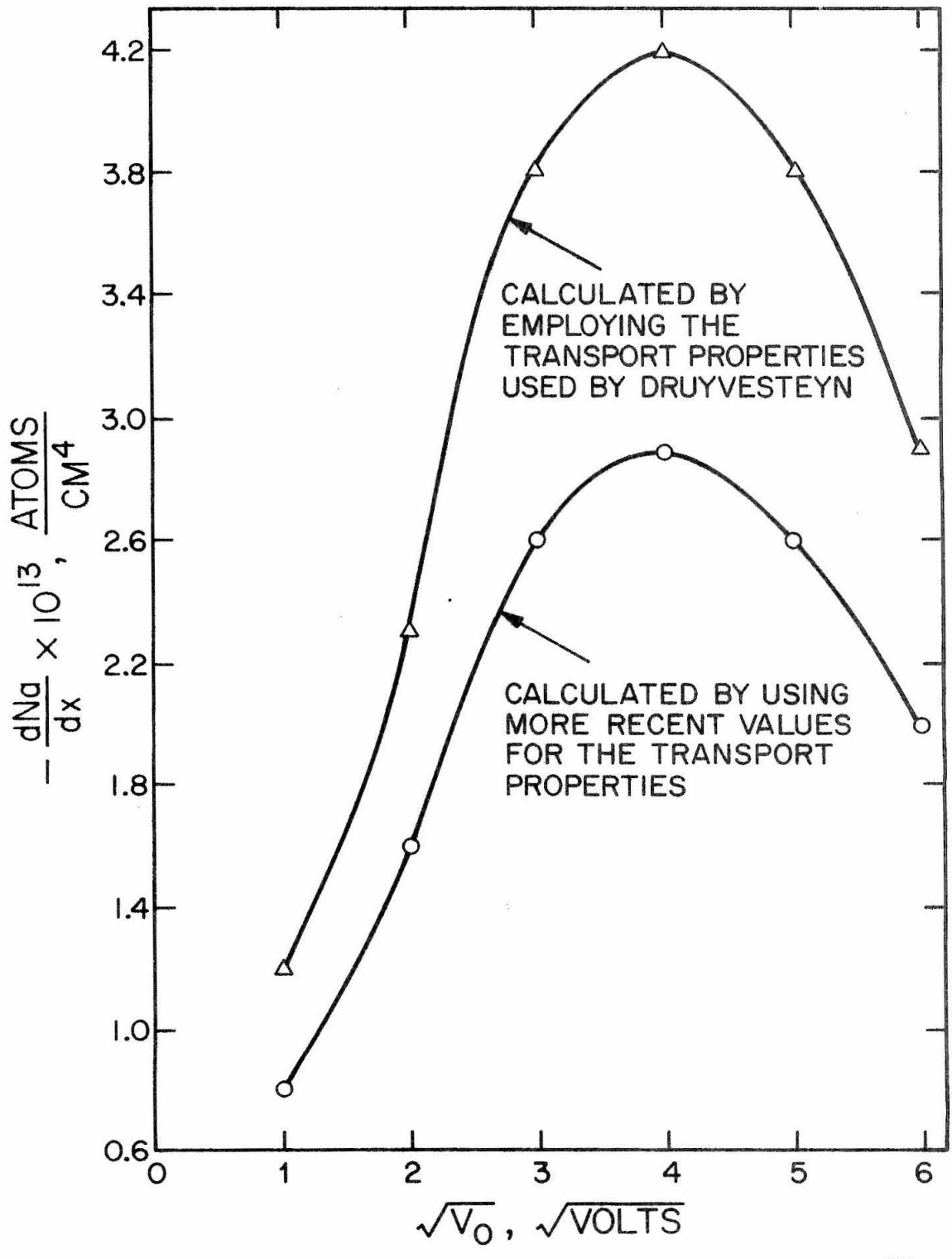

Figure A.1. Axial Gradient of the Hg Density as a Function of $\sqrt{V_o}$

APPENDIX B

A Theoretical Model for Gas Separation in a Glow Discharge: Cataphoresis

Reprinted from JOURNAL OF APPLIED PHYSICS, Vol. 39, No. 12, 5762-5767, November 1968

A Theoretical Model for Gas Separation in a Glow Discharge: Cataphoresis

FREDRICK H. SHAIR AND DONALD S. REMER
Division of Chemistry and Chemical Engineering, California Institute of Technology, Pasadena, California 91109
(Received 4 December 1967; in final form 29 July 1968)

A theoretical model for transient and steady-state cataphoresis is developed starting with the macroscopic equations of continuity. After a brief breakdown period, the impurity ions are assumed to be closely coupled with their neutral counterparts. The basic assumptions in the model are that after breakdown, the level of ionization of the impurity, and the axial electric field remain constant; it is demonstrated that under these conditions a system involving rapid ionization–recombination reactions is equivalent to a system in which no reaction occurs, but in which the "effective" ion mobility is a product of the true ion mobility and the fraction of impurity ionization. The influence of endbulbs commonly employed in experiments is analyzed and found to influence greatly the characteristic time required to reach steady state. Agreement is found between the model and available experimental data. Particular emphasis is placed upon mass spectrometer data reported by Matveeva, and by Beckey, Groth, and Welge; these data are for mixtures of rare gases and for mixtures of hydrogen and deuterium, and involve endbulbs. The ordinary diffusion case, associated with the collapse of the steady state cataphoretic profile, is also analyzed for a system containing endbulbs.

I. INTRODUCTION

It has been known for some time that longitudinal concentration gradients occurred within dc glow-discharge tubes containing various gas mixtures.[1] This effect, resulting from one component being drawn preferentially toward the cathode, has been termed cataphoresis.[2] This phenomenon has been known to occur in at least 23 different binary mixtures.[1–14] The work up to 1958, involving rare gases, was reviewed by Loeb.[15] Cataphoresis has been used primarily as a convenient technique to provide pure gases[16,17]; occasionally, cataphoresis has been used to obtain an impurity level of one part in 10^7 or less.[9,10] As pointed out by Oskam,[18] "even the application of the most refined ultrahigh vacuum techniques cannot remove the rare gas impurities in commercially available gases."[19] Consequently, it is of interest to obtain a better description on both the microscopic and macroscopic levels. Concerning the separation of isotopes, Groth and Harteck[12] found an enrichment of deuterium at the cathode in the case of hydrogen. Continuing along this line, Beckey, Groth, and Welge[14] reported experimental results in which a mass spectrometer was used to monitor the concentration of deuterium and hydrogen in the cathode and anode regions. Later, Matveeva[12] reported mass spectrometer data which she obtained during studies involving binary mixtures of He, Ar, and Ne. Often, the electrodes have been placed within bulbs which are located at the ends of the discharge tube.[9,12,14]

Druyvesteyn[8] presented an approximate treatment for a steady-state cataphoresis without endbulbs. Recently, Freudenthal[20,21] has developed a linearized model of transient cataphoresis when no endbulbs are present. Presented below is a linearized macroscopic model of transient cataphoresis when endbulbs are present.[22] Quantitative comparison is made between the model and the mass spectrometer data reported by Beckey, Groth, and Welge,[14] and by Matveeva.[12] The mass spectrometer data were favored because (1) the initial impurity compositions were reported, and (2) the problem associated with the optical spectroscopic technique near the cathode[11] was avoided. Due to the lack of completeness associated with the optical spectroscopic data reported previously, only a qualitative comparison was made between these data and the model.

Using a system containing endbulbs, Matveeva[12] also studied the collapse of the steady-state cataphoretic profile, after the electrical discharge was extinguished. It is mentioned that Hogervorst and Freudenthal[23] recently used this system *without* endbulbs to measure binary diffusion coefficients.

II. ANALYSIS

Cataphoresis

The mass conservation equations are applied to the impurity ions and to the impurity neutrals, immediately

[1] E. C. C. Baly, Phil. Mag **35**, 200 (1893).
[2] G. Francis, *Encyclopedia of Physics, XXII, Gas Discharges II*, (Springer-Verlag, Berlin, 1956), pl 195.
[3] J. J. Thompson, Proc. Roy. Soc. (London) **58**, 244 (1895).
[4] F. Skaupy, Verh. Deut. Phys. Ges. **18**, 230 (1916).
[5] F. Skaupy and F. Bobek, Z. Tech. Physik **6**, 284 (1925).
[6] F. M. Penning, Physica **1**, 763 (1933).
[7] M. J. Druyvesteyn and N. Warmoltz, Phil. Mag. **17**, 1, (1934).
[8] M. J. Druyvesteyn, Physica **2**, 255 (1935).
[9] R. Riesz and G. H. Dicke, J. Appl. Phys. **25**, 196 (1954).
[10] H. C. Miller, General Electric Research Rept. No. 63-RL-3462G (1963).
[11] A. L. Schmeltekopf, Jr., J. Appl. Phys. **35**, 1712 (1964).
[12] N. A. Matveeva, Bull. Acad. Sci. USSR Phys. Ser. (English Ed.) **23**, 1009 (1959).
[13] W. Groth and P. Harteck, Naturwiss. **22**, 391 (1939).
[14] H. D. Beckey, W. E. Groth, and K. H. Welge, Z. Naturforsch. **8a**, 556 (1953).
[15] L. B. Loeb, J. Appl. Phys. **29**, 1469 (1958).
[16] V. R. Mittelstadt and H. J. Oskam, Rev. Sci. Instr. **32**, 1408 (1961).
[17] L. B. Loeb, R. G. Westberg, and H. C. Huang, Phys. Rev. **123**, 43 (1961).
[18] H. J. Oskam, J. Appl. Phys. **34**, 711 (1963).
[19] The italics are Oskam's (Ref. 18).
[20] J. Freudenthal, Physica **36**, 354 (1967).
[21] J. Freudenthal, J. Appl. Phys. **38**, 4818 (1967).
[22] This research commenced independently of that reported by Freudenthal[20,21] and by Hogervorst and Freudenthal.[23]
[23] W. Hogervorst and J. Freudenthal, Physica **37**, 97 (1967).

after the electric discharge is established. Multiple ionization processes are neglected. Both the electric field, and the ratio of impurity ion concentration to impurity neutral concentration are taken to be constant. When endbulbs are present, the concentration throughout each endbulb is taken to be uniform and equal to the value of the composition at the nearest end of the discharge tube. Only electron impact ionization processes are considered. Whereas the ionization process is taken to be homogeneous in character, the main loss of charged particles is considered to be through ambipolar diffusion to the walls where recombination occurs; this has been the starting point in the development of other theories concerning the positive column.[2,24,25] Let the cathode be situated at $z=0$. The starting equation for the impurity ions is

$$\partial n_+/\partial t = D_+(\partial^2 n_+/\partial Z^2) + D_a(1/r)(\partial/\partial r)[r(\partial n_+/\partial r)] + \mu E(\partial n_+/\partial Z) + R_i. \quad (1)$$

The starting equation for the impurity neutrals is

$$\partial n_0/\partial t = D(\partial^2 n_0/\partial Z^2) + D(1/r)(\partial/\partial r)[r(\partial n_0/\partial r)] - R_i. \quad (2)$$

The first term on the right-hand side represents the ordinary diffusion in the direction parallel to the axis of the tube. We have assumed the diffusion coefficients to be independent of composition. The second term represents the radial diffusion of ions towards the wall, and the radial diffusion of neutrals away from the wall. The third term in the ion equation represents forced diffusion due to a uniform axial electric field. The last term represents the rate of homogeneous ionization which is a source for ions and a sink for neutrals. The quantities D, D_+, and D_a are the diffusion coefficients for neutral diffusion, ion diffusion, and ambipolar diffusion, respectively. As a first approximation, we shall treat the problem assuming $D \simeq D_+$. The nondimensional diffusion equations then become

$$\partial C_+/\partial\tau = (\partial^2 C_+/\partial\eta^2) + (L^2 D_a/R^2 D\rho)(\partial/\partial\rho)[\rho(\partial C_+/\partial\rho)] + [\beta(\partial C_+/\partial\eta)] + (L^2/D)R_i \quad (3)$$

and

$$\partial C_0/\partial\tau = (\partial^2 C_0/\partial\eta^2) + (L^2/R^2\rho)(\partial/\partial\rho)[\rho(\partial C_0/\partial\rho)] - (L^2/D)R_i, \quad (4)$$

where

$$\tau = tD/L^2, \quad \eta = Z/L, \quad \rho = r/R, \quad \beta = \mu EL/D, \quad C_+ = n_+/n_0^0$$

and $C_0 = n_0/n_0^0$. Here L represents the tube length, R the tube radius, and n_0^0 is the density of the impurity which is uniformly dispersed throughout the system before breakdown. The quantity β represents the ratio of the forced diffusion effect to the ordinary diffusion effect.

Multiplying Eqs. (3) and (4) by ρ and integrating from the tube center at $\rho=0$ to the wall at $\rho=1$ yields

$$\partial\langle C_+\rangle/\partial\tau = (\partial^2\langle C_+\rangle/\partial\eta^2) + (L^2 D_a/R^2 D)(\partial C_+/\partial\rho)_{\rho=1} + \beta(\partial\langle C_+\rangle/\partial\eta) + (L^2/D)\langle R_i\rangle \quad (5)$$

and

$$\partial\langle C_0\rangle/\partial\tau = \partial^2\langle C_0\rangle/\partial\eta^2 + (L^2/R^2)(\partial C_0/\partial\rho)_{\rho=1} - (L^2/D)\langle R_i\rangle. \quad (6)$$

The brackets indicate radially averaged quantities such as

$$\langle C_+\rangle = \int_0^1 \rho C_+(\rho)\, d\rho. \quad (7)$$

All ions diffusing to the wall are assumed to be lost, and to recombine rapidly as compared to the characteristic times associated with the diffusion processes. For small diameter tubes, the radial diffusion terms are much larger than the longitudinal diffusion terms. Thus,

$$D_a(\partial C_+/\partial\rho)_{\rho=1} = -D(\partial C_0/\partial\rho)_{\rho=1}. \quad (8)$$

Since $D_a \simeq D_+[1+(T_e/T_i)]$ and $T_e \gg T_i$ in the positive column of the glow discharge, then $|(\partial C_+/\partial\rho)_{\rho=1}| \ll |(\partial C_0/\partial\rho)_{\rho=1}|$.

The level of ionization of the impurity,

$$\langle C_+\rangle/(\langle C_+\rangle + \langle C_0\rangle),$$

is assumed constant and independent of time and of position in the discharge. This assumption implies that we do not treat the case where the ionization frequencies of the impurity and of the host gas are of the same order. Adding Eqs. (5) and (6) and rearranging yields a general equation for cataphoresis:

$$\partial\theta/\partial\tau = (\partial^2\theta/\partial\eta^2) + \alpha(\partial\theta/\partial\eta). \quad (9)$$

We have defined

$$\theta = (\langle C_0\rangle + \langle C_+\rangle)$$

and

$$\alpha = (\langle C_+\rangle/\langle C_0\rangle + \langle C_+\rangle)(\mu EL/D).$$

Thus, when the impurity ions and neutrals are tightly coupled, the reacting system is found to be equivalent to an inert system; however, the inert system is one in which the "effective" ion mobility is a product of the true ion mobility and the level of ionization of the impurity. When $\langle C_+\rangle \ll \langle C_0\rangle$, then $\alpha \sim (\langle C_+\rangle/\langle C_0\rangle)(\mu EL/D)$ and Eq. (9) reduces to Freudenthal's principle equation.[20,21]

Equation (9) must be solved under appropriate boundary conditions for the experiments considered. The boundary conditions which represent the influence of the endbulbs are

$$(\partial\theta/\partial\eta) + \alpha\theta = \delta(\partial\theta/\partial\tau) \quad \text{at } \eta=0 \quad (10)$$

[24] F. Llewelleyn-Jones, Methuen & Co., Ltd. (London) 1966.
[25] I. M. Cohen and M. D. Kruskal, Phys. Fluids 8, 920 (1965).

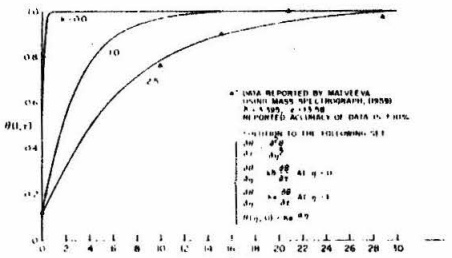

FIG. 1. Argon concentration vs time near the anode for backward diffusion in argon helium mixture.

and

$$(\partial\theta/\partial\eta) + \alpha\theta = -\epsilon(\partial\theta/\partial\tau) \qquad \text{at } \eta = 1. \qquad (11)$$

The quantity δ is the ratio of the volume of the bulb surrounding the cathode to the volume of the discharge tube. Similarly, ϵ, is the ratio of the volume of the bulb surrounding the anode to the volume of the discharge tube. Equation (10) states that a flux of impurity out of the tube at $\eta = 0$ results in an increase in the concentration of impurity in the bulb surrounding the cathode.

On the other hand, Eq. (11) states that a flux of impurity into the tube at $\eta = 1$ results in a decrease in the concentration of impurity in the bulb surrounding the anode. Each endbulb is assumed to be well mixed so that the impurity composition in the cathode bulb is uniform and equal to the impurity composition at $\eta = 0$; likewise, the impurity composition in the anode bulb is assumed uniform and equal to the impurity composition at $\eta = 1$.

The initial condition is

$$\theta = 1 \qquad \text{for all } \eta. \qquad (12)$$

It should be noted that the eigenfunctions for the above problem are not orthogonal in the usual sense. Since the problem has been solved elsewhere,[20] we shall merely write down the solution:

$$\theta(\eta, \tau) = Ke^{-\alpha\eta} + \alpha e^{-\alpha\eta/2} \exp(-\alpha^2\tau/4) \sum_{n=1}^{\infty} A_n^{-1} \times \{[\mu_n \cos\mu_n(1-\eta) + E_n \sin\mu_n(1-\eta)] - e^{\alpha/2}[\mu_n \cos\mu_n\eta - D_n \sin\mu_n\eta]\} \exp(-\mu_n^2\tau), \qquad (13)$$

where

$$A_n = [(\alpha^2/4) + \mu_n^2]^2\{[\delta\epsilon + (\delta+\epsilon)/2]\sin\mu_n - F_n(\cos\mu_n/2\mu_n)\} \qquad (14)$$

$$D_n = \tfrac{1}{2}\alpha[1 + \delta(\tfrac{1}{2}\alpha)] + \delta\mu_n^2 \qquad (15)$$

$$E_n = \tfrac{1}{2}\alpha[1 - \epsilon(\tfrac{1}{2}\alpha)] - \epsilon\mu_n^2 \qquad (16)$$

$$F_n = 1 + \delta + \epsilon + (\alpha/2)(\delta - \epsilon) - \delta\epsilon(\tfrac{1}{4}\alpha^2 + \mu_n^2) \qquad (17)$$

and

$$K = (1 + \delta + \epsilon)/(\delta + \epsilon e^{-\alpha} - e^{-\alpha}/\alpha + 1/\alpha). \qquad (18)$$

[20] F. H. Shair and D. S. Cohen, J. Chem. Eng. Sci (in press).

The terms, μ_n, are solutions to the following equation:

$$\tan\mu_n = -(\delta+\epsilon)\mu_n/[1 + \tfrac{1}{2}\alpha(\delta - \epsilon) - \delta\epsilon(\tfrac{1}{4}\alpha^2 + \mu_n^2)]. \qquad (19)$$

The first term in Eq. (13) represents the steady-state solution, while the rest represents the transient part which decays rapidly in time. The constant K was obtained from a mass balance between the final and initial concentration profiles.

$$\delta\theta(0, \infty) + \int_0^1 Ke^{-\alpha\eta}d\eta + \epsilon\theta(1, \infty) = 1 + \delta + \epsilon. \qquad (20)$$

Typical values of θ vs τ when $\delta = \epsilon$ are shown in Figs. 7 and 8.

Collapse of the Steady-State Cataphoretic Profile

At time equal to zero, the discharge is extinguished and the exponential concentration profile collapses in time to a flat uniform concentration profile. Here again, account is taken for the endbulbs present in the experiment. The equation to be solved is

$$\partial\theta/\partial\tau = \partial^2\theta/\partial\eta^2 \qquad (21)$$

with boundary conditions

$$\partial\theta/\partial\eta = \delta(\partial\theta/\partial\tau) \qquad \text{at } \eta = 0 \qquad (22)$$

and

$$\partial\theta/\partial\eta = -\epsilon(\partial\theta/\partial\tau) \qquad \text{at } \eta = 1. \qquad (23)$$

The initial condition for this case is

$$\theta = Ke^{-\alpha\eta}. \qquad (24)$$

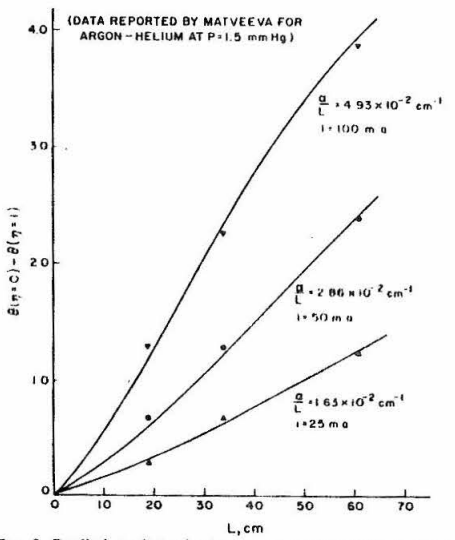

FIG. 2. Prediction of steady-state concentration difference as a function of L.

As before, the problem is non self-adjoint and has been solved elsewhere.[26] The solution is

$$\theta(\eta,\tau) = 1 + 2\alpha\Lambda \sum_{n=1}^{\infty} B_n^{-1}\{(1+\alpha\delta)B_n^{-1} \times[\cos\mu_n(1-\eta) - \epsilon\mu_n \sin\mu_n(1-\eta)] - (1-\alpha\epsilon)(\cos\mu_n\eta - \delta\mu_n \sin\mu_n\eta)\} \exp(-\mu_n^2\tau), \quad (25)$$

where

$$B_n = (\alpha^2+\mu_n^2)[(1+\delta+\epsilon-\delta\epsilon\mu_n^2)\cos\mu_n - (\delta+\epsilon+2\delta\epsilon)\mu_n \sin\mu_n]. \quad (26)$$

The terms μ_n for this problem are solutions to the following equation:

$$\tan\mu_n = -(\delta+\epsilon)\mu_n/(1-\delta\epsilon\mu_n^2). \quad (27)$$

III. DISCUSSION

Calculations with Eq. (13) indicate that the steady-state cataphoretic profile is much more sensitive to α than to δ and ϵ. On the other hand, the characteristic time τ_c associated with transient cataphoresis is quite *insensitive* to α but extremely sensitive to δ and ϵ.

Matveeva[12] monitored the composition near the anode during the buildup of the cataphoretic profile; in order to obtain agreement between the model and experiment an "effective" volume of each bulb, equal to 1.7 times that of the reported values, was required. This is not unexpected,[27] since Eq. (13) is the solution to an idealized problem in which the endbulbs are adequately stirred. In Matveeva's[12] transient cataphoretic experiment, it was found that $\tau_c = 3.4$ and $\alpha = 3.5$. Using the *actual* volumes of the endbulbs yields a $\tau_c = 2.0$. When no endbulbs are present, the calculated $\tau_c = 0.009$.

Matveeva[12] also monitored the composition near the anode during the collapse of the cataphoretic profile. As indicated in Fig. 1, in order to obtain agreement between Eq. (25) and experiment, we had to take an "effective" volume of each bulb equal to 2.5 times that of the reported values. The difference in the effective volumes required for the two experiments may be due to some endbulb mixing in the cataphoretic experiment; electrode heating along with the discharge within the endbulbs, may have caused free convection.

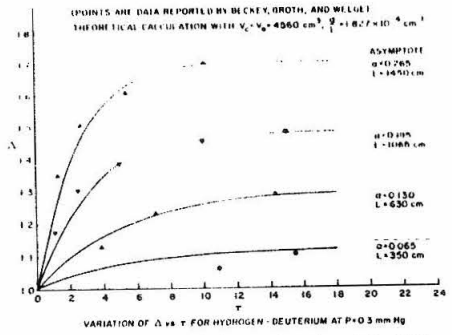

FIG. 3. Variation of Δ vs τ for hydrogen-deuterium at $P = 0.3$ Torr.

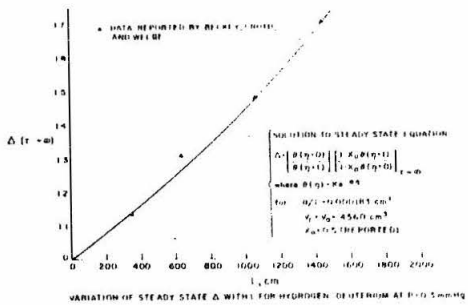

FIG. 4. Variation of steady-state Δ with L for hydrogen deuterium at $P = 0.3$ Torr.

The data reported in Matveeva's Figs. 3, 4, and 5 were then analyzed within the framework of our model. If $E \sim 10$ V/cm, then calculated values of $\langle n_+ \rangle$ near the cathode region ranged from 10^{10}-10^{12} ions/cm^3; the corresponding values near the anode ranged from 10^9-10^{11} ions/cm^3. These values appear to be reasonable. It should be mentioned that the data points were measured by tracings onto mm graph paper. A comparison between our model and the data reported in Fig. 7 of Matveeva[12] is shown in Fig. 2 of this text. For each of the three values of discharge currents, it was possible to obtain excellent agreement with a single value of α/L.

Beckey, Groth, and Welge[14] (referred to as BGW) monitored the concentration of D_2 and H_2 in both the anode and cathode regions. BGW reported their data using tau, which they defined

$$\tau_{BGW} = \left(\frac{\text{mole fraction of } D_2 \text{ at cathode}}{\text{mole fraction of } D_2 \text{ at anode}}\right) \times \left(\frac{\text{mole fraction of } H_2 \text{ at anode}}{\text{mole fraction of } H_2 \text{ at cathode}}\right). \quad (28)$$

In order to avoid any ambiguity, we shall define $\Delta \equiv \tau_{BGW}$, which is related to our θ by the following expression:

$$\Delta = [\theta(\eta=0,\tau)/\theta(\eta=1,\tau)] \times \{[1-0.5\theta(\eta=1,\tau)]/[1-0.5\theta(\eta=0,\tau)]\}. \quad (29)$$

In the above expression, τ refers to the dimensionless time as used in Eq. (13). The factor 0.5 is present because the initial mole fraction of deuterium was 0.5 in all the experiments reported. Unfortunately, BGW

[27] J. Crank, *The Mathematics of Diffusion* (Clarendon Press, Oxford, 1956).

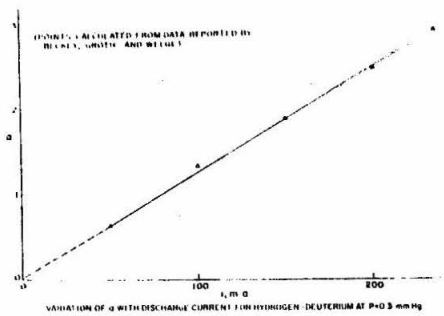

FIG. 5. Variation of α with discharge current for hydrogen–deuterium at $P=0.3$ Torr.

report neither electric field data nor the volumes of the "large flasks situated near the anode and cathode."[28] However, from their Fig. 1, it is reasonable to assume that the volumes of both flasks are approximately equal, i.e., $\delta=\epsilon$.

As shown in Figs. 3 and 4, values of $V_c=V_a=4560$ cm^3 and $\alpha/L=1.827\times10^{-4}$ allow agreement between our model and the data reported in Figs. 2 and 3 of BGW. If $E\sim10$ V/cm, then calculated values of $\langle n_1\rangle$ in the discharge ranged from 10^{10} to 10^{11} ions/cm^3. Figure 4 of BGW indicates that a plot of $\ln[\Delta(\tau\to\infty)-\Delta(\tau)]$ vs time is linear, which is in agreement with the model. Figure 5 of BGW indicates a linear relation between $\ln[\Delta(\tau\to\infty)]$ vs discharge current; as shown in our Fig. 5, these data suggest that the quantity $(\langle n_+\rangle/\langle n_0\rangle)E$ is linearly proportional to the discharge current. This conclusion appears reasonable as a number of investigators[29] have found that in the glow discharge the electron density at constant pressure is linearly proportional to the discharge current, while E does not change much at higher currents.

Volume of Endbulbs: Equation (13) indicates that τ_c is linearly proportional to $\delta+\epsilon$. Thus, when L and R are kept constant, both τ_c and t_c are linearly proportional to V_c+V_a. Riesz and Dicke[9] reported: "The time at which equilibrium is reached depends on the volume of the bulb B. (This was a bulb attached to the anode region.) The larger its volume, the longer it takes before equilibrium is reached. If it is omitted equilibrium is reached within a minute; ..."[30] Undoubtedly, the long characteristic times reported by Matveeva[12] and by BGW[14] are due to the large values of δ and ϵ present in their experiments. The calculated influence of bulb size upon τ_c relevant to the data reported by BGW, is shown in Fig. 6. As indicated in Fig. 6, τ_c is relatively insensitive to α.

A large endbulb at the cathode is predicted to decrease the steady state concentration of the impurity near the anode; the limiting value of θ at $\eta=1$ is predicted to be $e^{-\alpha}$. Regarding Matveeva's experiment,[12] she probably would have obtained much lower Ar concentrations at the anode had she reversed the electric field.

Tube Length: When δ and ϵ are kept constant, τ_c is also constant; thus t_c is proportional to L^2. When V_c and V_a are kept constant, both δ and ϵ vary inversely with L; then t_c is directly proportional to L. This prediction is in agreement with Matveeva[12] and BGW.[14]

Because of the exponential dependence of α, the tube length *greatly* influences the steady-state concentration profile. The longer the tube, the greater will be the concentration difference between the anode and cathode. This prediction is in agreement with experimental observations.[11,12,14]

Tube Radius: For fixed values of V_c and V_a, t_c is predicted to be proportional to R^{-2}. Unfortunately, there are no data available to test this prediction.

Concerning the steady-state concentration profile, changes in R will influence α. If the discharge current is kept constant, both the production rate of ions and the loss rate of ions should vary as R^{-2}; however, for small diameter tubes, E decreases as R increases.[2,24] Thus, α should decrease with increasing R; this is in agreement with Schmeltekopf[11] and with BGW.[14]

Pressure: Since the diffusion coefficient is inversely proportional to P, t_c is predicted to be directly proportional to P; this is in agreement with Matveeva[12] and BGW.[14]

Since both μ and D are inversely proportional to P, P affects α mainly through the ionizational fraction and through the electric field. Since the ambipolar diffusion coefficient is inversely proportional to P, the loss rate of ions should vary inversely with P. On the other hand,

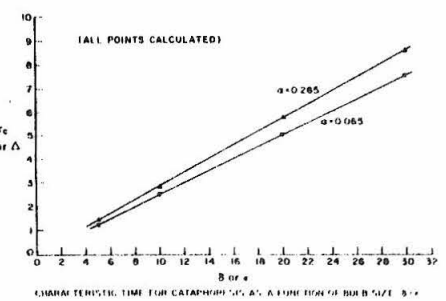

FIG. 6. Characteristic time for cataphoresis as a function of bulb size: $\delta=\epsilon$.

[28] The italics are BGW's (Ref. 14).
[29] Among others, J. F. Prince, and W. W. Robertson, J. Chem. Phys. 45, 2577 (1966).
[30] Yu. A. Pekar, Sov. Phys. 11, 1024 (1967).

the production rate of ions may increase with increasing P. Both these effects enhance the ionization fraction and increase α. The value of α may be further enhanced since the longitudinal electric field also increases with increasing pressure.[34] The actual pressure dependence will depend upon the ionization mechanism. In the case of neon with argon impurity, the Penning effect helps keep the separation relatively pressure independent.[18] Oskam[18] also points out that in the case of helium with neon impurity, an increase in pressure will increase the production rate of He_2^+ through the Hornbeck Molnar process, $He^* + He \rightarrow He_2^+ + e$, and through the three-body process $He^+ + 2He \rightarrow He_2^+ + He$. These processes are important since the neon is probably ionized by $He_2^+ + Ne \rightarrow Ne^+ + 2He$, as suggested by Loeb[16] and Oskam.[18] At higher pressures, three-body recombination may become important thus tending to minimize the influence of pressure. Aside from the early work of Skaupy and Bobek,[5] this is in agreement with experimental observations.[9,11,12,14]

Discharge Current: If heating effects upon the transport properties are negligible, t_e should not be significantly influenced by the discharge current; this is in agreement with experimental observations.[12]

Concerning the steady state, increasing the discharge current should increase α by increasing the ion production rate. As suggested in Schmeltekopf's empirical relation,[11] the current density is more fundamental than the actual discharge current. Experimental observations have shown that the cataphoretic separation is enhanced with increasing discharge current.[5,9,11-14]

Gas Temperature: The gas temperature is expected to influence t_e by changing the diffusion coefficient.

Regarding the steady state, increasing the gas temperature increases the loss rate of ions to the wall

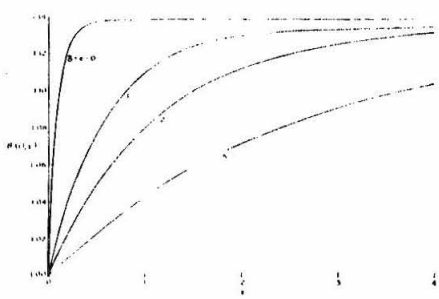

FIG. 7. Concentration at the cathode as a function of time for cataphoresis with equal size endbulbs ($\delta = \epsilon$) for the case where $\alpha = 0.265$

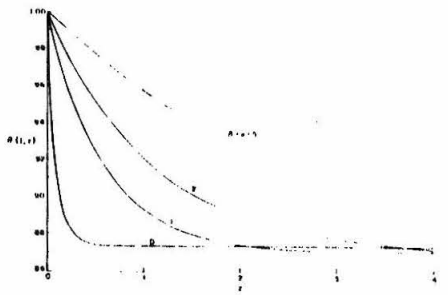

FIG. 8. Concentration at the anode as a function of time for cataphoresis with equal-size endbulbs ($\delta = \epsilon$) for the case where $\alpha = 0.265$.

and thus tends to reduce α by lowering the ionization fraction of the impurity. Experimental results[11,14] indicate that the steady-state separation is reduced with increasing gas temperature.

Initial Composition: The model suggests that t_e should be relatively independent of the initial composition of the impurity; this is in agreement with experiment[12].

These experimental results also indicate that the steady-state separation increases with decreasing initial impurity concentration. Possibly, the ionization fraction of the impurity increases with decreasing concentration of impurity. If this be the case, the variation of α within each of the experiments analyzed was apparently weak enough to allow agreement between a linear model and an inherently nonlinear phenomenon. However, there are initial values of the impurity composition which will lead to a transition regime, where the ionization frequencies for the impurity gas and for the host gas are of the same order of magnitude. Then the electric field and the level of impurity ionization will be dependent upon the longitudinal position.[30,31] In this case, variations from the linear model may be quite significant. Also, in some cases, the volume force in electrophoresis[32] may give rise to deviations from the assumed model.

ACKNOWLEDGMENT

This work was supported in part by grants from the Sloan Foundation and the Shell Oil Company. Grateful acknowledgment is made to the donors of said funds.

[31] Yu A. Pekar, Sov. Phys. 12, 800 (1967).
[32] C. C. Leiby, Jr. and H. J. Oskam, Phys. Fluids 10, 1992 (1967).

APPENDIX C

Use of a Tungsten Filament Lamp as a Pirani Gauge for Continuous Gas Analysis

Reprinted from THE REVIEW OF SCIENTIFIC INSTRUMENTS, Vol. 40, No. 7, 968-969, July 1969
Printed in U. S. A.

Use of a Tungsten Filament Lamp as a Pirani Gauge for Continuous Gas Analysis*

D. S. REMER AND F. H. SHAIR

Division of Chemistry and Chemical Engineering,
California Institute of Technology,
Pasadena, California 91109

(Received 17 October 1968; and in final form, 20 November 1968)

REPORTED herein is a thermal conductivity technique by which continuous and quantitative data have been obtained in a cataphoretic system without sample withdrawal. Spectroscopic techniques were the earliest ones used to measure cataphoresis.[1-5] When end bulbs are present in the discharge system, Mittelstadt and Oskam[6] have reported a clever way to periodically determine if the gas within an endbulb is spectroscopically pure. Mass spectrometers have been successfully used to obtain cataphoretic data, but samples must be removed from the discharge system.[5,7-9] Recent studies have been reported in which a thermal conductivity probe was utilized for measuring cataphoresis.[10,11] For this conductivity method, Flinn[10] stated "The removal of a sample from the discharge system tended to disturb the system somewhat, but the 7 minutes average time between samples was adequate to restore the steady-state condition."

The disturbance, associated with sample withdrawal in the above technique, may be eliminated by having each gas stream flow through a 60 W lamp. In the flow system the lamp filaments must be calibrated for both composition and flow rate. In the nonflow system involving endbulbs the 60 W lamp is connected directly behind a porous molybdenum screen serving as the anode. The molybdenum screen is rolled tightly inside a 9.5 mm Kovar glass-to-metal seal which is grounded. The gas discharge system is cooled by a constant temperature water bath. For typical operating conditions in nonflow cataphoretic systems, the product of the Grashof and Prandtl numbers is $\sim 10^{-8}$, thereby indicating that heat transfer from the filament by free convection is negligible.[12,13] Although the 60 W lamp filament is in a close helix-in-helix winding, a simple conduction analysis of a straight thin wire predicts the calibration curves quite accurately. Binary mixtures with helium or hydrogen are ideally suited to this technique because of their relatively high thermal conductivities. The lamp filament provides one leg in a Wheatstone bridge. The imbalance of the bridge circuit is amplified and recorded on a strip chart. Typical results, shown in Fig. 1, are in agreement with theory.[14]

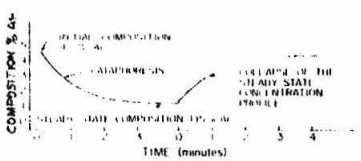

FIG. 1. Argon composition at the anode in a He+Ar mixture vs time for cataphoresis and for back diffusion after the discharge is turned off. Current = 100 mA; pressure = 3.2 mm.

* This work was supported in part with funds provided by the United States Atomic Energy Commission.

[1] E. C. C. Baly, Phil. Mag. **35**, 200 (1893).
[2] F. M. Penning, Physica **1**, 763 (1933).
[3] M. J. Druyvesteyn and N. Warmoltz, Phil. Mag. **17**, 1 (1934).
[4] R. Riesz and G. H. Dieke, J. Appl. Phys. **25**, 196 (1954).
[5] A. L. Schmeltekopf, Jr., J. Appl. Phys. **35**, 1712 (1964).
[6] V. R. Mittelstadt and H. J. Oskam, Rev. Sci. Instrum. **32**, 1408 (1961).
[7] N. A. Matveeva, Bull. Acad. Sci. USSR, Phys. Ser. **23**, 1009 (1959).
[8] J. Freudenthal, Physica **36**, 365 (1967).
[9] H. D. Berkey, W. E. Groth, and K. H. Welge, Z. Naturforsch. **8a**, 556 (1953).
[10] James E. Flinn, Doctoral dissertation, University of Cincinnati (University Microfilms, Inc., Ann Arbor, Michigan, 1965), p. 130.
[11] J. E. Flinn and R. H. Price, Ind. Eng. Chem. Process Design Develop. **5**, 75 (1966).
[12] N. V. Tsederberg, *Thermal Conductivity of Gases and Liquids* (The MIT Press, Cambridge, Massachusetts, 1965), Chap. 1, p. 22.
[13] William H. McAdams, *Heat Transmission* (McGraw-Hill Book Co., New York, 1954), 3rd ed., Chap. 7, p. 176.
[14] F. H. Shair and D. S. Remer, J. Appl. Phys. **39**, 5762 (1968).

APPENDIX D

Error Analysis

ERROR ANALYSIS

An error analysis of the directly measured quantities and the calculated quantities is considered in this appendix. The method of analysis is based on the discussion by Mickley, Sherwood, and Reed [42] on the interpretation of data and the propagation of errors.

In the first part of the appendix, the errors in the directly measured quantities are described. The pressure in the discharge chamber was measured with a McLeod gauge which was accurate to ±0.1 mm Hg in the range of 5 mm Hg to 10 mm Hg and ±0.05 mm Hg in the range of 1 mm Hg to 5 mm Hg. The mercury levels in the absolute-pressure manometer were read with the cathetometer to an uncertainty of ±0.01 mm Hg. The water-bath temperature was accurate to ±0.02°C. The characteristic time for cataphoresis was determined by using a scale to measure the distance to an uncertainty of ±1/16 inch. The distance was converted to a time with uncertainty of ±0.06 minutes by using the recorder speed of 1.0 inch/minute. The distance between the electric-field probes was measured with a scale to within ±1 mm. The length of the discharge tube was also measured with a scale to an uncertainty of ±2 cm. The current through the discharge tube was measured with a Simpson DC milliammeter, Model No. 1150-1, with an error of ±1 ma. The electric field was measured by using a Keithley, Model 601, electrometer with an uncertainty of ±1 volt.

The errors in the directly measured quantities are summarized below.

Measured Quantities and Estimated Errors

Variable	Measured to
P (McLeod gauge, 5 mm Hg to 10 mm Hg)	±0.1 mm Hg
P (McLeod gauge, 1 mm Hg to 5 mm Hg)	±0.05 mm Hg
P (manometer)	±0.01 mm Hg
T	±0.02°C
t_c	±0.06 min
d	±1 mm
L	±2 cm
i	±1 ma
V	±1 volt

In the second part of this appendix, the errors in the calculated quantities are described. The maximum and minimum values for each quantity are used in the following discussion. The electric field was between 8.5 volts/cm and 36.4 volts/cm. The error in the electric field for these two values was calculated to be 8.5 ± 0.9 volts/cm and 36.4 ± 2.2 volts/cm. Therefore, the bounds for the error in the reported values of the electric field were ±(0.9 to 2.2) volts/cm. The uncertainty in the initial composition of mixtures was calculated to be ±0.1 mole %.

The equation for K in Chapter IV is

$$K = \frac{1 + \delta + \varepsilon}{\delta + \varepsilon e^{-\alpha} - \frac{e^{-\alpha}}{\alpha} + \frac{1}{\alpha}} \tag{23}$$

The error in K was calculated using Eq. (2-5) in Mickley, Sherwood, and Reed [42]. If α is assumed constant and the denominator in Eq. (23) is denoted by $\underline{D}$, then

$$\Delta K = \frac{\underline{D} - (1+\delta+\varepsilon)}{\underline{D}^2} \Delta\delta + \frac{\underline{D} - (1+\delta+\varepsilon)e^{-\alpha}}{\underline{D}^2} \Delta\varepsilon \tag{34}$$

The values of ε and δ were $\varepsilon = 4.2 \pm 0.2$ and $\delta = 8.9 \pm 0.5$. The range of α was between 0.13 and 4.33. The results for ΔK were $\Delta K = \pm 0.003$ with $\alpha = 0.13$ and $\Delta K = \pm 0.050$ with $\alpha = 4.33$.

The composition is obtained from the calibration curve to about ±0.2 mole %; refer to Figs. 8 and 9. The error in the value of $\theta(1,\infty)$ is calculated to be within ±0.06.

The value of α was obtained from Eqs. (22) and (23). The error in the calculated value of α for the maximum and minimum values of α was 4.33 ± 1.10 and 0.12 ± 0.06.

The value of n_+/n_o was obtained from Eq. (25). The error in the calculated value of n_+/n_o for the maximum and minimum values of n_+/n_o was $(178 \pm 82) \times 10^{-6}$ and $(4.8 \pm 1.9) \times 10^{-6}$.

It is evident that the use of Eq. (2-5) in reference [42] probably overestimates the error because it is assumed that the error extremes are additive. However, the method still serves as a useful tool for estimating the maximum error in the calculated quantities.

APPENDIX E

Tables

TABLE E-1

THE VALUES OF α AND $\theta(1,\infty)$ FOR $\delta = 8.9$ AND $\varepsilon = 4.2$

α	$\theta(1,\infty)$	α	$\theta(1,\infty)$
0.05	0.967	1.20	0.395
0.10	0.935	1.25	0.378
0.15	0.903	1.30	0.362
0.20	0.872	1.35	0.347
0.25	0.841	1.40	0.332
0.30	0.811	1.45	0.318
0.35	0.782	1.50	0.304
0.40	0.754	1.55	0.291
0.45	0.726	1.60	0.278
0.50	0.699	1.65	0.266
0.55	0.673	1.70	0.254
0.60	0.647	1.75	0.243
0.65	0.622	1.80	0.232
0.70	0.598	1.85	0.221
0.75	0.575	1.90	0.211
0.80	0.552	1.95	0.202
0.85	0.530	2.00	0.193
0.90	0.509	2.05	0.184
0.95	0.488	2.10	0.176
1.00	0.468	2.15	0.168
1.05	0.449	2.20	0.160
1.10	0.430	2.25	0.153
1.15	0.412	2.30	0.146

TABLE E-1 - Continued

α	$\theta(1,\infty)$	α	$\theta(1,\infty)$
2.35	0.139	3.45	0.048
2.40	0.132	3.50	0.046
2.45	0.126	3.55	0.044
2.50	0.120	3.60	0.041
2.55	0.115	3.65	0.040
2.60	0.109	3.70	0.038
2.65	0.104	3.75	0.036
2.70	0.099	3.80	0.034
2.75	0.095	3.85	0.032
2.80	0.090	3.90	0.031
2.85	0.086	3.95	0.029
2.90	0.082	4.00	0.028
2.95	0.078	4.05	0.027
3.00	0.074	4.10	0.025
3.05	0.071	4.15	0.024
3.10	0.068	4.20	0.023
3.15	0.064	4.25	0.022
3.20	0.061	4.30	0.021
3.25	0.058	4.35	0.020
3.30	0.056	4.40	0.019
3.35	0.053	4.45	0.018
3.40	0.050	4.50	0.017

TABLE E-2

Results for Cataphoresis in He-Ar

Measured							Calculated			
n_o^o (% Ar)	i (ma)	P (mm Hg)	$\theta(1,\infty)$	E (V/cm)	t_c^E (min)	τ_c^E	t_c^M (min)	τ_c^M	α	$n_+/n_o \times 10^6$
4.7	25	3.2	0.915	12.6	1.12	2.39	1.37	2.92	0.13	4.8
4.7	100	3.2	0.245	8.5	1.00	2.13	0.91	1.94	1.74	96.3
4.7	50	3.2	0.681	10.2	1.31	2.79	1.26	2.68	0.53	24.2
4.7	25	5.5	0.894	15.5	2.62	3.24	2.35	2.90	0.16	4.8
4.7	100	5.5	0.138	10.7	1.44	1.78	1.26	1.56	2.36	103
4.7	50	5.5	0.585	12.7	1.38	1.70	2.07	2.55	0.73	26.7
4.7	25	8.9	0.790	20.0	3.75	2.86	3.67	2.80	0.34	7.9
4.7	100	8.9	0.030	13.7	1.40	1.07	--	--	3.92	133
4.7	50	8.9	0.383	15.9	3.13	2.39	2.93	2.24	1.24	36.3

TABLE E-3

Results for Cataphoresis in He-Ne

Measured							Calculated			
n_o^o (% Ne)	i (ma)	P (mm Hg)	$\theta(1,\infty)$	E (V/cm)	t_c^E (min)	τ_c^E	t_c^M (min)	τ_c^M	α	$n_+/n_o \times 10^6$
4.8	100	6.0	0.403	11.1	2.00	3.28	1.39	2.28	1.18	98.7
4.8	50	6.0	0.631	11.2	2.00	3.28	1.60	2.62	0.63	52.2
4.8	25	6.0	0.900	12.6	1.16	1.90	1.78	2.91	0.15	11.0
4.8	75	6.0	0.458	11.1	2.31	3.79	1.45	2.37	1.03	86.1
2.4	25	6.0	0.861	11.9	0.72	1.18	1.75	2.87	0.22	17.2
2.4	50	6.0	0.483	11.4	1.56	2.56	1.47	2.41	0.96	78.1
2.4	75	6.0	0.251	11.5	2.56	4.20	1.19	1.95	1.72	139
2.4	50	3.5	0.635	11.9	0.78	2.17	0.94	2.62	0.62	48.3
2.4	50	9.1	0.430	12.4	2.28	2.45	2.17	2.33	1.10	82.3

TABLE E-4

Results for Cataphoresis in He-N_2

Measured							Calculated			
n_o^o (% N_2)	i (ma)	P (mm Hg)	$\theta(1,\infty)$	E (V/cm)	t_c^E (min)	τ_c^E	t_c^M (min)	τ_c^M	α	$n_+/n_o \times 10^6$
4.8	15	6.3	0.864	33.5	2.90	2.94	2.83	2.87	0.21	5.2
4.8	25	6.3	0.600	32.9	2.73	2.77	2.53	2.57	0.70	17.7
4.8	50	6.3	0.173	29.2	1.86	1.89	1.69	1.71	2.12	60.5
4.8	75	6.3	0.021	27.6	1.10	1.12	--	--	4.33	131
2.2	7.5	6.3	0.728	27.3	4.38	4.44	2.69	2.73	0.45	13.7
2.2	15	6.3	0.445	26.3	2.65	2.68	2.31	2.35	1.06	33.5
2.2	25	6.3	0.241	23.4	3.69	3.74	1.90	1.93	1.76	62.6
2.2	50	6.3	0.022	21.6	2.17	2.20	--	--	4.33	168
1.2	5	6.3	0.433	26.7	1.73	1.75	2.35	2.37	1.09	33.9
1.2	9	6.3	0.267	27.8	2.04	2.07	1.97	2.00	1.64	49.1
1.2	20	6.3	0.020	26.9	1.22	1.24	--	--	4.33	133
4.8	50	8.8	0.160	36.4	1.69	1.23	2.29	1.66	2.20	50.0
4.8	50	2.7	0.275	17.7	1.25	2.96	0.85	2.02	1.61	75.6
4.8	50	4.3	0.190	21.7	1.75	2.60	1.19	1.77	2.01	77.2
4.8	50	2.2	0.379	15.8	1.12	3.25	0.77	2.24	1.25	65.7

TABLE E-5

Results for Cataphoresis in He-O_2

Measured							Calculated			
n_o^o (% O_2)	i (ma)	P (mm Hg)	$\theta(1,\infty)$	E (V/cm)	t_c^E (min)	τ_c^E	t_c^M (min)	τ_c^M	α	$n_+/n_o \times 10^6$
5.0	75	6.0	0.080	25.7	4.38	4.95	--	--	2.93	101
5.0	50	6.0	0.344	26.8	2.72	3.07	1.92	2.17	1.36	44.8
5.0	35	6.0	0.536	27.4	2.53	2.86	2.20	2.49	0.84	27.0
5.0	20	6.0	0.764	28.4	1.19	1.34	2.45	2.77	0.38	11.4
5.0	85	6.0	0.020	24.8	3.31	3.74	--	--	4.32	154
5.0	50	7.5	0.370	28.0	2.72	2.46	2.46	2.22	1.28	40.4
5.0	50	4.0	0.350	20.3	2.16	3.66	1.29	2.18	1.34	58.3
5.0	50	2.7	0.440	19.8	1.91	4.80	0.94	2.35	1.07	47.6
5.0	50	2.1	0.500	13.6	0.66	2.13	0.76	2.44	0.92	59.6
2.2	25	6.0	0.332	23.6	1.75	1.98	1.90	2.15	1.40	52.5
2.2	15	6.0	0.632	24.7	1.13	1.28	2.32	2.62	0.63	22.5
2.2	35	6.0	0.100	22.4	1.84	2.08	1.20	1.36	2.69	106
2.2	42.5	6.0	0.020	21.5	1.59	1.80	--	--	4.32	178
4.1	50	6.0	0.250	25.0	1.69	1.91	1.73	1.96	1.71	56.2
4.1	72.5	6.0	0.020	22.5	1.41	1.60	--	--	4.32	170
4.1	35	6.0	0.462	28.1	2.09	2.36	2.11	2.38	1.02	32.0
4.1	20	6.0	0.658	30.4	0.97	1.10	2.35	2.65	0.58	16.9

TABLE E-6

Results for Cataphoresis in He-CO

Measured							Calculated			
n_o^o (% CO)	i (ma)	P (mm Hg)	$\theta(1,\infty)$	E (V/cm)	t_c^E (min)	τ_c^E	t_c^M (min)	τ_c^M	α	$n_+/n_o \times 10^6$
4.9	50	6.3	0.575	28.7	0.94	1.00	2.38	2.54	0.75	12.2
4.9	25	6.3	0.698	30.7	0.91	0.97	2.53	2.695	0.50	7.64
4.9	15	6.3	0.755	31.9	2.69	2.87	2.59	2.76	0.40	5.90
4.9	75	6.3	0.482	26.2	0.66	0.70	2.26	2.41	0.97	17.4
4.9	50	4.4	0.654	23.4	0.59	0.90	1.73	2.64	0.59	11.8
4.9	50	8.8	0.472	35.8	2.47	1.88	3.15	2.40	0.99	12.9
4.9	50	2.8	0.711	17.3	0.22	0.53	1.13	2.71	0.48	12.9
2.3	25	6.3	0.587	24.6	1.63	1.74	2.40	2.56	0.72	13.7
2.3	15	6.3	0.643	27.1	1.50	1.60	2.47	2.63	0.61	10.5
2.3	75	6.3	0.348	21.4	2.31	2.46	2.05	2.18	1.35	29.4
2.3	50	4.25	0.479	18.0	0.75	1.18	1.355	2.41	0.97	25.2
2.3	50	8.6	0.412	28.1	2.12	1.66	2.95	2.30	1.15	19.1
2.3	50	2.3	0.531	12.45	0.69	2.01	0.85	2.48	0.85	31.9

TABLE E-6 - Continued

Measured							Calculated			
n_o^o (% CO)	i (ma)	P (mm Hg)	$\theta(1,\infty)$	E (V/cm)	t_c^E (min)	τ_c^E	t_c^M (min)	τ_c^M	α	$n_+/n_o \times 10^6$
2.3	50	6.3	0.461	21.4	1.94	2.07	2.24	2.38	1.02	22.3
1.2	25	6.3	0.350	21.7	2.19	2.33	2.05	2.18	1.34	28.9
1.2	75	6.3	0.158	18.4	0.94	1.00	1.55	1.65	2.21	56.2
1.2	15	6.3	0.425	21.7	1.31	1.40	2.18	2.32	1.12	24.2
1.2	50	6.3	0.233	19.3	1.56	1.66	1.79	1.91	1.79	43.4
1.2	50	2.5	0.261	11.1	0.71	1.91	0.74	1.98	1.67	70.2
1.2	50	4.4	0.248	15.0	1.20	1.83	1.27	1.94	1.73	53.8
1.2	50	8.7	0.218	24.2	2.28	1.76	2.42	1.87	1.86	35.9

TABLE E-7

Results for Dissociation in $He-CO_2$

i (ma)	P (mm Hg)	n_o^o (% CO_2)	F*
10	6.0	4.7	0.11
25	6.0	4.7	0.26
35	6.0	4.7	0.38
50	6.0	4.7	0.48
65	6.0	4.7	0.67
50	2.2	4.7	0.17
50	7.9	4.7	0.64
30	6.0	7.5	0.31
40	6.0	7.5	0.41
60	6.0	7.5	0.59

*The letter "F" is Fraction of CO_2 Dissociated.

TABLE E-8

Results for Cataphoresis in He-Ar Calculated from the Model with the Estimated Values of the Electrostatic Peclet Number

$\theta(1,\infty)$ vs i

i (ma)	P (mm Hg)	n_o^o (% Ar)	$\theta(1,\infty)$	α	E (V/cm)	$n_+/n_o \times 10^6$
25	3.2	4.7	0.931	0.105	10.2	4.8
50	3.2	4.7	0.681	0.53	10.2	24.2
100	3.2	4.7	0.338	1.38	10.2	63.0
25	5.5	4.7	0.915	0.13	12.7	4.8
50	5.5	4.7	0.585	0.73	12.7	26.7
100	5.5	4.7	0.207	1.925	12.7	70.5
25	8.9	4.7	0.829	0.27	15.9	7.9
50	8.9	4.7	0.383	1.24	15.9	36.3
100	8.9	4.7	0.062	3.19	15.9	93.4

$\theta(1,\infty)$ vs P

25	3.2	4.7	0.915	0.13	12.6	4.8
25	5.5	4.7	0.896	0.16	15.6	4.8
25	8.9	4.7	0.867	0.21	20.0	4.8
50	3.2	4.7	0.652	0.59	10.3	26.7
50	5.5	4.7	0.589	0.72	12.6	26.7
50	8.9	4.7	0.500	0.92	16.0	26.7
100	3.2	4.7	0.213	1.89	8.5	103
100	5.5	4.7	0.138	2.36	10.7	103
100	8.9	4.7	0.070	3.06	13.8	103

TABLE E-9

Results for Cataphoresis in He-Ne Calculated from the Model with the Estimated Values of the Electrostatic Peclet Number

$\theta(1,\infty)$ vs i

i (ma)	P (mm Hg)	n_o^o (% Ne)	$\theta(1,\infty)$	α	E (V/cm)	$n_+/n_o \times 10^6$
25	6.0	2.4	0.865	0.21	11.4	17.2
50	6.0	2.4	0.483	0.96	11.4	78.1
75	6.0	2.4	0.252	1.71	11.4	139
25	6.0	4.8	0.915	0.13	11.2	11.0
50	6.0	4.8	0.631	0.63	11.2	52.2
75	6.0	4.8	0.420	1.13	11.2	93.5
100	6.0	4.8	0.270	1.63	11.2	134

$\theta(1,\infty)$ vs P

50	3.5	2.4	0.476	0.98	11.6	78.1
50	6.0	2.4	0.468	1.00	11.9	78.1
50	9.1	2.4	0.460	1.02	12.1	78.1

TABLE E-10

Results for Cataphoresis in He-N_2 Calculated from the Model with the Estimated Values of the Electrostatic Peclet Number

$\theta(1,\infty)$ vs i

i (ma)	P (mm Hg)	n_o^o (% N_2)	$\theta(1,\infty)$	α	E (V/cm)	$n_+/n_o \times 10^6$
5	6.3	1.2	0.420	1.13	27.8	33.9
9	6.3	1.2	0.267	1.64	27.8	49.1
20	6.3	1.2	0.072	3.04	27.8	90.9
7.5	6.3	2.2	0.737	0.43	26.3	13.7
15	6.3	2.2	0.445	1.06	26.3	33.5
25	6.3	2.2	0.213	1.89	26.3	59.9
50	6.3	2.2	0.029	3.98	26.3	126
15	6.3	4.8	0.865	0.21	32.9	5.2
25	6.3	4.8	0.600	0.70	32.9	17.7
50	6.3	4.8	0.236	1.78	32.9	45.1
75	6.3	4.8	0.081	2.91	32.9	73.6
			$\theta(1,\infty)$ vs P			
50	2.2	4.8	0.412	1.15	15.8	60.5
50	2.7	4.8	0.372	1.27	17.4	60.5
50	4.3	4.8	0.270	1.63	22.4	60.5
50	6.3	4.8	0.177	2.09	28.7	60.5
50	8.8	4.8	0.103	2.66	36.5	60.5

TABLE E-11

Results for Cataphoresis in He-O_2 Calculated from the Model with the Estimated Values of the Electrostatic Peclet Number

i (ma)	P (mm Hg)	n_o^o (% O_2)	$\theta(1,\infty)$	α	E (V/cm)	$n_+/n_o \times 10^6$
			$\theta(1,\infty)$ vs i			
15	6.0	2.2	0.647	0.60	23.6	22.5
25	6.0	2.2	0.332	1.40	23.6	52.5
35	6.0	2.2	0.160	2.20	23.6	82.5
42.5	6.0	2.2	0.089	2.81	23.6	105
20	6.0	4.1	0.678	0.54	28.1	16.9
35	6.0	4.1	0.462	1.02	28.1	32.0
50	6.0	4.1	0.304	1.50	28.1	47.2
72.5	6.0	4.1	0.155	2.23	28.1	69.9
20	6.0	5.0	0.782	0.35	27.4	11.4
35	6.0	5.0	0.536	0.84	27.4	27.0
50	6.0	5.0	0.356	1.32	27.4	42.6
75	6.0	5.0	0.171	2.13	27.4	68.6
85	6.0	5.0	0.126	2.45	27.4	79.0
			$\theta(1,\infty)$ vs P			
50	2.1	5.0	0.548	0.81	15.9	44.8
50	2.7	5.0	0.517	0.88	17.4	44.8
50	4.0	5.0	0.453	1.04	20.6	44.8
50	6.0	5.0	0.366	1.29	25.5	44.8
50	7.5	5.0	0.309	1.48	29.1	44.8

TABLE E-12

Results for Cataphoresis in He-CO Calculated from the Model with the Estimated Values of the Electrostatic Peclet Number

$\theta(1,\infty)$ vs i

i (ma)	P (mm Hg)	n_o^o (% CO)	$\theta(1,\infty)$	α	E (V/cm)	$n_+/n_o \times 10^6$
15	6.3	1.2	0.427	1.11	21.7	24.0
25	6.3	1.2	0.344	1.36	21.7	29.4
50	6.3	1.2	0.195	1.99	21.7	42.9
75	6.3	1.2	0.108	2.61	21.7	56.4
15	6.3	2.3	0.668	0.56	24.6	10.6
25	6.3	2.3	0.587	0.72	24.6	13.7
50	6.3	2.3	0.414	1.15	24.6	21.8
75	6.3	2.3	0.288	1.56	24.6	29.7
15	6.3	4.9	0.765	0.38	30.7	5.8
25	6.3	4.9	0.699	0.50	30.7	7.7
50	6.3	4.9	0.548	0.81	30.7	12.4
75	6.3	4.9	0.420	1.13	30.7	17.2
			$\theta(1,\infty)$ vs P			
50	2.8	4.9	0.715	0.47	17.9	12.2
50	4.4	4.9	0.652	0.59	22.7	12.2
50	6.3	4.9	0.579	0.74	28.5	12.2
50	8.8	4.9	0.492	0.94	36.1	12.2
50	2.3	2.3	0.647	0.60	12.6	22.3
50	4.25	2.3	0.539	0.83	17.3	22.3
50	6.3	2.3	0.445	1.06	22.3	22.3
50	8.6	2.3	0.353	1.33	27.8	22.3
50	2.5	1.2	0.457	1.03	11.1	43.4
50	4.4	1.2	0.332	1.40	15.2	43.4
50	6.3	1.2	0.236	1.78	19.2	43.4
50	8.7	1.2	0.153	2.25	24.3	43.4

TABLE E-13

The Design Equations for the Electric Field as a Function of Pressure

$$E = mP + b$$

where E is the electric field in volts/cm and P is the total gas pressure in mm Hg

The values of m and b were calculated by the method of least squares. The tube inside diameter is 8 mm.

i (ma)	n_o^o (percentage of impurity)	m $(\frac{V/cm}{mm\ Hg})$	b (V/cm)	range of P (mm Hg)
25	4.7% Ar	1.30	8.41	3.2 - 8.9
50	4.7% Ar	.996	7.10	3.2 - 8.9
100	4.7% Ar	.910	5.63	3.2 - 8.9
50	2.4% Ne	.0985	11.3	3.5 - 9.1
50	4.8% N_2	3.14	8.90	2.2 - 8.8
50	5.0% O_2	2.445	10.8	2.1 - 7.5
50	4.9% CO	3.04	9.35	2.8 - 8.8
50	2.3% CO	2.41	7.085	2.3 - 8.6
50	1.2% CO	2.125	5.82	2.5 - 8.7

TABLE E-14

The Values of τ_c , u_1 , and α for $\delta = 8.9$ and $\varepsilon = 4.2$

α	u_1	τ_c	α	u_1	τ_c
0.10	0.583	2.92	1.10	0.359	2.32
0.20	0.582	2.87	1.15	0.327	2.29
0.30	0.578	2.80	1.20	0.288	2.26
0.40	0.569	2.75	1.25	0.242	2.23
0.45	0.563	2.72	1.30	0.181	2.20
0.50	0.556	2.69	1.33	0.129	2.18
0.55	0.548	2.66	1.35	0.08	2.16
0.60	0.539	2.63			
0.65	0.528	2.60			
0.70	0.517	2.57			
0.75	0.504	2.53			
0.80	0.489	2.50			
0.85	0.473	2.47			
0.90	0.455	2.44			
0.95	0.435	2.41			
1.00	0.412	2.38			
1.05	0.387	2.35			

APPENDIX F

Preliminary

Experimental Investigations

Preliminary Experimental Investigations

Two preliminary experimental systems were designed and constructed. The purpose of these investigations was to study the cataphoretic separation of binary mixtures flowing through a glow discharge between concentric electrodes. The results of these studies have been previously described in reports entitled, "Cataphoresis in Binary Gas Mixtures"[81] and "Cataphoresis in a Flowing System" [82]. Associates have redesigned the two-inch diameter system described in reference [82], and their current investigation is proceeding with the aid of a mass spectrometer.

VII. REFERENCES

1. Baly, E. C. C., Phil. Mag. 35, 200 (1893).

2. Thomson, J. J., Proc. Roy. Soc. Lond. 58, 244 (1895).

3. Groth, W., and Harteck, P., Naturwiss. 27, 390 (1939).

4. Beckey, H. D., Groth, W. E., and Welge, K. H., Z. Naturforsch. 8a, 556 (1953).

5. Skaupy, F., Verh. Phys. Ges. 18, 230 (1916).

6. Skaupy, F., and Bobek, F., Z. Tech. Phys. 6, 284 (1925).

7. Penning, F. M., Physica 1, 763 (1934).

8. Druyvesteyn, M. J., Physica 2, 255 (1935).

9. Riesz, R., and Dieke, G. H., J. Appl. Phys. 25, 196 (1954).

10. Kenty, C., Bull. Am. Phys. Soc., Ser. II, 3, 82 (1958).

11. Cobine, J. D., Gaseous Conductors, Dover Publications, Inc., New York, 1957.

12. Loeb, L. B., J. Appl. Phys. 29, 1369 (1958).

13. Oskam, H. J., Bull. Am. Phys. Soc., Ser. II, 3, 85 (1958).

14. Pahl, M., and Wermer, U., Naturwiss. 44, 487 (1957).

15. Matveeva, N. A., Bull. Acad. Sci. USSR, Phys. Ser. (English Ed.), 23, 1009 (1959).

16. Schmeltekopf, A. L., Doctoral Dissertation, Univ. of Texas, Univ. Microfilms, Ann Arbor, 1962.

17. Schmeltekopf, A. L., J. Appl. Phys. 35, 1712 (1964).

18. Flinn, J. E., and Price, R. H., Ind. Eng. Chem. Process Design and Development 5, 75 (1966).

19. Grew, K. E., and Ibbs, T. L., Thermal Diffusion in Gases, Cambridge University Press, London, 1952.

20. Freudenthal, J., Physica 36, 354 (1967).

21. Freudenthal, J., J. Appl. Phys. 38, 4818 (1967).

22. Shair, F. H., and Remer, D. S., J. Appl. Phys. 39, 5762 (1968).

23. Remer, D. S., and Shair, F. H., Rev. Sci. Instr. 40, 968 (1969).

24. Miller, H. C., J. Appl. Phys. 35, 1745 (1964).

25. Loeb, L. B., Westberg, R. G., Huang, H. C., Phys. Rev. 123, 43 (1961).

26. Oskam, H. J., and Mittelstadt, V. R., Phys. Rev. 132, 1435 (1963).

27. Druyvesteyn, M. J., and Penning, F. M., Rev. Mod. Phys. 12, 88 (1940).

28. Benton, E. E., Doctoral Dissertation, Univ. of Texas, Austin, 1962.

29. Hogervorst, W., and Freudenthal, J., Physica 37, 97 (1967).

30. Druyvesteyn, M. J., and Warmholtz, N., Phil. Mag. 17, 1 (1934).

31. Freudenthal, J., Physica 36, 365 (1967).

32. Francis, G., Encyclopedia of Physics XXII, Springer-Verlag, Berlin, 1956.

33. Biondi, M. A., Phys. Rev. 83, 1078 (1951).

34. Biondi, M. A., and Chanin, L. M., Phys. Rev. 94, 910 (1954).

35. Brode, R. B., Rev. Mod. Phys. 5, 257 (1933).

36. von Engel, A., Ionized Gases, 2nd Ed., Clarendon Press, Oxford, 1965.

37. Hirschfelder, J. O., Curtiss, C. F., Bird, R. B., Molecular Theory of Gases and Liquids, John Wiley and Sons, Inc., 1967.

38. Srivastava, K. P., Physica 25, 571 (1959).

39. Srivastava, B. N., and Srivastava, K. P., J. Chem. Phys. 30, 984 (1959).

40. Srivastava, K. P., and Barva, A. K., Indian J. Phys. 33, 229 (1959).

41. Llewellyn-Jones, F., The Glow Discharge, John Wiley, New York, 1966.

42. Mickley, H. S., Sherwood, T. K., and Reed, C. E., Applied Mathematics in Chemical Engineering, 2nd Ed., McGraw-Hill, New York, 1957.

43. Dalgarno, A., McDowell, M. R. C., and Williams, A., Phil. Trans. Roy. Soc. (London) A-250, 411 (1958).

44. Malmstadt, H. V., Enke, C. G., and Toren, E. C., Electronics for Scientists, W. A. Benjamin, Inc., New York, 1963.

45. Cook, G. A., Argon, Helium and the Rare Gases, 1, Interscience, New York, 1961.

46. Reid, R. C., and Sherwood, T. K., The Properties of Gases and Liquids, 2nd Ed., McGraw-Hill, New York, 1966.

47. Chanin, L. M., Phelps, A. V., and Biondi, M. A., Phys. Rev. 128, 219 (1962).

48. Seager, S. L., Geertson, L. R., and Giddings, J. C., J. Chem. Eng. Data 8, 168 (1963).

49. McDaniel, E. W., and Crane, H. R., Rev. Sci. Instr. 28, 684 (1957).

50. Jeans, J. H., The Dynamical Theory of Gases, Cambridge at the University Press, 3rd Ed., 1921.

51. Chanin, L. M., and Biondi, M. A., Phys. Rev. 107, 1219 (1957).

52. Tyndall, A. M., and Powell, C. F., Proc. Roy. Soc. (London) 134, 125 (1931); 136, 145 (1932); Nature 127, 592 (1931).

53. Loeb, L. B., Basic Processes of Gaseous Electronics, Univ. of Calif. Press, Berkeley, 1961.

54. Kruithoff, A. A., and Penning, F. M., Physica 3, 515 (1936); 4, 430 (1937); 5, 203 (1938).

55. Oskam, H. J., Philips Res. Rept. 13, 401 (1958).

56. Reed, R. I., Ion Production by Electron Impact, Academic Press, London, 1962.

57. Hornbeck, J. A., Phys. Rev. 84, 615 (1951).

58. Dahler, J. S., Franklin, J. L., Munson, M. S. B., Field, F. H., J. Chem. Phys. 36, 3332 (1962).

59. Brown, S. C., Basic Data of Plasma Physics, 2nd Ed., The M.I.T. Press, Cambridge, Massachusetts, 1966.

60. Massey, E. H. S., and Burhop, H. S. W. Electronic and Ionic Impact Phenomena, Clarendon Press, Oxford, 1952.

61. Varney, R. N., Phys. Rev. 89, 708 (1953).

62. McDaniel, E. W., Collision Phenomena in Ionized Gases, John Wiley and Sons, Inc., New York, 1964.

63. Gaydon, A. G., Pearse, R. W. B., The Identification of Molecular Spectra, 3rd Ed., John Wiley and Sons, Inc., New York, 1963.

64. Hagstrum, H. D., Rev. Mod. Phys. 23, 185 (1951).

65. Hagstrum, H. D., and Tate, J. T., Phys. Rev. 55, 1136 (1939); 59, 354 (1941).

66. Cottrell, T. L., The Strength of Chemical Bonds, 2nd Ed., Butterworths, London, 1958.

67. Sauter, G. F., Gerber, R. A., Oskam, H. J., Physica 32, 1921 (1966).

68. Gaur, J. P., and Chanin, L. M., J. Appl. Phys. 40, 256 (1969).

69. Ravimohan, A. L., and Shair, F. H., submitted to the J. Appl. Physics, 1970.

70. Rundle, H. W., Gillespie, K. A., Yealland, R. M., Sova, R., and Deckers, J. M., Can. J. Chem. 44, 2995 (1966).

71. Miller, H. C., Phys. Letters 5, 120 (1963).

72. Lochte-Holtgreven, W., Plasma Diagnostics, North Holland Pub. Co., Amsterdam, 1968.

73. McTaggert, F. K., Plasma Chemistry in Electrical Discharges, Elsevier Pub. Co., Amsterdam, 1967.

74. Blackwood, J. D., and McTaggart, F. K., Australian J. Chem. 12, 533 (1959).

75. O'Driscoll, W. G., Dunabin, J. E., Martin, W. H., and Walker, A., U.K. At. Energy Authority Ind. Group, IGR-TN/C, 1960.

76. Dixon, W. J., Massey, F. J., Introduction to Statistical Analysis, 3rd Ed., McGraw-Hill, New York, 1969.

77. Sosnowski, T. P., J. Appl. Phys. 40, 5138 (1969).

78. Buser, R. G., and Sullivan, J. J., J. Appl. Phys. 41, 472 (1970).

79. Shair, F. H., and Cohen, D. S., Chem. Eng. Sci. 24, 39 (1969).

80. Shilling, G. D., Process Dynamics and Control, Holt, Rinehart and Winston, Inc., New York, 1963.

81. Remer, D. S., "Cataphoresis in Binary Gas Mixtures," Caltech, Chemical Engineering Dept. Research Report RR-30, 1967.

82. Remer, D. S., "Cataphoresis in a Flowing System," Caltech, Chemical Engineering Student Report SR 1092, 1966.

83. Headrick, L. B., and Duffendack, O. S., Phys. Rev. 37, 736 (1931).

PROPOSITION I

This proposition was submitted and accepted by the Candidacy Examination Committee of Professors F. H. Shair, G. R. Gavalas, W. H. Corcoran, and S. K. Friedlander on May 3, 1967.

PROPOSITION I

List of Figures

The mortality of Drosophila melanogaster (D.m.) which are commonly referred to as fruit flies was investigated under partial vacuum. The experimental results appear in Fig. I-1. The life span was found to vary from approximately 3 minutes at 2 inches of mercury absolute to about 3 weeks at atmospheric pressure.

The reactions and mortality of Drosophila exposed to light, sound, pressure, temperature, chemicals, radiation, electrical properties, etc. have been found to be similar in many ways to other living things. Weltman [1] has studied the mortality and infertility effects of cold-shock treatments on D.m. Harnly and Goldsmith [2], under a grant from the National Cancer Institute, have investigated the effect of chemicals on the mortality of D.m. Muller [3], working with a grant from the U. S. Atomic Energy Commission, studied mortality induced by x-rays. He concluded that the mortality in Drosophila represents basically the same phenomenon which is described in the case of vertebrates as radiation aging. Scheltgen and Cole [4] investigated D.m. in the range of 5,200 lbs/in^2 to 9,000 lbs/in^2, and Pease and Regnery [5] studied D.m. at pressures of 10,000 lbs/in^2 to 15,000 lbs/in^2. Ingraham [6] has conducted experiments at 0.2 atmospheres pressure and found that vacuum treatment retarded the growth processes. No results have appeared in the literature where mortality of D.m. as a function of pressure has been investigated. A recent impetus for this work has been provided by the U. S. biosatellite program in which a capsule of living specimens, including D.m. has

been launched into orbit. The object of this Biosatellite 1 mission is to study biological hazards of space travel. Such questions as the effect of weightlessness, growth, heredity, reduced pressures, radiation, and subtle cellular changes for D.m. will be investigated [7,8].

The data obtained from Biosatellite 1 and later missions will indicate the mortality of D.m. under the influence of reduced pressure, increased radiation, and other factors. Because data for D.m. life span on earth under partial vacuum apparently is not reported in the literature, the present experimental investigation has been carried out to furnish this information and in effect serve as a control experiment.

The experimental apparatus appears in Fig. I-2 and a schematic diagram of the system is shown in Fig. I-3. The pressure was measured by a U-type absolute pressure gauge. A vacuum pump was used to obtain the reduced pressures and the system pressure was regulated by a valve which controlled the air leakage into the system. Cardboard barriers were used to prevent the D.m. from being pulled into the vacuum pump and to prevent their escape into the pressure gauge line. Since D.m. will only live about 20 hours without food under normal conditions, a supply of food-gelled medium consisting of maize meal, yeast, molasses, and agar was provided in the test cell. An anesthetizing bottle was used to transfer the D.m. into the apparatus. Ether was used as the anesthetic.

It was necessary to determine a criterion for D.m. mortality. Experimental tests were performed where the pressure was reduced and then returned to atmospheric pressure. A close surveillance of the D.m. indicated that those flies which rolled over on their backs under

the reduced pressure never regained consciousness at atmospheric pressure. Therefore, it was assumed that after a fly rolled over on its back, it was dead.

The results for the life span of D.m. as a function of pressure appear in Fig. I-1. The life span is approximately 3 weeks (500 hours) between atmospheric pressure and 26 in. Hg. As the pressure is reduced to 22 in. Hg, the life span begins to decrease rapidly to about 110 hours. Upon further reduction of the pressure, the life span decreases to 3 minutes at 2 in. Hg. The results are arithmetic averages of the life span for groups of ten flies at each pressure reported.

Continuous observations of D.m. lifetime were recorded at pressures below 6 in. Hg. At pressures in the range of 6 to 10 in. Hg, observations were made at least once every 10 minutes, and at pressures in the range of 10 to 29 in. Hg, the frequency of observations was at least once every seven hours.

D.m. species Oregon R were used in the investigation. The subjects studied were two days old when testing was initiated.

No conclusions about the cause of mortality can be inferred from the experimental data. Mortality may be dependent on the partial pressure of water vapor which might cause dehydration of D.m. The partial pressure of 0_2 or CO_2 may also be an important factor affecting mortality. Further experiments where the partial pressure of two of the three components 0_2, CO_2, and H_20 are held constant while varying the partial pressure of the third component would be necessary before any conclusions could be reached on the cause of mortality.

Meager experimental data on the influence of the partial pressure of O_2, CO_2, and H_2O have appeared in the literature. Goldsmith [9] investigated D.m. at atmospheric pressure in O_2 with partial pressures of CO_2 ranging from 0.2 - 0.5 atm. D.m. activity was depressed but increased mortality was not observed. Abrahamson [10] observed D.m. in an environment devoid of O_2 . D.m. were placed in a N_2 atmosphere for 1, 3, and 18 hour periods. 95% survival was obtained for the groups of D.m. in the 1 and 3 hour tests; however, 100% mortality was reported for the group in the 18 hour period. Herskowitz [11] found that the dehydration of D.m. increases the mortality effect of x-rays on D.m.

ACKNOWLEDGMENT

I would like to thank Dr. Edward B. Lewis, Professor of Biology at the California Institute of Technology, for furnishing a supply of Drosophila melanogaster and anesthetizing apparatus for this experiment.

REFERENCES

1. Weltman, A. S., Drosophila Information Service 29, 171-172 (1955).

2. Harnly, M. H., Goldsmith, E. D., Anatomical Record 108, 564-565 (1950).

3. Muller, H. J., International Journal of Radiation Biology (1959 Supplement), 321-325.

4. Scheltgen, E., Cole, K. M., Drosophila Information Service 27, 111 (1953).

5. Pease, D. C., Regnery, D., Journal of Cellular and Comparative Physiology 17, 397-398 (1947).

6. Ingraham, A., The Louisiana Academy of Sciences, 99-100 (1944).

7. Technology Week 19, No. 25, 13 (1966).

8. The Independent Star-News, Pasadena, California, 1 (12/18/66).

9. Goldsmith, M. H., Schneiderman, H. A., Anatomical Record 125, 557-558 (1956).

10. Abrahamson, S., Drosophila Information Service 32, 109 (1958).

11. Herskowitz, I. H., Genetics 42, 289-298 (1957).

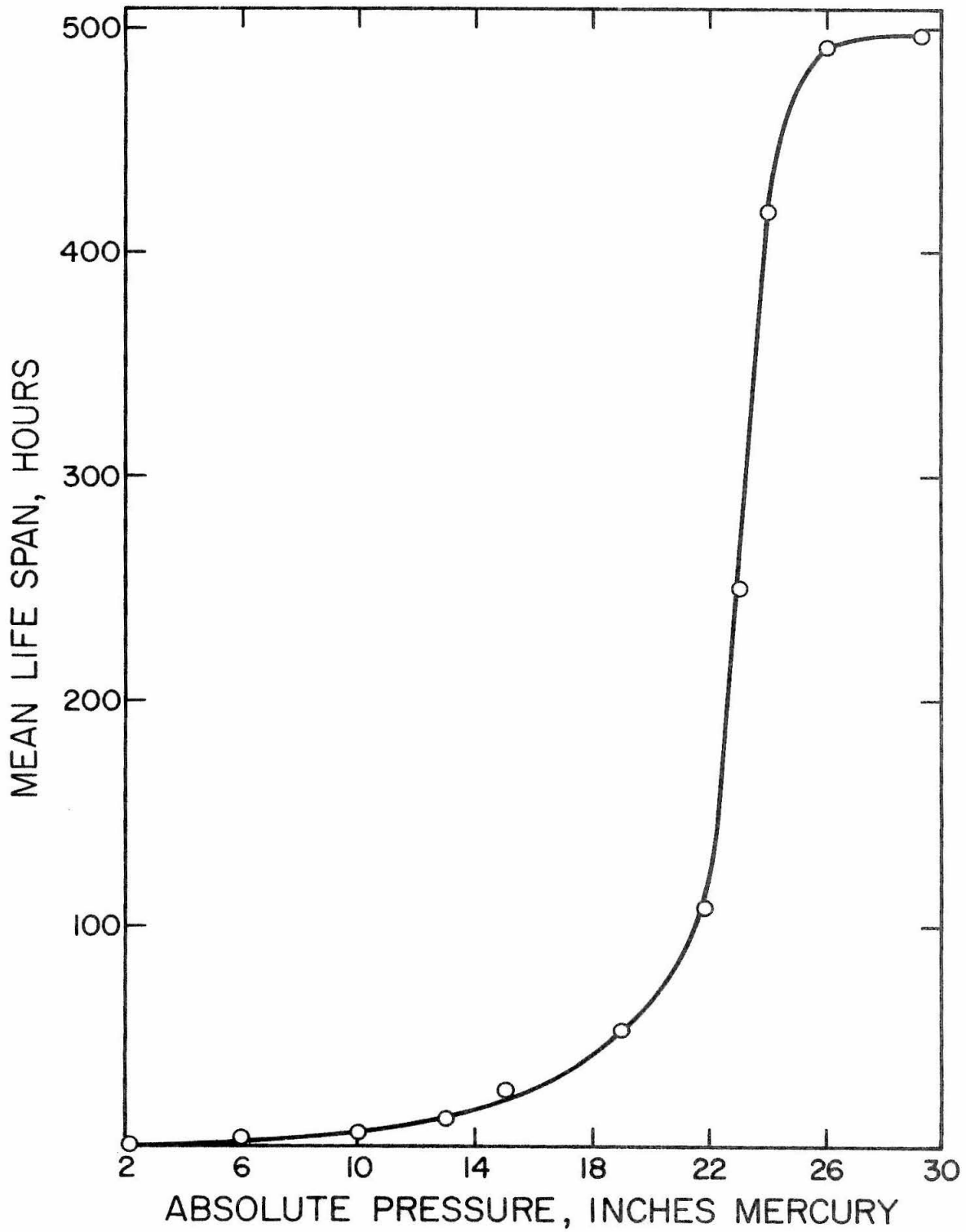

Figure I-1. Life Span of Drosophila Melanogaster as a Function of Pressure

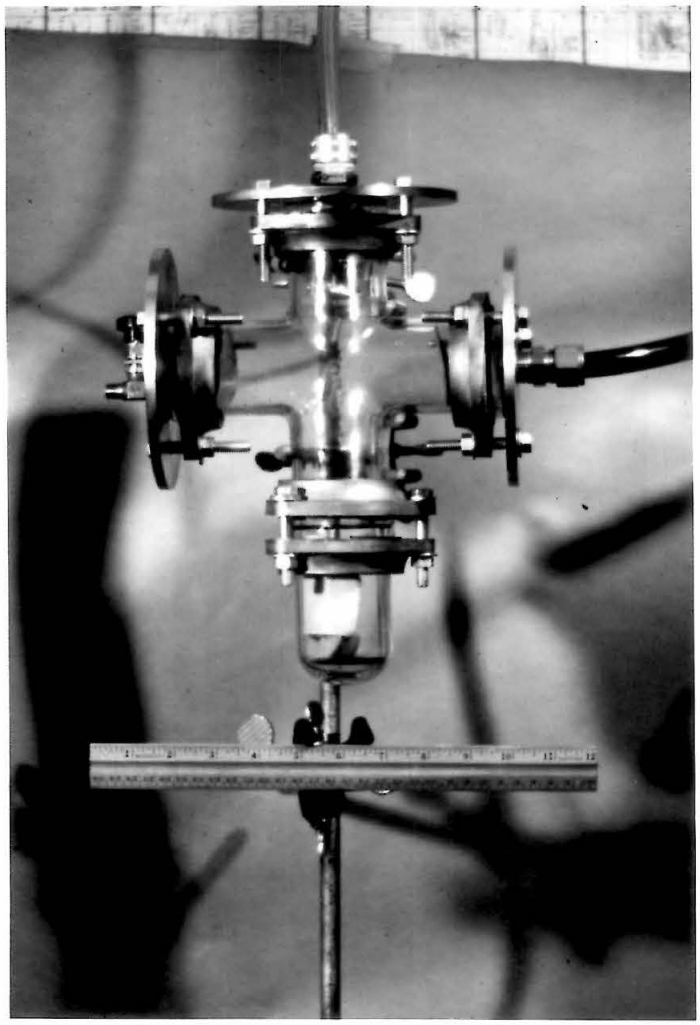

Figure I-2. Photograph of Apparatus for the Measurement of Mortality of Drosophila Melanogaster as a Function of Pressure

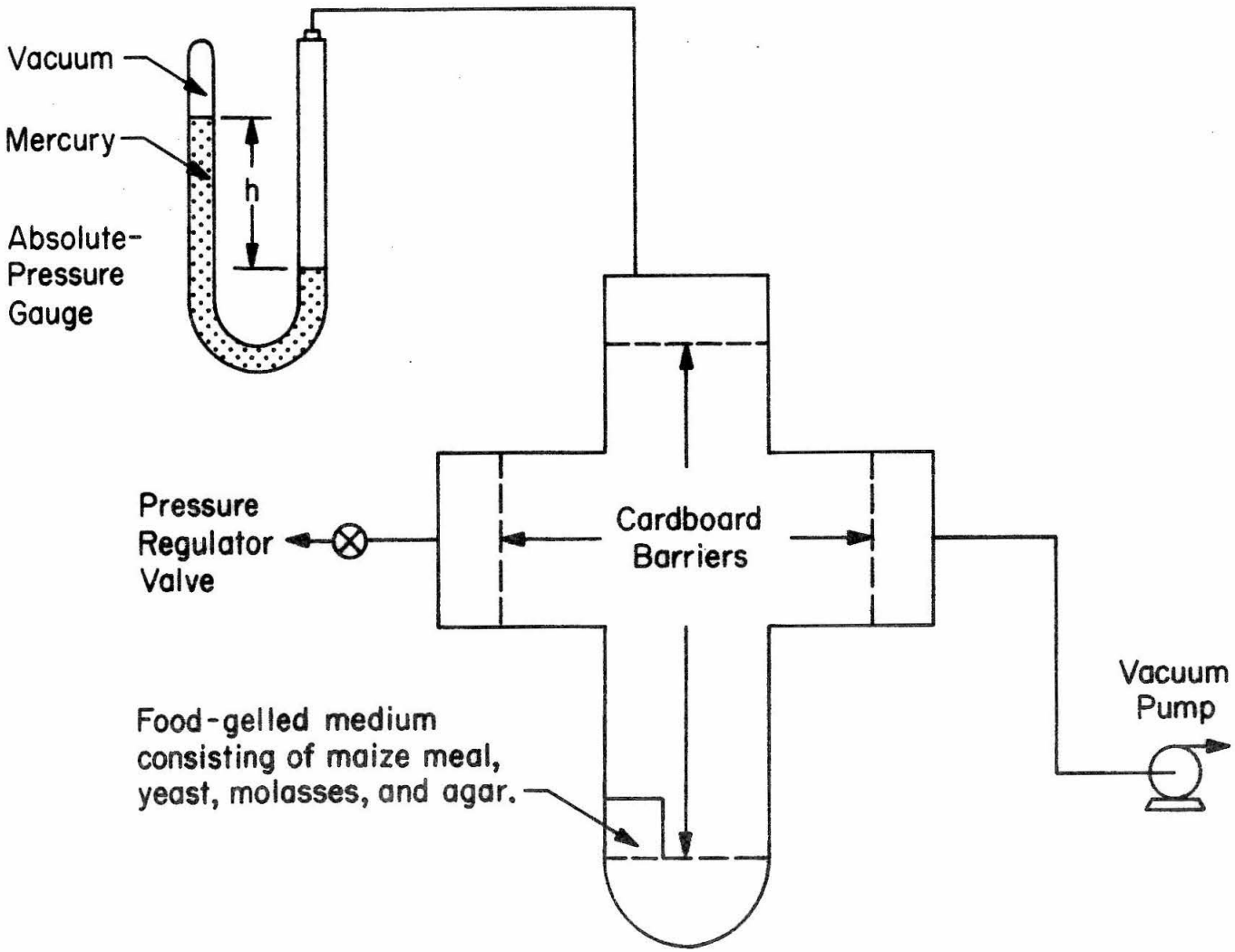

Figure I-3. Schematic Diagram of Apparatus for the Measurement of Mortality of Drosophila Melanogaster as a Function of Pressure

PROPOSITION II

This proposition was submitted and accepted by the Candidacy Examination Committee of Professors F. H. Shair, G. R. Gavalas, W. H. Corcoran, and S. K. Friedlander on May 3, 1967.

PROPOSITION II

List of Figures

It is proposed to revise the model for the Industrial Materials Price Index. Each component in the index was individually compared to the business cycle. It was found that five of the components did not forecast the contraction periods in the business cycle. These five components were removed from the index, and the remaining eight components were used to form a revised model. The revised model predicted the last four contractional periods in the business cycle an average of three months earlier than the original index ; refer to Fig. II-1.

During the last one hundred and fifty years the United States economy has undergone repeated expansion and contraction periods. An expansion period is characterized by rising employment, production, prices, wages, interest rates, and profits. The reverse is true of contraction periods. This recurring phenomenon is referred to as the business cycle. Two main methods of forecasting the business cycle have been used; analysis of economic aggregates, and empirical business cycle indicators. The latter method is considered in this discussion.

The concept of business cycle indicators was first introduced at the Harvard Business School in 1919. This study was abandoned in 1925 because the introduction of the Federal Reserve and the Central Bank were believed to be artificial stimuli that would destroy the natural business cycle trends. After World War II, the National Bureau of Economic Research (NBER) revived the interest in business cycle forecasting and is presently the leader in the field of research relating to business cycle indicators.

The principle behind the business cycle approach to economic forecasting is an outgrowth of the empirical work performed by the NBER which indicates that certain segments of our economy cyclically increase or decrease before, during, or after, an expansion or contraction period. These segments are referred to as leading, coincident, or lagging indicator time series, respectively.

One of the important leading series indicators is the Industrial Materials Price Index. The model presently being used by the U. S. Department of Commerce for this indicator is composed of an aggregate of thirteen components which are supposed to represent the cyclical nature of prices for industrial materials [1,2]. The thirteen components were originally selected for their historical importance in predicting trends. It was hypothesized that an individual analysis of these components might indicate that certain ones no longer predict current cyclical trends. Data [3,4,5] was obtained and the time series for each component was compared to the business cycle as defined by the Bureau of the Census [1] for the period 1947 to 1962. The data for each component is shown in Figs. II-2, II-3, II-4, and II-5, where the shaded regions represent the contraction periods and the unshaded regions represent the expansion periods. A summary of these results appears in Table II-1.

This table indicates that the Rosin price series predicted only one contraction period, and that the Copper, Zinc, Burlap, and Tin price series each predicted only two contraction periods.

The Copper, Tin, and Zinc series have been affected by two counteracting forces; namely, the increase in population, and the

inroads of new technology. The rate of increase in population, coupled with the relative rate of decrease in usage because of the introduction of plastic substitutes, new styles in packaging, etc., have caused these items to be insensitive to the relative variations in the business cycle. Rosin and Burlap usage has been affected by the paper and synthetic chemical replacements, respectively. Both of these items have relatively inelastic demand curves which would make them less sensitive to business fluctuaions.

When the five components, Copper, Tin, Zinc, Rosin, and Burlap are eliminated from the model for the industrial materials price index, the remaining eight components which each predicted at least three of the contraction periods are used to form a revised model. A comparison between the original model and the revised model indicates that the revised one forecasts the four contractional periods an average of about three months earlier than the original model; refer to Fig. II-1.

TABLE II-1

Component	Number of months before the contraction period that each component series started a downtrend				% of contraction periods predicted
	1948-49	1953-54	1957-58	1960-61	
Copper scrap	--	--	11	5	50
Lead scrap	--	16	2	6	75
Steel scrap	--	3	6	6	75
Tin	--	28	3	--	50
Zinc	--	14	8	--	50
Burlap	16	24	--	--	50
Cotton	4	24	13	11	100
Print cloth	11	25	19	5	100
Wool tops	4	30	--	5	75
Hides	10	30	12	11	100
Rosin	9	--	--	--	25
Rubber	2	31	18	--	75
Tallow	10	30	--	5	75

ACKNOWLEDGMENT

I would like to thank Professor Horace Gilbert for his stimulating lectures which introduced the writer to the field of business cycle forecasting.

REFERENCES

1. "Business Cycle Developments," U. S. Department of Commerce, Bureau of the Census, U. S. Government Printing Office, 1961-1966.

2. Shiskin, J., Review of the ISI 31, 3 (1963).

3. "Wholesale Prices and Price Indexes," U. S. Department of Labor Statistics, Group 6--Chemicals, 1947-1962.

4. "Standard and Poor's Trade and Securities Statistics," Orange, Conn. Editorial Offices, New York, N. Y., Vol. 29, No. 12, December 1963.

5. "Business Statistics," U. S. Department of Commerce, Office of Business Economics, Supplements to the Survey of Current Business, 1947-1962.

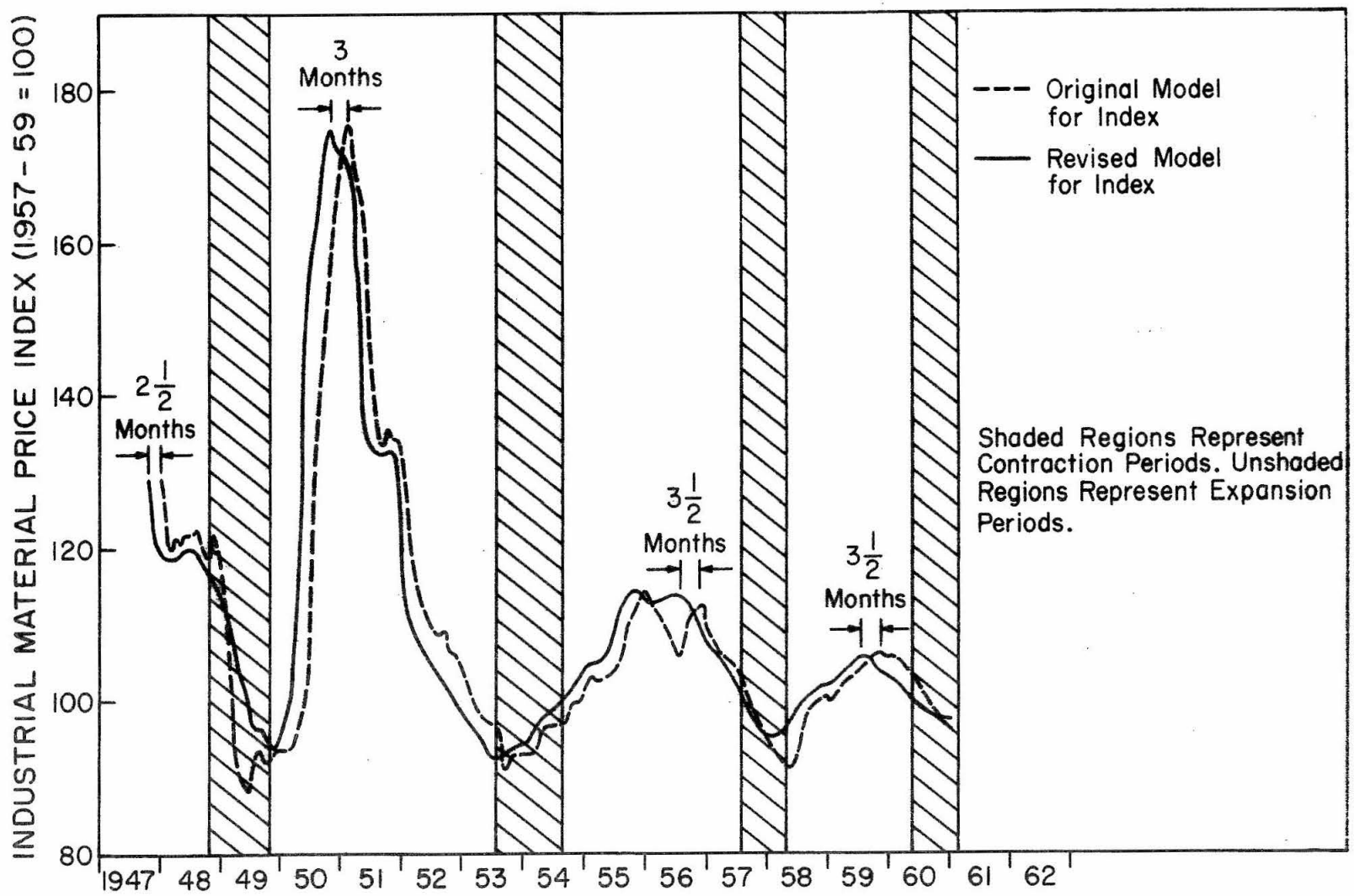

Figure II-1. Comparison of Original Model to Revised Model for the Industrial Materials Price Index

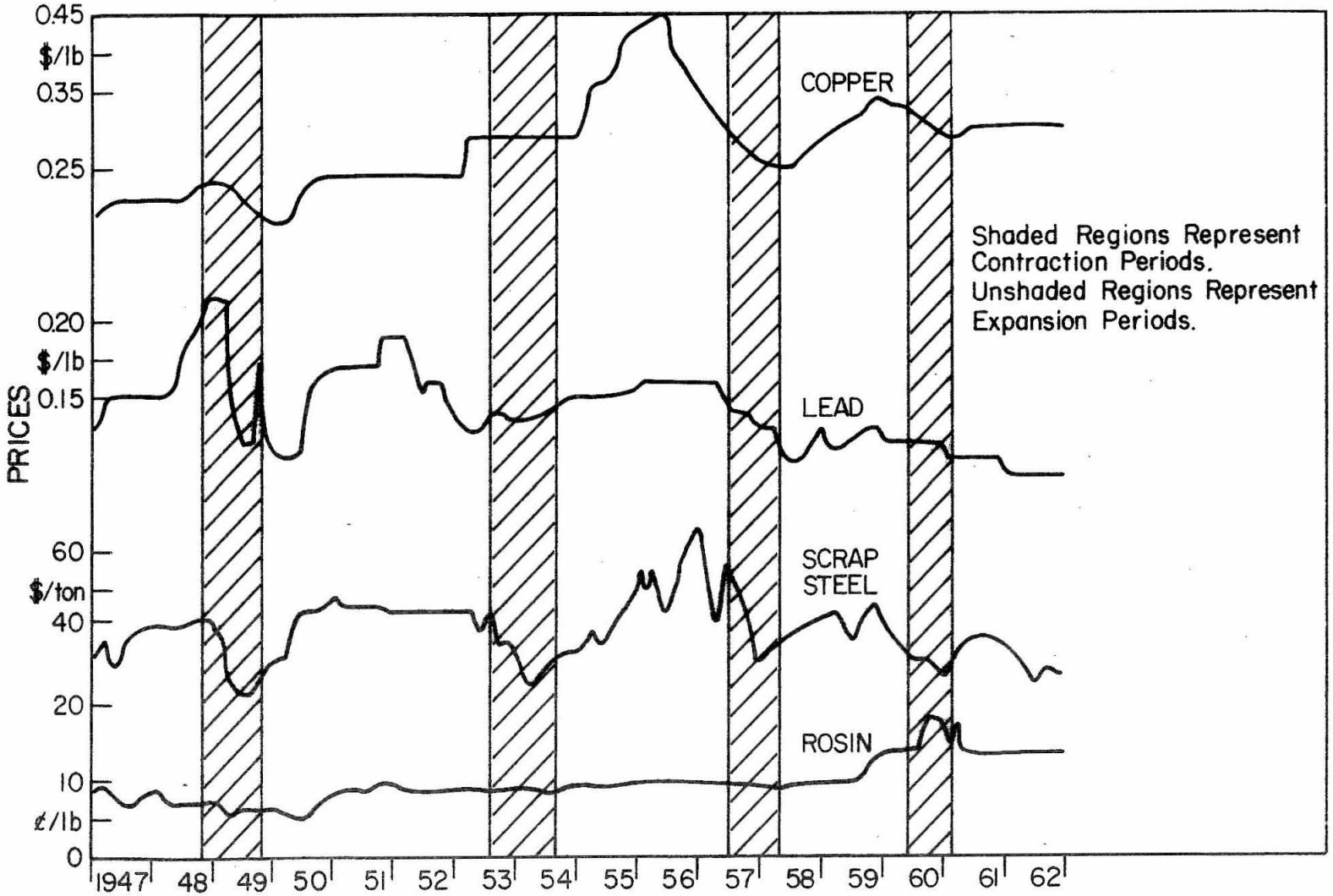

Figure II-2. Business Cycle Series for Copper, Lead, Scrap Steel, and Rosin

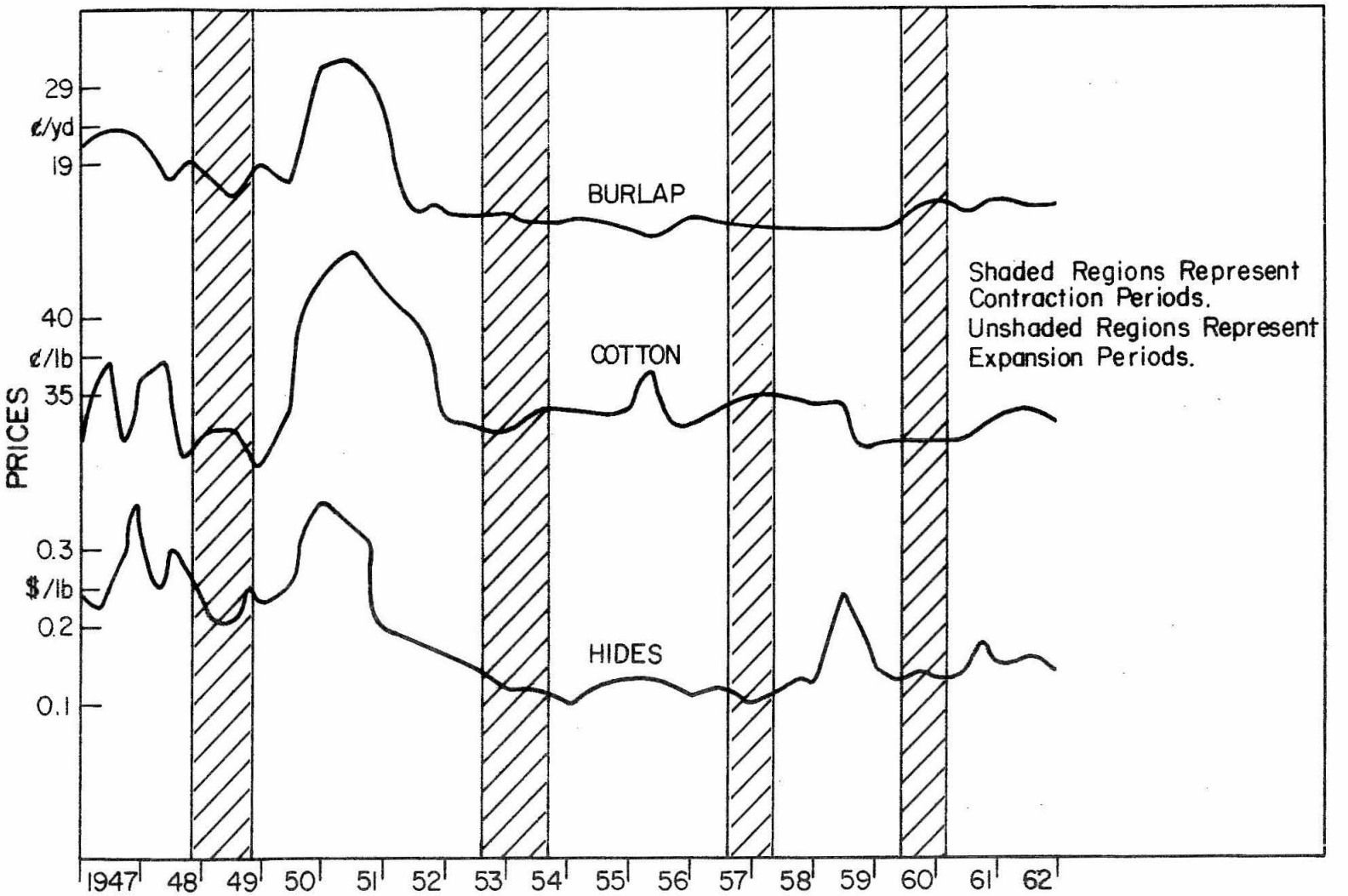

Figure II-3. Business Cycle Series for Burlap, Cotton, and Hides

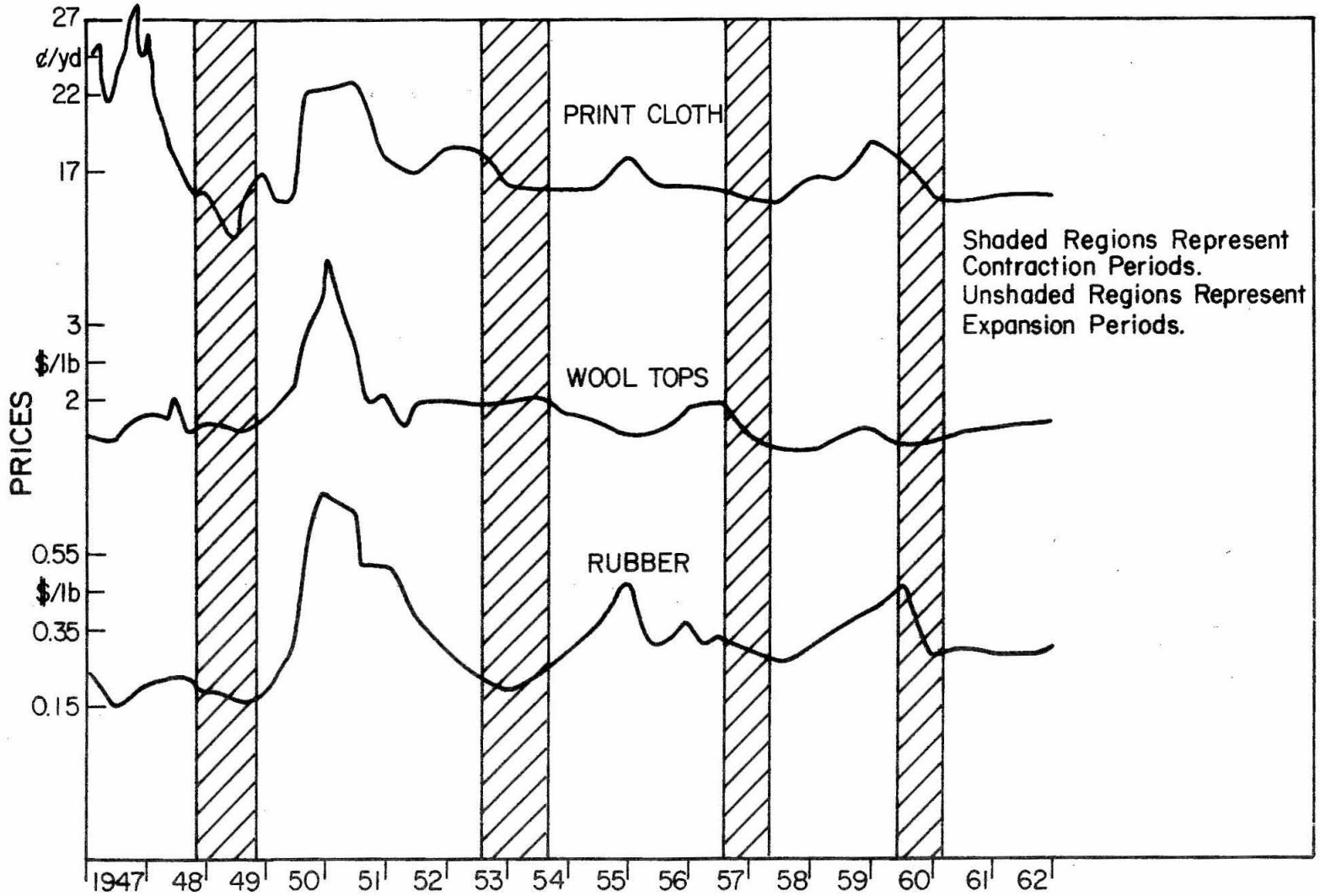

Figure II-4. Business Cycle Series for Print Cloth, Wool Tops, and Rubber

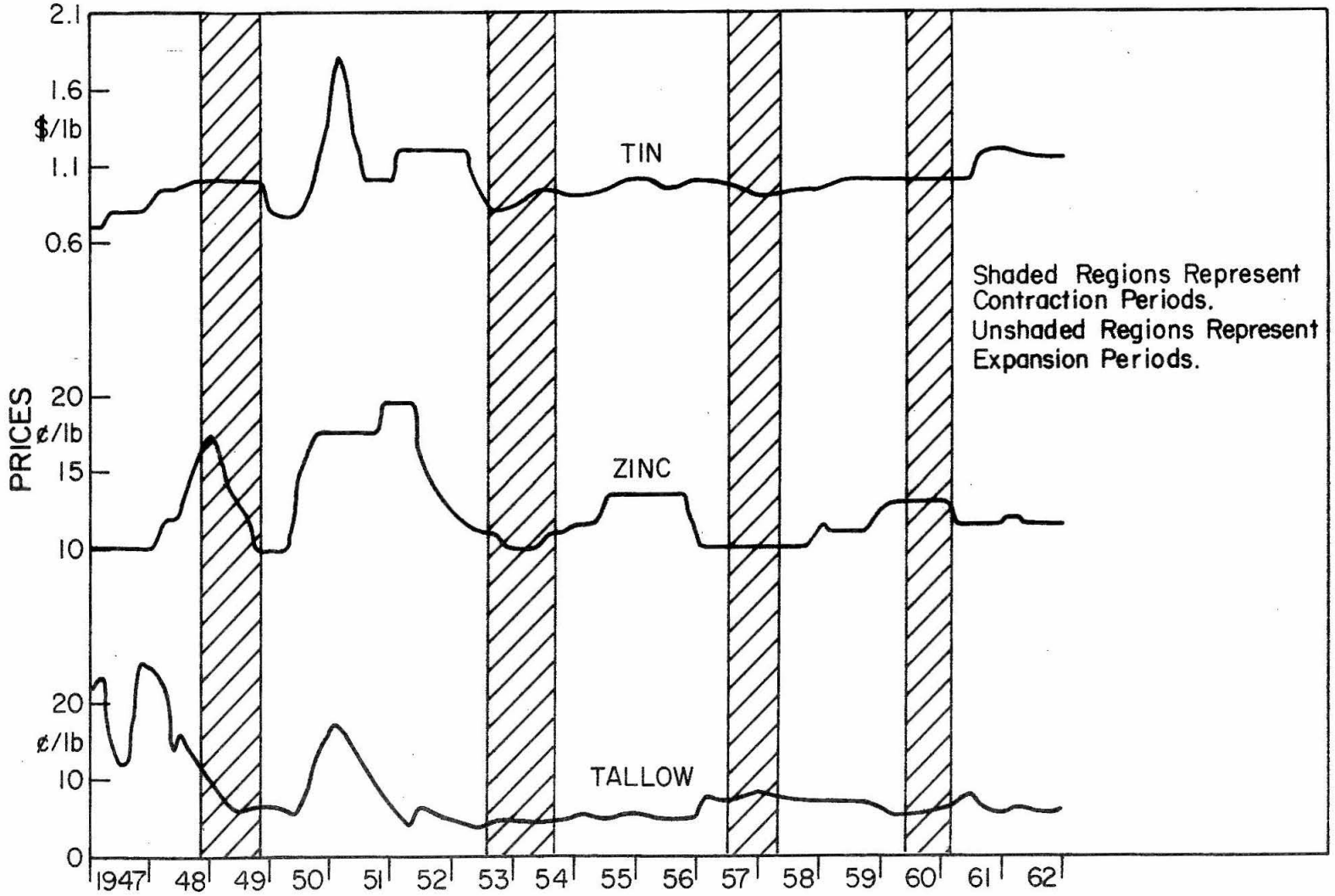

Figure II-5. Business Cycle Series for Tin, Zinc, and Tallow

PROPOSITION III

PROPOSITION III

List of Figures

Two new methods are proposed for the electrode-to-skin contact in routine clinical electrocardiography. The proposed methods are less expensive, less time-consuming, less corrosive, cleaner, and yield the same results as present methods. Experimental tests indicate the recommended methods yield electrocardiograms in agreement with conventional methods.

Introduction

The use of electrocardiography in the diagnosis of heart conditions has been well documented [1,2,3]. There are three basic components in electrocardiography: (1) electrocardiograph, (2) electrodes, and (3) patient. This discussion is primarily concerned with the interface between the electrodes and the patient, that is, the medium for electrode-to-skin contact; refer to Fig. III-1.

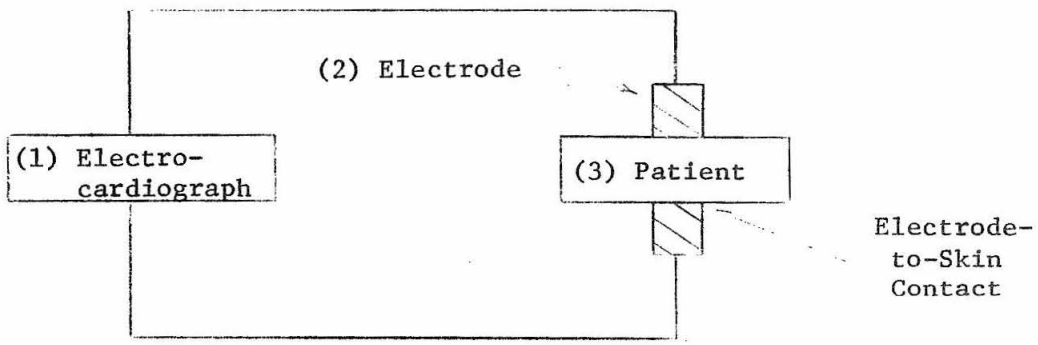

Fig. III-1. Basic Components in Electrocardiography

Recently, expensive and sophisticated methods have been developed to continuously monitor electrocardiograms in special applications such as for pilots, astronauts, and aquanauts [4,5]. However, this is outside the scope of the present investigation which is only concerned with routine clinical procedures.

Historical Perspective of the Problem

In the embryonic stage of electrocardiography, it was common practice to place a patient's two hands and one foot into three large pots of saline solution to reduce the electrical resistance of the skin to obtain satisfactory cardiograms. The inconvenience of this technique led James and Williams [6] in 1910 to introduce contact electrodes which were later improved by Cohn [7] in 1920. Cohn utilized saline pad bandages with the contact electrodes. These saline pads were messy and bedclothes became wet, often resulting in short-circuits. In 1928 Boas [8] dispensed with saline pads by introducing the use of cup-shaped metal electrodes filled with soft soap.

The modern era of electrode-to-skin contacts was initiated in 1935 when Jenks and Graybiel [9] introduced an electrode paste containing a pumice abrasive and salt. This electrode paste or jelly, consisting of sodium chloride and an abrasive, became an essential part of cardiography. Very similar pastes (or jellies or creams) are now commercially available. In fact, about 90% of electrode-to-skin contacts are made using commercial pastes (jellies or creams), for example, Electro Cream by Elma Schonander Company.

Cardiographers have continually complained about conventional electrode paste because it is messy, time-consuming, inconvenient, and unpleasant to patients, doctors, and technicians. Clothes become soiled, patients must wash after tests, and instruments and electrodes are corroded. These grievances were summarized by Littmann [10] in 1959. The inherent problems in the existing methods spurred Littmann to experiment with liquid solutions containing salt, propenol, and glycerine. He concluded that these liquid electrode solutions provided adequate electrode-to-skin contact and yielded results comparable to the jelly, and in addition, they eliminated all the objectionable features of the established jelly. These liquid solutions soon became available, for example, E-Graph manufactured by Hoyt Pharmaceutical Corporation. A slight improvement in this technique was introduced by using pads impregnated with the electrolyte solution, for example, Burdick Lectro-Pads produced by Burdick Corporation.

After a brief period of usage, it became apparent that these liquid solutions introduced another problem. For a complete examination, usually at least ten electrode positions and sometimes as many as twenty are required for the patient's chest and extremities. The patient often becomes chilled with these wet solutions and shivering occurs which causes muscular movements. These movements introduce artifacts in the traces destroying their accuracy and impairing their interpretation. In addition, grounding problems are encountered between the patient and the resting table.

At the present time, about 90% of cardiographers still use the jelly or cream and the remainder use a liquid solution or impregnated

pad [11] . In 1968 Marriott [3] recommended the use of jellies in his popular, standard text for cardiologists.

Historically, the need for a good electrode-to-skin contact was of essential importance. The skin resistance (usually about several thousand ohms) had to be overcome because of the low impedance of the string galvanometers. The electrode jelly, therefore, was necessary to reduce excessive A.C. interference which distorted traces. However, the recent electrocardiographs now being produced, for example by the Sanborn Division of Hewlett Packard, have input impedances of at least a factor of 10 to 100 times higher than string galvanometers.

In light of these new high-impedance circuits, an investigation of present electrode-to-skin contact materials was conducted.

The principal goal of this investigation is to see if the present electrode-to-skin contact materials are necessary and to find suitable alternatives to these materials without impairing diagnosis.

Purpose

The purpose of this study is to find a less time-consuming, less corrosive, less objectionable, and less expensive method for providing the electrode-to-skin contact required in clinical practice of cardiography. This method should provide the same quality of measurements as existing methods.

Experiment

The experiment was conducted to investigate several electrode-to-skin contact methods. The results of the electrocardiograms

obtained from both the conventional and recommended methods were compared. Both limb and chest measurements were taken using a direct-reading electrocardiograph under the supervision and operation of a cardiologist [11] . The author was the patient in the experiments described below.

Experimental Apparatus. The electrocardiograph was a Sanborn (Hewlett Packard) Model Viso 100. There were two visual outputs, a Biocom Scope, Model 430, and a Sanborn millivolt recorder. The sensitivity of the output was 1 cm = 1 millivolt with a chart speed of 25 mm/sec. Measurements were taken at rest and while the patient was on a M. D. Electronics Treadmill, Model E-6 at two mph and 10^{o} incline. Two types of electrodes were used. Chest measurements were taken while the patient was on the treadmill and while the patient was at rest using the M. D. Electronics Ag/AgCl electrodes with in-line insulated connectors; refer to Fig. III-2. These electrodes were supported by two-sided adhesive rings. The electrodes are about 2 cm diameter. Limb measurements were taken at rest using the Lumiscope Cardio Clamps; refer to Fig. III-2.

Six different electrode-to-skin contacts were investigated. They were (1) dry, that is direct electrode-to-skin contact, (2) tap water, (3) standard saline solution with 0.9 gms NaCl USP/100 cc, supplied by Cutter Laboratories, (4) Pacquins Hand Cream (for extra dry hands) produced by Charles Pfizer and Company, Inc., (5) standard EKG paste manufactured by Burton, Parsons, and Company, Inc., and (6) isopropyl alcohol, 70% by volume.

Preparations (3), (5), and (6) represent the conventional methods; preparations (1), (2), and (4) represent the proposed methods.

Experimental Procedure. The chest measurements were taken in the standard V-4 position using three probes and a ground. The hair was shaved in the area where electrodes were placed on the chest. The limb measurements were taken using two arms, and one leg as a ground which is called the standard limb lead I; refer to Fig. III-2.

Experimental Results. All six electrode-to-skin contact mediums gave similar traces for the limb electrocardiograms. A comparison of these cardiograms is shown in Fig. III-3. No differences between the cardiograms were discernible [11]. A comparison of the methods for limb measurements including costs is summarized in Table III-1.

The use of a dry skin-to-electrode contact is recommended for limb measurements because it is fast, cost-free, and noncorrosive. No application or removal of any messy material is required. Finally, and most important, the electrocardiograms are comparable to the other methods.

Some difficulty was encountered using the liquid contact methods with the chest measurements because the liquid run-off reduced the effectiveness of the adhesive tape in supporting the electrodes. However, the hand cream and EKG paste contacts yielded comparable cardiograms [11]. A dry contact was not used for the chest measurements during the movement on the treadmill because

Table III-1. Summary of Results for Limb Measurements Using Various Electrode-to-Skin Contact Methods

Electrode-to-Skin Contact Material	Cost of Contact Materials (per Patient)	Application and Removal of Contact Material	Cardiogram Results	Time-for Application and Removal/ Patient (minutes)	Corrosive Properties
(1) Dry	--	Nothing Required	Excellent	--	Negligible
(2) Tap Water	--	Easy	Excellent	2	Negligible
(3) Saline Solution	2¢	Must be Washed Off Electrodes	Excellent	2.5	Minor
(4) Hand Cream	4¢	May be Rubbed into Skin	Excellent	3.5	Negligible
(5) EKG Paste	10¢	Must be Washed Off Electrodes and Patient	Excellent	6.5	Serious Problem Unless Cleaned Very Carefully
(6) Isopropyl Alcohol	2¢	Easy	Excellent	2	Negligible

lubrication between the skin and electrode may reduce the possibility of chafing and artifacts.

The comparison of the hand cream and the EKG paste is interesting because after removal of the electrode, the hand cream can be simply rubbed into the skin like a vanishing cream. In comparison, the EKG paste is messy, must be wiped off, and usually is troublesome

to patient, doctor, technician, and especially to electrodes because of corrosion [10]. The use of hand cream will undoubtedly be favorably received by female patients.

These results are in substantial agreement with Lewes [12] who investigated very high-impedance research type instruments of about 4 megohm. The present investigation was conducted with an instrument of input impedance around 20 kilohm which is the type commonly used in routine clinical practice.

Conclusion

For limb measurements, all six electrode-to-skin contact methods yielded similar electrocardiograms. The dry contact method is recommended. Use of conventional EKG jellies, pastes, creams, alcohol solution, and electrolyte pads can be discontinued for routine clinical practice. The savings in time, effort, and money, and the elimination of shivering and corrosion problems will be the result.

For chest measurements, a commercial, noncorrosive hand cream was more convenient and yielded electrocardiograms comparable to the recommended EKG pastes which are messy and corrosive.

The standard recommended practices for electrode-to-skin contacts were developed in the 1930's for low input instruments, and these practices are no longer necessary with today's commercial electrocardiographs.

Acknowledgment

The consultation and donation of time, supplies, and equipment by George W. Collen, M.D., F.A.C.C. for this investigation is very much appreciated.

The EKG's were interpreted by Dr. Collen who has been active in the field of cardiology for 25 years in private practice, in education, and in research. He is presently engaged in private practice and is an Assistant Clinical Professor of Medicine at UCLA. From 1964 to 1966 he was Director of Vectorcardiography at Harbor General Hospital, Torrance, California.

References

1. Krupp, M. A., Sweet, N. J., Jawetz, E., and Biglieri, E. D., Physicians Handbook, Fourteenth Edition, Lange Medical Publications, Los Altos, California, 1966.

2. Goldman, M. J., Principles of Clinical Electrocardiography, Sixth Edition, Lange Medical Publications, Los Altos, California, 1967.

3. Marriott, H. J. L., Practical Electrocardiography, Fourth Edition, Williams and Wilkins Co., Baltimore, 1968.

4. Brown, M. K., Nature 180, 192 (1957).

5. Richardson, P. C., Aerospace Med. 39, 745 (1968).

6. James, W. B., and Williams, H. B., Amer. J. Med. Sci. 140, 408 (1910).

7. Cohn, A. E., Arch. Intern. Med. 26, 105 (1920).

8. Boas, E. P., Arch. Intern. Med. 41, 403 (1928).

9. Jenks, J. L., and Graybiel, A., Amer. Heart J. 10, 693 (1935).

10. Littmann, D., Amer. J. of Card. 4, 554 (1959).

11. Collen, G. W., personal communication, 1970.

12. Lewes, D., Br. Heart J. 27, 105 (1965).

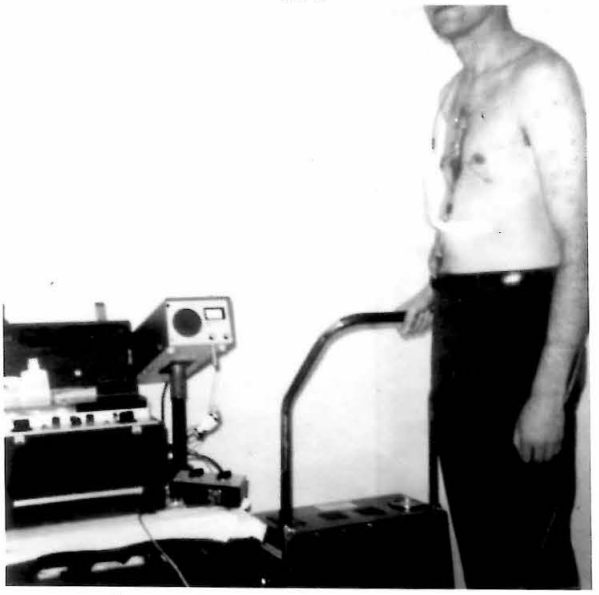

Chest
Hook
Up

Limb
Hook
Up

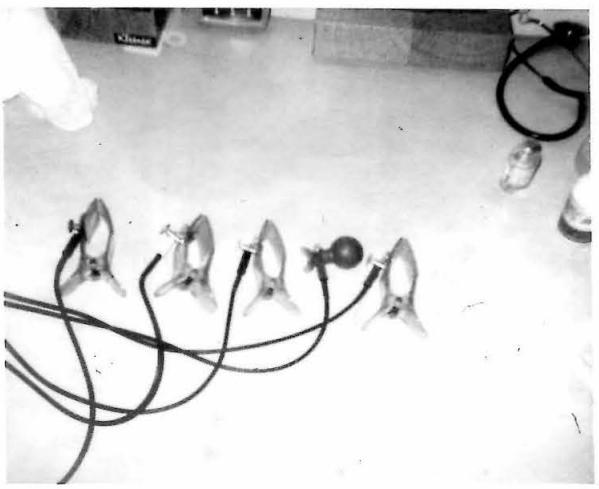

Limb
Electrodes

Figure III-2. Chest Hook Up, Limb Hook Up, and Limb Electrodes

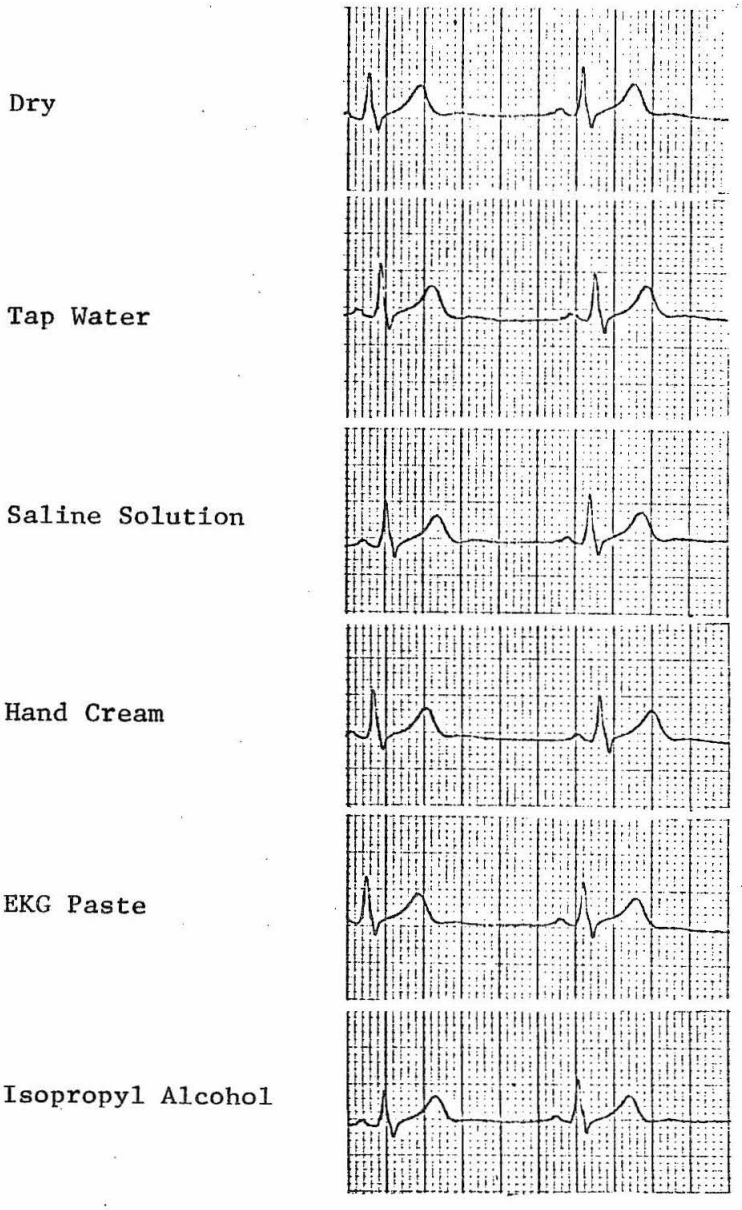

Fig. III-3. Limb Cardiograms for Six Electrode-to-Skin Contacts